Adaptive Refinement Algorithms for Optimization Problems in Energy Transport Networks

Dissertation approved by Faculty IV
of Trier University

for

the award of the academic degree
Doctor of Natural Sciences (Dr. rer. nat.)

by

J.-Marius Roland
born in Brussels, Belgium

Trier, September 2022

supervised by Prof. Dr. Martin Schmidt

Date of scientific debate:	November 7, 2022
Thesis committee:	Prof Dr. Martin Schmidt
	Prof Dr. Volker Mehrmann
	Prof Dr. Volker Schulz (Chair)

Acknowledgments

I would like to thank my supervisor Martin Schmidt. Your availability, perseverance, and desire to pass on your knowledge have strongly influenced me during the last three years. I am sure that your teachings will positively impact my future. You were not only a supervisor but also very quickly became a mentor and a friend. I wish you the best and I am sure that we will stay in contact.

I would like to thank Volker Mehrmann for being part of my thesis committee and the efficiency and responsiveness that he demonstrated for every step of my thesis defense.

I would like to show my gratitude to Volker Schulz for being the chair of my thesis defense.

I wish to thank all my co-authors for our fruitful collaboration: Diego Cattaruzza, Hannes Dänschel, Martine Labbé, Volker Mehrmann, Matteo Petris, and Martin Schmidt.

I want to thank all my colleagues at Trier University. Special thanks go to Marc Harmening, Lukas Mich, Britta Schmitt, Max Späth, and Michael Vu for making my integration very smooth from my first day at the department. My thanks also go to Lukas Winkel for his great smile and all the good times spent together. I would also like to thank Johannes Thürauf for the boosts of motivation that he gave me through our many fruitful discussions and for all his valuable comments. I thank Yasmine Beck for correcting large chunks of my thesis and for always keeping the comments positive.

My thanks go to my family for their huge support and understanding. More specifically, I thank my father for his kindness, will to pass on his life lessons, and his never-ending availability. I thank my mother for her generosity, everlasting smile, and for always making me feel welcome at home. I thank my sister for her kindness, and for giving me confidence at all times.

I would like to express my gratitude to all my close friends who helped me put things into perspective and take my thesis less seriously. In the first place, I would like to thank Celia Souralaysak. You were the sunshine I could always rely on when things became complicated. I changed so much thanks to you and I am very grateful for every second we spent together. Next, I thank Oliver Neumann for all the time spent together and the support he gave me during the last months of writing. Further, my thanks go to Darvin Hassan for the time spent together and our interesting discussions. Next, I thank the famous trio: Gaspard Berger, Dan Mardulyn, and Oskar de Wolf for the countless hours spent together. I am convinced that each weekend at the "depot" heavily influenced my mood and I am very grateful for the constant support that you have demonstrated. The three of you strongly influenced who I am now and I am very grateful for the life experiences that we had. More specifically, I thank Gaspard for his kindness, ever-lasting positive attitude, and for supporting me for so many years. I thank Dan for always showing interest and

support in my projects, his friendliness, and his will to always be there even when I am on the other side of the planet. I thank Oskar for making me feel at home at any time, his generosity, and the countless deep discussions that we had. Finally, I thank Quentin Dewint for the great times spent together and for being there when it mattered. Last but not least, I thank Quentin Roland and Charles Roland for being very supportive friends and cousins.

Curriculum Vitae

Personal Information

Name	Jacques-Marius Roland
Nationality	Belgian
Date and Place of Birth	September 7, 1996, Brussels, Belgium

Education

09/2019 – 11/2022	**Research Assistant at Trier University**
	Prof. Dr. Martin Schmidt
06/2019	**Master Degree in Mathematical Engineering**
09/2017 – 06/2019	Catholic University of Louvain
	Louvain-la-Neuve, Belgium
06/2017	**Bachelor Degree in Engineering**
09/2014 – 06/2017	Catholic University of Louvain
	Louvain-la-Neuve, Belgium
06/2017	**High School**
	Koninklijk Atheneum Etterbeek, Belgium

Abstract

Energy transport networks are one of the most important infrastructures for the planned energy transition. They form the interface between energy producers and consumers and their features make them good candidates for the tools that mathematical optimization can offer. Nevertheless, the operation of energy networks comes with two major challenges. First, the nonconvexity of the equations that model the physics in the network render the resulting problems extremely hard to solve for large-scale networks. Second, the uncertainty associated to the behavior of the different agents involved, the production of energy, and the consumption of energy make the resulting problems hard to solve if a representative description of uncertainty is to be considered.

In this cumulative dissertation we study adaptive refinement algorithms designed to cope with the nonconvexity and stochasticity of equations arising in energy networks. Adaptive refinement algorithms approximate the original problem by sequentially refining the model of a simpler optimization problem. More specifically, in this thesis, the focus of the adaptive algorithm is on adapting the discretization and description of a set of constraints.

In the first part of this thesis, we propose a generalization of the different adaptive refinement ideas that we study. We sequentially describe model catalogs, error measures, marking strategies, and switching strategies that are used to set up the adaptive refinement algorithm. Afterward, the effect of the adaptive refinement algorithm on two energy network applications is studied. The first application treats the stationary operation of district heating networks. Here, the strength of adaptive refinement algorithms for approximating the ordinary differential equation that describes the transport of energy is highlighted. We introduce the resulting nonlinear problem, consider network expansion, and obtain realistic controls by applying the adaptive refinement algorithm. The second application concerns quantile-constrained optimization problems and highlights the ability of the adaptive refinement algorithm to cope with large scenario sets via clustering. We introduce the resulting mixed-integer linear problem, discuss generic solution techniques, make the link with the generalized framework, and measure the impact of the proposed solution techniques.

The second part of this thesis assembles the papers that inspired the contents of the first part of this thesis. Hence, they describe in detail the topics that are covered and will be referenced throughout the first part.

Author's Contributions

[MR1] Roland, M. and M. Schmidt (2020). "Mixed-integer nonlinear optimization for district heating network expansion". In: *at - Automatisierungstechnik* 68.12, pp. 985–1000. DOI: 10.1515/auto-2020-0063.

The original idea of the paper came from Martin Schmidt. The model that is presented in the paper resulted from a joint discussion between both authors. The author of this dissertation was responsible for the implementations and the writing of the paper was primarily done by him.

[MR2] Dänschel, H., V. Mehrmann, M. Roland, and M. Schmidt (2022). "Adaptive Nonlinear Optimization of District Heating Networks Based on Model and Discretization Catalogs". Submitted. URL: https://optimization-online.org/2022/01/8779/.

The ideas of this paper originally came from Volker Mehrmann and Martin Schmidt. The author of this dissertation developed the model catalog as well as analytical solutions and proved the theoretical results in close collaboration with Hannes Dänschel. In addition, he strongly contributed to the code and performed the numerical study.

[MR3] Cattaruzza, D., M. Labbé, M. Petris, M. Roland, and M. Schmidt (2022). "Exact and Heuristic Solution Techniques for Mixed-Integer Quantile Minimization Problems". Submitted. URL: https://optimization-online.org/2021/11/8673/.

All authors contributed equally to the ideas of this paper. More specifically, the adaptive scenario clustering algorithm was proposed by the author of this dissertation. Therefore, he was the primary author of Section 5. Jointly with Matteo Petris, he was responsible for the implementation of the proposed techniques and wrote the numerical results section.

Contents

I Extended Summary **1**

1 Introduction **2**
1.1 Adaptive Refinement for General Optimization 4
1.2 Adaptive Refinement for Optimization with ODEs 4
1.3 Contributions and Structure 6

2 A Generalized Adaptive Refinement Framework **7**
2.1 General Problem 8
2.2 Fitted Surrogate Problem 9
2.3 Discretized Problem 11
2.4 Adaptive Refinement Algorithm 11

3 Optimization of District Heating Networks **20**
3.1 Introduction to District Heating Networks 20
3.2 Stationary District Heating Network Operation 21
3.3 Network Expansion 26
3.4 Realistic Solutions 32

4 Quantile-Constrained Optimization Problems **43**
4.1 Optimization Problem and Approximation 43
4.2 Preliminary Solution Techniques 45
4.3 Adaptive Scenario Clustering Algorithm 48
4.4 Numerical Results 52

5 Conclusion **56**

Bibliography **59**

II Reprints of Published Journal Articles and Preprints **68**

1 Mixed-Integer Nonlinear Optimization for District Heating Network Expansion **69**

2 Adaptive Nonlinear Optimization of District Heating Networks Based on Model and Discretization Catalogs **99**

3 Exact and Heuristic Solution Techniques for Mixed-Integer Quantile Minimization Problems **129**

Part I

Extended Summary

1 Introduction

When considering optimization problems corresponding to real applications, it is commonly accepted to use approximated representations of reality. Usually, these approximations are obtained through simplifying assumptions about the process that is considered. For instance, in the seminal papers by Markowitz and Manne (1957) and Dantzig (1960) it was discussed how nonlinear functions could be replaced by piecewise linear functions. Naturally, the authors made the simplifying assumption that enough points were selected for the piecewise function to accurately mimic the original function. Their aim was to consider an, in that time, easier to solve mixed-integer linear optimization problem (MILP) instead of a nonlinear optimization problem (NLP).

One issue that is often abstracted from in the literature is that solutions of the approximated model are not necessarily feasible for the original model. Consequently, the resulting solutions may not properly mimic the real process that is considered. Moreover, realistic solutions can generally not be obtained by solving the original model in reasonable computing times. This discrepancy highlights the usual trade-off in application-driven optimization: the time requirement of many applications that benefit from optimization limits the quality of the solution that can be obtained.

Energy transport networks constitute one of these applications. Interestingly, the optimization of energy networks comes with two challenges that can be coped with the use of simplified models. First, detailed descriptions of the physics that govern such networks result in huge nonconvex and nonlinear optimization problems. With the current state of the computational hardware and software, these problems cannot be solved in reasonable times. For the case of electricity networks, this issue was highlighted by Aravena et al. (2022) that summarize the approaches taken in the first challenge of the ARPA-E Grid Optimization Competition[1], a challenge aimed at modernizing the state-of-the-art power grid optimization software. Much attention is

[1] See https://gocompetition.energy.gov/.

consequently pointed towards approximating the expressions that describe energy transport. Catalogs of optimization models with a decreasing amount of nonlinear terms exist for describing the network's physics; see, e.g., Molzahn and Hiskens (2019) for a detailed list of stationary optimal power flow approximations. Often, bounds on the approximation accuracy of such simplified models exist. These upper bounds allow to use simplified models while keeping the accuracy of the solution below a certain threshold. Similarly, the dynamics of some energy networks such as gas networks or district heating networks (DHNs) have to be described by partial differential equations (PDEs); see, e.g., Domschke et al. (2021). The most intuitive way of dealing with such constraints is to use discretization techniques that yield a large set of constraints. For this approach, error measures exist that quantify the accuracy that the discretization provides. This allows to use coarse discretizations that reduce the size of the resulting optimization problem as long as the error measures are small.

Second, the behavior of the various agents in energy networks are not known in advance. This motivates the use of probabilistic optimization models; see, e.g., Conejo et al. (2010). In many cases, uncertainty is dealt with a representative selection of scenarios that yield an optimization problem of smaller size. This selection of scenarios is often obtained by clustering a larger set of scenarios. Depending on the uncertainty that is studied, statistical error bounds exist to describe the accuracy of the scenario-based approximation, once more, showing that simplified models may be used to get realistic solutions to energy network optimization problems.

Due to the current energy turnaround, energy networks have become a popular topic in optimization. Hence, this popularization motivated the development of optimization techniques that exploit simplified models of energy transport and uncertainty quantification. As discussed, the aim here is to bypass the associated challenges and efficiently yield solutions of good quality. Nevertheless, the problem of accuracy guarantees is usually not the primary focus in the literature and is the topic of this dissertation. We study a technique that designs approximated optimization problems with accuracy guarantees. More specifically, we examine an adaptive optimization algorithm that yields realistic solutions to energy network applications.

Adaptive optimization algorithms, sometimes referred to as decomposition techniques, are methods that iteratively switch between solving and improving the approximation accuracy of a simplified optimization problem. Many groundbreaking optimization methods can be described in this way. For instance, in the case of mixed-integer linear programming, one can, e.g., think about cutting-plane algorithms, see Wolsey (1998), and Benders decomposition, see Benders (1962) and Geoffrion (1972). The same holds for nonlinear programming where methods such as outer approximation as described in Duran and Grossmann (1986) as well as Fletcher and Leyffer (1994) follow the same adaptive structure.

In more detail, the focus of this dissertation is on adaptive refinement algorithms (ARAs), a specific type of adaptive optimization algorithm that iteratively improves the accuracy guarantee of the approximation model by refining the description and discretization of a set of constraints. Two branches of the optimization literature are related to the topics considered in this thesis. The first branch is

concerned with approximating a class of optimization problems by a "simpler" class of optimization problem. Here, the simpler problems are inner or outer approximations of the original problem and are obtained through the partitioning of the feasible set of a variable. The second branch studies the approximation of ordinary differential equations (ODEs) in optimization problems. Here, the ODEs are discretized to yield optimization problems in closed form and the resulting discretization is adaptively refined until realistic solutions of the original problem are obtained. In the following two sections we review the literature of the two aforementioned branches with a specific focus on energy network applications. We mention that this literature review is not comprehensive and is designed to give an overview of the different research directions linked to the topic of this thesis.

1.1 Adaptive Refinement for General Optimization

ARAs are part of the large set of optimization techniques concerned with solving specific classes of optimization problems. Various authors in the field of mixed-integer nonlinear programming (MINLP) propose adaptive algorithms that iteratively refine outer approximations. Usually, the construction of outer approximations differ based on the assumptions that are made about the MINLP that is considered; see, e.g., Schmidt et al. (2019), Schmidt et al. (2022), Grübel et al. (2022), Lundell et al. (2013), and Leyffer et al. (2008). A notable application related to this thesis is the adaptive refinement of MILP outer approximations applied to the case of gas networks discussed as in Geißler et al. (2012), Geißler et al. (2013), Burlacu et al. (2020), Burlacu et al. (2019), and Aigner et al. (2020). Similarly, Gupte et al. (2022) propose an adaptive refinement technique for inner approximations of quadratically constrained quadratic problems. Goderbauer et al. (2016) and Koster and Kuhnke (2019) apply the same ideas for linearizing bilinear terms in MINLPs arising in design of decentralized energy supply systems and water usage and treatment networks. Furthermore, adaptive refinement is a popular topic in the field of semi-infinite programming. Here, most approaches are based on the founding works of Blankenship and Falk (1976) that iteratively refine a discretization of the infinite-dimensional domain. Finally, Berthold et al. (2022) applied a similar approach for solving optimization problems with so-called probust constraints that arise, e.g., in the case of gas transport problems.

1.2 Adaptive Refinement for Optimization with ODEs

We now focus on the literature related to the core topic of this thesis, i.e., ARAs for optimization problems with ODEs. The motivation for adaptive refinement can be traced back to the a-posteriori error estimates for finite element methods (FEMs) presented in Babuška and Rheinboldt (1977). For the first time, the value of the exact approximation error could be bounded from above by a sum of finite-element cell contributions. This gave rise to two new branches of the FEM literature. The first one introduced the concept of adaptive finite element methods (AFEMs) that

sequentially solve a finite element discretization and refine the underlying grid until the approximate solution is close enough to the exact solution; see, e.g., Bangerth and Rannacher (2003) and Nochetto et al. (2009). The second branch corresponds to the study and establishment of tight error estimates for finite element methods, see, e.g., Verfürth (1994), Hintermüller and Hoppe (2008), and Leykekhman and Vexler (2016). Moreover, a new error estimation approach called the dual-weighted residual method that makes it possible to compute error estimates w.r.t. a specific quantity of interest was proposed during that period by Becker et al. (2000). This opened the door to algorithms that couple optimal control with AFEMs as discussed in the survey by Becker and Rannacher (2001) and enhanced by, e.g., Becker et al. (2000), Becker and Rannacher (2001), Ziems and Ulbrich (2011), and Liu et al. (2015).

Furthermore, multifidelity methods are numerical optimization methods that have a strong link to the field of adaptive optimal control. In the field of multifidelity methods the focus is on unconstrained optimization problems with objective functions that have varying fidelity w.r.t. the reality. Because this topic is not at the core of this thesis, we refer the interested reader to Polak (1997), Alexandrov et al. (1998), Gratton et al. (2008), and Peherstorfer et al. (2018) for a subset of papers that discuss this topic.

Recently, adaptive refinement algorithms have been applied to energy networks. As mentioned previously, the behavior of some energy networks have to be described by PDEs that motivate the use of such algorithms. Due to the nonconvexity of the equations modeling energy transport, the focus has initially been on developing model catalogs that define a sequence of models with decreasing accuracy guarantees w.r.t. the exact physics of the energy network; see, e.g., Domschke et al. (2021) for gas networks, Mehrmann et al. (2018a) for electricity networks, and Hauschild et al. (2020) for district heating networks. Domschke et al. (2015) propose discretization and model error estimates for a subset of models in the gas network model catalog by Domschke et al. (2021). Moreover, Stolwijk and Mehrmann (2018) provide an error and sensitivity analysis of the gas equations with a specific focus on data uncertainty. The error estimates of Domschke et al. (2015) are combined with an adaptive refinement algorithm in Domschke et al. (2018) for transient gas network simulation. Another approach for the simulation of gas networks is taken by Rüffler et al. (2018), where a mode optimal switching control problem is proposed that optimizes a performance index, which balances model accuracy and computational cost for a simulation of the entire network. In the optimization literature, Schmidt et al. (2015) and Schmidt et al. (2016) propose to iteratively solve an enhanced version of a gas network optimization problem by increasing the model level of all the pipes. Finally, Mehrmann et al. (2018b) use the error estimates of Stolwijk and Mehrmann (2018) to set up an ARA that considers both model level switching and discretization stepsize modification. This inspired the ideas presented in [MR2] and [MR3]. To the best knowledge of the author of this thesis, these papers are the only applications of adaptive refinement techniques that combine model level

switching and discretization stepsize modification for the case of energy network optimization with ODE constraints.

1.3 Contributions and Structure

This cumulative dissertation is divided in two parts. Part I, referred to as the extended summary, summarizes the content of the papers that make up this thesis. Here, we refrain from repeating the proofs of the theoretical results. Furthermore, Part II contains the reprints of the journal articles and preprints that Part I summarizes. We now discuss the contributions of this thesis by referring to the respective chapters of Part I.

In Section 1.2 we highlighted that ARAs have rarely been used for approximating ODEs in energy network optimization problems. This thesis is an attempt to contribute to this branch of the optimization literature. The primary objective is to set up a generalization of ARAs for solving energy network optimization problems with discretizable constraints. In more detail, the contributions of this cumulative dissertation are threefold.

First, we contribute to the energy network optimization literature by presenting a generalized optimization framework in Chapter 2. This framework bridges the gap between energy networks and ARAs. Moreover, we pave the way for future works that study theoretical aspects of generalized ARAs applied to energy network problems with discretizable constraints. We first construct a general optimization model. Then, two ways of coping with the discretizable constraints are discussed through the lens of this general optimization problem. The first method, which can only be applied in very specific cases, replaces the troublesome constraints with a surrogate function; see, e.g., Sobester et al. (2008). The second method is a generalization of the ARAs presented in Mehrmann et al. (2018b), [MR2], and [MR3].

Second, we consider two optimization problems originating from energy networks that benefit from the application of ARAs; a stationary district heating network operational optimization problem and a quantile-constrained optimization problem. They are presented in Chapter 3 and 4, respectively. Additionally, the models are reformulated to fit into the new generalized framework, and solved with the techniques of Chapter 2. Hence, we highlight the applicability of the approach and discuss both the strengths and weaknesses of the studied ARA.

Finally, through the applications that we consider, two extensions of the ARA are presented. In Chapter 3, we focus on extending the algorithm with a coarsening and down-switching step for the case of district heating network operation. In Chapter 4 the ARA is extended so that it provably terminates at a global optimal solution of the quantile-constrained problem.

2

A Generalized Adaptive Refinement Framework

This chapter presents a generalization of the adaptive refinement algorithms considered in Stolwijk and Mehrmann (2018), [MR2], and [MR3]. We remark that the generalization that we propose is new and is uniquely inspired by the ideas in Stolwijk and Mehrmann (2018), [MR2], and [MR3]. The concepts are illustrated using the example of ODEs. Therefore, we expect the reader to have basic knowledge regarding discretization of ODEs as described in, e.g., Süli and Mayers (2003) or Quarteroni et al. (2007).

We shortly discuss the contents of this chapter. First, a general optimization problem is presented that captures the characteristics of the optimization problems considered in Stolwijk and Mehrmann (2018), [MR2], and [MR3]. Preliminary assumptions about this general problem are stated. Second, the fitted surrogate optimization problem and the discretized optimization problem are described on the basis of these assumptions. Both problems approximate the general problem. Then, the main contribution of this chapter is presented; a generalized adaptive refinement algorithm designed to cope with the issues of the discretized problem.

In more detail, this chapter is outlined as follows. Section 2.1 introduces the general optimization problem and states the assumptions about the problem. Then, Section 2.2 presents the fitted surrogate optimization problem. Section 2.3 presents the discretized optimization problem. Finally, Section 2.4 describes the functioning of the adaptive refinement algorithm using the discretized problem presented in Section 2.3. In addition, we lay the foundation for applying the adaptive refinement algorithm in the next chapters.

2.1 General Problem

We now state the general optimization problem that we consider throughout this chapter and state the preliminary assumptions about its structure.

Let $u \in U \subseteq \mathbb{R}^m$ and $w \in W \subseteq \mathbb{R}^o$ be two sets of variables. Here u represents the exact decisions to be made and the set w represents the auxiliary variables that are uniquely determined by the constraints of the optimization problem when u is fixed. For example, the w variables could be linked to the underlying application's internal dynamics, which are implicitly determined given a fixed value for the u variables. Furthermore, a non-overlapping partition of w in $\alpha + 1$ disjoint vectors of variables w_j is assumed such that $w := \left(w_1^\top, \ldots, w_\alpha^\top, w_{\alpha+1}^\top\right)^\top$ holds. We define the set $J := \{1, \ldots, \alpha\}$ associated to all disjoint variable sets of w except for $w_{\alpha+1}$. Additionally, I represents an arbitrary subset of $\mathbb{N}$. Then, the general optimization problem reads

$$\begin{aligned} \min_{u,w} \quad & f(u, w) \\ \text{s.t.} \quad & g_i(u, w) = 0, \quad i \in I, \\ & h_j(u, w_j) = 0, \quad j \in J, \\ & u \in U, \ w \in W. \end{aligned} \tag{G}$$

The first assumption specifies the type of functions h_j that we are interested in.

Assumption 1 *The function $h_j : U \times W_j \to \mathbb{R}$ defined for all $j \in J$ does not describe an analytical expression, i.e., it cannot be represented with a finite number of standard mathematical operations and functions.*

Examples of functions that satisfy Assumption 1 are ordinary differential equations. By definition, they contain differential operators and thus describe mathematical expressions that are not analytical. In other words, unless they have an analytical solution, no closed-form formula exists to compute their value.

Next, the functions $f : U \times W \to \mathbb{R}$ and $g_i : U \times W \to \mathbb{R}$ for $i \in I$ designate functions whose expressions are given explicitly in closed-form. The constraints $g_i(u, w) = 0$ therefore encompass all the remaining closed-form constraints of the underlying optimization problem. These constraints typically pose fewer challenges when translating the original application into an optimization problem.

For the sake of illustration, we consider the case of optimal control problems, as, e.g., described in Sethi and Thompson (2000). By associating the u variables to the "controls" of the problem and the w variables to the "state" variables we can easily cast any optimal control problem to the form of (G). Indeed, the ODEs governing the controlled physics can then be represented with the constraints $h_j(u, w_j) = 0$ whereas the initial and boundary conditions can then be represented with $g_i(u, w) = 0$ constraints.

In general, (G) cannot explicitly be solved by state-of-the art optimization solvers due to Assumption 1. Consequently, there is a need for accurate approximations of h_j. In Stolwijk and Mehrmann (2018), [MR2], and [MR3] the constraints $h_j(u, w_j) = 0$

can be approximated with a set of discretized closed-form constraints. In the field of optimization with ODE constraints this idea is commonly referred to as the first-discretize-then-optimize approach; see Hinze et al. (2009).

We now introduce the notation associated to this discretization. Hence, we have the set of discretization variables $z_j \in Z_j \subseteq \mathbb{R}^{n_j}$ and the set of discretization constraints $\tilde{h}_{j,k}(u, w_j, z_j) = 0$ defined for all $k \in K(j)$ where $K(j) \subseteq \mathbb{N}$. Moreover, the variables z_j link the constraints $\tilde{h}_{j,k}$ together. As a consequence, $|K(j)|$ is expected to be of $O(n_j)$, where n_j denotes the dimension of z_j.

We now state the second assumption about (G). To do so, we first define the sets of feasible solutions. Hence, for $j \in J$, we define

$$\mathcal{G}_j := \{(u, w_j) \in U \times W_j : \ h_j(u, w_j) = 0\},$$
$$\tilde{\mathcal{G}}_j := \{(u, w_j) \in U \times W_j : \ \exists z_j \in Z_j, \ \tilde{h}_{j,k}(u, w_j, z_j) = 0, \ k \in K(j)\}.$$

Then, for all $j \in J$, the second assumption links the set $K(j)$ of discretization functions $\tilde{h}_{j,k}$ and the original function h_j.

Assumption 2 *For any $\varepsilon > 0$ and for any $j \in J$ there exists a value for n_j such that*

$$|h_j(u, w_j)| \leq \varepsilon$$

holds for all $(u, w_j) \in \tilde{\mathcal{G}}_j$.

Assumption 2 implies that there exists a large enough value for n_j such that any point inside $\tilde{\mathcal{G}}_j$ will be "nearly" inside of $\mathcal{G}_j$.

Going back to the ODE example, we highlight that a wide range of discretization techniques exist for approximating differential operators; see, e.g., Quarteroni et al. (2007). These techniques yield a set of constraints satisfying the description of $\tilde{h}_{j,k}(u, w_j, z_j) = 0$ with associated discretization variables z_j. Furthermore, upper bounds exist on the distance between the exact solution and the discretized solution of an ODE, depending on the discretization stepsize, i.e., the value of n_j. Again, we refer to Quarteroni et al. (2007) for more details about convergence analysis of numerical solutions to ODEs.

In the next two sections two closed-form optimization problems that approximate (G) are presented. The first problem uses a surrogate function to replace h_j that can only be used if $h_j(u, w_j)$ can be evaluated for all $(u, w_j) \in U \times W_j$. The second problem uses the set $K(j)$ of discretization functions $\tilde{h}_{j,k}$ to set up a closed-form approximation problem.

2.2 Fitted Surrogate Problem

In this section we highlight the specific case in which the function h_j has a closed-form reformulation that can be used to set up an approximation problem. Naturally, we consider the case where this reformulation can be evaluated but cannot directly be used to replace h_j in (G). Otherwise, the reformulation would make the ideas of this chapter unnecessary. For example, such a closed-form reformulation of h_j

exists when h_j describes an ODE that has a continuous closed-form solution that is parameterized by a case distinction. Then, the reformulation cannot be used directly for replacing h_j in (G) since state-of-the-art optimization solvers do not accept case-distinctions; see, e.g., Byrd et al. (2006) for the KNITRO solver.

If such a reformulation exists, a closed-form surrogate function can be designed to approximate h_j in (G), see, e.g., Sobester et al. (2008) and Peherstorfer et al. (2018). One way of designing such a surrogate function is to fit an ansatz function h_j^{fit} to h_j on a sample of the set of feasible u and w_j values. If a large enough sample of $U \times W_j$ exists and h_j is continuous over $U \times W_j$, then an approximation function h_j^{fit} might be sufficient for replacing h_j in (G). This is the idea of the fitted surrogate optimization problem that we consider.

Thus, we can select a finite subset $\mathcal{D} \subseteq U \times W_j$, a loss function $\ell : \mathbb{R} \times \mathbb{R} \to \mathbb{R}^+$, and an ansatz function $h_j^{\text{fit}} : U \times W \times \Lambda_j \to \mathbb{R}$ where $\Lambda_j \subseteq \mathbb{R}^o$ models the set of feasible parameters. Using the classic fitting problem, see Deisenroth et al. (2020, p. 260), we look for $\lambda_j^* \in \Lambda_j$ that minimizes

$$\min_{\lambda_j \in \Lambda_j} \frac{1}{|\mathcal{D}|} \sum_{(u,w_j)\in\mathcal{D}} \ell(h_j(u,w_j), h_j^{\text{fit}}(u,w_j,\lambda_j)). \tag{2.1}$$

The objective function value of optimization problem (2.1) is a measure for the fitting accuracy of h_j^{fit} with respect to h_j over $\mathcal{D}$. This allows to judge the quality of the approximation over the set $\mathcal{D}$.

Given h_j^{fit} with $\lambda_j^* \in \Lambda_j$ that solves (2.1), we define the fitted surrogate optimization problem

$$\begin{aligned} \min_{u,w} \quad & f(u,w) \\ \text{s.t.} \quad & g_i(u,w) = 0, \quad i \in I, \\ & h_j^{\text{fit}}(u,w_j,\lambda_j^*) = 0, \quad j \in J, \\ & u \in U,\ w \in W. \end{aligned} \tag{F}$$

We draw the attention to the fact that the fitting presented in (2.1) does not necessarily give good results if used in (F). It might indeed happen that some very precise dynamics of h_j cannot be captured by an ansatz function h_j^{fit} with a reasonable amount of nonlinear terms, see Fajemisin et al. (2021). Furthermore, an accurate representation of the challenging dynamics of h_j over $U \times W_j$ can require a dense set of samples inside $U \times W_j$. Depending on the size of $U \times W_j$, this set of samples might have to be too large for (2.1) to stay solvable. Hence, if one of these prerequisites is not met, the use of a fitted function can introduce approximation errors that will likely lead to solutions that are far away from any feasible solution of (G).

In more detail, for $j \in J$, we define

$$\mathcal{G}_j^{\text{fit}} := \left\{(u,w_j) \in U \times W_j : \ h_j^{\text{fit}}(u,w_j) = 0\right\}.$$

Then, Assumption 2 does not necessarily hold if we replace $\tilde{\mathcal{G}}_j$ by $\mathcal{G}_j^{\text{fit}}$. As a consequence, this creates the need for different algorithmic techniques that exploit the

feasibility guarantees of the $\tilde{h}_{j,k}$ functions over the entirety of $U \times W_j$, as stated in Assumption 2. In the next section we will therefore introduce the closed-form optimization problem that approximates (G) using the functions $\tilde{h}_{j,k}$.

2.3 Discretized Problem

As a first step towards exploiting Assumption 2 inside the adaptive refinement algorithm, we state the optimization problem that replaces the constraints $h_j(u, w_j) = 0$ with the set $K(j)$ of approximation constraints $\tilde{h}_{j,k}(u, w_j, z_j) = 0$.

To keep the notation simple we merge the non-overlapping variable vectors z_j using $z := \left(z_1^\top, \ldots, z_\alpha^\top\right)^\top \in Z \subseteq \mathbb{R}^n$. Then, by adding z to (G) and applying the constraint approximations for all $j \in J$ in (G) we get the discretized optimization problem

$$\begin{aligned} \min_{u,w,z} \quad & f(u, w) \\ \text{s.t.} \quad & g_i(u, w) = 0, \quad i \in I, \\ & \tilde{h}_{j,k}(u, w_j, z_j) = 0, \quad j \in J,\ k \in K(j), \\ & u \in U,\ w \in W,\ z \in Z. \end{aligned} \tag{D}$$

The functions $\tilde{h}_{j,k}$ allow to find "near"-feasible solutions to problems like (G) but are in practice complicated to deal with. First, it can happen in practice that the constraints $\tilde{h}_{j,k}(u, w_j, z_j) = 0$ have varying steep gradients. This phenomenon is a consequence of the amount of nonlinear terms in the expression of the $\tilde{h}_{j,k}$ functions. In fact, some nonlinear terms in the expression of $\tilde{h}_{j,k}$ may not be necessary for every $j \in J$ to get "near"-feasible solutions of (G). Second, n_j needs to be large enough so that Assumption 2 is satisfied. However, an unnecessary high value of n_j increases the size of the optimization problem, hence making it harder solve. A trade-off therefore exists for the choice of the amount of nonlinear terms in the description of $\tilde{h}_{j,k}$ and the size of n_j to get good quality decisions u while keeping the resulting (D) solvable in reasonable time by a state-of-the-art optimization solver.

In what follows, we consider optimization models that have the structure of (G) and satisfy Assumptions 1 and 2. We focus on how to choose the expression of $\tilde{h}_{j,k}$ and the value of n_j in (D) and present a generalized adaptive refinement framework that automates this decision making.

2.4 Adaptive Refinement Algorithm

Adaptive refinement algorithms cope with the challenges associated with choosing the expression of $\tilde{h}_{j,k}$ and the value of n_j by bridging the gap between (G) and (D).

In a nutshell, an ARA iteratively solves a version of (D) and uses the resulting solution to improve the approximation accuracy of the next instance of (D). This version of (D) is then solved and the process is repeated. Therefore, the ARA

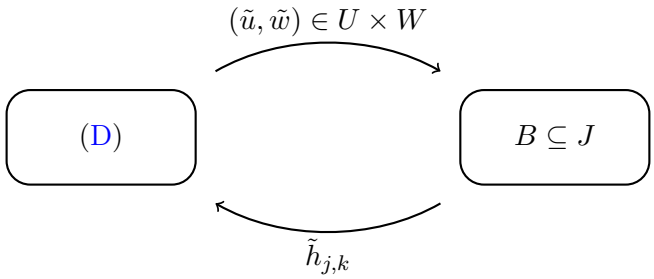

Figure 2.1: State diagram of the ARA. The state on the left-hand side corresponds to solving (D) and the state on the right-hand side corresponds to the creation of $B \subseteq J$.

sequentially enhances (D) through the results of the previous iteration of the ARA as is commonly done in adaptive optimal control, see; e.g., Bangerth and Rannacher (2003).

We now explain in detail the general ideas of the ARA that we study with the help of Figure 2.1. It shows a state diagram describing the ARA process. Two states that summarize how the algorithm functions are visible in the schematic of Figure 2.1. The first state, located on the left side of the schematic, corresponds to the solve phase of the ARA. Here, the ARA takes a specific version of (D) and solves it using an optimization solver. The decision variables $\tilde{u}$ and the remaining variables $\tilde{w}$ resulting from the first state are then transferred to the second state located on the right side of the schematic. Here, the ARA checks for feasibility w.r.t. (G) of $(\tilde{u}, \tilde{w})$. If $h_j(\tilde{u}, \tilde{w}_j)$ is close enough to 0 for all $j \in J$ then the ARA is stopped. Otherwise, a subset of indices $B \subseteq J$ is selected. For all $j \in B$, the accuracy of the set $K(j)$ of functions $\tilde{h}_{j,k}$ in (D) is improved. Two changes can be made. Either the amount of nonlinear terms of $\tilde{h}_{j,k}$ or the value of n_j can be increased. Then, the ARA proceeds back to the first state where the ARA solves the new version of (D).

The general idea of this scheme is to get near-feasible solutions to (G) while keeping the intermediate (D)s tractable. Moreover, the quantification of infeasibility allows to identify the indices $j \in J$ whose functions need a more refined approximation while leaving unchanged the remaining indices.

In what follows, we introduce the components that specify the exact functioning of the generalized adaptive refinement framework. We start by introducing the concepts of model catalogs that are used to reduce the complexity of solving (D) when a simpler mathematical expression for $\tilde{h}_{j,k}$ could yield similar near-feasible solutions. Then, we define the idea of error measures that quantify the degree of infeasibility of $h_j(\tilde{u}, \tilde{w}_j) = 0$ given a point $(\tilde{u}, \tilde{w}) \in U \times W$ and $j \in J$. Additionally, we define the concept of ε-feasibility, that formalizes near feasibility and is the stopping criterion of the ARA. Next, the ideas of marking and switching strategies are introduced. They define a set of strategies for selecting the elements of B and a set of strategies for modifying (D) to increase the approximation accuracy of the resulting model, respectively. Finally, the adaptive algorithm is specified with the use of the aforementioned building blocks.

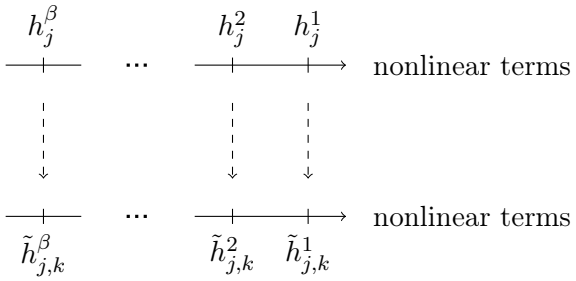

Figure 2.2: Model catalog of h_j obtained by sequentially modifying the amount of nonlinear terms.

2.4.1 Model Catalogs

In general, for some $j \in J$, the expressions of $\tilde{h}_{j,k}$ can have an unnecessarily high amount of nonlinear terms in order for (D) to return near-feasible solutions. In the ARA this is dealt with using a set $\mathcal{L} := \{1, \dots, \beta\} \subseteq \mathbb{N}$ of model simplifications of h_j, indicated by h_j^θ for $\theta \in \mathcal{L}$. These simplified models yield a set of approximation functions $\tilde{h}_{j,k}^\theta$ with a decreasing amount of nonlinear terms and result from applying the same problem-specific numerical techniques used for getting $\tilde{h}_{j,k}$ from h_j. We refer to Domschke et al. (2021) for a detailed catalog of models derived for the case of gas networks and to Schmidt et al. (2015) and Schmidt et al. (2016) for the study of optimization problems that consider different model levels in this model catalog. Similar model catalogs exist for electricity networks, see; e.g., Mehrmann et al. (2018a) for the transient case and Molzahn and Hiskens (2019) for the stationary case.

The general idea is illustrated in Figure 2.2; we use a catalog that consists of functions with a decreasing amount of nonlinear terms that lead to a catalog of discretized closed-form functions. It is usually the case that h_j^1 equals h_j and is therefore considered to be the most detailed level in the catalog. In the case that function h_j describes an ODE, we can obtain such a catalog by, e.g., sequentially dropping nonlinear terms. The terms of h_j can then, for instance, be dropped depending on their modeling importance.

With this model catalog $\mathcal{L}$ at hand and by selecting a model level $\ell_j \in \mathcal{L}$ for all $j \in J$, we replace $\tilde{h}_{j,k}$ in (D) by $\tilde{h}_{j,k}^{\ell_j}$ yielding the simplified discretized optimization problem

$$\begin{aligned} \min_{u,w,z} \quad & f(u,w) \\ \text{s.t.} \quad & g_i(u,w) = 0, \quad i \in I, \\ & \tilde{h}_{j,k}^{\ell_j}(u, w_j, z_j) = 0, \quad j \in J,\ k \in K(j), \\ & u \in U,\ w \in W,\ z \in Z. \end{aligned} \tag{SD}$$

We note that the choice of n_j and ℓ_j will highly influence the time to solve (SD). A less detailed version of (SD) is, in theory, computationally easier to solve but

might lead to infeasible solutions w.r.t. (G). On the contrary, a more detailed version of (SD) will be computationally more challenging but will more likely lead to near feasible solutions of (G). This mismatch highlights the importance of the ARA that is constructed to gradually increase n_j and switch down ℓ_j for specific $j \in J$. In doing so, error measures play an important role and are the topic of the next section.

2.4.2 Error Measures

We now introduce the concept of error measures in adaptive refinement algorithms. For a given point $(u, w) \in U \times W$ and $j \in J$, error measures quantify the degree of infeasibility of $h_j(u, w_j) = 0$. They allow to identify the indices $j \in J$ for which the increase of n_j and switch-up of ℓ_j will increase the approximation accuracy of (SD) in the next ARA iteration. Hence, they are used to select the elements $B \subseteq J$ that is introduced in Section 2.4.

Error measures were initially used to bound the error induced by finite element approximations of PDEs; see, e.g., Becker and Rannacher (2001). We adapt this concept to the case of optimization with discretizable constraints.

We make a case distinction between exact errors and error estimates. We begin by presenting exact errors and differentiate between three different error types; the exact total error, the exact model error, and the exact discretization error. Then, we derive the concept of error estimates by highlighting the conceptual weaknesses of the exact errors.

Exact Errors

We now define the exact total error that quantifies the infeasibility w.r.t. (G) of a solution originating from the approximation considered in (SD). For a specific $j \in J$, the exact total error highlights how far a point $(\tilde{u}, \tilde{w}) \in U \times W$ is from satisfying $h_j(\tilde{u}, \tilde{w}_j) = 0$. According to this idea, let n_j and ℓ_j be fixed for all $j \in J$ and $(\tilde{u}, \tilde{w}, \tilde{z}) \in U \times W \times Z$ be a point that satisfies the constraints of (SD). For $j \in J$ we define the exact total error as

$$\nu_j(\tilde{u}, \tilde{w}) := |h_j^1(\tilde{u}, \tilde{w}_j)|. \tag{2.2}$$

Hence, the exact total error is the absolute value of $h_j^1(\tilde{u}, \tilde{w}_j)$, i.e., the distance between the most detailed model h_j^1 evaluated at $(\tilde{u}, \tilde{w}_j)$ and zero.

Next, we derive an important feature of the exact total error. This feature allows to express $\nu_j(\tilde{u}, \tilde{w})$ as a difference of variables that satisfy $h_j(u, w_j) = 0$ and variables that satisfy $\tilde{h}_{j,k}^{\ell_j}(u, w_j, z_j) = 0$ for all $k \in K(j)$. On a first glance, rewriting exact errors in this way might not seem necessary. However, e.g., for ODEs, problem-specific upper bounds of this variable difference that depend on n_j exist; see, e.g., Quarteroni et al. (2007). These results can be used to show that (G) satisfies Assumption 2.

We now describe this feature. For all $\theta \in \mathcal{L}$, let $\kappa^\theta : \mathbb{R}^m \times \mathbb{R}^{p-1} \to \mathbb{R}$ be a predetermined function and let $w_j(\iota)$ denote the variable at index $\iota \in \{1, \dots, p\}$ of variable vector w_j. It may happen that a fixed index $\delta \in \{1, \dots, p\}$ exists such that

for all $\theta \in \mathcal{L}$ we can rewrite the constraint $h_j^\theta(u, w_j) = 0$ in the form

$$h_j^\theta(u, w_j) = \kappa^\theta\left(u, w_j(1), \ldots, w_j(\delta-1), w_j(\delta+1), \ldots, w_j(p)\right) - w_j(\delta) = 0. \tag{2.3}$$

In other words, we can isolate the variable $w_j(\delta)$ in the mathematical expression of $h_j^\theta(u, w_j)$. Furthermore, let $\psi_j^\theta(\delta)$ be the value of variable $w_j(\delta)$ in Equation (2.3) when we set $u = \tilde{u}$ and $w_j(\iota) = \tilde{w}_j(\iota)$ for all $\iota \in \{1, \ldots, p\} \setminus \{\delta\}$. Then, by replacing $h_j^1(\tilde{u}, \tilde{w}_j)$ in (2.2) with its reformulation in (2.3) it holds

$$\nu_j(\tilde{u}, \tilde{w}) = |\psi_j^1(\delta) - \tilde{w}_j(\delta)|. \tag{2.4}$$

Similarly to the exact total error, we define the exact model error that computes the error due to the model selection in (SD) and use Equation (2.3) to reformulate it. Hence, the exact model error reads

$$\begin{aligned} \nu_j^{\mathrm{m}}(\tilde{u}, \tilde{w}) &:= |h_j^1(\tilde{u}, \tilde{w}_j) - h_j^{\ell_j}(\tilde{u}, \tilde{w}_j)| && (2.5)\\ &= |\psi_j^1(\delta) - \psi_j^{\ell_j}(\delta)|. && (2.6) \end{aligned}$$

We note that $\nu_j^{\mathrm{m}}(\tilde{u}, \tilde{w})$ computes the error due to the model selection in (SD) and is not related to the value of n_j.

Furthermore, we define the exact discretization error that computes the error due to the chosen discretization in (SD), i.e., due to the value of n_j. Again, we use Equation (2.3) to reformulate it. Hence, the exact model error is defined as

$$\begin{aligned} \nu_j^{\mathrm{d}}(\tilde{u}, \tilde{w}) &:= |h_j^{\ell_j}(\tilde{u}, \tilde{w}_j)| && (2.7)\\ &= |\psi_j^{\ell_j}(\delta) - \tilde{w}_j(\delta)|. && (2.8) \end{aligned}$$

we note that that $\nu_j^{\mathrm{d}}(\tilde{u}, \tilde{w})$ computes the error due to the chosen discretization in (SD) and hence fixes the model level to ℓ_j.

Error Estimates and Relationship with Exact Errors

The exact errors require the value of $h_j^\theta(\tilde{u}, \tilde{w}_j)$ or $\psi_j^\theta(\delta)$ which are not available in general. Nevertheless, the exact errors can be bounded from above via problem-specific estimates in some applications. We call them error estimates because they bound the associated exact error to a certain order of accuracy without having to evaluate $h_j^\theta(\tilde{u}, \tilde{w}_j)$ or $\psi_j^\theta(\delta)$. We refer to Stoer and Bulirsch (2002, p. 482) for an introduction to error estimates. Moreover, we highlight that, in the following, the relation $f_1(x) \dot{\leq} f_2(x)$ states that a function f_2 is a first-order upper bound of the function f_1 if and only if $f_1(x) \leq f_2(x) + r(x)$ for $x \to 0$ and some function $r \in o(\|f_2\|_\infty)$.

Then, for every feasible solution $(\tilde{u}, \tilde{w}, \tilde{z}) \in U \times W \times Z$ of (SD) and for every index $j \in J$, we introduce the model error estimate denoted by $\eta_j^{\mathrm{m}}(\tilde{u}, \tilde{w})$ and the discretization error estimate denoted by $\eta_j^{\mathrm{d}}(\tilde{u}, \tilde{w})$ such that they satisfy

$$\begin{aligned} \nu_j^{\mathrm{m}}(\tilde{u}, \tilde{w}) &\dot{\leq} \eta_j^{\mathrm{m}}(\tilde{u}, \tilde{w}), && (2.9)\\ \nu_j^{\mathrm{d}}(\tilde{u}, \tilde{w}) &\dot{\leq} \eta_j^{\mathrm{d}}(\tilde{u}, \tilde{w}). && (2.10) \end{aligned}$$

Using the definitions in Equations (2.2), (2.5), (2.7), (2.9), and (2.10), we can derive the upper bound

$$\nu_j(\tilde{u},\tilde{w}) := |h_j^1(\tilde{u},\tilde{w}_j)| = |h_j^1(\tilde{u},\tilde{w}_j) - h_j^{\ell_j}(\tilde{u},\tilde{w}_j) + h_j^{\ell_j}(\tilde{u},\tilde{w}_j)| \tag{2.11a}$$

$$\leq \nu_j^{\mathrm{m}}(\tilde{u},\tilde{w}) + \nu_j^{\mathrm{d}}(\tilde{u},\tilde{w}) \dot{\leq} \eta_j^{\mathrm{m}}(\tilde{u},\tilde{w}) + \eta_j^{\mathrm{d}}(\tilde{u},\tilde{w}), \tag{2.11b}$$

where we used the triangular inequality. For the sake of completeness, we use the result of Line (2.11b) to define the total error estimate

$$\eta_j(\tilde{u},\tilde{w}) := \eta_j^{\mathrm{m}}(\tilde{u},\tilde{w}) + \eta_j^{\mathrm{d}}(\tilde{u},\tilde{w}), \tag{2.12}$$

implying that

$$\nu_j(\tilde{u},\tilde{w}) \dot{\leq} \eta_j(\tilde{u},\tilde{w}).$$

We extract two main take-aways from (2.11). First, the influence of the model error and the discretization error on the total error can be identified. Hence, this feature tells us if the ARA needs to focus on increasing n_j or switching up ℓ_j for a specific $j \in J$. Second, we can use estimates instead of exact errors in the ARA. Indeed, once estimates are proved for exact errors and a feasible solution $(\tilde{u},\tilde{w},\tilde{z}) \in U \times W \times Z$ of (SD) is provided we can easily identify how to decrease the total exact error without the need to evaluate $h_j^\theta(\tilde{u},\tilde{w}_j)$ or $\psi_j^\theta(\delta)$.

2.4.3 Stopping Criterion: ε-Feasibility

To terminate the ARA, we need to specify what a solution of (SD) needs to satisfy to be near-feasible w.r.t. (G). This criterion is called ε-feasibility and is discussed in, e.g., Locatelli and Schoen (2013, p. 289). With the use of the newly introduced error measures defined in Section 2.4.2 we can state the definition of ε-feasibility of an ARA solution.

Definition 1 *Let $\varepsilon > 0$ be a given tolerance. The feasible point $(\tilde{u},\tilde{w},\tilde{z}) \in U \times W \times Z$ of (SD) is called* ε-feasible *if*

$$\bar{\nu}(\tilde{u},\tilde{w}) := \frac{1}{|J|}\sum_{j\in J} \nu_j(\tilde{u},\tilde{w}) \leq \varepsilon,$$

where $\bar{\nu}(\tilde{u},\tilde{w})$ is called the total average exact error.

Hence, as long as we keep increasing n_j and switching up ℓ_j for all $j \in J$, Assumption 2 of Section 2.1 forces the total average exact error to decrease until it is smaller than ε.

We remark that, in practice, the total average error estimate $\bar{\eta}(\tilde{u},\tilde{w}) := \frac{1}{|J|}\sum_{j\in J} \eta_j(\tilde{u},\tilde{w})$ is used instead. This can be done because, by construction of the error estimates, $\bar{\eta}(\tilde{u},\tilde{w})$ is an upper bound for $\bar{\nu}(\tilde{u},\tilde{w})$.

2.4.4 Marking and Switching Strategies

In the ARA case, marking strategies select the subset of indices B of J to be modified in the next (SD) that is solved, as discussed in Section 2.4. In more detail, marking strategies return a subset of J by using error estimates computed for a point of the feasible region of (SD). In general, they focus on selecting a subset of indices with the largest error estimate value. We refer to Nochetto et al. (2009, p. 93) for a list of the most popular AFEM marking strategies.

We distinguish between the discretization refinement marking strategy $\sigma_{\mathcal{R}}$ and the model up-switching marking strategy $\sigma_{\mathcal{U}}$ that respectively yield the sets $\mathcal{R},\mathcal{U} \subseteq J$. The sets $\mathcal{R}$ and $\mathcal{U}$ contain the elements for which n_j and ℓ_j are modified, respectively. As the name suggests, the discretization refinement marking strategy selects the elements of $\mathcal{R}$ based on $\eta_j^{\mathrm{d}}(\tilde{u},\tilde{w})$. Similarly, the model up-switching marking strategy selects the elements of $\mathcal{U}$ based on $\eta_j^{\mathrm{m}}(\tilde{u},\tilde{w})$.

Switching strategies determine how to modify n_j and ℓ_j in (SD) for the elements of $\mathcal{R}$ and $\mathcal{U}$. We therefore consider two types of switching strategies. First, we introduce the discretization refinement rule $\xi_{\mathcal{R}} : \mathbb{N} \to \mathbb{N}$ as an increasing function applied on every $j \in \mathcal{R}$ that acts on n_j. Second, we introduce the model up-switching rule $\xi_{\mathcal{U}} : \mathcal{L} \to \mathcal{L}$ as an decreasing function applied on every element $j \in \mathcal{U}$ that acts on ℓ_j.

2.4.5 Detailed Description of the ARA

We have introduced all the necessary concepts for discussing the exact functioning of the ARA. Hence, in the following, we describe the adaptive refinement algorithm in detail. Algorithm 1 shows the pseudo-code of the algorithm. The inputs are the error tolerance ε, the marking strategies $\sigma_{\mathcal{R}}, \sigma_{\mathcal{U}}$, and the switching strategies $\xi_{\mathcal{R}}, \xi_{\mathcal{U}}$. The output is an ε-feasible solution of (G) arising from a detailed version of (SD).

We now explain the main parts of the algorithm. Before entering the main for loop in Line 6, the ARA initializes the parameters n_j and ℓ_j with a small and a large value, respectively. The first optimization problem that is instantiated and solved, i.e., $(\mathrm{SD})^0$, therefore is a low-detail approximation of (G). Then, the resulting solution $(\tilde{u},\tilde{w})^0$ of $(\mathrm{SD})^0$ is checked for ε-feasibility. If $(\tilde{u},\tilde{w})^0$ is ε-feasible, which is very unlikely as $(\mathrm{SD})^0$ approximates (G) poorly, the ARA terminates. Otherwise, we leave the initialization phase and enter the main for loop of the ARA in Line 6. Moving forward, we use the subscript k to indicate the current iteration of the ARA. First, we create the sets $\mathcal{R}^k$ and $\mathcal{U}^k$ with the help of the marking strategies. In Lines 8 and 9, we update the discretization of the resulting $(\mathrm{SD})^k$. For every $j \in \mathcal{R}^k$, the value of n_j^k is computed using the improvement rule $\xi_{\mathcal{R}}$ applied to n_j^{k-1}. In Lines 10 and 11, the same ideas are applied for the model switch in $(\mathrm{SD})^k$, yielding the new model level ℓ_j^k for all $j \in \mathcal{U}^k$. Finally, in the last part of the main for loop, we instantiate and solve model $(\mathrm{SD})^k$. As before, we check for ε-feasibility of the resulting $(\tilde{u},\tilde{w})^k$ solution. Unless ε-feasibility of $(\tilde{u},\tilde{w})^k$ is achieved, the same process is repeated until ε-feasibility is satisfied.

Algorithm 1: Adaptive refinement algorithm

Input: error tolerance $\varepsilon > 0$, marking strategies $\sigma_{\mathcal{R}}, \sigma_{\mathcal{U}}$, and improvement rules $\xi_{\mathcal{R}}, \xi_{\mathcal{U}}$
Output: ε-feasible solution (u, w) of (G)

foreach $j \in J$ **do**
  Initialize ℓ_j^0 and n_j^0
$(\tilde{u}, \tilde{w}, \tilde{z})^0 \leftarrow$ Solve $(\mathrm{SD})^0$
if $(\tilde{u}, \tilde{w})^0$ *is* ε*-feasible* **then**
  return $(u, w) \leftarrow (\tilde{u}, \tilde{w})^0$
for $k = 1, 2, \ldots$ **do**
  Compute sets $\mathcal{R}^k, \mathcal{U}^k$ according to $\sigma_{\mathcal{R}}, \sigma_{\mathcal{U}}$
  foreach $j \in \mathcal{R}^k$ **do**
    Increase n_j^k according to $\xi_{\mathcal{R}}$
  foreach $j \in \mathcal{U}^k$ **do**
    Switch-up ℓ_j^k according to $\xi_{\mathcal{U}}$
  $(\tilde{u}, \tilde{w}, \tilde{z})^k \leftarrow$ Solve $(\mathrm{SD})^k$
  if $(\tilde{u}, \tilde{w})^k$ *is* ε*-feasible* **then**
    return $(u, w) \leftarrow (\tilde{u}, \tilde{w})^k$

Figure 2.3 is a more detailed version of Figure 2.1 that includes the new concepts and notation introduced for explaining the ARA in Algorithm 1.

2.4.6 Features

We now highlight two features of the ARA that show why it is a well-suited candidate for solving problems like (G).

The ARA can terminate at ε-feasible solutions by only relying on error estimates. Indeed, the use of error estimates in the ARA is straightforward. Once we prove that error estimates bound the exact errors from above, we can easily replace the exact errors with their associated estimates in the ARA. Therefore, this removes the need for any evaluation of h_j while still ensuring termination at ε-feasible points of (G). Also, the error origin is easily identified due to the distinction between the model error and the discretization error. This strengthens the ARA and highlights its adaptivity regarding the specific problem that is considered.

Next, the ARA inherently produces good warmstarts for the successive instances of (SD) that are solved. The point $(\tilde{u}, \tilde{w}, \tilde{z})^{k-1}$ can be close to a feasible point of $(\mathrm{SD})^k$ depending on the application that is considered and the size of $\mathcal{R}^k$ and $\mathcal{U}^k$. Hence, this makes it a good initial iterate for optimization solvers. Consequently, the warmstart of the successive $(\mathrm{SD})^k$ can speed up the time for the ARA to reach its termination criterion.

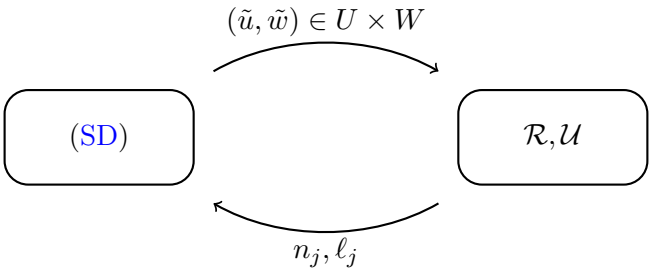

Figure 2.3: State diagram of Figure 2.1 enhanced with the new concepts and notation of Algorithm 1. In the state on the left-hand side (SD) is solved and in the state on the right-hand side we select the sets $\mathcal{R}, \mathcal{U} \subseteq J$.

2.4.7 Extensions

This section concludes this chapter by presenting a series of extensions from which the ARA can benefit depending on the specificities of the underlying problem.

First, the ARA can be subject to the curse of dimensionality, i.e., the subsequent (SD) instances explode in size. This is usually due to the parameterization of the ARA that orients the focus toward improving the approximation accuracy of (SD) without considering the size of the resulting models. More specifically, the marking and switching strategies are at the core of this issue as they determine how the model structure evolves. For handling this, we refer to Chapter 3, which is based on [MR2] and deals with this challenge by adding a coarsening and model down-switching step to the ARA.

Second, a proof of finite termination at an ε-feasible point is an important feature to look for. It might in some applications even be necessary to make the correct choice of marking and switching strategies. To obtain such a result one usually proves that between two iterations of the ARA the total average error estimate decreases. Therefore, it is common practice to show that there exists a constant $C > 0$, such that

$$\bar{\eta}^k(\tilde{u}, \tilde{w}) - \bar{\eta}^{k+1}(\tilde{u}, \tilde{w}) > C,$$

for all iterations k of the ARA. In [MR2], summarized in Chapter 3, we prove finite termination of an adaptive optimization algorithm given a set of conditions on the parameters of the algorithm.

Finally, in some applications, finite termination at an ε-feasible points comes for granted because of the structure of the underlying problem. This is the case in Chapter 4 where we discuss the content of [MR3]. In this paper, we enhance the ARA so that it finitely terminates at a global optimal solution of (G).

3

Optimization of District Heating Networks

This chapter summarizes [MR1] and [MR2] where the optimization of stationary district heating networks (DHNs) is considered. First, we present an operational optimization model, discuss it, and show that it can be reformulated as (G). Moreover, we demonstrate that the operational optimization model satisfies the assumptions made about (G) stated in Section 2.1. Then, we sequentially extend this model for the cases considered in [MR1] and [MR2]. Furthermore, the concepts of Chapter 2 are applied to approximate specific ODE constraints of the models. Finally, the numerical results of both papers are presented.

In more detail, Section 3.1 introduces district heating networks. Afterward, the functioning principles of DHNs are translated into a mathematical optimization framework in Section 3.2. Then, Section 3.3 extends this model to the case of [MR1], where DHN expansion decision making is considered. Here, the ideas of Section 2.2 are applied. Similarly, Section 3.4 extends the original model to the case of [MR2] and applies the ideas of Section 2.4 to compute ε-feasible controls for DHN operation.

3.1 Introduction to District Heating Networks

District heating networks are energy transportation networks that allow to efficiently connect heat producers to many individual heat consumers. They are composed of four parts; energy producers, the forward flow network, the energy consumers, and the backward flow network. Water flows through the network to transport the heat from the producers to the consumers.

We now explain in detail how DHNs work and explain how each part contributes to the heat transfer. First, the energy producers transfer energy to incoming water under the form of heat. More specifically, the water flows through depots where the

energy transfer takes place. This energy can originate from various sources, e.g., through renewable energy production, heat production from industrial processes, or simply from burning gas.

Second, the outgoing hot water is transported to the consumers of the network using a network of insulated pipes, called the forward flow network. The aim is to transport the energy with as little losses as possible.

Third, after being transported through this network of insulated pipes, the water reaches the third component of the network, the energy consumers. Here, heat exchangers extract heat from the incoming water and transfer it to the consumers' water. It should be noted that, usually, the heat exchange occurs without mixing of the incoming water and the consumers' water. The water that is now hot on the consumer side is used for satisfying the consumers' heat demand. The outgoing water of the heat exchangers, i.e., the water flowing through the DHN, significantly decreases in temperature as a result of the heat transfer.

Finally, the heat exchangers' outgoing water enters the last part of the network, the backward flow network, a network of pipes in the opposite direction of the forward flow that transports the cooled water back to the depots of the network. Hence, we draw attention to the fact that a DHN fundamentally represents a closed-loop energy-distribution network. In other words, no water enters or leaves the network.

3.2 Stationary District Heating Network Operation

As a first step towards presenting the results of [MR1] and [MR2], we show how to mathematically model stationary DHN operation. Therefore, the modeling of every component that is introduced in Section 3.1 is discussed here. We first focus on describing the network using graphs. With the help of this graph description, we present how we model the behavior of water inside the pipes, the interaction of water at pipe intersections, and the effect of both depots and consumers on incoming water. We conclude this section with a generalized stationary operational optimization problem that is later used for describing [MR1] and [MR2].

3.2.1 Graph Description of the Network Topology

To describe the structure of a DHN we introduce a graph $G = (V, A)$ that mimics the topological characteristics of the network. In what follows, we use the four components of Section 3.1 to introduce associated arc sets that are part of A. Furthermore, Figure 3.1 shows an exemplary graph of a small DHN to visually support this interpretation.

First, we introduce the depot arc set A_{d}, shown as a solid red arc in Figure 3.1. Second, we represent the consumers of the network with the arc set A_{c} illustrated by dotted green arcs in Figure 3.1. Finally, we divide the network of pipes into the arc set of forward flow pipes A_{ff} and the arc set of backward flow pipes A_{bf}. Figure 3.1 shows the elements of A_{ff} in dashed black and the elements of A_{bf} in dashed blue. As a consequence, A_{ff} and A_{bf} span the set of pipes A_{p} such that $A_{\mathrm{p}} := A_{\mathrm{ff}} \cup A_{\mathrm{bf}}$. The

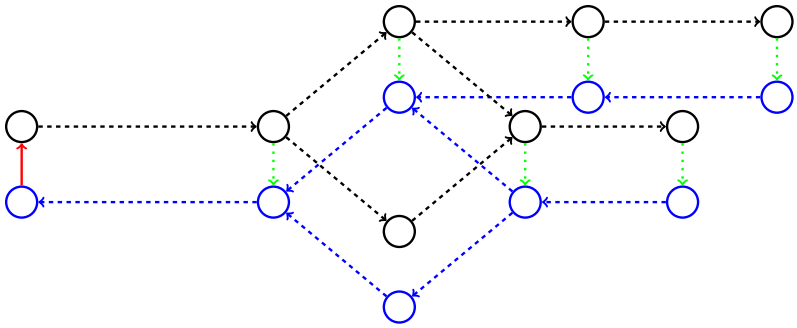

Figure 3.1: Visualization of the associated graph for a small size DHN. The solid red arc corresponds to the depot of the network $a_{\mathrm{d}} \in A_{\mathrm{d}}$, the dashed black arcs correspond to the forward flow pipes $a \in A_{\mathrm{ff}}$, the dotted green arcs correspond to the consumers $a \in A_{\mathrm{c}}$, and the dashed blue arcs correspond to the backwards flow pipes $a \in A_{\mathrm{bf}}$.

junctions and the union of the arcs of $A_{\mathrm{ff}}, A_{\mathrm{bf}}, A_{\mathrm{c}}$, and A_{d} create the set of nodes V and the set of arcs A. In particular, this means that $A := A_{\mathrm{ff}} \cup A_{\mathrm{bf}} \cup A_{\mathrm{c}} \cup A_{\mathrm{d}}$.

3.2.2 Modeling of Hot Water Inside the Pipes

The transport of hot water inside of the pipes is modeled with the Euler equations for compressible fluids in cylindrical pipes; see, e.g., Chorin and Marsden (1993) or Hauschild et al. (2020). In their most detailed version, they induce equations that cannot be treated by state-of-the-art optimization solvers on realistic networks. It is therefore reasonable to assume a simplified behavior. To this end, we summarize the simplifying assumptions that we make. First, the pipes are assumed to have a constant cylindrical shape, i.e., they have a constant radius and a constant slope. Furthermore, we assume that the fluid is incompressible and that its state only changes in the direction of the pipe. Finally, we focus on stationary operation of the network, hence, resulting in physical quantities that evolve only over space (x), i.e., the axis induced by the direction of the pipe. Here and in what follows, let L_a, D_a, λ_a, and h'_a be the length, the diameter, the friction coefficient, and the slope of pipe $a \in A_{\mathrm{p}}$, respectively. Moreover, we denote the gravitational acceleration by g. Further, let ρ represent the density, p the pressure, and v the velocity of the water flowing inside the network. These are all variables which are indexed over $a \in A_{\mathrm{p}}$ and which model functions that map any spatial position $x \in [0, L_a]$ to the respective physical quantity inside the pipe. Additionally, they also capture the associated nodal quantity when indexed over $u \in V$.

Due to the simplifying assumptions, the first Euler equation, also called the continuity equation, reduces to $v_a(x)$ and $\rho_a(x)$ being constant for all $x \in [0, L_a]$. In what follows, v_a and ρ_a are therefore considered unique on every arc $a \in A_{\mathrm{p}}$. Furthermore, the second Euler equation, when complemented with the simplifying

assumptions, reduces to

$$0 = \frac{p_a(L_a) - p_a(0)}{L_a} + \frac{\lambda_a \rho_a}{2D_a}|v_a|v_a + g\rho_a h'_a, \tag{3.1}$$

where we compute the friction coefficient λ_a with the law of Nikuradse; see, e.g., Borsche et al. (2019). For a more detailed discussion of the Euler equations, we refer to [MR2] or Krug et al. (2021b). Since incompressible flow is considered, we complement Equation (3.1) with the constant state equation

$$\rho_a = 997\,\mathrm{kg\,m^{-3}}$$

for all $a \in A_\mathrm{p}$. Consequently, ρ_a is replaced by a scalar parameter ρ for every pipe of the network.

Next, the thermal behavior of water is described through the last Euler equation, i.e., the internal energy density equation, as discussed in Hauschild et al. (2020) and Domschke et al. (2021). We denote by e and T the internal energy density and the temperature of the water, respectively. Under the simplifying assumptions, the internal energy density equation reads

$$0 = v_a \frac{\mathrm{d}e_a}{\mathrm{d}x}(x) - \frac{\lambda_a}{2D_a}\rho|v_a|v_a^2 + \frac{4U_a}{D_a}(T_a(x) - T_\mathrm{W}), \tag{3.2}$$

where T_W is the temperature of the soil surrounding the pipe and U_a denotes the heat transfer parameter of the pipe. In addition to Equation (3.2), a second state equation is considered to close the resulting system. Different versions of such a state equation exist, which influence the modeling accuracy. We refer to Hauschild et al. (2020, p. 5) for a discussion of state equations of hot water flowing in a pipe. Since, in what follows, two different expressions are used we keep the description general. Hence, we consider a state function $\zeta : \mathbb{R}^+ \times \mathbb{R}^+ \to \mathbb{R}^+$ that complements Equation (3.2) such that

$$T_a(x) = \zeta(e_a(x), \rho) \tag{3.3}$$

holds for all $a \in A_\mathrm{p}$.

3.2.3 Nodal Coupling

All network elements are coupled via equations defined over the set V. Schmidt et al. (2016) introduce and discuss the modeling of nodal interactions in gas networks. We follow this approach and apply it to DHNs as presented in Hauschild et al. (2020) and Krug et al. (2021b). Three conservation laws are necessary for modeling arc intersections: the conservation of mass, the pressure continuity, and the conservation of energy. For node $u \in V$, let $\delta^\mathrm{in}(u), \delta^\mathrm{out}(u) \subseteq A$ be the set of ingoing and outgoing arcs of u. Let the variable q_a denote the mass flow inside pipe $a \in A_\mathrm{p}$ that is proportional to v_a and ρ such that $q_a = \rho v_a A_a$, where A_a is the cross-sectional area of a. Since ρ_a and v_a are constant for all $a \in A$, q_a is constant as well. Then, mass conservation and pressure continuity read

$$\sum_{a \in \delta^\mathrm{in}(u)} q_a = \sum_{a \in \delta^\mathrm{out}(u)} q_a, \quad u \in V, \tag{3.4}$$

and

$$\begin{aligned} p_u &= p_a(0), \quad u \in V,\ a \in \delta^{\text{out}}(u), \\ p_u &= p_a(L_a), \quad u \in V,\ a \in \delta^{\text{in}}(u). \end{aligned} \tag{3.5}$$

Finally, we consider the conservation of energy via the complementarity-constrained reformulation presented in Hante and Schmidt (2019). Therefore, it holds for all $u \in V$ that

$$\begin{aligned} \sum_{a \in \delta^{\text{in}}(u)} \frac{e_a(L_a) q_a}{\rho} &= \sum_{a \in \delta^{\text{out}}(u)} \frac{e_a(0) q_a}{\rho}, \\ 0 &= \beta_a (e_a(0) - e_u), \quad a \in \delta^{\text{out}}(u), \\ 0 &= \gamma_a (e_a(L_a) - e_u), \quad a \in \delta^{\text{in}}(u), \end{aligned} \tag{3.6}$$

with the variables β_a and γ_a that satisfy the complementarity constraints

$$q_a = \beta_a - \gamma_a, \quad \beta_a \geq 0, \quad \gamma_a \geq 0, \quad \beta_a \gamma_a = 0, \tag{3.7}$$

for all $a \in A$.

3.2.4 Depots and Consumers

The depots and the consumers of the network inject and extract energy in and from the network, respectively. We refer to Krug et al. (2021b) for a detailed discussion of depot and consumer constraints.

We first summarize the depot constraints. For $a_{\text{d}} \in A_{\text{d}}$, we have

$$\begin{aligned} p_u &= p_{\text{s}}, \\ P_{\text{p}} &= \frac{q_{a_{\text{d}}}}{\rho} \left(p_{a_{\text{d}}}(L_{a_{\text{d}}}) - p_{a_{\text{d}}}(0) \right), \\ P_{\text{w}} + P_{\text{g}} &= \frac{q_{a_{\text{d}}}}{\rho} \left(e_{a_{\text{d}}}(L_{a_{\text{d}}}) - e_{a_{\text{d}}}(0) \right), \end{aligned} \tag{3.8}$$

where p_{s} is the stagnation pressure and P_{p}, P_{w}, and P_{g} are power variables that influence pressure increase, the internal energy density of the water obtained by recuperating heat from industrial processes, and the internal energy of the water obtained by burning natural gas.

Furthermore, we model the consumers $a = (u, v) \in A_{\text{c}}$ using

$$P_a = \frac{q_a}{\rho} \left(e_a(0) - e_a(L_a) \right), \tag{3.9a}$$

$$e_a(0) \geq e_a^{\text{ff}}, \tag{3.9b}$$

$$e_a(L_a) = e^{\text{bf}}, \tag{3.9c}$$

$$p_v \leq p_u, \tag{3.9d}$$

where P_a is the heat power consumed by consumer a, e_a^{ff} is the lower bound on the incoming internal energy density, and e^{bf} is the value of the internal energy density of the outgoing water.

3.2.5 Bounds

We now introduce bounds on the variables which originate from physical and technical network characteristics. First, the massflow of every arc $a \in A$ is bounded such that

$$q_a^- \leq q_a \leq q_a^+ \tag{3.10}$$

holds, where $q_a^- = 0$ for all $a \in A_\mathrm{d} \cup A_\mathrm{c}$. Next, for every node $u \in V$, we have bounds on pressure and temperature,

$$p_u \in [p_u^-, p_u^+], \quad T_u \in [T_u^-, T_u^+]. \tag{3.11}$$

Finally, the depot power variables are also bounded,

$$P_\mathrm{p} \in [0, P_\mathrm{p}^+], \quad P_\mathrm{w} \in [0, P_\mathrm{w}^+], \quad P_\mathrm{g} \in [0, P_\mathrm{g}^+]. \tag{3.12}$$

We highlight the fact that P_p^+ and P_g^+ will likely be equal to infinity, whereas P_w^+ is finite. Indeed, excess power originating from industry is in practice bounded unlike gas power or electrical power (for increasing the depot pressure) that are, except in unforeseen circumstances, always available.

3.2.6 Operational Optimization Problem

The complete behavior of a DHN can now be captured in an operational optimization problem. Therefore, we add the objective function

$$C_\mathrm{p} P_\mathrm{p} + C_\mathrm{w} P_\mathrm{w} + C_\mathrm{g} P_\mathrm{g} \tag{3.13}$$

to the model. Here, $C_\mathrm{p}, C_\mathrm{w}$, and C_g denote the cost of pressure increase, waste incineration, and natural gas, respectively. Expression (3.13) models the total payment incurred by the network operator to satisfy the consumers' power demand. This yields the stationary district heating network operational optimization model

$$\begin{aligned}
\min \quad & \text{objective: (3.13)}, \\
\text{s.t.} \quad & \text{momentum: (3.1)} \\
& \text{internal energy density: (3.2) with (3.3)}, \\
& \text{mass conservation: (3.4)}, \\
& \text{pressure continuity: (3.5)}, \\
& \text{energy conservation: (3.6) with (3.7)}, \\
& \text{depot constraints: (3.8)}, \\
& \text{consumer constraints: (3.9)}, \\
& \text{bounds: (3.10)–(3.12)}.
\end{aligned} \tag{O-DHN}$$

3.2.7 Discussion of the Model

Model (O-DHN) can, in its current form, not be solved with optimization solvers. Indeed, the internal energy density equation (3.2) is an ODE and therefore is not a analytical expression. This makes it a candidate for the approximation techniques discussed in Chapter 2. Therefore, we first show that (O-DHN) can be reformulated in the structure of (G) of Section 2.1. Moreover, we discuss why (O-DHN) satisfies the assumptions stated about (G).

To reformulate (O-DHN) as (G), we associate the set of variables u from Chapter 2 to $P_\mathrm{p}, P_\mathrm{w}, P_\mathrm{g}$, and q_{a_d} for all $a_\mathrm{d} \in A_\mathrm{d}$. As elaborated in Section 2.1, u models the exact decisions to be taken for the underlying application, which, in the case of DHN operation, are the controls of the system. Indeed, once these variables are fixed, it holds that the remaining constraints allow for a unique state of the system; see, e.g., Lagnese et al. (1994), Leugering et al. (2017), or Krug et al. (2021a) for results on well-posedness of similar graph-structured systems.

Next, the w variables of Chapter 2 contain all the remaining variables of (O-DHN). They model the state of the system and are thus uniquely determined by the constraints of the optimization problem if u is fixed. Then, by setting $w_a = (e_a(0), e_a(L_a), v_a)^\top$ for all $a \in A_\mathrm{p}$ we can rewrite the internal energy density equation of (3.2) as $h_a(u, w_a) = 0$ for all $a \in A_\mathrm{p}$. To complete the modeling, we define $w_{\alpha+1}$ as the vector of all the remaining variables inside of w, such that $w = \left(w_1^\top, \dots, w_\alpha^\top, w_{\alpha+1}^\top\right)^\top$ holds. Then, by simply setting $J = A_\mathrm{p}$ and rewriting all the remaining constraints as $g_i(u, w) = 0$ indexed over $i \in I$, we obtain (O-DHN) in the structure of (G).

Furthermore, we show that (O-DHN) cast in the form of (G) fulfills the assumptions made in Section 2.1. Assumption 1 is clearly satisfied as h_a models an ODE and hence cannot be described with a analytical expression. For $a \in A_\mathrm{p}$, we select a discretization scheme and a step size Δx_a, yielding equidistant discretization points $0 = x_0 < \dots < x_{n_a} = L_a$. By introducing $z_a = (e_a(x_1), \dots, e_a(x_{n_a-1}))^\top$ we can denote the resulting discretized equations as $\tilde{h}_{a,k}(u, w_a, z_a) = 0$ for $k \in K(a) \subseteq \mathbb{N}$, where the expression of $\tilde{h}_{a,k}$ and the expression of $|K(a)|$ arise from the used discretization scheme. Therefore, if we adequately choose a discretization scheme and the value of n_a w.r.t. the convergence of numerical solutions to exact solutions of ODEs, then Assumption 2 holds. As a result, we apply the techniques presented in Chapter 2 on (O-DHN).

Finally, we draw attention to the fact that, in what follows, u, w_a, z_a, h_a, and $\tilde{h}_{a,k}$ now refer to the case of stationary DHN operation.

3.3 Network Expansion

This section concerns the results of [MR1], where we consider expansion decision making for tree-shaped DHNs. The DHN expansion literature can be categorized depending on the approach that is used. The first category concerns scenario-based stationary mixed-integer linear models, which usually induce a significant amount of

integer variables to linearize the nonlinear constraints that model the water physics; see, e.g., Bracco et al. (2013), Haikarainen et al. (2016), and Bordin et al. (2016). The second category concerns mixed-integer nonlinear models, see e.g. Blommaert et al. (2018). As a consequence of the nonlinearity of the constraints, the resulting problems are harder to solve. Almost all papers of this category use heuristics to find solutions; see, e.g., Guelpa et al. (2018) and Mertz et al. (2017). This is the category [MR1] belongs to as well. We propose a stationary nonconvex mixed-integer nonlinear district heating network expansion model for tree-shaped networks that accurately takes into account pressure as well as thermal losses. In contrast to the aforementioned papers, we reach global optimal solutions by using global optimization solvers.

To describe the results of [MR1], we first specify the expression of the energy density state equation (3.2) and introduce two additional model simplifications. Then, under these simplifications, we extend (O-DHN) with expansion decision variables and constraints. Furthermore, we address the approximation of the h_a functions by applying the technique presented in Section 2.2 resulting in a model of type (F). Finally, with the resulting expansion decision model, we present the results and conclusions of [MR1].

3.3.1 State Equation Specification and Model Simplifications

First, we specify (O-DHN) by refining the description of state equation (3.2). Hence, we assume that ζ in Equation (3.3) is linear and depends on the specific heat capacity c_p of water. This expression is commonly used in the case of nonisothermal gas flow as discussed in Domschke et al. (2021) and reads

$$e_a(x) = c_\mathrm{p}\rho T_a(x). \tag{3.14}$$

Note that (3.14) is a coarse linear approximation of the real state of the system. Additionally, it allows to eliminate either the variable e or the variable T in the description of (O-DHN). In the following, we will hence only consider variable T because it yields solutions that can be easily interpreted. Moreover, by using state equation (3.14) we may rewrite Equation (3.2) in the form

$$0 = v_a \frac{\mathrm{d}T_a}{\mathrm{d}x}(x) - \frac{\lambda_a}{2c_\mathrm{p}D_a}|v_a|v_a^2 + \frac{4U_a}{c_\mathrm{p}\rho D_a}(T_a(x) - T_\mathrm{W}). \tag{3.15}$$

Furthermore, we state two simplifications of the underlying physics that make the expansion model more tractable for optimization solvers. First, we assume that, for small velocities v_a, the friction term $\frac{\lambda_a}{2c_\mathrm{p}D_a}|v_a|v_a^2$ in Equation (3.15) can be neglected, yielding

$$0 = v_a \frac{\mathrm{d}T_a}{\mathrm{d}x}(x) + \frac{4U_a}{c_\mathrm{p}\rho D_a}(T_a(x) - T_\mathrm{W}). \tag{3.16}$$

The ODE of Equation (3.16) has an analytical solution as presented in the following lemma.

Lemma 1 (Lemma 1 in [MR1]) *The ODE (3.16),*

$$v_a \frac{\mathrm{d}T_a}{\mathrm{d}x}(x) + \frac{4U_a}{c_\mathrm{p}\rho D_a}(T_a(x) - T_W) = 0,$$

has the solution

$$T_a(x; v_a) = \begin{cases} T_W, & \text{if } v_a = 0, \\ Ce^{-\frac{4U_a x}{c_\mathrm{p}\rho D_a v_a}} + T_W, & \text{if } v_a > 0, \end{cases} \tag{3.17}$$

where $C \in \mathbb{R}$ is a constant. The solution is continuous for all $x \in [0, L_a]$ and all $v_a \geq 0$.

A valid expression for C is easily obtained using the initial condition at $T_a(0)$. Replacing C by this expression then results in a constraint linking $T_a(0)$ and $T_a(L_a)$. However, this function is defined by a case distinction ($v_a = 0$ vs. $v_a \neq 0$). The integration of (3.17) into a model that can be solved by an optimization solver requires additional variables and constraints that lead to further computational challenges. In particular, it is not possible to simply include the second case of the definition standalone in the model since the resulting constraint would not be well-defined in all cases in which an arc has a zero flow. As will be discussed in the next section, this is, e.g., the case for all candidate pipes that are not built. To tackle this problem, we will derive an approximation h_a^{fit} in Section 3.3.3 so that Equation (3.17) is approximately captured via the equality constraint $h_a^{\mathrm{fit}}(u, w_a, \lambda_a^*) = 0$.

The second and last assumption that we make is that the DHN has exactly one depot and that both the forward and backward flow network are tree-shaped. Consequently, a unique forward flow path exists from the depot to any consumer. Similarly, it means that a unique backward flow path exists from any consumer to the depot. If this is the case, the sign of all mass flow variables q_a can be inferred from the network structure. Thus, by only considering tree-shaped networks, we simplify the modeling of the DHN's physics and make (O-DHN) less computationally challenging compared to the original formulation.

Then, if we assume that the arcs are oriented in the inferred flow direction and if we replace e by T through the use of state equation (3.14), the set of energy conservation constraints (3.6) and (3.7) simplify to

$$\begin{aligned} \sum_{a \in \delta^{\mathrm{in}}(u)} c_\mathrm{p} T_a(L_a) q_a = \sum_{a \in \delta^{\mathrm{out}}(u)} c_\mathrm{p} T_a(0) q_a, \\ T_u = T_a(0), \quad a \in \delta^{\mathrm{out}}(u). \end{aligned} \tag{3.18}$$

This means that we eliminate the need for the complementarity pair (β_a, γ_a) described in the set of Equations (3.7).

3.3.2 Modeling the Expansion Decisions

Model (O-DHN) is now enhanced so that a point originating from its feasible domain results in expansion decisions regarding a set of candidate pipes and consumers. With

this in mind, we split the set A_c in A_c^e, the set of existing consumers, and A_c^c, the set of candidate consumers. Similarly, we split the set A_p in A_p^e, the set of existing pipes, and A_p^c, the set of candidate pipes. Naturally it holds that $A_\mathrm{c}^\mathrm{e} \cup A_\mathrm{c}^\mathrm{c} = A_\mathrm{c}$ and $A_\mathrm{p}^\mathrm{e} \cup A_\mathrm{p}^\mathrm{c} = A_\mathrm{p}$. We refer to Table 1 of [MR1] for a detailed arc and node set summary. Moreover, Figure 1 of [MR1] shows a schematic of the graph representation for a small DHN example with expansion extensions.

Next, we introduce the expansion decision variable $x_a \in \{0, 1\}$ that models if arc $a \in A_\mathrm{c}^\mathrm{c} \cup A_\mathrm{p}^\mathrm{c}$ is built or not. Naturally, the set of variables u that is specified in Section 3.2.7 now also includes the expansion variables x_a as they model exact decisions that are linked to the underlying application.

Furthermore, we adapt the constraints of (O-DHN) to account for expansion decisions. First, we replace the mass flow bounds (3.10) for $a \in A_\mathrm{p}^\mathrm{c} \cup A_\mathrm{c}^\mathrm{c}$ by

$$0 \leq q_a \leq x_a q_a^+. \tag{3.19}$$

Thus, they force $q_a = 0$ for $a \in A_\mathrm{p}^\mathrm{c} \cup A_\mathrm{c}^\mathrm{c}$ if $x_a = 0$. To avoid changing the set of feasible states of the system, the consumer power consumption constraint (3.9a) and the momentum equation (3.1) have to be deactivated if $x_a = 0$ for candidate arcs. Therefore, we replace (3.9a) for all $a \in A_\mathrm{c}^\mathrm{c}$ by

$$x_a P_a = q_a c_\mathrm{p} \left(T_a(L_a) - T_a(0)\right) \tag{3.20}$$

and replace (3.1) for all $a \in A_\mathrm{p}^\mathrm{c}$ by the big-M reformulation

$$p_v - p_u + L_a g \rho h_a' + \lambda_a \frac{|v_a| v_a \rho L_a}{2 D_a} \leq (1 - x_a) M_a^1, \tag{3.21a}$$

$$p_v - p_u + L_a g \rho h_a' + \lambda_a \frac{|v_a| v_a \rho L_a}{2 D_a} \geq -(1 - x_a) M_a^2 \tag{3.21b}$$

with suitably large constants M_a^1, M_a^2 as discussed in Section 2.6 of [MR1].

Furthermore, we add valid inequalities to the expansion model. Again, we refer to Section 2.7 of [MR1] for a detailed discussion. For $a \in A_\mathrm{p}^\mathrm{c} \cup A_\mathrm{c}^\mathrm{c}$, the valid inequalities read

$$x_a \leq x_{\bar{a}}, \quad \bar{a} \in P(a), \tag{3.22}$$

where $P(a) \subseteq A$ represents the set of arcs created by the unique forward and backward flow paths from arc a to the existing network.

Finally, the objective function is modified to take the expansion decisions into account. It reads

$$\sum_{a \in A_\mathrm{c}^\mathrm{c}} P_a w \pi x_a - \sum_{a \in A_\mathrm{p}^\mathrm{c} \cup A_\mathrm{c}^\mathrm{c}} C_a^\mathrm{inv} x_a - w \left(C_\mathrm{p} P_\mathrm{p} + C_\mathrm{w} P_\mathrm{w} + C_\mathrm{g} P_\mathrm{g}\right), \tag{3.23}$$

where $w = 24\,\mathrm{h}$ and π, C_a^inv stand for the energy price per kWh and the daily annuity costs of arc a, respectively.

3.3.3 An Internal Energy Density Equation Approximation

The closed-form reformulation of h_a presented in (3.17) cannot be used as a constraint. As indicated previously, its case-distinction and numerical ill-conditioning for positive values of v_a close to zero make it badly suited for optimization solvers. However, the expression of Equation (3.17) does form a good candidate for applying the ideas of Section 2.2. Consequently, we propose to replace the closed-form expression of h_a by a fitted surrogate function h_a^{fit} that is better suited for global optimization solvers. Hence, we use a modified multivariate polynomial ansatz function to replace Equation (3.17). Let d be the degree of the considered polynomial and let α_{klm} denote a fitting parameter defined for all Θ_d, where

$$\Theta_d := \left\{(k,l,m) \in \mathbb{N}^3 \colon k \neq 0 \text{ and } k+l+m \leq d\right\}.$$

Then, we set $\lambda_a := \{\alpha_{klm} : (k,l,m) \in \Theta_d\}$ resulting in the ansatz function

$$h_a^{\text{fit}}(u, w_a, \lambda_a) = \sum_{(k,l,m)\in\Theta_d} \alpha_{klm}\, v_a^k\, T_a(0)^l\, T_a(L_a)^m + T_a(L_a) - T_{\text{W}}. \tag{3.24}$$

When $v_a = 0$ holds, Equation (3.24) is constructed so that the closed-form constraint $h_a^{\text{fit}}(u, w_a, \lambda_a) = 0$ reduces to $T_a(L_a) = T_{\text{W}}$. This property ensures that the resulting optimization model stays feasible even if a candidate arc is not built. By doing so, we highlight the strength of the approach presented in Section 2.2, i.e., the flexibility in terms of the ansatz function allows to keep specific features of function h_a. Additionally, outer approximations of monomial and bilinear terms have been thoroughly studied and are part of most global optimization solvers; see, e.g., Misener and Floudas (2014) for a summary of the outer approximations implemented in the ANTIGONE solver. As a consequence, global optimization solvers are built to efficiently tackle equations of the form (3.24), making the proposed ansatz function well suited for the expansion application that is considered.

Finally, the ansatz function of Equation (3.24) is fitted as discussed in Section 2.2 with a quadratic loss function and a large set of samples that satisfy Equation (3.17). The interested reader is referred to Section 3 of [MR1] for a detailed discussion about the approximation accuracy of the resulting fitted function.[1]

[1] In [MR1], $f_{\text{approx}}(v_a, T_a(0), T_a(L_a))$ is the notation used for $h_a^{\text{fit}}(u, w_a, \lambda_a)$.

3.3.4 Expansion Optimization Problem

With the extensions of Sections 3.3.1, 3.3.2, and 3.3.3 we summarize the stationary district heating network expansion optimization problem

$$
\begin{aligned}
\min \quad & \text{objective: (3.23)}, \\
\text{s.t.} \quad & \text{momentum: (3.1) or (3.21)}, \\
& \text{internal energy density approximation: (3.24)}, \\
& \text{mass conservation: (3.4)}, \\
& \text{pressure continuity: (3.5)}, \\
& \text{energy conservation: (3.18)}, \\
& \text{depot constraints: (3.8)}, \\
& \text{consumer constraints: (3.9) with (3.9a) or (3.20)}, \\
& \text{massflow bounds: (3.10) or (3.19)}, \\
& \text{nodal and power bounds: (3.11) and (3.12)}, \\
& \text{valid inequalities: (3.22)}.
\end{aligned}
\tag{E-DHN}
$$

We remark that (E-DHN) is a special case of (F) described in Chapter 2 for stationary expansion decision making in tree-shaped district heating networks.

Furthermore, we highlight that (E-DHN) belongs to the nonconvex MINLP class. Consequently, global MINLP solvers are needed for solving this problem to global optimality.

3.3.5 Numerical Results

To study (E-DHN), we use the AROMA network from Krug et al. (2021b) and remove one arc in the forward and backward flow networks that make it a tree-shaped network. Five candidate consumers are added to the optimization problem. Costs and prices are taken from Nussbaumer and Thalmann (2016) and TWL (2020), respectively. For specifications of hardware, software, and the test instances, we refer to Section 4.1 and 4.2 of [MR1].

We first discuss the results of the base test case shown in Figure 3.2. Despite that the cost of pressure increase is the highest among all costs, it can be observed that a non-negligible pressure difference is induced at the depot of the network. This is a consequence of the thermal energy equation (3.17) that has decreasing thermal losses when the velocity v_a is increased via a pressure difference.

Through a sensitivity analysis of the instance shown in Figure 3.2 that is carried out in Section 4.3 of [MR1], we identify the three main parameters that drive the investment decisions:

- First, the estimated power demand of the candidate consumer directly influences the objective function (3.23). In fact, in (E-DHN), the resulting consumer payment is the only way of reimbursing the investment costs incurred to establish a connection with the consumer. Consequently, this motivates the

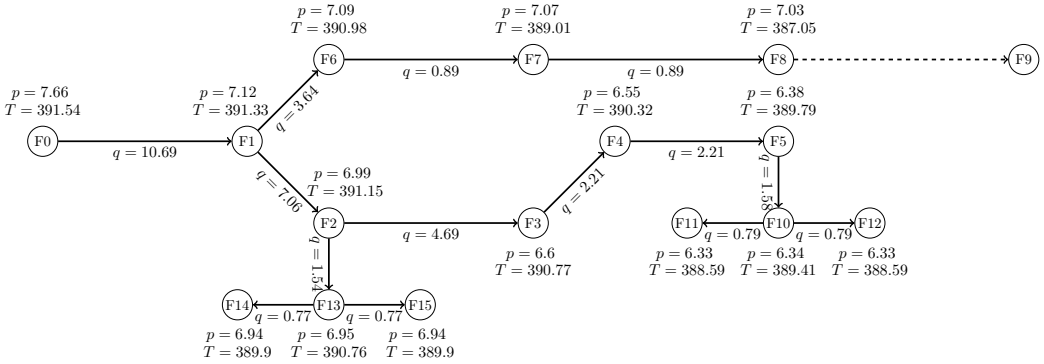

Figure 3.2: Illustration of the solution of Problem (E-DHN) on the modified AROMA network. Solid arcs represent existing and newly constructed candidate pipes, whereas dashed arcs represent candidate pipes that are not built. The figure also provides parts of the physical solution (T in K and p in bar at nodes and q in $\mathrm{kg\,s^{-1}}$ on arcs).

accurate estimation of consumer power demand, which is a research topic on its own, see, e.g., Werner (2017).

- Second, as can be seen in Equation (3.23), a candidate consumer who is located far away from the network incurs larger trench digging and pipe placement costs for connecting him to the network. Thus, the distance of a candidate consumer to the existing network directly increases the value of the objective function when an expansion decision is made.

- Finally, for some consumers, the heat transfer coefficients U_a of the pipes that connect them to the depot are what makes them financially attractive for the network operator. Indeed, higher thermal losses implies that more heat is needed for the transport of water to the candidate consumers, i.e., a larger amount of money is spent by the network operator to satisfy the same demand. Moreover, this result highlights the importance of the expansion model that we present. We accurately take into account the influence of thermal losses induced by the network of pipes on the expansion decisions.

The interested reader is referred to Section 4.3 of [MR1] for a more detailed description of the results.

3.4 Realistic Solutions

We now present the content of [MR2] that focuses on obtaining accurate solutions of (O-DHN) via adaptive refinement algorithms. Interestingly, the literature on mathematical optimization for DHN operation is rather sparse. For closed-loop control strategies of instationary variants of the problem, we refer to Sandou et al. (2005), Verrilli et al. (2017), Benonysson et al. (1995), and to Krug et al. (2021b)

for open-loop optimization approaches. The interested reader is referred to Section 1 of [MR2] for more DHN optimization references.

In the following, we begin by specifying the internal energy density state equation that is kept general in the description of (O-DHN). Then, we present a model catalog for approximating the internal energy density equation of (O-DHN). This yields a reformulation that is in line with the description of (SD) in Chapter 2. With this new description at hand, Algorithm 1 discussed in Section 2.4 is applied and extended with a coarsening and model down-switching step. Finally, the numerical results presented in [MR2] are summarized.

To keep this extended summary self-contained and for the ease of presentation, we present the ideas of [MR2] by relying on the notation of Chapters 2 and 3.

3.4.1 State Equation Specification

As for the expansion decision model, we specify the expression of the internal energy density state equation (3.2). We consider the state equation proposed by Hauschild et al. (2020), i.e.,

$$T_a = \theta_2 (e_a^*)^2 + \theta_1 e_a^* + \theta_0 \tag{3.25}$$

with

$$e_a^* := \frac{e_a}{e_0}, \quad e_0 := 10^9 \,\mathrm{J\,m^{-3}},$$
$$\theta_2 = 59.2453\,\mathrm{K}, \quad \theta_1 = 220.536\,\mathrm{K}, \quad \theta_0 = 274.93729\,\mathrm{K}.$$

Equation (3.25) provides a more detailed second-order polynomial relationship between e and T in comparison to state equation (3.14). Moreover, it can be shown that state equation (3.25) combined with ODE (3.2) has an analytical solution.

Lemma 2 (Lemma 1 in [MR2]) *The differential equation (3.2), i.e.,*

$$0 = v_a \frac{\mathrm{d}e_a}{\mathrm{d}x} - \frac{\lambda_a}{2D_a}\rho |v_a| v_a^2 + \frac{4U_a}{D_a}(T_a - T_W)$$

with initial condition

$$e_a(0) = e_a^0 > 0$$

and state equation (3.25) has the exact solution

$$e_a(x) = \frac{\sqrt{\beta^2 - 4\alpha\gamma}}{2\alpha} \frac{1 + \exp\left(\frac{x\sqrt{\beta^2-4\alpha\gamma}}{\zeta}\right)\left(\frac{2\alpha e_a^0 + \beta - \sqrt{\beta^2-4\alpha\gamma}}{2\alpha e_a^0 + \beta + \sqrt{\beta^2-4\alpha\gamma}}\right)}{1 - \exp\left(\frac{x\sqrt{\beta^2-4\alpha\gamma}}{\zeta}\right)\left(\frac{2\alpha e_a^0 + \beta - \sqrt{\beta^2-4\alpha\gamma}}{2\alpha e_a^0 + \beta + \sqrt{\beta^2-4\alpha\gamma}}\right)} - \frac{\beta}{2\alpha}$$

with

$$\alpha := -\frac{4U\theta_2}{D_a (e_0)^2}, \quad \beta := -\frac{4U\theta_1}{D_a e_0}, \quad \zeta := v_a,$$
$$\gamma := \frac{\lambda_a}{2D_a}\rho |v_a| v_a^2 - \frac{4U}{D_a}(\theta_0 - T_W),$$

if $4\alpha\gamma - \beta^2 < 0$ *is satisfied.*

Interestingly, we note that the condition $4\alpha\gamma - \beta^2 < 0$ is always satisfied for usual pipe parameters.

The analytical solution derived in Lemma 2 could, in principle, be used as a constraint in a nonlinear optimization model. However, the fractions, square roots, and exponential functions would lead to a badly posed problem resulting in a significant numerical challenge even for state-of-the-art solvers. Additionally, this analytical solution yields a specific behavior that cannot easily be mimicked by a fitted approximation function. As a consequence, no guarantee of obtaining ε-feasible solutions to (O-DHN) exists. Hence the ideas of Section 2.2 cannot be used anymore if accurate solutions are needed.

Therefore, we focus on applying the generalized adaptive refinement algorithm ideas of Section 2.4 for the case of stationary DHN operation. The next subsections hence specify the components that we consider in Algorithm 1.

3.4.2 Model Catalog

The expression of the internal energy density equation (3.2) has a high amount of nonlinear terms. When discretized and considered as a constraint this equations would induce varying steep gradients that can make the resulting optimization problems hard to solve. As described in Section 2.4.1, we create a set of model levels with decreasing amount of nonlinear terms to cope with this issue. They read

$$0 = v_a \frac{\mathrm{d}e_a}{\mathrm{d}x} - \frac{\lambda_a}{2D_a}\rho|v_a|v_a^2 + \frac{4U_a}{D_a}(T_a - T_\mathrm{W}), \tag{M1}$$

$$0 = v_a \frac{\mathrm{d}e_a}{\mathrm{d}x} + \frac{4U}{D_a}(T_a - T_\mathrm{W}), \tag{M2}$$

$$0 = e_a(L_a) - e_a(0), \tag{M3}$$

where (M1) and (M2) are complemented with state equation (3.25). The highest model level (M1) equals Equation (3.2). Then, by sequentially dropping terms $\lambda_a/(2D_a)\rho v_a^2|v_a|$ and $4U_a/D_a(T_a - T_\mathrm{W})$, respectively, we get model levels (M2) and (M3). As in Section 2.4.1, let $\mathcal{L}$ be the set that captures the different levels, i.e., $\mathcal{L} := \{(\mathrm{M1}), (\mathrm{M2}), (\mathrm{M3})\}$. In addition, Corollary 1 of [MR2] gives the analytical solution of (M2). We do not include this corollary here to keep the extended summary short.

Since we follow the approach presented in Section 2.4, we need a set of functions $\tilde{h}^\theta_{a,k}$ with $k \in K(a)$, that can replace h^θ_a for all $a \in A_\mathrm{p}$ and all $\theta \in \mathcal{L}$. Consequently, we introduce an equidistant discretization $\mathit{\Gamma}_a$ of the spatial domain $[0, L_a]$ using the discretization points $x_k \in \mathit{\Gamma}_a$ such that $0 = x_0 < x_1 < \cdots < x_{n_a} = L_a$ with the step size $\Delta x_a = x_{k+1} - x_k$ for $k = 0, 1, \ldots, n_a - 1$. We use the implicit mid-point rule to discretize the separate levels of the catalog, i.e., Systems (M1)–(M3), as well as the state equation (3.25). Using the abbreviation $e_a^k := e_a(x_k)$, we obtain the

associated discretized model levels

$$0 = v_a \left(\frac{e_a^k - e_a^{k-1}}{\Delta x} \right) - \frac{\lambda_a \rho}{2D_a} |v_a| v_a^2 + \frac{4U_a}{D_a} \left(T_a(e_a^k, e_a^{k-1}) - T_{\mathrm{W}} \right), \tag{D1}$$

$$0 = v_a \left(\frac{e_a^k - e_a^{k-1}}{\Delta x} \right) + \frac{4U}{D_a} \left(T_a(e_a^k, e_a^{k-1}), -T_{\mathrm{W}} \right) \tag{D2}$$

$$0 = e_a(L_a) - e_a(0), \tag{D3}$$

where (D1) and (D2) hold for $k = 1, \ldots, n_a$. The set of equations (D1) and (D2) are complemented with the discretized state equation (3.25), i.e.,

$$T_a(e_a^k, e_a^{k-1}) := \frac{\theta_2}{4e_0^2} \left(e_a^k + e_a^{k-1} \right)^2 + \frac{\theta_1}{2e_0} \left(e_a^k + e_a^{k-1} \right) + \theta_0 \tag{3.26}$$

for all $k = 1, \ldots, n_a$.

3.4.3 Adaptive Optimization Problem

The new discretized model level equations (D1)–(D3) yield the adaptive optimization problem for stationary DHN operation[2]

min	objective: (3.13),	
s.t.	momentum: (3.1)	
	internal energy density: (3.26) and (D1), (D2), or (D3),	
	mass conservation: (3.4),	
	pressure continuity: (3.5),	(A-DHN)
	energy conservation: (3.6) with (3.7),	
	depot constraints: (3.8),	
	consumer constraints: (3.9),	
	bounds: (3.10)–(3.12).	

This model is the equivalent of (SD) in Chapter 2. Because (O-DHN) is a special case of (G) and since (A-DHN) also is a special case of (SD), we can apply the ARA presented in Section 2.4.

Furthermore, we highlight that (A-DHN) belongs to the class of nonconvex nonlinear optimization problem with complementarity constraints. Since we want to obtain accurate solutions for realistic networks we will not consider global optimization solvers as their solution time does not scale well with the size of the resulting models. In fact, we use generic nonlinear solvers that do not yield optimality guarantees when applied to our problem. Nevertheless, in practice, their use does result in good-quality solutions for the sequence of problems that are solved.

[2] In [MR2], (NLP) is the abbreviation used for (A-DHN).

3.4.4 Components of the Algorithm

The details about the components of the ARA presented in Section 2.4 applied to (O-DHN) are now discussed.

First, we specify the exact error measures that quantify the infeasibility of a solution of (A-DHN) w.r.t. the domain of (O-DHN). Suppose that (A-DHN) is solved and let $(\tilde{u}, \tilde{w}) \in U \times W$ be the resulting solution in which $\tilde{e}_a(x_k)$ and $\tilde{v}_a$ are the value of the internal energy density at point $x_k \in \Gamma_a$ of arc $a \in A_\mathrm{p}$ and the value of the velocity of arc $a \in A_\mathrm{p}$, respectively.[3] In addition, for $x \in [0, L_a]$, let $\epsilon_a^\theta(x)$ be the result of evaluating the right-hand side of the analytical solution to Constraints (M1), (M2), or (M3) with $e_a(0) = \tilde{e}_a(0)$ and $v_a = \tilde{v}_a$. Then, the reformulation of the exact total error (2.4) over variable $e_a(L_a)$ yields

$$\nu_a(\tilde{u}, \tilde{w}) := |\epsilon_a^1(L_a) - \tilde{e}_a(L_a)|. \tag{3.27}$$

However, let Γ_0 be a predetermined discretization grid $\Gamma_0 = \{x_0, \ldots, x_r\}$ with $x_0 = 0$ and $x_r = L_a$. Then, we remark that in [MR2] the exact total error is defined as

$$\nu_a(\tilde{u}, \tilde{w}) := \|\epsilon_a^1(\Gamma_0) - \tilde{e}_a(\Gamma_0)\|_\infty, \tag{3.28}$$

where $\tilde{e}_a(\Gamma_0) := (\tilde{e}_a(x_0), \ldots, \tilde{e}_a(x_r))^\top$ and $\epsilon_a^\theta(\Gamma_0) := (\epsilon_a^\theta(x_0), \ldots, \epsilon_a^\theta(x_r))^\top$.[4] Nevertheless, Equation (3.28) gives an upper bound on Equation (3.27) because $x_r = L_a$ is always part of the chosen discretization. Moreover, it holds by construction that both definitions are equal when $\Gamma_0 = \{0, L_a\}$. The definition of (3.28) is motivated by the theory of numerical solutions to Cauchy problems. In fact, convergence results of numerical solutions to exact solutions of ODEs, see, e.g., Süli and Mayers (2003, p. 318), are used in [MR2]. These convergence properties allow to prove finite termination of the ARA applied to (O-DHN) at ε-feasible points.

Next, we introduce the exact model error and the exact discretization error as in [MR2]:

$$\nu_a^\mathrm{m}(\tilde{u}, \tilde{w}) := \|\epsilon_a^1(\Gamma_0) - \epsilon_a^{\ell_a}(\Gamma_0)\|_\infty, \tag{3.29}$$

$$\nu_a^\mathrm{d}(\tilde{u}, \tilde{w}) := \|\epsilon_a^{\ell_a}(\Gamma_0) - \tilde{e}_a(\Gamma_0)\|_\infty. \tag{3.30}$$

Similar to $\nu_a(\tilde{u}, \tilde{w})$ it holds that the right-hand side of Equations (3.29) and (3.30) bound the right-hand side of Equations (2.6) and (2.8) adapted for (A-DHN) from above, respectively.

As the definition of the error estimates requires additional notation and as they are not necessary for understanding this extended summary we omit their description. In short, both estimates are obtained via asymptotic expansions of numerical solutions as described in Stoer and Bulirsch (2002, p. 481). Hence, we refer to Section 3.2 of [MR2] for the definition and discussion of the model error estimate $\eta_a^\mathrm{m}(\tilde{u}, \tilde{w})$ and the discretization error estimate $\eta_a^\mathrm{d}(\tilde{u}, \tilde{w})$. Naturally, in [MR2], we prove that $\nu_a^\mathrm{m}(\tilde{u}, \tilde{w})$ and $\nu_a^\mathrm{d}(\tilde{u}, \tilde{w})$ are bounded from above by the estimates $\eta_a^\mathrm{m}(\tilde{u}, \tilde{w})$ and $\eta_a^\mathrm{d}(\tilde{u}, \tilde{w})$ when

[3] In [MR2], y is the notation used for $(\tilde{u}, \tilde{w})$.

[4] In [MR2], $e_a^\ell(\Gamma_0; \Delta x_i)$ is the notation used for $\tilde{e}_a(\Gamma_0)$ and $e_a^\theta(\Gamma_0)$ is the notation used for $\epsilon_a^\theta(\Gamma_0)$.

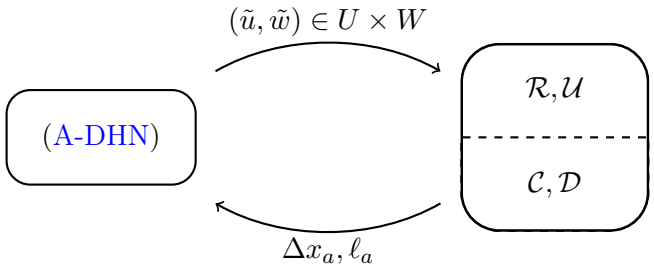

Figure 3.3: State diagram of Algorithm 1 tailored to return ε-feasible controls for stationary DHN operation. The state on the right-hand side is split into an approximation accuracy improvement phase, i.e., corresponding to the creation of $\mathcal{R}$,$\mathcal{U}$, and a model simplification phase, i.e., corresponding to the creation of $\mathcal{C}, \mathcal{D}$.

the discretization step size Δx_a tends to zero, i.e., $\Delta x_a \to 0$. By construction, it also holds that the set of Inequalities (2.11) are valid. Hence, we define the total error estimate $\eta_a(\tilde{u}, \tilde{w})$ exactly as in Equation (2.12). This then completes the error measure definitions of [MR2] explained with the concepts of Section 2.4.2.

For the case of marking and switching strategies, we restrict ourselves to the concepts introduced in Section 2.4. Hence, we refer the interested reader to Section 4.1 of [MR2] for a detailed description. In summary, the switching strategies that we use are the same as Mehrmann et al. (2018b). The marking strategies are based on Dörfler's rule, see Nochetto et al. (2009, p. 93), and are also used in Mehrmann et al. (2018b).

We now draw our attention to the fact that, as discussed in Section 2.4.7, a coarsening step and a model down-switching step are added to the algorithm with associated marking and switching strategies. Moreover, w.l.o.g., the refinement and coarsening switching strategies take effect on the discretization stepsize Δx_a instead of the dimension n_a.

3.4.5 Adaptive Refinement Algorithm and Finite Termination

The state diagram in Figure 3.3 describes the ARA of [MR2] by replacing the concepts and notation of Chapter 2 in Figure 2.3 with the concepts and notation of this chapter. Moreover, the extensions that we consider in this chapter, i.e., a coarsening and down-switching step, are added to the schematic.

We now discuss the functioning of the ARA applied on (O-DHN) by means of Figure 3.3. Generally speaking, the ARA of this chapter and the ARA of Chapter 2 are similar. Indeed, for each iteration of the algorithm, a version of (A-DHN) is solved and the resulting solution $(\tilde{u}, \tilde{w}) \in U \times W$ characterizes how the the next (A-DHN) is designed. Then, subsets of A_p are created such that the values of Δx_a and ℓ_a are changed for their elements. Hence, meaning that we go back to solving (A-DHN), where the entire process can start again.

Nevertheless, a coarsening step and a model down-switching step are added to the algorithm to keep the size of the subsequent instances of (A-DHN) solvable in

Algorithm 2: Adaptive optimization algorithm extended with a coarsening and down-switching phase

Input: error tolerance $\varepsilon > 0$, marking strategies $\sigma_{\mathcal{R}}, \sigma_{\mathcal{U}}, \sigma_{\mathcal{C}}, \sigma_{\mathcal{D}}$, improvement rules $\xi_{\mathcal{R}}, \xi_{\mathcal{U}}, \xi_{\mathcal{C}}, \xi_{\mathcal{D}}$
Output: ε-feasible solution (u, w) of (O-DHN)

foreach $a \in A_p$ **do**
  Initialize ℓ_a^0 and Δx_a^0
$(\tilde{u}, \tilde{w}, \tilde{z})^0 \leftarrow$ Solve (A-DHN)^0
if $(\tilde{u}, \tilde{w})^0$ *is* ε*-feasible* **then**
  return $(u, w) \leftarrow (\tilde{u}, \tilde{w})^0$
for $k = 1, 2, \ldots$ **do**
  for $j = 1, 2, \ldots, \mu$ **do**
    Compute sets $\mathcal{R}^{k,j}, \mathcal{U}^{k,j}$ according to $\sigma_{\mathcal{R}}, \sigma_{\mathcal{U}}$
    foreach $a \in \mathcal{R}^{k,j}$ **do**
      Increase $\Delta x_a^{k,j}$ according to $\xi_{\mathcal{R}}$
    foreach $a \in \mathcal{U}^{k,j}$ **do**
      Switch-up $\ell_a^{k,j}$ according to $\xi_{\mathcal{U}}$
    $(\tilde{u}, \tilde{w}, \tilde{z})^{k,j} \leftarrow$ Solve (A-DHN)^{k,j}
    if $(\tilde{u}, \tilde{w})^{k,j}$ *is* ε*-feasible* **then**
      return $(u, w) \leftarrow (\tilde{u}, \tilde{w})^{k,j}$
  Compute sets $\mathcal{C}^{k,j}, \mathcal{D}^{k,j}$ according to $\sigma_{\mathcal{C}}, \sigma_{\mathcal{D}}$
  foreach $a \in \mathcal{C}^{k,j}$ **do**
    Increase $\Delta x_a^{k,j}$ according to $\xi_{\mathcal{R}}$
  foreach $a \in \mathcal{D}^{k,j}$ **do**
    Switch-down $\ell_a^{k,j}$ according to $\xi_{\mathcal{D}}$
  $(\tilde{u}, \tilde{w}, \tilde{z})^{k,j} \leftarrow$ Solve (A-DHN)^{k,j}
  if $(\tilde{u}, \tilde{w})^{k,j}$ *is* ε*-feasible* **then**
    return $(u, w) \leftarrow (\tilde{u}, \tilde{w})^{k,j}$

a reasonable amount of time. The right-hand side of the schematic in Figure 3.3 consequently describes the subset selection state of the ARA that is split in two phases. The first phase corresponds to the improvement of the accuracy of (A-DHN) and is discussed in Chapter 2. The second phase is associated with reducing the computational challenge of (A-DHN) and creates the coarsening set $\mathcal{C}$ and the model down-switching set $\mathcal{D}$. Here, the discretization step size Δx_a of each element in $\mathcal{C}$ is increased whereas the model level ℓ_a of each element in $\mathcal{D}$ is switched down.

Finally, once an ε-feasible solution is reached, the algorithm stops and returns the solution.

To complete the current section, Algorithm 2 extends Algorithm 1 by adding the specifications described in the previous paragraph. The approximation improvement phase is shown in Lines 8–12 of Algorithm 2 and is scheduled to happen μ times more compared to the approximation simplification phase shown in Lines 16–20 of Algorithm 2. The parameter μ, also referred to as the safeguard parameter, ensures that the approximation accuracy keeps augmenting as long as no ε-feasible solution is found. In fact, μ is part of the finite termination conditions and therefore influences the time required to achieve termination of the algorithm. More information about the safeguard parameter can be found in Mehrmann et al. (2018b, p. 789). Naturally, $(\text{A-DHN})^{k,j}$ is solved and the resulting solution is checked for ε-feasibility as is shown in Lines 13–15 and Lines 21–23 of Algorithm 2.

We now state a series of lemmas that are used to prove finite termination of Algorithm 2 at ε-feasible solutions given a set of conditions on the parameters of the algorithm. Before stating the lemmas, we remark that $\Theta_{\mathcal{R}}, \Theta_{\mathcal{C}}, \Theta_{\mathcal{U}}$, and $\Theta_{\mathcal{D}}$ are parameters that influence the marking strategies that we consider. We omit their description and refer the interested reader to Section 4.1 of [MR2] for more details.

Lemma 3 (Lemma 2 in [MR2]) *Suppose that the model level $\ell_a \in \{1, 2, 3\}$ is fixed for every pipe $a \in A_p$. Let the resulting set of model levels be denoted by $\mathcal{M}$. Suppose further that $\eta_a(\tilde{u}, \tilde{w}) = \eta_a^d(\tilde{u}, \tilde{w})$ holds in (2.12) and that every (A-DHN) is solved to local optimality. Consider Algorithm 2 without applying the model switching steps in Lines 12 and 20. Then, the algorithm terminates after a finite number of refinements in Line 10 and coarsenings in Line 18 with an ε-feasible solution w.r.t. model level set $\mathcal{M}$ if there exists a constant $C > 0$ such that*

$$\frac{1}{4}\Theta_{\mathcal{R}}\mu \geq \Theta_{\mathcal{C}} + C \tag{3.31}$$

holds and if the step sizes of the initial discretizations are chosen sufficiently small.

Lemma 4 (Lemma 3 in [MR2]) *Suppose that the discretization stepsize Δx_a is fixed for every pipe $a \in A_p$. Suppose further that $\eta_a(\tilde{u}, \tilde{w}) = \eta_a^m(\tilde{u}, \tilde{w})$ holds in (2.12) and that every (A-DHN) is solved to local optimality. Consider Algorithm 2 without applying the discretization refinements in Line 10 and the coarsening step in Line 18. Then, the algorithm terminates after a finite number of model switches in Lines 12 and 20 with an ε-feasible solution w.r.t. the step sizes Δx_a, $a \in A_p$, if there exists a constant $C > 0$ such that*

$$\Theta_{\mathcal{U}}\mu \geq \tau\Theta_{\mathcal{D}}|A_p| + C. \tag{3.32}$$

Lemma 5 (Lemma 4 in [MR2]) *Let $(\tilde{u}, \tilde{w}, \tilde{z})^{\mu}$ and $(\tilde{u}, \tilde{w}, \tilde{z})^{\mu+1}$ be the solution of the optimization problem before and after a refinement or coarsening step, respectively. Let $\eta_a^d(\tilde{u}, \tilde{w})$ and $\eta_a^m(\tilde{u}, \tilde{w})$ be the discretization and model error estimate for a given solution $(\tilde{u}, \tilde{w}, \tilde{z})$ of (A-DHN). Then, if*

$$\eta_a^{d,\mu}(\tilde{u}, \tilde{w}) \ll \eta_a^{m,\mu}(\tilde{u}, \tilde{w})$$

is satisfied, it holds that

$$\eta_a^{m,\mu+1}(\tilde{u}, \tilde{w}) = \eta_a^{m,\mu}(\tilde{u}, \tilde{w}). \tag{3.33}$$

Assumption 3 (Assumption 1 in [MR2]) *Let $(\tilde{u}, \tilde{w}, \tilde{z})^{\mu}$ and $(\tilde{u}, \tilde{w}, \tilde{z})^{\mu+1}$ be the solution of the optimization problem before and after a model up- or down-switching step, respectively. Moreover, let us denote with λ^{μ} and $\lambda^{\mu+1}$ the corresponding sensitivities. Then, there exists a constant $C > 0$ with $\|\lambda^{\mu} - \lambda^{\mu+1}\| \leq C$.*

Lemma 6 (Lemma 5 in [MR2]) *Let $(\tilde{u}, \tilde{w}, \tilde{z})^{\mu}$ and $(\tilde{u}, \tilde{w}, \tilde{z})^{\mu+1}$, respectively, be the solution of the optimization problem before and after a model up or down switching step. Let $\eta_a^d(\tilde{u}, \tilde{w})$ and $\eta_a^m(\tilde{u}, \tilde{w})$ be the discretization and model error estimate for a given solution $(\tilde{u}, \tilde{w}, \tilde{z})$ of (A-DHN). Finally, suppose that Assumption 3 holds. Then,*

$$\eta_a^{m,\mu+1}(\tilde{u}, \tilde{w}) = \eta_a^{m,\mu}(\tilde{u}, \tilde{w}) \tag{3.34}$$

holds.

Next, we state the finite termination theorem of Algorithm 2 that is proven with Lemmas 3–6.

Theorem 1 (Theorem 1 in [MR2]) *Suppose that $\eta_a^d \ll \eta_a^m$ for every $a \in A_p$ and that every (A-DHN) is solved to local optimality. Moreover, suppose that Assumption 3 holds. Then, Algorithm 2 terminates after a finite number of refinements, coarsenings, and model switches in Lines 10, 18, 12, and 20 with an ε-feasible solution w.r.t. the reference problem if there exist constants $C_1, C_2 > 0$ such that*

$$\frac{1}{4}\Theta_{\mathcal{R}}\mu \geq \Theta_{\mathcal{C}} + C_1 \quad \text{and} \quad \Theta_{\mathcal{U}}\mu \geq \tau\Theta_{\mathcal{D}}|A_p| + C_2$$

hold.

Finally, we remark that in [MR2] the parameters $\Theta_{\mathcal{R}}, \Theta_{\mathcal{C}}, \Theta_{\mathcal{U}}, \Theta_{\mathcal{D}}, \mu$, and τ are indexed over the parameter k, the outer loop iteration index of Algorithm 2. This makes the conditions in Lemma 3, Lemma 4, and Theorem 1 iteration-specific and thus allows for modifying these parameters, if necessary, over the course of the iterations. We omit this notation here on purpose to keep the explanation clear.

3.4.6 Numerical Results

Algorithm 2 is tested on the AROMA and STREET networks originating from Krug et al. (2021b). Power costs are again taken from Nussbaumer and Thalmann (2016). The interested reader is referred to Section 5.1, 5.2, and 5.3 of [MR2] for the detailed discussion of the hardware setup, the software setup, the test instances, and the parameterization of the algorithm. In the following, we summarize the numerical results via a set of key points:

- In practice, the algorithm works as requested with both the exact errors and the error estimates on all considered instances. Therefore, it finitely terminates with an ε-feasible solution. Figure 3.4 highlights this by displaying the error decrease of the algorithm over the course of the iterations for both error

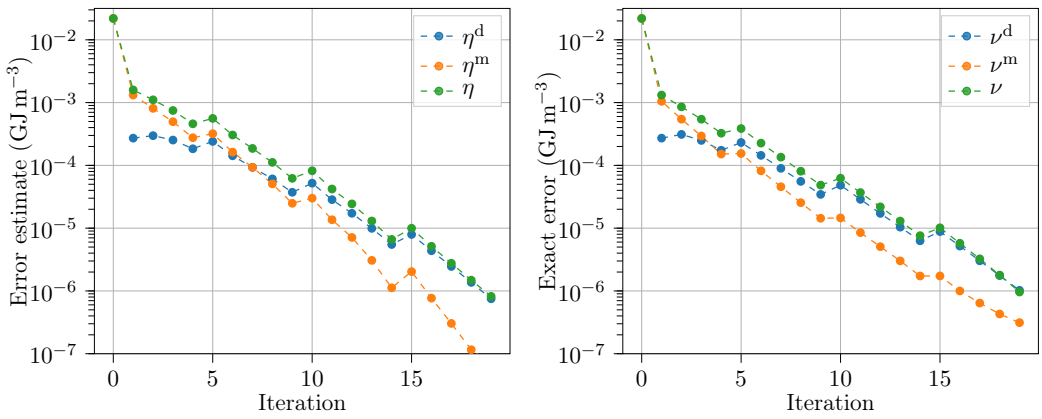

Figure 3.4: Error decrease of the ARA applied on the STREET network instance for the error estimates (left) and exact errors (right).

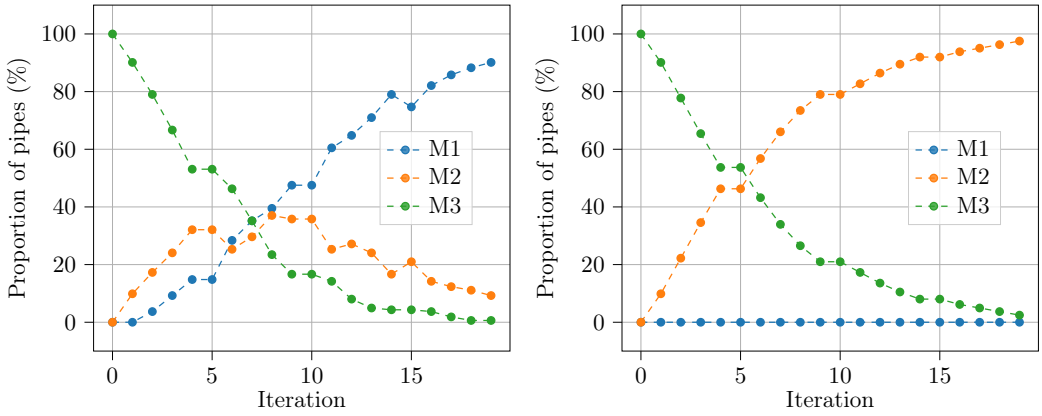

Figure 3.5: Proportion of pipes in each model level set of the ARA applied on the STREET network instance with error estimates (left) and exact errors (right).

measures. Moreover, for some instances, the algorithm is able to obtain high-detail solutions that state-of-the-art solvers cannot compute from scratch when the same level of detail is considered.

- We demonstrate that the use of error estimates, in the case of stationary DHN operation, results in similar behavior of the algorithm compared to the exact error case. Moreover, as can be seen in Figure 3.4, it needs exactly the same amount of iterations when the error estimates instead of the exact errors are used. Therefore, this makes Algorithm 2 coupled with error estimates a useful tool for obtaining ε-feasible solutions when exact error measures are not available. However, as the error estimates upper bound the exact errors, they might result in an overestimation of the discretization error or the model error. This can lead to approximations of the functions h_a that are too detailed. Figure 3.5 shows the proportion of pipes inside each model level set over the course of the

iterations when error estimates and exact errors are used. The error estimates overestimate the exact model error, hence, resulting in more pipes that reach the highest model level when the algorithm terminates. Naturally, this results in intermediate (A-DHN) problems that are harder to solve and can consequently increase the time needed to reach an ε-feasible solution.

- The variable values $(\tilde{u}, \tilde{w})^0$and $(\tilde{u}, \tilde{w})^{k_{\text{end}}}$, where k_{end} denotes the index of the last ARA iteration before ε-feasibility is reached, are strikingly different. This is a consequence of the increasing approximation accuracy of the $(\text{A-DHN})^{k,j}$ that are solved in every iteration of the algorithm. Such a discrepancy in the value of the solutions shows why we should always try to get physically accurate solutions if the resulting controls shall be practically useful.

4

Quantile-Constrained Optimization Problems

We now present solution techniques for quantile-constrained optimization problems as considered in [MR3]. First, quantile-constrained optimization problems and a scenario-based approximation are discussed in Section 4.1. Then, in Section 4.2, commonly used optimization techniques are developed for the problem that is considered. With the help of these solution techniques, an adaptive scenario clustering algorithm (ASCA) is presented in Section 4.3. This algorithm enhances the ideas of the ARA discussed in Section 2.4 so that it terminates at a global optimal solution. Finally, all techniques are tested and the computational results are compared in Section 4.4.

4.1 Optimization Problem and Approximation

This section describes quantile-constrained optimization problems and a tailored scenario-based approximation of the original problem.

We consider a discrete set of indices $t \in \mathcal{T} = \{1, \dots, T\}$. For each index t an unknown stochastic cost vector $c_t \in \mathbb{R}^N$ exists. Let f be an application-specific function. Furthermore, we merge all decision variables in a vector $x \in X \subseteq \mathbb{R}^N$. Then, the quantile-constrained optimization problem reads

$$\begin{aligned} \min_{x} \quad & \alpha \sum_{t \in \mathcal{T}} \mathbb{E}[c_t^\top x] + (1-\alpha) \sum_{t \in \mathcal{T}} f\left(q_t\right), \\ \text{s.t.} \quad & q_t = \mathbb{Q}[c_t^\top x], \\ & x \in X \subseteq \mathbb{R}^N, \end{aligned} \tag{Q}$$

where $\mathbb{E}$, $\mathbb{Q}$, and X model the expectation, the τ-quantile and the non-empty closed set of feasible decisions that may also include integrality restrictions for all or some of the variables, respectively. Here, contrarily to [MR3], variables q_t are introduced

w.l.o.g., so that the link with Chapter 2 can be made. In fact, in [MR3], $\mathbb{Q}[c_t^\top x]$ is directly part of the objective function.

We shortly summarize two examples that can be modeled by (Q): A maintenance planning problem in electricity networks as it was posed in the EURO/ROADEF challenge 2020[1] and a variant of the classic portfolio optimization problem.

The first problem is the grid operation based outage maintenance planning problem and consists in determining the start time of maintenance interventions in a high-voltage transmission network over a given time horizon. More specifically, the goal is to minimize a combination of the expectation and the quantile of the cost associated with the schedule. The second problem is the portfolio optimization where the goal is twofold: maximize the return and minimize the risk for which different measures have been proposed; see, e.g., Gaivoronski and Pflug (2005), Mansini et al. (2003), Benati and Rizzi (2007), and Lin (2009). Among them, the Value at Risk (VaR) or quantile has attracted particular attention, namely because it is used to measure market risk by regulators; see, e.g., Artzner et al. (1999) and the references therein. We refer to Section 2.1 and 2.2 of [MR3] for a detailed description of both models and their MILP approximation.

It often holds that the expression of $\mathbb{Q}[c_t^\top x]$ is unknown or that it cannot be described with finitely many variables. Therefore, an arguably good approximation of (Q) can be obtained by sampling a finite set $\mathcal{S}_t$ of scenarios for all $t \in \mathcal{T}$. In this case, every $s \in \mathcal{S}_t$ is associated to a finite cost vector c_t^s and a probability $p_t^s \in [0,1]$ such that $\sum_{s\in\mathcal{S}_t} p_t^s = 1$. Then, for a specific $t \in \mathcal{T}$, the expected value is approximated via

$$\mathbb{E}[c_t^\top x] = \sum_{s\in\mathcal{S}_t} p_t^s (c_t^s)^\top x.$$

Furthermore, the quantile is approximated with the result of the following optimization problem:

$$\begin{aligned}
\mathbb{Q}[c_t^\top x] = \min_{q_t, y_t^s} \quad & q_t && && \text{(4.1a)}\\
\text{s.t.} \quad & q_t \geq (c_t^s)^\top x + M_t^s(y_t^s - 1), && s \in \mathcal{S}_t, && \text{(4.1b)}\\
& \sum_{s\in\mathcal{S}_t} y_t^s p_t \geq \tau, && && \text{(4.1c)}\\
& y_t^s \in \{0,1\}, && s \in \mathcal{S}_t, && \text{(4.1d)}
\end{aligned}$$

Here, the big-M parameters are computed on an application-specific basis as highlighted in Sections 2.1 and 2.2 of [MR3].

We remark that for any $t \in \mathcal{T}$, Problem (4.1) can be solved in polynomial time if we are given a solution $x \in X$. More specifically, y_t^s is first initialized to zero for all $s \in \mathcal{S}_t$. Then, the vector products $(c_t^s)^\top x$ are sorted in increasing value over all $s \in \mathcal{S}_t$. Finally, the y_t^s variables are fixed to one by iterating over the ordered scenarios until (4.1c) is satisfied.

[1] See https://www.roadef.org/challenge/2020/en/index.php.

If the function f is nondecreasing and because both (Q) and (4.1) are minimization problems, we can replace $\mathbb{E}[c_t^\top x]$ and $\mathbb{Q}[c_t^\top x]$ by the scenario-dependent approximations yielding the scenario-based quantile-constrained optimization problem

$$\begin{aligned} \min_x \quad & \alpha \sum_{s\in\mathcal{S}_t} p_t^s (c_t^s)^\top x + (1-\alpha) \sum_{t\in\mathcal{T}} f(q_t) \\ \text{s.t.} \quad & q_t \geq (c_t^s)^\top x + M_t^s (y_t^s - 1), \quad t \in \mathcal{T}, s \in \mathcal{S}_t, \\ & \sum_{s\in\mathcal{S}_t} y_t^s p_t \geq \tau, \quad t \in \mathcal{T}, \\ & y_t^s \in \{0,1\}, \quad t \in \mathcal{T}, s \in \mathcal{S}_t, \\ & x \in X \subseteq \mathbb{R}^N. \end{aligned} \tag{S-Q}$$

We draw attention to the fact that (S-Q) is an MILP in the case of the maintenance planning problem and the portfolio optimization problem. Indeed, the effect of function f can, for both applications, be reformulated by a set of continuous variables and linear inequalities.

4.2 Preliminary Solution Techniques

We now discuss the preliminary solution techniques that we propose. All techniques of this section will be used to improve the behavior of the ARA applied to quantile-constrained problems. It can be observed in (S-Q) that the scenario-based approximation of $\mathbb{Q}[c_t^\top x]$ has more influence on the size of the resulting optimization problem compared to the approximation of $\mathbb{E}[c_t^\top x]$. Hence, the solution techniques are designed to simplify the computational aspects related to the quantile part of the objective function.

4.2.1 Valid Inequalities

Valid inequalities are commonly used to improve optimization solver performance; see, e.g., Wolsey (1998).

We focus on obtaining lower bounds on the variable q_t. For the ease of notation, we omit the index t if there is no possible ambiguity. In what follows, we set $p(\bar{\mathcal{S}}) := \sum_{s\in\bar{\mathcal{S}}} p^s$ and $c_i(\bar{\mathcal{S}}) := \sum_{s\in\bar{\mathcal{S}}} p^s c_i^s$ for $\bar{\mathcal{S}} \subseteq \mathcal{S}$. Moreover, for a subset $\bar{\mathcal{S}} \subseteq \mathcal{S}$, we define

$$b_i(\bar{\mathcal{S}}) := \min_w \left\{ \sum_{s\in\mathcal{S}\setminus\bar{\mathcal{S}}} c_i^s w^s : \sum_{s\in\mathcal{S}\setminus\bar{\mathcal{S}}} w^s = \tau - p(\bar{\mathcal{S}}), 0 \leq w^s \leq p^s, s \in \mathcal{S}\setminus\bar{\mathcal{S}} \right\}.$$

This new notation allows to construct two lower bounds on q.

The first lower bound uses a strong-duality property and is a specific case of the valid inequalities discussed in Kleinert et al. (2021) for bilevel optimization.

Proposition 1 (Proposition 1 in [MR3]) *The following inequality is valid for the quantile problem (4.1) for all subsets $\bar{\mathcal{S}} \subseteq \mathcal{S}$ with $p(\bar{\mathcal{S}}) < \tau$:*

$$\big(\tau - p(\bar{\mathcal{S}})\big)\, q \geq \sum_{i=1}^{N} \big(b_i(\emptyset) - c_i(\bar{\mathcal{S}})\big)\, x_i. \tag{4.2}$$

Furthermore, it can be separated in polynomial time.

The second lower bound is based on a covering argument and is a generalization of the idea proposed by Qiu et al. (2014) for the case where at most k linear inequalities among n given ones are allowed to be violated.

Proposition 2 (Proposition 2 in [MR3]) *The following inequality is valid for the quantile problem (4.1) for all subsets $\bar{\mathcal{S}} \subseteq \mathcal{S}$ with $p(\bar{\mathcal{S}}) < \tau$:*

$$\big(\tau - p(\bar{\mathcal{S}})\big)\, q \geq \sum_{i=1}^{N} b_i(\bar{\mathcal{S}}) x_i. \tag{4.3}$$

Moreover, Proposition 3 in [MR3] states that, when we fix $p(\bar{\mathcal{S}})$, the separation problem for the inequalities in (4.3) is NP-hard even in the special case where $p^s = 1/|\mathcal{S}|$ for all $s \in \mathcal{S}$, $\tau = k/|\mathcal{S}|$ with $k \in \mathbb{N}^+$, and $c_i^s \in \{0, 1\}$.

Finally, Proposition 4 in [MR3] shows that the inequalities in (4.3) are stronger than the inequalities in (4.2). More specifically, for a predetermined $\bar{\mathcal{S}} \in \mathcal{S}$, Inequality (4.3) dominates Inequality (4.2). Consequently, this suggests to use the separation procedure for Inequality (4.2) but to add the corresponding stronger inequality (4.3).

4.2.2 Clustering

In practice, when considering a set of scenarios $\mathcal{S}_t$ that allows for representative approximation of $\mathbb{Q}[c_t^\top x]$ for all $t \in \mathcal{T}$, we obtain an optimization problem for which state-of-the-art optimization solvers struggle to close the gap. If this is the case, we can reduce the size of the resulting optimization problem by introducing a clustering of all scenario sets. In addition, if we are given a solution $x \in X$, we observe that when we solve (4.1) to optimality, at least one of the Constraints (4.1b) associated to a specific scenario $\tilde{s} \in \mathcal{S}_t$ will be binding. This means that the value of $(c_t^{\tilde{s}})^\top x$ equals q_t and shows that the other scenarios may not need to be considered individually but can be clustered. In the following, we describe two ways of getting the cost vectors associated to a cluster and highlight the properties of the resulting clustered optimization problems.

More precisely, let $\mathcal{C}_t$ be a partition of $\mathcal{S}_t$ into $K_t \leq |\mathcal{S}_t|$ nonempty clusters. Each cluster $\gamma \in \mathcal{C}_t$ has a cost vector c_t^γ and a probability p_t^γ. The probability p_t^γ of cluster $\gamma \in \mathcal{C}_t$ is given by

$$p_t^\gamma = \sum_{s \in \gamma} p_t^s,$$

such that

$$\sum_{\gamma \in \mathcal{C}_t} p_t^\gamma = 1$$

holds.

We consider two strategies to associate a cost vector to a cluster of scenarios. First, the average scenario clustering (ASC) associates with each cluster $\gamma \in \mathcal{C}_t$ a cost vector c_t^γ that is defined as follows:

$$(c_t^\gamma)_i = \frac{1}{|\gamma|} \sum_{s \in \gamma} (c_t^\gamma)_i, \quad i \in N.$$

Let us indicate with $\mathcal{C}_t^{\text{ASC}}$ the corresponding clustering of scenarios. The ASC hence creates a representative scenario by taking the centroid of the cluster, as is classically done in the well-known MSSC problem, initially proposed in MacQueen (1967) and Lloyd (1982).

Second, the minimum scenario clustering (MSC) associates with each cluster $\gamma \in \mathcal{C}_t$ a cost vector c_t^γ that is defined as

$$(c_t^\gamma)_i = \min \left\{ (c_t^\gamma)_i \colon s \in \gamma \right\}, \quad i \in N.$$

Let us indicate with $\mathcal{C}_t^{\text{MSC}}$ the corresponding clustering of scenarios.

With the the help of the ASC and the MSC, we can state a series of propositions that provide tools for approximating the objective function value of any global optimal solution of (S-Q) on $\mathcal{S}_t$.

Proposition 3 (Proposition 7 in [MR3]) *Let x^* be an optimal solution of Problem (S-Q) solved on the scenario set $\mathcal{S}_t$ and let x^*_{ASC} as well as x^*_{MSC} denote optimal solutions of Problem (S-Q) solved on the scenarios set $\mathcal{C}_t^{ASC}$ and $\mathcal{C}_t^{MSC}$, respectively. For a vector $x \in X$, let $v(x)$ and $v_{MSC}(x)$ denote the objective value of (S-Q) w.r.t. x and defined over $\mathcal{S}_t$ and $\mathcal{C}_t^{MSC}$, respectively. Then,*

$$v_{MSC}(x^*_{MSC}) \leq v(x^*) \leq \min\{v(x^*_{ASC}), v(x^*_{MSC})\}$$

holds.

Proposition 3 shows that there exists a way of bounding $v(x^*)$ when we are given a clustering of $\mathcal{C}_t$ of $\mathcal{S}_t$ for all $t \in \mathcal{T}$. Additionally, it highlights that the clustering described by $\mathcal{C}_t$ strongly influences the tightness of the bounds. As discussed in Corollary 1 of [MR3], if $v_{\text{MSC}}(x^*_{\text{MSC}})$ equals $\min\{v(x^*_{\text{ASC}}), v(x^*_{\text{MSC}})\}$ for a given clustering, it holds that either x^*_{ASC} or x^*_{MSC} is an optimal solution of (S-Q) solved on the scenario set $\mathcal{S}_t$.

Furthermore, the MSC can be strengthened with the following proposition.

Proposition 4 *Let $\mathcal{C}_t^{MSC}$ be given for a specific $t \in \mathcal{T}$ and let γ be a cluster in $\mathcal{C}_t^{MSC}$ such that $p_t^\gamma > 1 - \tau$ holds. Then, in Problem (4.1) defining the quantile for t, it holds*

$$y_t^\gamma = 1$$

and the resulting inequality (4.1b) is dominated by the valid inequality (4.3) for $\bar{\mathcal{S}} = \mathcal{S}_t \setminus \gamma$.

From Proposition 4 we therefore know that, given the set

$$\mathcal{B} := \left\{\gamma \in \mathcal{C}_t^{\text{MSC}} : p_t^\gamma > 1 - \tau\right\},$$

we can replace the quantile constraint (4.1b) associated to $\gamma \in \mathcal{B}$ by the valid inequality (4.3) applied to the set $\mathcal{S}_t \setminus \gamma$, in (S-Q) solved on the scenario sets $\mathcal{C}_t^{\text{MSC}}$. Moreover, Constraint (4.1c) reduces to

$$\sum_{\gamma \in \mathcal{C}_t^{\text{MSC}} \setminus \mathcal{B}} y_t^\gamma p_t^\gamma \geq \tau - \sum_{\gamma \in \mathcal{B}} p_t^\gamma.$$

We denote by MSC$^+$ the resulting optimization problem. By construction, we thus have that

$$v_{\text{MSC}}(x^*_{\text{MSC}}) \leq v_{\text{MSC}^+}(x^*_{\text{MSC}^+}) \leq v(x^*)$$

holds.

At last, we highlight that clustering is a very popular topic in the field of optimization. Therefore, many ways of obtaining the set of clusters $\mathcal{C}_t$ exist, see, e.g., the doctoral thesis of Moreira Costa (2022) that discusses the results of Burgard et al. (2022b), Moreira Costa et al. (2022), and Burgard et al. (2022a). In the following, we focus on applying the ARA ideas of Chapter 2 to design clusters $\mathcal{C}_t$ that yield smaller sized (S-Q) instances. The algorithmic ideas of ARAs are well suited for setting up a series of smaller-size clustered problems that can result in tight bounds on $v(x^*)$. In fact, after each iteration, the ARA yields a solution $x \in X$ that will be used to improve the clustering in the next iteration. As a consequence, this allows to focus on the important scenarios that influence the quantile estimation w.r.t. the solution x, i.e., the scenarios for which Constraint (4.1b) is binding if we solve (S-Q) with $\mathcal{S}_t$ and fix x. Finally, the ARA makes it possible to easily integrate the upper and lower bound computation given by $\mathcal{C}_t^{\text{MSC}^+}$ and $\mathcal{C}_t^{\text{ASC}}$ as will be seen later.

4.3 Adaptive Scenario Clustering Algorithm

The adaptive scenario clustering algorithm from [MR3] is now described. Here, we rely on the ARA of Chapter 2 to set up a sequence of refined clusters $\mathcal{C}_t$ that continuously improve in approximating $\mathcal{S}_t$ until a global optimal solution of (Q) is found. To achieve this, the ARA of this chapter is modified to consider the ASC and MSC$^+$ clusterings that yield bounds on the objective function value of any global optimal solution of (Q), as described in Proposition 3.

Hence, we first show that the ARA can be applied to (Q). Then, the ARA components are discussed and the structure of the algorithm is described.

4.3.1 Discussion of the Model

Before applying Algorithm 1 of Section 2.4.5 to quantile-constrained problems, we show that it can be applied. To do so we rewrite (Q) as (G) and show that (Q) satisfies the assumptions stated in Section 2.1.

We start by showing that (Q) can be reformulated as (G). To this end, we set $u = x$, $w_t = q_t$ for all $t \in \mathcal{T}$ and we introduce $w = (w_1, \ldots, w_{|\mathcal{T}|})^\top$. Then, the constraint $q_t - \mathbb{Q}[c_t^\top x] = 0$ can be written as $h_t(u, w_t) = 0$ for all $t \in \mathcal{T}$. By setting $J = \mathcal{T}$ and $I = \emptyset$, we obtain (Q) reformulated as (G). It can be observed that, in the quantile-constrained case, w.l.o.g., the set of variables $w_{\alpha+1}$ is discarded from (G). Similarly, $I = \emptyset$, thus discarding the constraints $g_i(u, w) = 0$ from (G).

If we set $z_t = (y_t^1, \ldots, y_t^{|\mathcal{C}_t|})^\top$ we may write Constraints (4.1b) and (4.1c) as $\tilde{h}_{t,k}(u, w_t, z_t) \geq 0$, with $k \in K(t) \subseteq \mathbb{N}$ and $|K(t)| = |\mathcal{C}_t| + 1$ for all $t \in \mathcal{T}$. Then, by introducing slack variables for every $k \in K(t)$ and adding them to z_t for all $t \in \mathcal{T}$, the constraints can be rewritten as $\tilde{h}_{t,k}(u, w_t, z_t) = 0$. Additionally, the set Z describes the positivity of the newly introduced slack variables. Hence, for all $t \in \mathcal{T}$, we have replaced the constraint $h_t(u, w_t) = 0$ by a set $K(t)$ of discretization constraints $\tilde{h}_{t,k}(u, w_t, z_t) = 0$.

Next, we discuss why (Q) satisfies the assumptions stated in Section 2.1 about (G). First, unless the mathematical expression of the $\mathbb{Q}$ operator is known, which is rarely the case in practice, the function h_t satisfy Assumption 1. Second, Assumption 2 holds if two conditions are met. The first condition states that the global optimal objective function value of (4.1) over the precomputed set of scenarios $\mathcal{S}_t$ exactly equals the value of the real quantile $\mathbb{Q}[c_t^\top x]$ for any $x \in X$. This condition is quite strong but, e.g., holds when $\mathcal{S}_t$ is shown to be large enough w.r.t. the probability distribution of c_t. For every solution $x \in X$ and for every $t \in \mathcal{T}$ the second condition states that the associated value of variable q_t coming from (S-Q) always is the global optimal solution of (4.1). As explained in Section 4.1 this global optimal value for q_t can be computed in polynomial time in a post-processing step for a given $x \in X$. Then, if both conditions are met, Assumption 2 is satisfied if we keep increasing the size of the clusters until $\mathcal{C}_t = \mathcal{S}_t$ for all $t \in \mathcal{T}$, i.e., when we consider (S-Q) over the entire scenario set. Indeed, if $\mathcal{C}_t = \mathcal{S}_t$ for all $t \in \mathcal{T}$, we know from the first condition that the global optimal objective function value of the scenario-based approximation results in the exact value for $\mathbb{Q}[c_t^\top x]$ and from the second condition that we compute it correctly.

Thus, we may now apply the ARA of Chapter 2 to (Q). In the next sections the ARA is tweaked to result in a global optimal solution of (Q) with the use of Proposition 3. We first present the individual components of the ARA that we consider and then give a detailed description of the algorithm.

4.3.2 Components of the Algorithm

We now summarize each component of the ARA considered in this chapter.

Because the expression of (4.1b) is linear, we restrain from setting up a model catalog.

Next, we define the error measures by declining the concepts of Section 2.4.2 to the problem that we consider. Suppose that (S-Q) is solved over a clustering $\mathcal{C}_t$ for all $t \in \mathcal{T}$ and let $(\tilde{u}, \tilde{w}) \in U \times W$ be the resulting solution. In addition, let $\tilde{x}$ and $\tilde{q}_t$ be the decision variables and the value of the estimated quantile recomputed

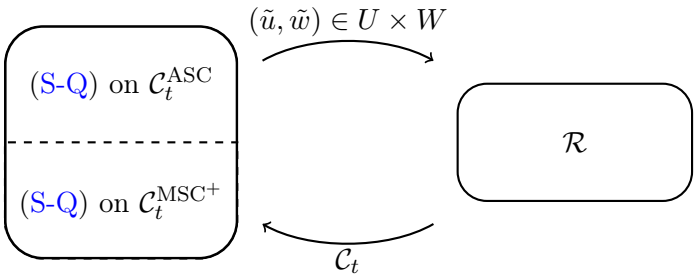

Figure 4.1: State diagram of Algorithm 1 tailored to solving quantile-constrained optimization problems to global optimality. The state on the left-hand side is split into an upper-bound phase, i.e., we solve (S-Q) on $\mathcal{C}_t^{\text{ASC}}$, and a lower-bound phase, i.e., we solve (S-Q) on $\mathcal{C}_t^{\text{MSC}^+}$.

with (4.1) using $\mathcal{C}_t$ and $x = \tilde{x}$, respectively. Then, it holds that the reformulation of the exact total error (2.4) over variable q_t yields

$$\nu_a(\tilde{u}, \tilde{w}) := |\mathbb{Q}[c_t^\top \tilde{x}] - \tilde{q}_t|.$$

Moreover, the exact value of $\mathbb{Q}[c_t^\top \tilde{x}]$ can be computed because the first condition in Section 4.3.1 states that it is equal to the optimal solution of (4.1) with $\mathcal{S}_t$ and $x = \tilde{x}$.

We remark that in [MR3], no discretization and model error are introduced because no model catalog is needed.

In the same way as in Section 3.4.5 the marking strategies are based on Dörfler's rule, see Nochetto et al. (2009, p. 93), for selecting the subset of $\mathcal{R} \subseteq \mathcal{T}$ to be re-clustered. The switching strategies use the solution of the previous ARA iteration to split a subset of $\mathcal{C}_t$ that is considered in the previous ARA iteration. This splitting is done using kernel density estimation (KDE), as described in Silverman (1986). The interested reader is referred to point one of Remark 1 in [MR3] for a detailed description of how KDE is used for cluster splitting.

4.3.3 Description of the Algorithm

Figure 4.1 specifies the state diagram of Figure 2.3 discussed in Section 2.4.5 by adding the additional notation and ARA extensions that we consider in this chapter.

Hence, we now describe the ARA that we consider through the description of the state diagram of Figure 4.1. The algorithm iteratively solves a version of (S-Q) over a clustering $\mathcal{C}_t$, yielding a solution $(\tilde{u}, \tilde{w}) \in U \times W$. With this solution, the algorithm refines the existing clustering with switching strategy $\xi_{\mathcal{R}}$ for a subset $\mathcal{R} \subseteq \mathcal{T}$ that is selected with marking strategy $\sigma_{\mathcal{R}}$. Problem (S-Q) is then solved on this new clustering and the process is repeated until the stopping criterion is reached.

Because ε-feasibility can be achieved in a polynomial-time post processing step, the algorithm instead focuses on improving the clusterings with the goal of obtaining a global optimal solution. In other words, we now look for decision variables $\tilde{u}$ that are provably globally optimal for (Q). Hence, three conceptual differences exist compared to the original ideas presented in Chapter 2. The first difference, as

Algorithm 3: Adaptive refinement algorithm extended with an upper-and lower-bound phase.

Input: error tolerance $\varepsilon > 0$, marking strategy $\sigma_{\mathcal{R}}$, improvement rule $\xi_{\mathcal{R}}$
Output: ε-optimal solution u_{UB} of (S-Q) on $\mathcal{S}_t$

foreach $t \in \mathcal{T}$ **do**
  Initialize $\mathcal{C}_t^0 \leftarrow \{\mathcal{S}_t\}$
Set $v_{\text{UB}} \leftarrow +\infty$, $v_{\text{LB}} \leftarrow -\infty$, and $\kappa \leftarrow$ true
for $k = 0, 1, \ldots$ **do**
  if κ **then**
    $(\tilde{u}, \tilde{w}, \tilde{z})^k \leftarrow$ Solve (S-Q) on $\mathcal{C}_t^{\text{ASC},k}$
    if $v(\tilde{u}) < v_{UB}$ **then**
      set $u_{\text{UB}} \leftarrow \tilde{u}$ and $v_{\text{UB}} \leftarrow v(\tilde{u})$
    else
      set $\kappa \leftarrow$ false.
  else
    $(\tilde{u}, \tilde{w}, \tilde{z})^k \leftarrow$ Solve (S-Q) on $\mathcal{C}_t^{\text{MSC}^+,k}$
    if $v_{MSC^+}(\tilde{u}) > v_{LB}$ **then**
      set $u_{\text{LB}} \leftarrow \tilde{u}$ and $v_{\text{LB}} \leftarrow v_{\text{MSC}^+}(\tilde{u})$
    else
      set $\kappa \leftarrow$ true
    if $v(\tilde{u}) < v_{UB}$ **then**
      set $u_{\text{UB}} \leftarrow \tilde{u}$ and $v_{\text{UB}} \leftarrow v(\tilde{u})$
  if $(v_{UB} - v_{LB})/v_{UB} \leq \varepsilon$ **then**
    return u_{UB}
  Compute set $\mathcal{R}^k$ according to $\sigma_{\mathcal{R}}$
  foreach $t \in \mathcal{R}^k$ **do**
    Refine $\mathcal{C}_t^k$ according to $\xi_{\mathcal{R}}$, yielding $\mathcal{C}_t^{k+1}$

discussed previously, is that no model switching is carried out and it is therefore removed from the state on the right-hand side of Figure 4.1. Second, an upper-and lower-bound phase are added to the algorithm. Depending on the considered phase, the algorithm solves (S-Q) on $\mathcal{C}_t^{\text{ASC}}$ or on $\mathcal{C}_t^{\text{MSC}+}$. The state diagram of Figure 4.1 highlights this by splitting the left-hand side state in an upper-and lower-bound phase. Finally, the most important difference is the stopping criterion that we use. For the case of quantile-constrained optimization problems we keep the value of the best found upper bound v_{UB} and the value of best found lower bound v_{LB}. Then, for a given $\varepsilon > 0$, we stop the algorithm if $(v_{\text{UB}} - v_{\text{LB}})/v_{\text{UB}} \leq \varepsilon$, i.e., when ε-global optimality is achieved.

Algorithm 3 describes the detailed functioning of the ARA that is considered for

solving quantile-constrained optimization problems. We now shortly point at the aforementioned parts that compose the algorithm. The initial clusters $\mathcal{C}_t^0$, the upper bound v_{UB}, the lower bound v_{LB}, and the Boolean parameter κ are initialized in Lines 1–3. Afterward, the main for-loop of the ARA is started in Line 4. Here, κ indicates if the ASC or MSC$^+$ is considered. Once a clustering is selected, the model is solved, either with the goal of decreasing the best found upper bound v_{UB} in Lines 6–10 or with the goal of increasing the best found lower bound v_{LB} in Lines 12–18. Then, the algorithm inverts κ if the value of the bound respective to the current phase is not improved. Thus, switching the focus of the next ARA iteration on the opposite bound. We additionally remark that, when the MSC$^+$ is selected, we also check if the resulting solution $\tilde{u}$ increases the value of v_{LB} as described in Proposition 3. Ultimately, the ε-global optimality stopping criterion that compares v_{UB} and v_{LB} is computed in Line 19. Unless the algorithm is stopped there, a selection of clusters inside $\mathcal{C}_t$ are split with KDE, for every $t \in \mathcal{R} \subseteq \mathcal{T}$, in Lines 21–23. Moreover, the second item of Remark 1 in [MR3] describes a set of improvements that increase the computational performances of the algorithm.

Finally, it can be shown that Algorithm 3 finitely terminates at an ε-global optimal solution of (S-Q) solved on $\mathcal{S}_t$, i.e., at an ε-global optimal solution of (Q) if the conditions of Section 4.3.1 are satisfied, as long as the size of $\mathcal{C}_t^k$ keeps increasing.

Theorem 2 (Theorem 1 in [MR3]) *Let u^* be an optimal solution of Problem (Q) and let $v(u^*)$ be its value. Moreover, let $\mathcal{C}_t^k$ be the clustering of $\mathcal{S}_t$ for index $t \in \mathcal{T}$ in iteration k. Suppose further that there exists an index $t \in \mathcal{T}$ such that*

$$|\mathcal{C}_t^k| > |\mathcal{C}_t^{k-1}|$$

for all iterations k. Then, Algorithm 3 terminates after a finite number of cluster refinements with a point $\tilde{u} \in U$ such that

$$\frac{v(\tilde{u}) - v(u^*)}{v(\tilde{u})} \leq \varepsilon.$$

4.4 Numerical Results

The preliminary solution techniques of Section 4.2 along with the ASCA of Section 4.3 are now compared with each other. For the sake of conciseness, we restrict to presenting the results of the maintenance planning problem instances. The interested reader is therefore referred to Section 6.2 of [MR3] for the numerical results of the portfolio optimization problem. Moreover, we highlight the results of the maintenance planning problem by only considering the semi-final instances of the EURO/ROADEF challenge 2020 as they are sufficient for describing how the aforementioned methods behave on the complete instance set. The characteristics of the EURO/ROADEF challenge 2020 instances are displayed in Table 1 of [MR3]. We refer to the beginning of Section 6 in [MR3] for a discussion about additional notation, implementation details, hardware setup, and software setup that we use.

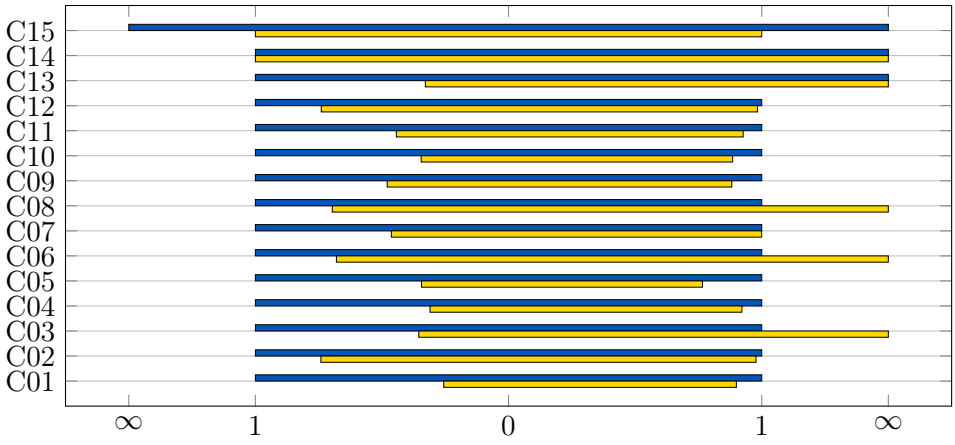

Figure 4.2: Bar plot for $\min_{m' \in \mathcal{M}'}\{v_{\mathrm{LB}}^{m'} \colon v_{\mathrm{LB}}^{m'} > 0\}/v_{\mathrm{LB}}^{m}$ (left side) and $v_{\mathrm{UB}}^{m}/\max_{m' \in \mathcal{M}'}\{v_{\mathrm{UB}}^{m'} \colon v_{\mathrm{UB}}^{m'} < \infty\}$ (right side), where $\mathcal{M}'$ is composed of MILP (blue) and $\mathrm{MILP}_{\mathrm{VI}^*}$ (yellow).

Before discussing the results, we draw attention to the fact that no instance is solved to global optimality within the allocated time of 90 minutes for any of the considered methods. Hence, we shortly explain how the bar plots of Figures 4.2–4.5 are created, that allow to visually compare the effect of the methods on the value of v_{UB} and v_{LB}. Let $\mathcal{M}'$ be the subset of methods considered in the bar plot. Then, for all $m \in \mathcal{M}'$ the bar plots show the re-scaled value of v_{LB}^{m} (left side) and v_{UB}^{m} (right side) on all instances. The bars' lengths are determined as follows. The left side of the bar plots is equal to $\min_{m' \in \mathcal{M}'}\{v_{\mathrm{LB}}^{m'} \colon v_{\mathrm{LB}}^{m'} > 0\}/v_{\mathrm{LB}}^{m}$. The numerator $\min_{m' \in \mathcal{M}'}\{v_{\mathrm{LB}}^{m'} \colon v_{\mathrm{LB}}^{m'} > 0\}$ takes the value of the smallest lower bound obtained by the methods in $\mathcal{M}'$ while ignoring a lower bound if the method m' does not improve on $v_{\mathrm{LB}}^{m'} = 0$. We apply a similar rule for the right side of the bar plots using $v_{\mathrm{UB}}^{m}/\max_{m' \in \mathcal{M}'}\{v_{\mathrm{UB}}^{m'} \colon v_{\mathrm{UB}}^{m'} < \infty\}$. Here, $\max_{m' \in \mathcal{M}'}\{v_{\mathrm{UB}}^{m} \colon v_{\mathrm{UB}}^{m'} < \infty\}$ takes the value of the largest upper bound obtained by the two compared methods without considering $v_{\mathrm{UB}}^{m'}$ if no incumbent is found during the solution process of m'.

Thus, we begin the comparison by considering the generic MILP with the $\mathrm{MILP}_{\mathrm{VI}^*}$, i.e., the MILP enriched with the valid inequalities of Proposition 2, in Figure 4.2. For the majority of the instances we observe that the valid inequalities have a strong influence on v_{UB} as well as v_{LB} where the biggest impact can be observed on the value of time limit. Most likely, this has two reasons. First, additional time is needed to separate violated inequalities in the first node of the branch-and-bound tree. Second, the model relaxations are harder to solve after adding valid inequalities due their increased size.

Consequently, we decided to add an initial heuristic to overcome this effect. More specifically, in Section 4 of [MR3] we propose an Overlapping Alternating Direction Method (OADM) for finding primal solutions to (S-Q). Hence, we use the notation $\mathrm{MILP}_{\mathrm{VI}^*}^{\mathrm{OADM}}$ when we refer to $\mathrm{MILP}_{\mathrm{VI}^*}$ enhanced with an initial OADM heuristic. Figure 4.3 then compares $\mathrm{MILP}_{\mathrm{VI}^*}$ and $\mathrm{MILP}_{\mathrm{VI}^*}^{\mathrm{OADM}}$ on the instances that

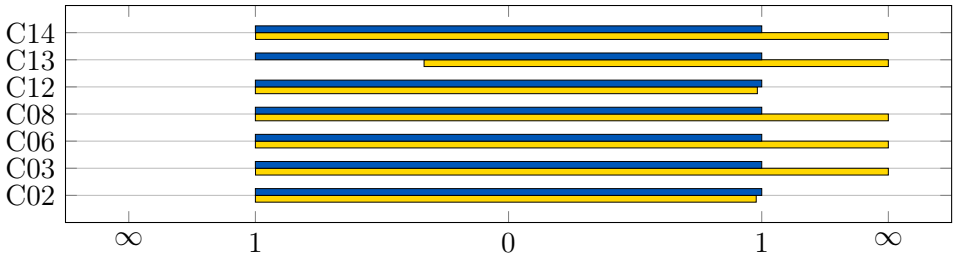

Figure 4.3: Bar plot for $\min_{m' \in \mathcal{M}'}\{v_{\mathrm{LB}}^{m'} \colon v_{\mathrm{LB}}^{m'} > 0\}/v_{\mathrm{LB}}^{m}$ (left side) and $v_{\mathrm{UB}}^{m}/\max_{m' \in \mathcal{M}'}\{v_{\mathrm{UB}}^{m'} \colon v_{\mathrm{UB}}^{m'} < \infty\}$ (right side), where $\mathcal{M}'$ is composed of $\mathrm{MILP}_{\mathrm{VI}^*}^{\mathrm{OADM}}$ (blue) and $\mathrm{MILP}_{\mathrm{VI}^*}$ (yellow). Only the instances with a significant difference in the results for v_{LB} and v_{UB} are displayed.

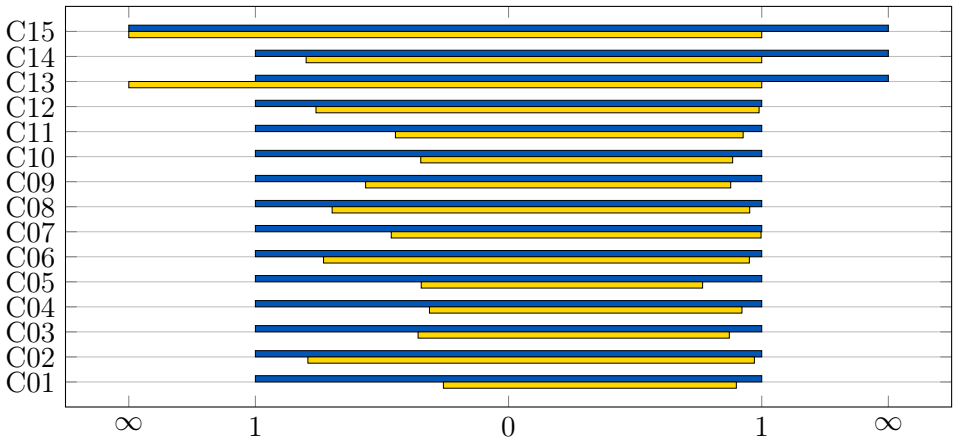

Figure 4.4: Bar plot for $\min_{m' \in \mathcal{M}'}\{v_{\mathrm{LB}}^{m'} \colon v_{\mathrm{LB}}^{m'} > 0\}/v_{\mathrm{LB}}^{m}$ (left side) and $v_{\mathrm{UB}}^{m}/\max_{m' \in \mathcal{M}'}\{v_{\mathrm{UB}}^{m'} \colon v_{\mathrm{UB}}^{m'} < \infty\}$ (right side), where $\mathcal{M}'$ is composed of MILP (blue) and ASCA (yellow).

show a significant difference in the results for v_{LB} and v_{UB}. It can be observed that the OADM finds an upper bound for every problematic instance. Nevertheless, e.g., for instance C02, the OADM is not competitive compared to $\mathrm{MILP}_{\mathrm{VI}^*}$ on v_{UB}. Moreover, the OADM has a negative influence on the value of v_{LB} for instance C13. This is explained by the fact that the time spent in one OADM iteration is rather long–hence harming the impact of the valid inequalities on v_{LB}.

Next, Figure 4.4 compares the results of the generic MILP with the ASCA. The ASCA clearly outperforms the generic MILP both in terms of upper and lower bound. But, in the case of instances C13 and C15, the ASCA does not improve on the lower bound $v_{\mathrm{LB}} = 0$. In fact, the ASCA keeps improving v_{UB} using the ASC problem during the initial iterations of the algorithm. Since v_{UB} keeps decreasing in every iteration, ASCA never enters the MSC^{+} problem before reaching the given time limit. It can therefore also be observed that the ASCA always finds a better upper bound compared to the generic MILP.

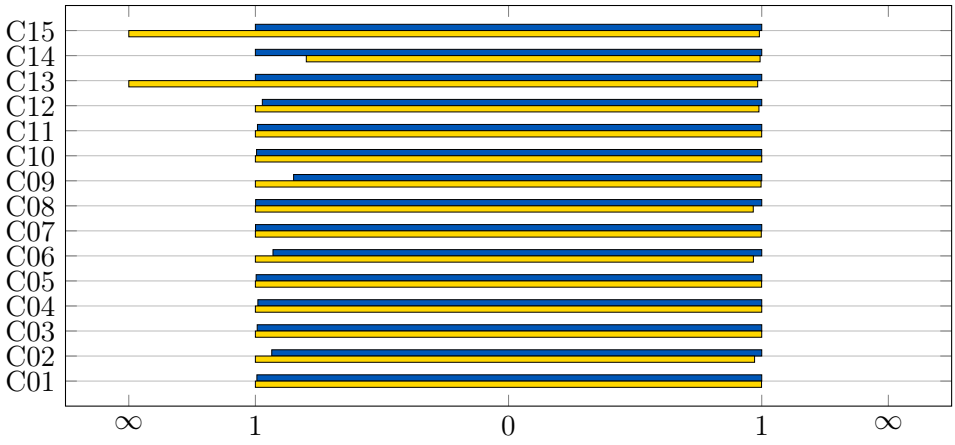

Figure 4.5: Bar plot for $\min_{m' \in \mathcal{M}'}\{v_{\mathrm{LB}}^{m'} \colon v_{\mathrm{LB}}^{m'} > 0\}/v_{\mathrm{LB}}^{m}$ (left side) and $v_{\mathrm{UB}}^{m}/\max_{m' \in \mathcal{M}'}\{v_{\mathrm{UB}}^{m'} \colon v_{\mathrm{UB}}^{m'} < \infty\}$ (right side), where $\mathcal{M}'$ is composed of $\mathrm{MILP}_{\mathrm{VI}^*}^{\mathrm{OADM}}$ (blue) and ASCA (yellow).

Finally, the two winner methods, i.e., $\mathrm{MILP}_{\mathrm{VI}^*}^{\mathrm{OADM}}$ and ASCA, are compared in Figure 4.5. Both methods result in values for v_{UB} and v_{LB} that are close to each other. Considering the values of v_{LB}, we see that $\mathrm{MILP}_{\mathrm{VI}^*}^{\mathrm{OADM}}$ always slightly outperforms ASCA except for the instance C14. The opposite situation occurs when the two configurations are compared w.r.t. the values of v_{UB}.

5 Conclusion

We now conclude Part I of this thesis by discussing the challenges that we solved as well as some future research avenues.

In Chapter 2, we presented a generalized framework for applying ARAs to energy network optimization problems. This framework ties together the ideas considered in the papers that make up this cumulative thesis. More specifically, the objective of this chapter is to pave the way for future works that propose a general theory for ARAs applied to energy network applications.

The theoretical analysis of the proposed framework is a topic of future research. Given the assumptions about the general model, we could, e.g., study the finite termination of the generalized ARA at ε-feasible points. Moreover, we did not combine the coarsening and down-switching step extension from Chapter 3 and the lower bound extension from Chapter 4. The resulting ARA would consider optimization problems that stay solvable in a reasonable amount of time while being parameterized to reach the optimal objective value of the original problem.

Afterward, we highlighted the versatility of the framework by demonstrating the applicability of the generalized ARA to two entirely different energy network optimization problems. The stationary operation of district heating networks is considered in Chapter 3. A model is presented and reformulated to fit into the generalized framework. Then, the same model is specified to respectively coincide with the models considered in [MR1] and [MR2], respectively.

For the case of [MR1], a surrogate function is fitted to approximate the nonlinear internal energy density equation. Moreover, expansion decisions are added to the model, which yields a nonconvex MINLP. A test case is constructed that allows to identify the three parameters that influence the expansion decision making: the estimated power demand of the candidate consumer, the distance of the candidate consumer to the existing network, and the thermal losses of the pipes. Here, one could extend the framework for DHNs with cycles in the forward and backward flow network. This would naturally require additional modeling and hence would increase

the time needed to solve the model. If this extension is considered, it might be possible to identify additional parameters that drive the expansion decision making. Some authors have considered the case with cycles by abstracting from other difficulties that are considered in [MR1]; see, e.g., Bordin et al. (2016) and Blommaert et al. (2018).

For the case of [MR2], the operational optimization problem is enhanced by a second-order polynomial state equation yielding a nonconvex NLP with complementarity constraints. Hence, in [MR2] the focus is on obtaining accurate ε-feasible controls for stationary operation of DHNs. The effect of the generalized ARA is studied and extended with a coarsening and a model down-switching step. Two test cases are used to produce the ARA results. For both instances, the ARA terminates at an ε-feasible solution. However, this is not the case for larger networks because the nonlinear solvers converge to infeasible points. Nevertheless, we observe that the ARA outperforms NLP optimization solvers. In fact, the NLP solvers do not yield any feasible solution for the degree of accuracy that the ARA provides. Moreover, the influence of using exact errors and error estimates is studied. We observe that the benefit of using exact errors is small. Yet, the results obtained with exact errors yield optimization models with constraints that have less nonlinear terms in comparison with the error estimates results.

In fact, the main reason that prevents the ARA from solving the operational optimization problem on larger networks are the internal energy density mixing equations. If we were able to predict the flow directions of the pipes inside the network this would highly strengthen the ARA approach. One could, e.g., set up a preprocessing step that extracts flow directions using the Euler equations of the pipes and the demand of the consumers. If this approach does not work, machine learning techniques could be used instead. Machine learning has successfully been applied to similar tasks arising in the power systems literature, see, e.g., Pineda et al. (2020) or Chatzos et al. (2022) and might therefore be a good candidate for predicting flow directions.

Another important topic that has not been discussed in this thesis is the transient dynamics that govern the behavior of the water. By removing the stationary assumption, the operational optimization problem becomes much harder to solve. Model order reduction (MOR) techniques, as discussed in Brunton and Kutz (2022), are a tool to bypass this challenge. There exist research that combines MOR and PDE constrained optimization; see, e.g., the survey by Benner et al. (2014). Moreover, in the recent works by Egger et al. (2018), Himpe et al. (2021), and Liljegren-Sailer and Marheineke (2022b), MOR methods for the damped wave equation and the Euler equations on networks are studied. These works focus on the preservation of port-Hamiltonian structures. The port-Hamiltonian paradigm, see, e.g., Schaft and Jeltsema (2014) or the discussion in Beattie et al. (2017), intuitively couples systems from different physical domains through energy exchange. We also refer to Hauschild and Marheineke (2021), Mehrmann et al. (2018a) and Liljegren-Sailer and Marheineke (2022a) for the modeling and approximation of energy networks in port-Hamiltonian form. Consequently, this progress opens the door to adaptive MOR for port-Hamiltonian formulations of energy transport.

Finally, in Chapter 4 we summarize the results of [MR3] where quantile-constrained optimization problems are considered. As a first step towards solving such problems, we define the scenario-based quantile-constrained optimization problem. This scenario-based model approximates the original quantile-constrained optimization problem and is an MILP for the examples that are presented. Then, solution techniques are developed for solving the scenario-based problem; valid inequalities and clustering of the scenarios. Afterward, the connection between the generalized ARA framework and the quantile-constrained optimization is presented. We tweak the ARA to the problem at hand and extend it with a complementary lower bound step. This new algorithm is called the adaptive scenario clustering algorithm. We prove that the ASCA finitely terminates at an ε-global optimal solution of the original problem. Ultimately, the complete set of solution techniques are compared on a set of instances. We observe that the proposed solution methods beat the MILP solver.

In this chapter, we assumed that enough scenarios are sampled to sufficiently describe the uncertain cost vector. In practice, this assumption is rarely satisfied. Therefore, future works could study adaptive refinement of the scenario set through sampling instead of clustering. Furthermore, future research should be concerned with applying the proposed techniques to chance constraints, see, e.g., Peña-Ordieres et al. (2020). In fact, Espinoza and Moreno (2014) and Ahmed et al. (2017) proposed similar but different scenario grouping techniques for quantile and chance-constrained optimization problems, respectively.

Bibliography

Ahmed, S., J. Luedtke, Y. Song, and W. Xie (2017). "Nonanticipative duality, relaxations, and formulations for chance-constrained stochastic programs". In: *Mathematical Programming* 162.1-2, Ser. A, pp. 51–81. DOI: 10.1007/s10107-016-1029-z.

Aigner, K.-M., R. Burlacu, F. Liers, and A. Martin (2020). "Solving AC Optimal Power Flow with Discrete Decisions to Global Optimality". URL: https://opus4.kobv.de/opus4-trr154/frontdoor/index/index/year/2020/docId/323.

Alexandrov, N. M., J. E. Dennis, R. M. Lewis, and V. Torczon (Feb. 1998). "A trust-region framework for managing the use of approximation models in optimization". In: *Structural optimization* 15.1, pp. 16–23. DOI: 10.1007/BF01197433.

Aravena, I., D. K. Molzahn, S. Zhang, C. G. Petra, F. E. Curtis, S. Tu, A. Wächter, E. Wei, E. Wong, A. Gholami, K. Sun, X. A. Sun, S. T. Elbert, J. T. Holzer, and A. Veeramany (2022). *Recent Developments in Security-Constrained AC Optimal Power Flow: Overview of Challenge 1 in the ARPA-E Grid Optimization Competition*. DOI: 10.48550/ARXIV.2206.07843.

Artzner, P., F. Delbaen, J.-M. Eber, and D. Heath (1999). "Coherent measures of risk". In: *Mathematical Finance* 9.3, pp. 203–228. DOI: 10.1111/1467-9965.00068.

Babuška, I. and W. C. Rheinboldt (1977). "A-posteriori error estimates for the finite element method". In: *International Journal for Numerical Methods in Engineering* 12.10, pp. 1597–1615. DOI: 10.1002/nme.1620121010.

Bangerth, W. and R. Rannacher (2003). *Adaptive finite element methods for differential equations*. Lectures in Mathematics ETH Zürich. Birkhäuser Verlag, Basel. DOI: 10.1007/978-3-0348-7605-6.

Beattie, C., V. Mehrmann, H. Xu, and H. Zwart (2017). *Port-Hamiltonian descriptor systems*. DOI: 10.48550/ARXIV.1705.09081.

Becker, R., H. Kapp, and R. Rannacher (2000). "Adaptive finite element methods for optimal control of partial differential equations: basic concept". In: *SIAM Journal on Control and Optimization* 39.1, pp. 113–132. DOI: 10.1137/S0363012999351097.

Becker, R. and R. Rannacher (2001). "An optimal control approach to a posteriori error estimation in finite element methods". In: *Acta Numerica* 10, pp. 1–102. DOI: 10.1017/S0962492901000010.

Benati, S. and R. Rizzi (2007). "A mixed integer linear programming formulation of the optimal mean/value-at-risk portfolio problem". In: *European Journal of Operational Research* 176.1, pp. 423–434. DOI: 10.1016/j.ejor.2005.07.020.

Benders, J. F. (1962). "Partitioning procedures for solving mixed-variables programming problems". In: *Numerische Mathematik* 4, pp. 238–252. DOI: 10.1007/BF01386316.

Benner, P., E. Sachs, and S. Volkwein (2014). "Model order reduction for PDE constrained optimization". In: *Trends in PDE constrained optimization*. Vol. 165. Inter-

national Series of Numerical Mathematics. Birkhäuser/Springer, Cham, pp. 303–326. DOI: 10.1007/978-3-319-05083-6_19.

Benonysson, A., B. Bøhm, and H. F. Ravn (1995). "Operational optimization in a district heating system". In: *Energy Conversion and Management* 36.5, pp. 297–314. DOI: 10.1016/0196-8904(95)98895-T.

Berthold, H., H. Heitsch, R. Henrion, and J. Schwientek (2022). "On the algorithmic solution of optimization problems subject to probabilistic/robust (probust) constraints". In: *Mathematical Methods of Operations Research* 96.1, pp. 1–37. DOI: 10.1007/s00186-021-00764-8.

Blankenship, J. W. and J. E. Falk (1976). "Infinitely constrained optimization problems". In: *Journal of Optimization Theory and Applications* 19.2, pp. 261–281. DOI: 10.1007/BF00934096.

Blommaert, M., R. Salenbien, and M. Baelmans (2018). "An adjoint approach to thermal network topology optimization". In: *International Heat Transfer Conference Digital Library*. Begel House Inc., pp. 2081–2089. DOI: 10.1615/IHTC16.cms.024074.

Bordin, C., A. Gordini, and D. Vigo (2016). "An optimization approach for district heating strategic network design". In: *European Journal of Operational Research* 252.1, pp. 296–307. DOI: 10.1016/j.ejor.2015.12.049.

Borsche, R., M. Eimer, and N. Siedow (2019). "A local time stepping method for thermal energy transport in district heating networks". In: *Applied Mathematics and Computation* 353, pp. 215–229. DOI: 10.1016/j.amc.2019.01.072.

Bracco, S., G. Dentici, and S. Siri (2013). "Economic and environmental optimization model for the design and the operation of a combined heat and power distributed generation system in an urban area". In: *Energy* 55, pp. 1014–1024. DOI: 10.1016/j.energy.2013.04.004.

Brunton, S. L. and J. N. Kutz (2022). *Data-driven science and engineering—machine learning, dynamical systems, and control*. Second edition. Cambridge University Press. DOI: 10.1017/9781009089517.

Burgard, J. P., C. Moreira Costa, C. Hojny, T. Kleinert, and M. Schmidt (2022a). "Mixed-Integer Programming Techniques for the Minimum Sum-of-Squares Clustering Problem". URL: https://optimization-online.org/2022/03/8823/.

Burgard, J. P., C. Moreira Costa, and M. Schmidt (2022b). "Robustification of the k-means clustering problem and tailored decomposition methods: when more conservative means more accurate". In: *Annals of Operations Research*. DOI: 10.1007/s10479-022-04818-w.

Burlacu, R., H. Egger, M. Groß, A. Martin, M. E. Pfetsch, L. Schewe, M. Sirvent, and M. Skutella (2019). "Maximizing the storage capacity of gas networks: a global MINLP approach". In: *Optimization and Engineering* 20.2, pp. 543–573. DOI: 10.1007/s11081-018-9414-5.

Burlacu, R., B. Geißler, and L. Schewe (2020). "Solving mixed-integer nonlinear programmes using adaptively refined mixed-integer linear programmes". In: *Optimization Methods & Software* 35.1, pp. 37–64. DOI: 10.1080/10556788.2018.1556661.

Byrd, R. H., J. Nocedal, and R. A. Waltz (2006). "KNITRO: An integrated package for nonlinear optimization". In: *Large-scale nonlinear optimization*. Vol. 83. Nonconvex Optim. Appl. Springer, New York, pp. 35–59. DOI: 10.1007/0-387-30065-1_4.

Chatzos, M., T. W. K. Mak, and P. V. Hentenryck (2022). "Spatial Network Decomposition for Fast and Scalable AC-OPF Learning". In: *IEEE Transactions on Power Systems* 37.4, pp. 2601–2612. DOI: 10.1109/TPWRS.2021.3124726.

Chorin, A. J. and J. E. Marsden (1993). *A mathematical introduction to fluid mechanics*. Third edition. Vol. 4. Texts in Applied Mathematics. Springer-Verlag, New York. DOI: 10.1007/978-1-4612-0883-9.

Conejo, A. J., M. Carrión, and J. M. Morales (2010). *Decision Making Under Uncertainty in Electricity Markets*. Boston, MA: Springer US. DOI: 10.1007/978-1-4419-7421-1.

Dantzig, G. B. (1960). "On the significance of solving linear programming problems with some integer variables". In: *Econometrica. Journal of the Econometric Society* 28, pp. 30–44. DOI: 10.2307/1905292.

Deisenroth, M. P., A. A. Faisal, and C. S. Ong (2020). *Mathematics for machine learning*. Cambridge University Press, Cambridge. DOI: 10.1017/9781108679930.

Domschke, P., A. Dua, J. J. Stolwijk, J. Lang, and V. Mehrmann (2018). "Adaptive refinement strategies for the simulation of gas flow in networks using a model hierarchy". In: *Electronic Transactions on Numerical Analysis* 48, pp. 97–113. DOI: 10.48550/ARXIV.1701.09031.

Domschke, P., B. Hiller, J. Lang, V. Mehrmann, R. Morandin, and C. Tischendorf (2021). "Gas Network Modeling: An Overview". URL: https://opus4.kobv.de/opus4-trr154/frontdoor/index/index/docId/411.

Domschke, P., O. Kolb, and J. Lang (2015). "Adjoint-based error control for the simulation and optimization of gas and water supply networks". In: *Applied Mathematics and Computation* 259, pp. 1003–1018. DOI: 10.1016/j.amc.2015.03.029.

Duran, M. A. and I. E. Grossmann (1986). "An outer-approximation algorithm for a class of mixed-integer nonlinear programs". In: *Mathematical Programming* 36.3, pp. 307–339. DOI: 10.1007/BF02592064.

Egger, H., T. Kugler, B. Liljegren-Sailer, N. Marheineke, and V. Mehrmann (2018). "On structure-preserving model reduction for damped wave propagation in transport networks". In: *SIAM Journal on Scientific Computing* 40.1, pp. A331–A365. DOI: 10.1137/17M1125303.

Espinoza, D. and E. Moreno (2014). "A primal-dual aggregation algorithm for minimizing conditional value-at-risk in linear programs". In: *Computational Optimization and Applications* 59.3, pp. 617–638. DOI: 10.1007/s10589-014-9692-6.

Fajemisin, A., D. Maragno, and D. d. Hertog (2021). *Optimization with Constraint Learning: A Framework and Survey*. DOI: 10.48550/ARXIV.2110.02121.

Fletcher, R. and S. Leyffer (1994). "Solving mixed integer nonlinear programs by outer approximation". In: *Mathematical Programming* 66.3, Ser. A, pp. 327–349. DOI: 10.1007/BF01581153.

Gaivoronski, A. A. and G. Pflug (2005). "Value-at-Risk in Portfolio Optimization: Properties and Computational Approach". In: *Journal of Risk* 7.2, pp. 1–31. DOI: 10.21314/JOR.2005.106.

Geißler, B., A. Martin, A. Morsi, and L. Schewe (2012). "Using piecewise linear functions for solving MINLPs". In: *Mixed Integer Nonlinear Programming*. Vol. 154. The IMA Volumes in Mathematics and its Applications. Springer, New York, pp. 287–314. DOI: 10.1007/978-1-4614-1927-3_10.

Geißler, B., A. Morsi, and L. Schewe (2013). "A new algorithm for MINLP applied to gas transport energy cost minimization". In: *Facets of Combinatorial Optimization*. Springer, Heidelberg, pp. 321–353. DOI: 10.1007/978-3-642-38189-8_14.

Geoffrion, A. M. (1972). "Generalized Benders decomposition". In: *Journal of Optimization Theory and Applications* 10, pp. 237–260. DOI: 10.1007/BF00934810.

Goderbauer, S., B. Bahl, P. Voll, M. E. Lübbecke, A. Bardow, and A. M. Koster (2016). "An adaptive discretization MINLP algorithm for optimal synthesis of decentralized energy supply systems". In: *Computers & Chemical Engineering* 95, pp. 38–48. DOI: 10.1016/j.compchemeng.2016.09.008.

Gratton, S., A. Sartenaer, and P. L. Toint (2008). "Recursive trust-region methods for multiscale nonlinear optimization". In: *SIAM Journal on Optimization* 19.1, pp. 414–444. DOI: 10.1137/050623012.

Grübel, J., R. Krug, M. Schmidt, and W. Wollner (2022). "A Successive Linear Relaxation Method for MINLPs with Multivariate Lipschitz Continuous Nonlinearities with Applications to Bilevel Optimization and Gas Transport". URL: https://opus4.kobv.de/opus4-trr154/frontdoor/index/index/docId/498.

Guelpa, E., G. Mutani, V. Todeschi, and V. Verda (2018). "Reduction of CO2 emissions in urban areas through optimal expansion of existing district heating networks". In: *Journal of Cleaner Production* 204, pp. 117–129. DOI: 10.1016/j.jclepro.2018.08.272.

Gupte, A., A. M. C. A. Koster, and S. Kuhnke (2022). "An Adaptive Refinement Algorithm for Discretizations of Nonconvex QCQP". In: *20th International Symposium on Experimental Algorithms (SEA 2022)*. Vol. 233. Leibniz International Proceedings in Informatics (LIPIcs). Dagstuhl, Germany: Schloss Dagstuhl – Leibniz-Zentrum für Informatik, 24:1–24:14. DOI: 10.4230/LIPIcs.SEA.2022.24.

Haikarainen, C., F. Pettersson, and H. Saxén (2016). "A decomposition procedure for solving two-dimensional distributed energy system design problems". In: *Applied Thermal Engineering* 100, pp. 30–38. DOI: 10.1016/j.applthermaleng.2016.02.012.

Hante, F. M. and M. Schmidt (2019). "Complementarity-based nonlinear programming techniques for optimal mixing in gas networks". In: *EURO Journal on Computational Optimization* 7.3, pp. 299–323. DOI: 10.1007/s13675-019-00112-w.

Hauschild, S.-A. and N. Marheineke (2021). "Structure-preserving discretization of a port-Hamiltonian formulation of the non-isothermal Euler equations". In: *PAMM* 20.1. DOI: 10.1002/pamm.202000014.

Hauschild, S.-A., N. Marheineke, V. Mehrmann, J. Mohring, A. M. Badlyan, M. Rein, and M. Schmidt (2020). "Port-Hamiltonian modeling of district heating networks".

In: *Progress in differential-algebraic equations II*. Differential-Algebraic Equations Forum. Springer, Cham, pp. 333–355. DOI: 10.1007/978-3-030-53905-4_11.

Himpe, C., S. Grundel, and P. Benner (2021). "Model order reduction for gas and energy networks". In: *Journal of Mathematics in Industry* 11, Paper No. 13, 46. DOI: 10.1186/s13362-021-00109-4.

Hintermüller, M. and R. H. W. Hoppe (2008). "Goal-oriented adaptivity in control constrained optimal control of partial differential equations". In: *SIAM Journal on Control and Optimization* 47.4, pp. 1721–1743. DOI: 10.1137/070683891.

Hinze, M., R. Pinnau, M. Ulbrich, and S. Ulbrich (2009). *Optimization with PDE constraints*. Vol. 23. Mathematical Modelling: Theory and Applications. Springer, New York. DOI: 10.1007/978-1-4020-8839-1.

Kleinert, T., M. Labbé, F. Plein, and M. Schmidt (2021). "Closing the Gap in Linear Bilevel Optimization: A New Valid Primal-Dual Inequality". In: *Optimization Letters* 15, pp. 1027–1040. DOI: 10.1007/s11590-020-01660-6.

Koster, A. M. C. A. and S. Kuhnke (2019). "An adaptive discretization algorithm for the design of water usage and treatment networks". In: *Optimization and Engineering* 20.2, pp. 497–542. DOI: 10.1007/s11081-018-9413-6.

Krug, R., G. Leugering, A. Martin, M. Schmidt, and D. Weninger (2021a). "Time-domain decomposition for optimal control problems governed by semilinear hyperbolic systems". In: *SIAM Journal on Control and Optimization* 59.6, pp. 4339–4372. DOI: 10.1137/20M138329X.

Krug, R., V. Mehrmann, and M. Schmidt (2021b). "Nonlinear optimization of district heating networks". In: *Optimization and Engineering* 22.2, pp. 783–819. DOI: 10.1007/s11081-020-09549-0.

Lagnese, J. E., G. Leugering, and E. J. P. G. Schmidt (1994). *Modeling, analysis and control of dynamic elastic multi-link structures*. Systems & Control: Foundations & Applications. Birkhäuser Boston, Inc., Boston, MA. DOI: 10.1007/978-1-4612-0273-8.

Leugering, G., A. Martin, M. Schmidt, and M. Sirvent (2017). "Nonoverlapping domain decomposition for optimal control problems governed by semilinear models for gas flow in networks". In: *Control and Cybernetics* 46.3, pp. 191–225. URL: https://opus4.kobv.de/opus4-trr154/frontdoor/index/index/year/2017/docId/202.

Leyffer, S., A. Sartenaer, and E. Wanufelle (2008). "Branch-and-refine for mixed-integer nonconvex global optimization". URL: https://wiki.mcs.anl.gov/leyffer/images/1/15/SOS-OA-ANL.pdf.

Leykekhman, D. and B. Vexler (2016). "A priori error estimates for three dimensional parabolic optimal control problems with pointwise control". In: *SIAM Journal on Control and Optimization* 54.5, pp. 2403–2435. DOI: 10.1137/15M1028042.

Liljegren-Sailer, B. and N. Marheineke (2022a). "On port-Hamiltonian approximation of a nonlinear flow problem on networks". In: *SIAM Journal on Scientific Computing* 44.3, pp. B834–B859. DOI: 10.1137/21M1443480.

Liljegren-Sailer, B. and N. Marheineke (2022b). "On snapshot-based model reduction under compatibility conditions for a nonlinear flow problem on networks". In: *Journal of Scientific Computing* 92.2. DOI: 10.1007/s10915-022-01901-z.

Lin, C.-C. (2009). "Comments on: "A mixed integer linear programming formulation of the optimal mean/value-at-risk portfolio problem" [European Journal of Operational Research 176.1 (2007), pp. 423–434] by S. Benati and R. Rizzi". In: *European Journal of Operational Research* 194.1, pp. 339–341. DOI: 10.1016/j.ejor.2008.01.041.

Liu, F., W. W. Hager, and A. V. Rao (2015). "Adaptive mesh refinement method for optimal control using nonsmoothness detection and mesh size reduction". In: *Journal of the Franklin Institute* 352.10, pp. 4081–4106. DOI: 10.1016/j.jfranklin.2015.05.028.

Lloyd, S. P. (1982). "Least squares quantization in PCM". In: *IEEE Transactions on Information Theory* 28.2, pp. 129–137. DOI: 10.1109/TIT.1982.1056489.

Locatelli, M. and F. Schoen (2013). *Global Optimization*. Vol. 15. SIAM Series on Optimization. Society for Industrial and Applied Mathematics. DOI: 10.1137/1.9781611972672.

Lundell, A., A. Skjäl, and T. Westerlund (2013). "A reformulation framework for global optimization". In: *Journal of Global Optimization* 57.1, pp. 115–141. DOI: 10.1007/s10898-012-9877-4.

MacQueen, J. (1967). "Some methods for classification and analysis of multivariate observations". In: *Proceedings of the Fifth Berkeley Symposium on Mathematical Statistics and Probability*. University California Press, pp. 281–297. URL: https://projecteuclid.org/euclid.bsmsp/1200512992.

Mansini, R., W. Ogryczak, and M. G. Speranza (2003). "LP solvable models for portfolio optimization: a classification and computational comparison". In: *IMA Journal of Management Mathematics* 14.3, 187–220 (2004). DOI: 10.1093/imaman/14.3.187.

Markowitz, H. M. and A. S. Manne (1957). "On the Solution of Discrete Programming Problems". In: *Econometrica* 25.1, pp. 84–110. URL: http://www.jstor.org/stable/1907744.

Mehrmann, V., R. Morandin, S. Olmi, and E. Schöll (2018a). "Qualitative stability and synchronicity analysis of power network models in port-Hamiltonian form". In: *Chaos* 28.10. 101102. DOI: 10.1063/1.5054850.

Mehrmann, V., M. Schmidt, and J. J. Stolwijk (2018b). "Model and discretization error adaptivity within stationary gas transport optimization". In: *Vietnam Journal of Mathematics* 46.4, pp. 779–801. DOI: 10.1007/s10013-018-0303-1.

Mertz, T., S. Serra, A. Henon, and J. Reneaume (2017). "A MINLP optimization of the configuration and the design of a district heating network: study case on an existing site". In: *Energy Procedia* 116. 15th International Symposium on District Heating and Cooling, 4-7 September 2016, Seoul, South Korea, pp. 236–248. DOI: 10.1016/j.egypro.2017.05.071.

Misener, R. and C. A. Floudas (2014). "ANTIGONE: Algorithms for coNTinuous/Integer Global Optimization of Nonlinear Equations". In: *Journal of Global Optimization* 59.2-3, pp. 503–526. DOI: 10.1007/s10898-014-0166-2.

Molzahn, D. K. and I. A. Hiskens (2019). "A Survey of Relaxations and Approximations of the Power Flow Equations". In: *Foundations and Trends in Electric Energy Systems* 4.1-2, pp. 1–221. DOI: 10.1561/3100000012.

Moreira Costa, C. (2022). "Computational Techniques for Minimum Sum-of-Squares Clustering, Cardinality-Constrained Optimization, and Robust Clustering Problems". PhD thesis. Universität Trier. DOI: 10.25353/ubtr-xxxx-5bc7-30f0.

Moreira Costa, C., D. Kreber, and M. Schmidt (2022). "An Alternating Method for Cardinality-Constrained Optimization: A Computational Study for the Best Subset Selection and Sparse Portfolio Problems". In: *INFORMS Journal on Computing*. DOI: 10.1287/ijoc.2022.1211.

Nochetto, R. H., K. G. Siebert, and A. Veeser (2009). "Theory of adaptive finite element methods: an introduction". In: *Multiscale, nonlinear and adaptive approximation*. Springer, Berlin, pp. 409–542. DOI: 10.1007/978-3-642-03413-8_12.

Nussbaumer, T. and S. Thalmann (2016). "Influence of system design on heat distribution costs in district heating". In: *Energy* 101, pp. 496–505. DOI: 10.1016/j.energy.2016.02.062.

Peherstorfer, B., K. Willcox, and M. Gunzburger (2018). "Survey of multifidelity methods in uncertainty propagation, inference, and optimization". In: *SIAM Review* 60.3, pp. 550–591. DOI: 10.1137/16M1082469.

Peña-Ordieres, A., J. R. Luedtke, and A. Wächter (2020). "Solving chance-constrained problems via a smooth sample-based nonlinear approximation". In: *SIAM Journal on Optimization* 30.3, pp. 2221–2250. DOI: 10.1137/19M1261985.

Pineda, S., J. M. Morales, and A. Jiménez-Cordero (2020). "Data-Driven Screening of Network Constraints for Unit Commitment". In: *IEEE Transactions on Power Systems* 35.5, pp. 3695–3705. DOI: 10.1109/TPWRS.2020.2980212.

Polak, E. (1997). *Optimization: Algorithms and Consistent Approximations*. New York, NY: Springer New York. DOI: 10.1007/978-1-4612-0663-7.

Qiu, F., S. Ahmed, S. S. Dey, and L. A. Wolsey (2014). "Covering linear programming with violations". In: *INFORMS Journal on Computing* 26.3, pp. 531–546. DOI: 10.1287/ijoc.2013.0582.

Quarteroni, A., R. Sacco, and F. Saleri (2007). *Numerical mathematics*. Second Edition. Vol. 37. Texts in Applied Mathematics. Springer-Verlag, Berlin. DOI: 10.1007/b98885.

Rüffler, F., V. Mehrmann, and F. M. Hante (2018). "Optimal model switching for gas flow in pipe networks". In: *Networks and Heterogeneous Media* 13.4, pp. 641–661. DOI: 10.3934/nhm.2018029.

Sandou, G., S. Font, S. Tebbani, and Hiret (2005). "Predictive Control of a Complex District Heating Network". In: *Proceedings of the 44th IEEE Conference on Decision and Control*, pp. 7372–7377. DOI: 10.1109/CDC.2005.1583351.

Schaft, A. van der and D. Jeltsema (2014). "Port-Hamiltonian Systems Theory: An Introductory Overview". In: *Foundations and Trends® in Systems and Control* 1.2-3, pp. 173–378. DOI: 10.1561/2600000002.

Schmidt, M., M. Sirvent, and W. Wollner (2019). "A decomposition method for MINLPs with Lipschitz continuous nonlinearities". In: *Mathematical Programming* 178.1-2, Ser. A, pp. 449–483. DOI: 10.1007/s10107-018-1309-x.

Schmidt, M., M. Sirvent, and W. Wollner (June 2022). "The cost of not knowing enough: mixed-integer optimization with implicit Lipschitz nonlinearities". In: *Optimization Letters* 16.5, pp. 1355–1372. DOI: 10.1007/s11590-021-01827-9.

Schmidt, M., M. C. Steinbach, and B. M. Willert (2015). "High detail stationary optimization models for gas networks". In: *Optimization and Engineering* 16.1, pp. 131–164. DOI: 10.1007/s11081-014-9246-x.

Schmidt, M., M. C. Steinbach, and B. M. Willert (2016). "High detail stationary optimization models for gas networks: validation and results". In: *Optimization and Engineering* 17.2, pp. 437–472. DOI: 10.1007/s11081-015-9300-3.

Sethi, S. P. and G. L. Thompson (2000). *Optimal control theory*. Second. Applications to management science and economics. Kluwer Academic Publishers, Boston, MA. DOI: 10.1007/978-3-319-98237-3.

Silverman, B. W. (1986). *Density estimation for statistics and data analysis*. Monographs on Statistics and Applied Probability. Chapman & Hall, London. DOI: 10.1201/9781315140919.

Sobester, A., A. Forrester, and A. Keane (2008). *Engineering Design via Surrogate Modelling*. John Wiley & Sons, Ltd. DOI: 10.1002/9780470770801.

Stoer, J. and R. Bulirsch (2002). *Introduction to numerical analysis*. Third edition. Vol. 12. Texts in Applied Mathematics. Springer-Verlag, New York. DOI: 10.1007/978-0-387-21738-3.

Stolwijk, J. J. and V. Mehrmann (2018). "Error analysis and model adaptivity for flows in gas networks". In: *Mathematical Journal of the Ovidius University of Constantza* 26.2, pp. 231–266. DOI: 10.2478/auom-2018-0027.

Süli, E. and D. F. Mayers (2003). *An introduction to numerical analysis*. Cambridge University Press, Cambridge. DOI: 10.1017/CBO9780511801181.

TWL (2020). *Preise für Fernwärme*. Last accessed 2020-03-25. URL: https://www.twl.de/privatkunden/meine-energie/fernwaerme/.

Verfürth, R. (1994). "A posteriori error estimation and adaptive mesh-refinement techniques". In: *Proceedings of the Fifth International Congress on Computational and Applied Mathematics (Leuven, 1992)*. Vol. 50. 1-3, pp. 67–83. DOI: 10.1016/0377-0427(94)90290-9.

Verrilli, F., S. Srinivasan, G. Gambino, M. Canelli, M. Himanka, C. Del Vecchio, M. Sasso, and L. Glielmo (2017). "Model Predictive Control-Based Optimal Operations of District Heating System With Thermal Energy Storage and Flexible Loads". In: *IEEE Transactions on Automation Science and Engineering* 14.2, pp. 547–557. DOI: 10.1109/TASE.2016.2618948.

Werner, S. (2017). "District heating and cooling in Sweden". In: *Energy* 126, pp. 419–429. DOI: 10.1016/j.energy.2017.03.052.

Wolsey, L. A. (1998). *Integer programming*. Second edition. Wiley-Interscience Series in Discrete Mathematics and Optimization. John Wiley & Sons, Inc., New York. DOI: 10.1002/9781119606475.

Ziems, J. C. and S. Ulbrich (2011). "Adaptive multilevel inexact SQP methods for PDE-constrained optimization". In: *SIAM Journal on Optimization* 21.1, pp. 1–40. DOI: 10.1137/080743160.

Part II

Reprints of Published Journal Articles and Preprints

Article 1

Mixed-Integer Nonlinear Optimization for District Heating Network Expansion

Marius Roland, Martin Schmidt
at - Automatisierungstechnik (2020), DOI: 10.1515/auto-2020-0063
©2020 Walter de Gruyter GmbH, Berlin/Boston

Marius Roland, Martin Schmidt

Mixed-Integer Nonlinear Optimization for District Heating Network Expansion

Abstract: We present a mixed-integer nonlinear optimization model for computing the optimal expansion of an existing tree-shaped district heating network given a number of potential new consumers. To this end, we state a stationary and nonlinear model of all hydraulic and thermal effects in the pipeline network as well as nonlinear models for consumers and the network's depot. For the former, we consider the Euler momentum and the thermal energy equation. The thermal aspects are especially challenging. Here, we develop a novel polynomial approximation that we use in the optimization model. The expansion decisions are modeled by binary variables for which we derive additional valid inequalities that greatly help to solve the highly challenging problem. Finally, we present a case study in which we identify three major aspects that strongly influence investment decisions: the estimated average power demand of potentially new consumers, the distance between the existing network and the new consumers, and thermal losses in the network.

Keywords: District heating networks, Network expansion, Mixed-integer nonlinear optimization

1 Introduction

Decarbonization and defossilization are at the core of the European energy transition and the European Green Deal, which has been announced at the end of 2019; see, e.g., [7]. Besides measures such as the reduction of CO_2 emissions by coal power plants or a better level of insulation of buildings, the efficient use of the existing energy transport infrastructure is of key importance. The latter aspect can be considered from at least to two different angles. On the one hand, the operation, maintenance, and expansion of energy transport infrastructures such as power or gas networks cost both money and energy and should thus be done in the most efficient way. On the other hand, the consideration of, e.g., the power network, standalone often lead to congestion issues in the recent past, which was more and more governed by highly volatile and uncertain renewable production. This aspect also leads to severe economic implications such as negative electricity prices at the

Marius Roland, Martin Schmidt, Trier University, Department of Mathematics, Universitätsring 15, 54296 Trier, Germany

energy exchange in certain days of the year with a high share of renewable energy. The reason is the missing capability of many power systems to store electrical energy or to transform it to other energy forms, i.e., to use power-to-X technologies. At this point, sector coupling enters the scene, which is considered as one of the key technologies towards a successful energy turnaround. Maybe the most intensively discussed sectors to be coupled are gas and electricity, since gas networks itself can be used as large-scale energy storages due to the compressibility of natural gas.

In this paper, we consider another type of energy networks that is not as frequently discussed in the literature: district heating networks. These networks are used to provide households with heat power by a network that transports hot water to the consumers, which is heated usually by waste incineration in a depot. Hence, district heating networks can also be seen as a large-scale energy storage (where energy is stored in terms of thermal energy), e.g., at days with a high renewable share.

To this end, there is a strong need to both operate and extend district heating networks in an optimal way. However, a rigorous mathematical modeling of hydraulic and thermal aspects in district heating networks together with a proper engineering modeling of the depot's processes and consumers leads to highly complex and nonlinear optimization models. Consequently, the literature on the computation of cost-optimal controls of district heating networks mainly uses nonlinear optimization models allowing to accurately describe the physics of the system. However, solving these models over large time horizons induces large computation times. As a remedy, model predictive control approaches are used in [32, 38, 2] to optimally operate the system. In contrast, a highly nonlinear closed-loop model for cost-optimal control of an existing district heating network is presented and solved over long time horizons in [18]. To this end, the authors use different preprocessing and other optimization techniques to reduce computation times.

Besides the optimal control and operation of an existing district heating network, the expansion of existing networks as well as the design of newly built parts are important. Obviously, network expansion is only carried out based on self-interested economic reasoning of the network operator who mainly earns money due to the power consumption of the connected consumers. This network expansion problem is studied in this paper for the special case of tree-shaped networks. We consider an existing district heating network, a set of consumers that are already connected to the network, and another set of potentially new consumers to be given. Based on this data, our model allows to compute the cost-optimal expansion of the network, i.e., the decisions which new consumers should be connected and which new pipes need to be built. Since this decision still depends on the physics in the network, we obtain a nonconvex mixed-integer nonlinear optimization problem (MINLP), which is very challenging to solve.

Mainly two approaches are considered in the related branch of the literature. The most frequently used approach consists in stating the design problem as a mixed-integer linear optimization problem (MILP). This means that all nonlinearities in the system need to be simplified or—at least—linearized to obtain a mixed-integer linear problem, usually at the cost of a significantly larger number of integer variables. Power losses in the system can still be considered, but in a (piecewise) linear fashion. The advantage of the MILP approach is that it usually delivers globally optimal solutions. The models usually incorporate decisions on the layout of the resulting network and on which technologies are installed based on minimizing the total costs of the entire system. These total costs consist of the investment and operational costs, where the latter are based on a cost-optimal control of the system for a set of typical days. Plenty of papers follow this approach and can be further distinguished along the set of technologies that can be installed in the nodes of the system; see, e.g., [1, 6, 36]. Commercial solvers are then usually used to find the optimal solution of the problem. In some cases, the diameter of the pipes is also considered as a decision variable; see, e.g., [29]. Additionally, in some papers, these models are extended towards a multi-objective setting, which allows to minimize the total costs as well as the CO_2 production of the entire system. In [8], this is done using the ε-constraint method and in [26], a genetic algorithm is used. In other papers, the authors also try to reduce the computational complexity by using heuristics to reduce the size of the network [12].

The last papers and the ones discussed in what follows are in contrast to the MILP approach since they do not consider approaches for computing global optima but use heuristics. Genetic algorithms are used as well in the second approach, which consists in describing the design problem as a mixed-integer nonlinear model [11, 20]. However, these algorithms come with a huge disadvantage because they do not allow for any (sub-)optimality guarantees. Another heuristic technique (however, with a mathematically more solid foundation) is to apply local mixed-integer nonlinear solvers or heuristics are used as, e.g., in [23, 24, 3]. The strength of the mixed-integer nonlinear approach relies on the fact that it allows to include all nonlinearities of the system and thus to have a more accurate description of all power losses.

The papers discussed so far deal with the design problem. In these problems, a completely new district heating network is designed from scratch. In contrast, expansion problems consider an already existing network to be given and ask for an optimal expansion. The expansion of existing district heating systems has been investigated less in the literature. In [4], an MILP is proposed for this problem. No thermal losses are considered and pressure losses are introduced to avoid reaching the pressure bounds of the system. However, pressure losses are not reflected in costs for increasing the pressure in the system.

In the light of the cited papers, our contribution is the following. To the best of our knowledge, we are the first ones who propose a stationary nonconvex mixed-integer nonlinear district heating network expansion model for tree-shaped networks that accurately takes into account pressure losses as well as thermal losses. Let us note that the assumption of a tree-like network is crucial for our modeling of the problem since it significantly reduces the models complexity because flow directions are known in advance and, thus, nonsmooth and highly nonlinear mixing models for the water temperature are not required. The entire model is presented in Section 2, where we also derive some further valid binary inequalities that greatly help to solve the problem. Afterward, in Section 3, we derive a novel polynomial approximation of the solution of the thermal energy equation that we then use in our optimization model. Finally, the model is applied to a realistic test case in Section 4 and we identify the main driving factors that influence investments in new district heating network infrastructure. The paper closes with some concluding remarks and some topics of future research in Section 5.

2 Problem Statement

In this section, we present a model for optimal district heating network expansion. The model makes it possible to decide if it is economically reasonable to connect potential new consumers to an existing district heating network that is assumed to be tree-shaped. We distinguish between investment decisions (i.e., which pipes and consumers should be connected to the existing network) and operational decisions for controlling the network. To keep the resulting problem tractable, we restrict ourselves to the stationary setting. This can be seen as that the investment decisions are taken up-front and that the computed operational decisions are optimal for the expanded network. Obviously, investment decisions influence operational decisions and vice versa.

First, we introduce the graph describing the already existing network as well as the potential new consumers and pipes that can be added to the network. Then, the constraints of the optimization problem are presented, followed by the objective function and an overall model summary.

2.1 Network Topology

To describe the topology of a district heating network, we first discuss the relevant network elements and the corresponding arc set A and and node set V of the

underlying directed and connected graph $G = (V, A)$. To this end, we mainly follow the notation introduced in [18] and extend it. A typical district heating network consists of the following parts:

(i) A depot $a_\mathrm{d} \in A$ at which the water is heated to satisfy the energy demand of the connected consumers. Moreover, the pressure is increased to propel the water flow in the network.

(ii) Consumers $a \in A_\mathrm{c} \subset A$ that extract energy from the hot water circulating in the network.

(iii) A forward-flow part consisting of pipes $a \in A_\mathrm{ff}$, which are used to transport the heated water from the depot to the consumers. The node set V_ff represents the nodes in the forward-flow part of the network. These nodes serve as intersections between the depot and adjacent consumers and pipes.

(iv) A backward-flow part consisting of pipes $a \in A_\mathrm{bf}$, which transport the cooled water from consumers back to the depot. The node set V_bf represents the nodes in the backward-flow part of the network as it is the case for the forward-flow network.

In particular, consumers are always of the type $a \in A_\mathrm{c}$ with $a = (u, v)$ and $u \in V_\mathrm{ff}$, $v \in V_\mathrm{bf}$. Contrarily, the single depot of the network is of type $a_\mathrm{d} = (u_\mathrm{d}, v_\mathrm{d})$ with $u_\mathrm{d} \in V_\mathrm{bf}$ and $v_\mathrm{d} \in V_\mathrm{ff}$. With these notations at hand, we have

$$A = \{a_\mathrm{d}\} \cup A_\mathrm{c} \cup A_\mathrm{ff} \cup A_\mathrm{bf}, \quad V = V_\mathrm{ff} \cup V_\mathrm{bf}.$$

Moreover, the set of consumers A_c is split up into already connected consumers $a \in A_\mathrm{c}^\mathrm{e}$ and potential new, i.e., candidate, consumers $a \in A_\mathrm{c}^\mathrm{c}$. Thus, we have $A_\mathrm{c} = A_\mathrm{c}^\mathrm{e} \cup A_\mathrm{c}^\mathrm{c}$. Other existing network elements are also super-indexed with "e", whereas potential new, i.e., candidate, elements are super-indexed with "c". Consequently, we also have $A_\mathrm{ff} = A_\mathrm{ff}^\mathrm{e} \cup A_\mathrm{ff}^\mathrm{c}$ and $A_\mathrm{bf} = A_\mathrm{bf}^\mathrm{e} \cup A_\mathrm{bf}^\mathrm{c}$ as well as $V_\mathrm{ff} = V_\mathrm{ff}^\mathrm{e} \cup V_\mathrm{ff}^\mathrm{c}$ and $V_\mathrm{bf} = V_\mathrm{bf}^\mathrm{e} \cup V_\mathrm{bf}^\mathrm{c}$.

As already discussed in the introduction, we restrict ourselves to the case in which the district heating network is tree-shaped. In this context, a tree-shaped district heating network is a graph for which both the forward and the backward flow part standalone are trees, i.e., directed acyclic graphs. To be more specific, the forward flow part of the network is a rooted out-tree and the backward flow part is a rooted in-tree, where the root is depot of the network. Note, however, that the entire network always contains cycles since the forward and backward flow parts are connected via the depot and the consumers. Table 1 summarizes the graph notation and Figure 1 shows an exemplary district heating network with additional candidate consumers and pipes.

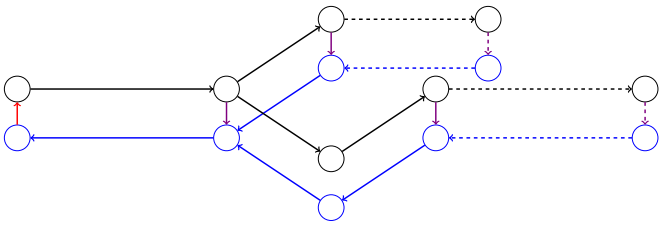

Fig. 1: Schematic illustration of a district heating network. Black arcs and nodes represent pipes in A_{ff} and nodes in V_{ff}. Blue arcs and nodes represent pipes in A_{bf} and nodes in V_{bf}. Purple arcs are consumers in A_{c} and the red arc is the depot a_{d}. Overall, solid arcs represent existing arcs in $A^{\mathsf{e}}_{\mathsf{ff}} \cup A^{\mathsf{e}}_{\mathsf{bf}} \cup A^{\mathsf{e}}_{\mathsf{c}}$, whereas dashed arcs represent for candidate arcs in $A^{\mathsf{c}}_{\mathsf{ff}} \cup A^{\mathsf{c}}_{\mathsf{bf}} \cup A^{\mathsf{c}}_{\mathsf{c}}$.

Tab. 1: Arc and node sets.

Symbol	Description
a_{d}	Depot
A_{c}	Consumers
$A^{\mathsf{e}}_{\mathsf{c}} \subset A_{\mathsf{c}}$	Existing consumers
$A^{\mathsf{c}}_{\mathsf{c}} \subset A_{\mathsf{c}}$	Candidate consumers
A_{ff}	Pipes in the forward-flow network
$A^{\mathsf{e}}_{\mathsf{ff}} \subset A_{\mathsf{ff}}$	Existing pipes in the forward-flow network
$A^{\mathsf{c}}_{\mathsf{ff}} \subset A_{\mathsf{ff}}$	Candidate pipes in the forward-flow network
A_{bf}	Pipes in the backward-flow network
$A^{\mathsf{e}}_{\mathsf{bf}} \subset A_{\mathsf{bf}}$	Existing pipes in the backward-flow network
$A^{\mathsf{c}}_{\mathsf{bf}} \subset A_{\mathsf{bf}}$	Candidate pipes in the backward-flow network
V_{ff}	Nodes in the forward-flow network
$V^{\mathsf{e}}_{\mathsf{ff}} \subset V_{\mathsf{ff}}$	Existing nodes in the forward-flow network
$V^{\mathsf{c}}_{\mathsf{ff}} \subset V_{\mathsf{ff}}$	Candidate nodes in the forward-flow network
V_{bf}	Nodes in the backward-flow network
$V^{\mathsf{e}}_{\mathsf{bf}} \subset V_{\mathsf{bf}}$	Existing nodes in the backward-flow network
$V^{\mathsf{c}}_{\mathsf{bf}} \subset V_{\mathsf{bf}}$	Candidate nodes in the backward-flow network

2.2 Existing Pipes

In this section, we describe the modeling of all pipes that are already existing in the network, i.e., of all arcs $a = (u, v) \in A^{\mathrm{e}}_{\mathrm{ff}} \cup A^{\mathrm{e}}_{\mathrm{bf}}$. First, we derive the required equations to model the hot water flow in the network; see, e.g., [5, 19, 31]. Note that these equations are very similar to the Euler equations that are typically used for natural gas network optimization; see, e.g., [33, 35, 9]. To this end, let L_a denote the length of pipe a and let $x \in [0, L_a]$ be the spatial position in the pipe. For the ease of presentation and since we are only considering the stationary case in this paper, we directly state the stationary variants of the corresponding nonlinear partial differential equations. The one-dimensional stationary continuity equation for compressible fluids in cylindrical pipes is given by

$$\frac{\mathrm{d}(\rho_a v_a)}{\mathrm{d}x} = 0, \tag{1}$$

where $\rho_a(\cdot)$ and $v_a(\cdot)$ denote the density and the velocity of the water depending on the spatial position in the pipe, respectively; see e.g., [18, 17] for the instationary setting. Obviously, Equation (1) is equivalent to

$$\rho_a \frac{\mathrm{d}v_a}{\mathrm{d}x} + v_a \frac{\mathrm{d}\rho_a}{\mathrm{d}x} = 0.$$

Using the incompressibility of water, which is modeled via

$$v_a \frac{\mathrm{d}\rho_a}{\mathrm{d}x} = 0,$$

see, e.g., [21], we see that Equation (1) reads

$$\rho_a \frac{\mathrm{d}v_a}{\mathrm{d}x} = 0$$

in the incompressible case. Since $\rho_a(x) > 0$ for all x, we finally obtain

$$\frac{\mathrm{d}v_a}{\mathrm{d}x} = 0, \tag{2}$$

which implies that velocity $v_a(x) = v_a$ is constant in a pipe.

Next, we consider the one-dimensional stationary momentum equation for compressible fluids in cylindrical pipes, which is given by the nonlinear differential equation

$$\frac{\mathrm{d}p_a}{\mathrm{d}x} + \frac{\mathrm{d}(\rho_a v_a^2)}{\mathrm{d}x} + g\rho_a h'_a + \lambda_a \frac{|v_a| v_a \rho_a}{2D_a} = 0;$$

see again [18, 17] for the instationary setting. The function p_a represents the water pressure at the spatial position x and g, h'_a, and D_a represent gravitational acceleration, the pipe's slope, and the inner diameter of pipe a, respectively.

Friction λ_a at the rough inner pipe wall is modeled using the law of Nikuradse [5], i.e.,

$$\lambda_a = \left(2\log_{10}\left(\frac{D_a}{k_a}\right) + 1.138\right)^{-2},$$

where k_a is the roughness of the inner pipe's wall. Incompressibility and (2) imply

$$\frac{\mathrm{d}(\rho_a v_a^2)}{\mathrm{d}x} = 0,$$

which yields

$$\frac{\mathrm{d}p_a}{\mathrm{d}x} = -g\rho_a h_a' - \lambda_a \frac{|v_a| v_a \rho}{2D_a}. \tag{3}$$

The additional assumption that the density $\rho_a(x) = \rho_a = \rho$ is constant in the entire network leads to a right-hand side in (3) that is independent of x. Thus, the pressure $p_a(x)$ is linear in x, which leads to the momentum equation

$$\frac{p_a(L_a) - p_a(0)}{L_a} = -g\rho h_a' - \lambda_a \frac{|v_a| v_a \rho}{2D_a}, \tag{4}$$

where L_a denotes the length of pipe a.

Next, we describe the thermal behavior of water flow in the pipe using the one-dimensional stationary thermal energy equation

$$v_a \frac{\mathrm{d}T_a}{\mathrm{d}x} + \frac{4U_a}{c_\mathrm{p}\rho D_a}(T_a - T_\mathrm{soil}) = 0; \tag{5}$$

see again [18, 17] for the instationary setting. Here and in what follows, water temperature at the spatial position x is denoted with $T_a(x)$ and the parameters U_a, c_p, and T_soil represent the heat transfer coefficient of the pipe's wall, the specific heat capacity of water, and the temperature of the surrounding soil of the pipe, respectively. Equation (5) is a first-order ordinary differential equation (ODE) and can be solved as stated in the following lemma. To simplify the presentation let us remark that both water flows as well as velocities can be assumed to be nonnegative since the network is a tree and we have only a single depot.

Lemma 1. *The ODE* (5)*,*

$$v_a \frac{\mathrm{d}T_a}{\mathrm{d}x}(x) + \frac{4U_a}{c_\mathrm{p}\rho D_a}(T_a(x) - T_{soil}) = 0,$$

has the solution

$$T_a(x; v_a) = \begin{cases} T_{soil}, & \text{if } v_a = 0, \\ Ce^{-\frac{4U_a x}{c_\mathrm{p}\rho D_a v_a}} + T_{soil}, & \text{if } v_a > 0, \end{cases} \tag{6}$$

where $C \in \mathbb{R}$ is a constant. The solution is continuous for all $x \in [0, L_a]$ and all $v_a \geq 0$.

The proof of this lemma is rather straightforward and can be found in Appendix A.

For a macroscopic network modeling, we are again mainly interested in the relation between the quantities at the end nodes of the pipes as it is also the case for the pressure loss equation (4) that couples inflow and outflow pressure as well as the water flow on the arc. Regarding the temperature loss model, we aim for something similar but for a coupling of inflow and outflow temperature as well as the flow on the arc. As usual, the constant C appears in the general solution of the stationary thermal energy equation as given in Lemma 1. If the latter ODE is considered as an initial value problem with the initial value being the inflow water temperature, this constant can be specified in dependence of the initial value, i.e.,

$$T_a(0; v_a) = C + T_{\text{soil}}$$

holds for $v_a > 0$. This means that the constant represents the offset between the inflow and the soil temperature. Going further, we can rewrite the solution as

$$T_a(L_a; v_a) = \begin{cases} T_{\text{soil}}, & v_a = 0, \\ (T_a(0) - T_{\text{soil}})\, e^{-\frac{4U_a L_a}{c_p \rho D_a v_a}} + T_{\text{soil}}, & v_a > 0. \end{cases} \tag{7}$$

It is easy to see that $T_a(L_a; v_a)$ is smooth at $v_a = 0$. However, the problem is that this function is defined by a case distinction ($v_a = 0$ vs. $v_a \neq 0$) since the second part of the function's definition is not defined for $v_a = 0$. This renders the integration of (7) into a model that should later be solved by a global MINLP solver impossible. Furthermore, it is not possible to simply include the second part of the definition standalone in the model since the resulting constraint would not be well-defined in all cases in which an arc has a zero flow, which is, e.g., the case for all candidate pipes that are not built. To tackle this problem, we will derive an approximation f_{approx} in Section 3 so that (7) is approximately captured via using the equality constraint $f_{\text{approx}} = 0$.

Finally note that all physical equations in this section are stated using the velocity v_a of the water flow in the pipe. Using the formula $q_a = \rho A_a v_a$ with $A_a = \pi(D_a/2)^2$, which directly connects velocity v_a with the mass flow q_a (note again that ρ is constant), we can also state all equations such as the momentum or the thermal energy equation in terms of mass flow instead of velocity.

2.3 Nodes

Nodes are used to connect adjacent pipes or other types of arcs. At nodes, we need to model three different phenomena:

(i) mass conservation,

(ii) pressure continuity, and
(iii) mixing of different inflowing water temperatures.

For stating mass conservation, we introduce the notations

$$\delta^{\text{in}}(u) := \{a \in A \colon \exists v \in V \text{ with } a = (v, u)\},$$
$$\delta^{\text{out}}(u) := \{a \in A \colon \exists v \in V \text{ with } a = (u, v)\}$$

for incoming and outgoing arcs at node $u \in V$. With this, the mass flow q_a needs to satisfy

$$\sum_{a \in \delta^{\text{in}}(u)} q_a = \sum_{a \in \delta^{\text{out}}(u)} q_a, \quad u \in V. \tag{8}$$

Pressure continuity at nodes is easily modeled using

$$\begin{aligned} p_u &= p_a(0), \quad u \in V,\ a \in \delta^{\text{out}}(u), \\ p_u &= p_a(L_a), \quad u \in V,\ a \in \delta^{\text{in}}(u), \end{aligned} \tag{9}$$

where p_u is the pressure at node u.

Finally, we need to model the mixing of different inflowing water temperatures at a node of the network. In [18], a formulation of the required nodal mixing constraints has been introduced for general district heating networks, which is based on analogous models for natural gas networks; see, e.g., [34, 14, 10]. In general network structures, which can also contain cycles, the directions of water flow are not known in advance. This leads to nonsmooth constraints that introduce significant additional hardness to the overall problem. Due to our simplifying assumption of only considering tree-shaped networks (i.e., the graphs of the forward and the backward-flow part of the network are trees), we can fix the direction of the flow in the pipes in advance. This is explained by the fact that a consumer cannot obtain water if the flow direction in a pipe on the unique path from the depot to the consumer changes. The same applies for the backward-flow part but in the opposite direction. This also implies that we can w.l.o.g. assume that all mass flows in the network are positive. Thus, the model introduced in [18] specifies to

$$T_u = \frac{\sum_{a \in \delta^{\text{in}}(u)} c_{\text{p}} q_a T_{a,\text{out}}}{\sum_{a \in \delta^{\text{in}}(u)} c_{\text{p}} q_a}, \quad u \in V, \tag{10a}$$

$$T_u = T_a(0), \quad u \in V,\ a \in \delta^{\text{out}}(u). \tag{10b}$$

Here, $T_{a,\text{out}}$ stands for the water temperature at the outlet of arc a. For pipes, this corresponds to $T_a(L_a)$. Equation (10a) is obtained by using the law of conservation of energy. If c_{p} is a constant throughout the network and the same for all pipes,

we finally obtain

$$T_u = \frac{\sum_{a\in\delta^{\mathrm{in}}(u)} q_a T_{a,\mathrm{out}}}{\sum_{a\in\delta^{\mathrm{in}}(u)} q_a}, \quad u \in V,$$
$$T_u = T_a(0), \quad u \in V,\ a \in \delta^{\mathrm{out}}(u).$$

2.4 Depot and Consumers

We now state the constraints modeling the depot and the consumers. For the depot $a_{\mathrm{d}} = (u_{\mathrm{d}}, v_{\mathrm{d}})$ we have,

$$p_{u_{\mathrm{d}}} = p_{\mathrm{s}}, \tag{11a}$$
$$P_{\mathrm{p}} = \frac{q_{a_{\mathrm{d}}}}{\rho}\left(p_{v_{\mathrm{d}}} - p_{u_{\mathrm{d}}}\right), \tag{11b}$$
$$P_{\mathrm{w}} + P_{\mathrm{g}} = q_{a_{\mathrm{d}}} c_{\mathrm{p}}\left(T_{a,\mathrm{out}} - T_{a,\mathrm{in}}\right). \tag{11c}$$

Here, $T_{a,\mathrm{in}}$ and $T_{a,\mathrm{out}}$ represent the inflow and outflow water temperature at the depot. Moreover, p_{s} stands for the stagnation pressure. The stagnation pressure, to which the depot's inflow pressure is set, leads to pressure values in the entire network that are uniquely determined by the pressure loss constraints (4). The variables P_{p}, P_{w}, and P_{g} stand for the power needed to increase the water pressure, the power used for heating the water obtained by waste incineration, and the power produced by burning natural gas. As one can see, power consumption mainly depends on the products of temperature or pressure differences and the mass flow.

The constraints modeling consumers $a = (u, v)$ read

$$P_a = q_a c_{\mathrm{p}}\left(T_{a,\mathrm{out}} - T_{a,\mathrm{in}}\right), \qquad a \in A_{\mathrm{c}}^{\mathrm{e}}, \tag{12a}$$
$$x_a P_a = q_a c_{\mathrm{p}}\left(T_{a,\mathrm{out}} - T_{a,\mathrm{in}}\right), \qquad a \in A_{\mathrm{c}}^{\mathrm{c}}, \tag{12b}$$
$$T_{a,\mathrm{out}} = T^{\mathrm{bf}}, \qquad a \in A_{\mathrm{c}}, \tag{12c}$$
$$T_{a,\mathrm{in}} \geq T_a^{\mathrm{ff}}, \qquad a \in A_{\mathrm{c}}, \tag{12d}$$
$$p_v \leq p_u, \qquad a \in A_{\mathrm{c}}. \tag{12e}$$

In (12a) and (12b), the parameter P_a stands for the average power demand of the consumer. Additionally, the binary variable $x_a \in \{0, 1\}$ is introduced for deciding if arc $a \in A_{\mathrm{c}}^{\mathrm{c}}$ is connected or not. We show in Section 2.5 that x_a is also used to force a zero mass flow in arc a if the decision is made to not connect a ($x_a = 0$). Since in this case, the right-hand side of (12b) is zero, we multiply the left-hand side by x_a to ensure the validity of the constraint. The parameter T^{bf} is the consumer's outlet water temperature and is the same for all consumers. The parameter T_a^{ff} represents

the contractually fixed lower bound of the consumer's inflow temperature. Finally, Constraint (12e) implies that the outlet pressure of the consumer is not greater than its inlet pressure.

2.5 Bounds

We now introduce bounds on the variables of our model and make a distinction between existing and candidate arcs if needed. First, we state the bounds on mass flow,

$$0 \leq q_a \leq q_a^+, \qquad a \in A_{\mathrm{ff}}^{\mathrm{e}} \cup A_{\mathrm{bf}}^{\mathrm{e}} \cup A_{\mathrm{c}}^{\mathrm{e}}, \tag{13a}$$

$$0 \leq q_a \leq x_a q_a^+, \qquad a \in A_{\mathrm{ff}}^{\mathrm{c}} \cup A_{\mathrm{bf}}^{\mathrm{c}} \cup A_{\mathrm{c}}^{\mathrm{c}}, \tag{13b}$$

where the parameters q_a^+ define upper bounds on the mass flow and are usually imposed for avoiding pipe damages as well as excessive noise emissions. In the latter constraint we again use the binary variables $x_a \in \{0,1\}$ for all possibly built arcs $a \in A_{\mathrm{ff}}^{\mathrm{c}} \cup A_{\mathrm{bf}}^{\mathrm{c}} \cup A_{\mathrm{c}}^{\mathrm{c}}$. Thus, this constraint obviously enforces $q_a = 0$ for $a \in A^{\mathrm{c}}$ if $x_a = 0$; cf. (12b). Note also that this immediately implies $v_a = 0$ as well. Next, we introduce bounds on the nodal pressure variables

$$0 \leq p_u \leq p_u^+, \quad u \in V. \tag{14}$$

Moreover, we have bounds on the nodal water temperature, i.e.,

$$T_u \in [T_u^-, T_u^+], \quad u \in V. \tag{15}$$

Finally, we incorporate bounds on the power consumption, i.e.,

$$P_{\mathrm{p}} \in [0, P_{\mathrm{p}}^+], \quad P_{\mathrm{w}} \in [0, P_{\mathrm{w}}^+], \quad P_{\mathrm{g}} \in [0, P_{\mathrm{g}}^+]. \tag{16}$$

2.6 Candidate Pipes

For candidate pipes, we need to make some adaptions to the equations presented in Section 2.2. For existing pipes, the hydraulic effects are modeled using (4), i.e.,

$$p_v - p_u + L_a g \rho h'_a + \lambda_a \frac{|v_a| v_a \rho L_a}{2 D_a} = 0,$$

and by the constraint $f_{\mathrm{approx}} = 0$ as discussed at the end of the Section 2.2. Obviously, both constraints need to be present if a candidate pipe $a = (u, v) \in A_{\mathrm{ff}}^{\mathrm{c}} \cup A_{\mathrm{bf}}^{\mathrm{c}}$ is decided to be installed. However, if the pipe is not built, these constraints

need to be de-activated. To this end, we introduce a binary variable $x_a \in \{0,1\}$ for every candidate pipe with $x_a = 0$ if the pipe is not built and $x_a = 1$ if it is built. With this decision variable at hand, we then restate the momentum equation as

$$p_v - p_u + L_a g \rho h'_a + \lambda_a \frac{|v_a| v_a \rho L_a}{2 D_a} \leq (1 - x_a) M_a^1, \tag{17a}$$

$$p_v - p_u + L_a g \rho h'_a + \lambda_a \frac{|v_a| v_a \rho L_a}{2 D_a} \geq -(1 - x_a) M_a^2 \tag{17b}$$

with suitably large constants M_a^1, M_a^2 that can be chosen as

$$M_a^1 = p_v^+ - p_u^- + L_a g \rho h'_a,$$
$$M_a^2 = p_v^- - p_u^+ + L_a g \rho h'_a.$$

Note that the friction part of the momentum equation (4) can be ignored due to the implied bounds in (13b). Interestingly, an analogous big-M formulation is not required for the approximation of the thermal energy equation; see Section 3.

2.7 Valid Inequalities for Candidate Arcs

In this section, we briefly derive valid inequalities for the binary expansion decision variables of the model. These additional inequalities are not required to obtain a correct model but we will later show that they greatly help global solvers to solve the problem.

We split the description of the inequalities into three cases and start with a candidate pipe $a \in A_{\text{ff}}^{\text{c}}$ in the forward-flow part of the network. Let $P(a) \subseteq A_{\text{ff}}^{\text{c}}$ be the set of arcs of the path connecting a to the existing forward-flow network. This path is unique since we consider tree-shaped networks. The valid additional constraints

$$x_a \leq x_{\bar{a}}, \quad \bar{a} \in P(a), \tag{18}$$

then model that all pipes on the way from the existing forward-flow part of the network to the newly built pipe also need to be built.

For a candidate pipe $a \in A_{\text{bf}}^{\text{c}}$ in the backward-flow part of the network, the idea and the valid inequalities are the same. The only difference is that the arcs in the path $P(a)$ are now part of the backward-flow network and are oriented in the other direction compared to the path in the forward-flow network.

Third and finally, if $a = (u, v) \in A_{\text{c}}^{\text{c}}$ is a potential new consumer, we combine both ideas and introduce (18) for the forward-flow part of the network (using the path that connects the consumer's inlet node $u \in V_{\text{ff}}$ with the existing forward-flow part of the network) as well as for the backward-flow part of the network (using the path that connects the consumer's outlet node $v \in V_{\text{bf}}$ with the existing backward-flow part of the network).

2.8 Objective Function

The objective function to maximize reads

$$\sum_{a \in A_{\mathrm{c}}^{\mathrm{c}}} P_a w \pi x_a - \sum_{a \in A^{\mathrm{c}}} C_a^{\mathrm{inv}} x_a - w \left(C_{\mathrm{p}} P_{\mathrm{p}} + C_{\mathrm{w}} P_{\mathrm{w}} + C_{\mathrm{g}} P_{\mathrm{g}} \right), \tag{19}$$

where $w = 24$ and π, C_a^{inv}, C_{p}, C_{w}, and C_{g} stand for the energy price per kWh, the daily annuity costs of arc a, the price per pressure increase (measured in kWh), the price of energy from waste incineration per kWh, and the price of energy from gas per kWh, respectively. The first part of the objective, corresponding to the candidate consumer payments, models how much a new consumer pays in average over a day if connected to the network. The second part, which corresponds to investment costs, represents how much is paid per day in order to install arc $a \in A^{\mathrm{c}}$. The last part, corresponding to the power cost, represents how much the network operator pays to satisfy the energy demand of the possibly extended district heating system. Here, we abstract from operation and maintenance costs.

2.9 Model Summary

For later reference, we now finally state the complete optimization problem for computing the optimal investments to connect new consumers to an existing district heating network:

max	objective (19),	(20a)
s.t.	stationary incompressible Euler equation (4) or (17),	(20b)
	stationary thermal energy equation (7),	(20c)
	mass conservation (8),	(20d)
	pressure continuity (9),	(20e)
	temperature mixing equations (10),	(20f)
	depot constraints (11),	(20g)
	consumer constraints (12),	(20h)
	mass flow bounds (13),	(20i)
	pressure bounds (14),	(20j)
	temperature bounds (15),	(20k)
	power bounds (16),	(20l)
	valid binary inequalities (18).	(20m)

All variables are listed in Table 2.

Tab. 2: Variables of Problem (20)

Variable	Index Set
$P_\mathrm{p}, P_\mathrm{w}, P_\mathrm{g}$	—
x_a	$a \in A_{\mathsf{ff}}^{\mathsf{c}} \cup A_{\mathsf{bf}}^{\mathsf{c}} \cup A_{\mathsf{c}}^{\mathsf{c}}$
v_a	$a \in A_{\mathsf{ff}} \cup A_{\mathsf{bf}}$
q_a	$a \in A_{\mathsf{ff}} \cup A_{\mathsf{bf}} \cup A_{\mathsf{c}} \cup \{a_{\mathsf{d}}\}$
p_u, T_u	$u \in V$
$p_a(0), p_a(L_a)$	$a \in A_{\mathsf{ff}} \cup A_{\mathsf{bf}}$
$T_{a,\mathsf{in}}, T_{a,\mathsf{out}}$ (resp. $T_a(0), T_a(L_a)$)	$a \in A$

3 Approximation of the Thermal Energy Equation

We now deduce the approximation of the solution of the thermal energy equation for all pipes $a = (u, v) \in A_{\mathrm{ff}} \cup A_{\mathrm{bf}}$. As already mentioned in Section 2.2, the main goal is to obtain a constraint using a single symbolic expression (instead of the case distinction in (7)) so that inflow and outflow water temperature of a pipe are coupled to the water flow through the pipe as given in (7). To this end, we define the function $f(v_a, T_a(0), T_a(L_a))$, which depends on the three discussed physical quantities, based on Equation (7) as

$$f(v_a, T_a(0), T_a(L_a)) := \begin{cases} \big(T_a(0) - T_{\mathrm{soil}}\big) e^{-\frac{4U_a L_a}{c_\mathrm{p} \rho D_a v_a}} + T_{\mathrm{soil}} - T_a(L_a), & v_a > 0, \\ T_{\mathrm{soil}} - T_a(L_a), & v_a = 0. \end{cases}$$

Ideally, we would like to incorporate the constraint $f(v_a, T_a(0), T_a(L_a)) = 0$ that couples the inlet and outlet temperature of a pipe with the velocity of hot water flow in our model. However, this is not possible directly due to the function f being defined via a case distinction. Thus, we design a continuous ansatz function $f_{\mathrm{approx}}(v_a, T_a(0), T_a(L_a))$ satisfying the following conditions:

(i) If $v_a = 0$, then $f_{\mathrm{approx}}(v_a, T_a(0), T_a(L_a)) = 0$ reduces to $T_a(L_a) = T_{\mathrm{soil}}$.

(ii) The approximation f_{approx} is continuous and as close as possible to 0 for all reasonable combinations of $v_a \in [0, v_a^+]$ and $T_a(0), T_a(L_a) \in [T_v^-, T_v^+]$ that satisfy the thermal energy equation.

The main rationale is to use a polynomial of degree d as the ansatz function, i.e.,

$$f_{\mathrm{approx}}(v_a, T_a(0), T_a(L_a)) = \sum_{(k,l,m) \in \Gamma_d} \alpha_{klm}\, v_a^k\, T_a(0)^l\, T_a(L_a)^m,$$

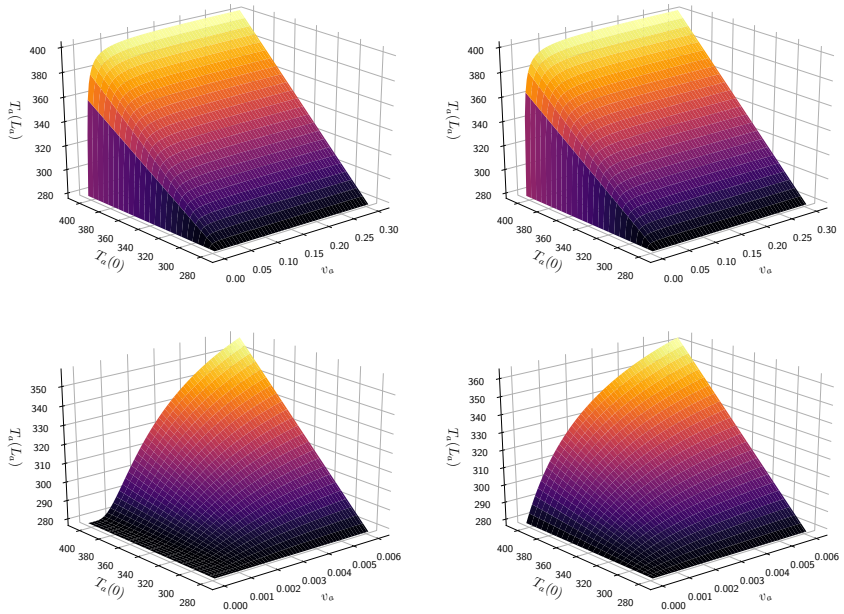

Fig. 2: Solution of the thermal energy equation (left figures) and its degree-2 polynomial approximation (right figures) for $U_a = 0.5\,\mathrm{W\,m^{-2}\,K^{-1}}$, $c_\mathrm{p} = 4181.3\,\mathrm{J\,kg^{-1}\,K^{-1}}$, $\rho_a = 1000\,\mathrm{kg\,m^{-3}}$, $D_a = 0.07\,\mathrm{m}$, $L_a = 400\,\mathrm{m}$, and $T_\mathsf{soil} = 278\,\mathrm{K}$. For larger values of v_a (top figures) the approximation is nearly identical to the original thermal energy equation solution. Whereas the approximation does not possess similar curvature for values of v_a close to 0 (bottom figures).

with coefficients α_{klm} and

$$\Gamma_d := \left\{(k,l,m) \in \mathbb{N}^3 \colon k+l+m \leq d\right\}.$$

However, it is reasonable to slightly modify this ansatz and to replace it with

$$f_{\text{approx}}(v_a, T_a(0), T_a(L_a)) = \sum_{(k,l,m)\in\Theta_d} \alpha_{klm}\, v_a^k\, T_a(0)^l\, T_a(L_a)^m + T_a(L_a) - T_{\text{soil}} \tag{21}$$

and

$$\Theta_d := \left\{(k,l,m) \in \mathbb{N}^3 \colon k \neq 0 \text{ and } k+l+m \leq d\right\}.$$

By doing so, the Condition (i) above is always satisfied by construction. Let us also note that Condition (i) is sufficient to exclude the trivial solution $\alpha_{klm} = 0$ for all $(k,l,m) \in \Theta_d$. To satisfy the Condition (ii) we compute the polynomial's coefficients α_{klm} in (21) using the least-squares fit

$$\min_{\alpha} \quad \sum_{i\in I} f_{\text{approx}}(v_a^i, T_a(0)^i, T_a(L_a)^i)^2.$$

For our computations, we use a large number of equidistant vectors

$$(v_a, T_a(0)) \in [0, v_a^+] \times [T_v^-, T_v^+]$$

and compute the corresponding outlet temperature $T_a(L_a)$ by solving the thermal energy equation. The resulting vectors in $\mathbb{R}^3$ then form the set I for the least-squares fit.

Figure 2 shows the degree-2 approximation for a certain pipe. One can see that the approximation is pretty accurate. However, for positive values of v_a very close to zero the approximation is not able to reflect the curvature of the original thermal energy equation.

We close this section with a discussion of the introduced approximation of the solution of the stationary thermal energy equation in the context of candidate pipes. In Section 2.6, we explicitly reformulated the momentum equation for candidate pipes. This is not required for the approximation of the thermal energy equation's solution since we can always include the corresponding constraint as it is—independent of whether the candidate pipe is built or not. The reason is as follows. If a candidate pipe is not built, the constraints in (13) force the velocity, and thus the mass flow, to zero. However, in this case, $f_{\text{approx}}(0, T_a(0), T_a(L_a)) = 0$ implies $T_a(L_a) = T_{\text{soil}}$; see (21). Since $T_{\text{soil}} \in [T_u^-, T_u^+]$ always holds, no adaptions are required for the thermal modeling on candidate pipes.

To conclude, the final model is given by Problem (20) with Constraint (7) replaced by $f_{\text{approx}}(0, T_a(0), T_a(L_a)) = 0$ for every pipe $a \in A_{\text{ff}} \cup A_{\text{bf}}$.

4 Numerical Results

In this section, we first describe the software and hardware setup that we use for our numerical tests, then present a basic test case, and discuss its numerical results. Afterward, we slightly modify the network's setup to carry out a sensitivity analysis that allows to conclude on the key decision parameters for optimal district heating network expansion. To the best of our knowledge, we are the first to consider a district heating network expansion problem equipped with the level of physical and technical detail as discussed in this paper. Thus, the aim of the following discussion of the numerical results is to showcase the impact of certain key aspects on the expansion decisions. This means that we try to answer the question on what the governing factors for expansions are if an accurate nonlinear physics model is used. To this end, we choose a network size that is non-trivial but that still allows to discuss the physical and investment solution in detail for different parameterizations of the problem at hand.

4.1 Software and Hardware Setup

We implemented the model in Python v.3.7.4 using the Pyomo v.5.6.8 package [16, 15] and solve the resulting MINLPs using ANTIGONE, which is interfaced via the Pyomo-GAMS interface. We also tested other global MINLP solvers but the branch-and-cut based global optimization solver ANTIGONE turned out to be the most reliable and best performing one. All details of the algorithms inside ANTIGONE can be found in [25] and the references therein. In our computations, we use a relative optimality gap of 0.1 %. All other parameters are the default values of GAMS. The computations are executed on a computer with an Intel(R) Core(TM) i7-8550U processor with eight threads at 1.90 GHz and 16 GB RAM.

4.2 Test Cases

We carry out our case study on the network shown in Figure 3. This network is based on the AROMA network used in [18], which we adapt and extend to our needs of computing optimal district heating network expansion decisions. In particular, the original network from the literature is modified so that it is tree-shaped, while keeping its other major characteristics. Table 3 (left) provides the diameters of all pipes in the forward-flow part of the network. The diameters of the corresponding pipes of the backward-flow part of the network are chosen identical.

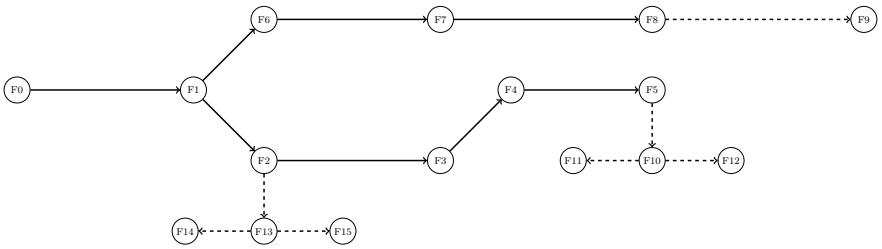

Fig. 3: The tree-shaped forward-flow part of the network used in our case study. Solid lines are existing pipes and dashed lines correspond to candidate pipes. The node F0 is the depot.

As introduced previously, the parameter P_a represents the average demand of the consumer $a \in A_\mathrm{c}$; see Table 3 (right). The costs for connecting a new consumer are 100 000 €. The investment costs per meter of pipe as well as the mass flow's upper bound (both depending the chosen diameter) are given in Table 4 and taken from [28]. The costs C_a^inv in (19) thus correspond to the daily annuity of 100 000 € for consumers $a \in A_\mathrm{c}^\mathrm{c}$ and to the daily annuity of $C^\mathrm{inv} L_a$ for $a \in A_\mathrm{ff}^\mathrm{c} \cup A_\mathrm{bf}^\mathrm{c}$, where C^inv is given in Table 4.

We now discuss the operating costs of the depot. The price of waste incineration, of gas combustion, and the price of electricity (for increasing the pressure) are given by $C_\mathrm{w} = 0$ €/kWh, $C_\mathrm{g} = 0.0415$ €/kWh, and $C_\mathrm{p} = 0.165$ €/kWh, respectively. These cost data are also taken from [28]. A discount factor of 3 % per year is used to compute daily annuities. The energy selling price π, see (19), is based on [37]. We suppose that no upper bound on P_g and P_p exists. Contrarily, we impose a bound of 500 kW for P_w.

Finally, the approximation of the solution of the thermal energy equation is chosen to be of degree 2 and is computed separately for each pipe using a fine grid of 32 000 sample points on the domain imposed by the bounds on velocities and inlet temperatures; cf. Section 3. We also carried out an extensive computational sensitivity analysis to check if the results qualitatively change if the approximation is changed. To this end, we tested approximations obtained from a range between 8000 to 128 000 sample points. Since all results stayed very much the same, we do not discuss this sensitivity analysis in more detail.

4.3 Discussion of the Results

We start by discussing the results obtained for the parameterization of the problem discussed above. Figure 4 illustrates the solution, i.e., the solution of (20), in the

Tab. 3: Left: Diameters of all pipes $a \in A_{\mathsf{ff}}$ in the forward-flow part of the network. Right: Average demands P_a for all consumers $a \in A_{\mathsf{c}}$.

Pipe	D **(in** mm**)**
(F0,F1)	107
(F1,F2)	107
(F1,F6)	107
(F2,F3)	83
(F2,F13)	70
(F3,F4)	83
(F4,F5)	70
(F5,F10)	70
(F6,F7)	83
(F7,F8)	70
(F8,F9)	70
(F10,F11)	70
(F10,F12)	70
(F13,F14)	70
(F13,F15)	70

Consumer	P **(in** kW**)**
(F2,B2)	200.00
(F3,B3)	600.00
(F5,B5)	150.00
(F6,B6)	666.66
(F8,B8)	200.00
(F9,B9)	183.33
(F11,B11)	183.33
(F12,B12)	183.33
(F14,B14)	183.33
(F15,B15)	183.33

Tab. 4: Investment costs per pipe length and upper bounds on mass flow for all pipe diameters.

D_a **(**mm**)**	**70**	**83**	**107**
C^{inv} (€/m)	537.0	616.0	760.0
q_a^+ ($\mathrm{kg\,s^{-1}}$)	24.6	38.9	68.3

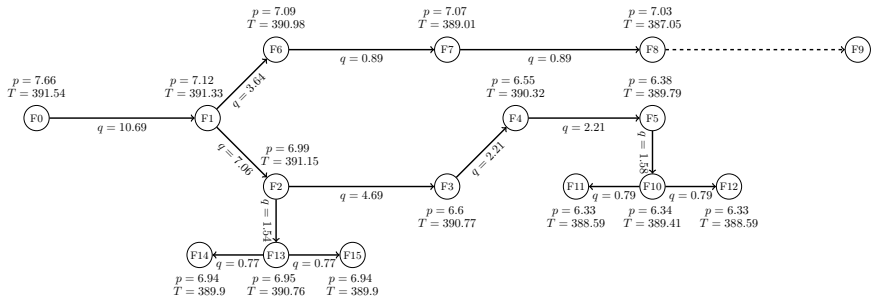

Fig. 4: Illustration of the solution of Problem (20). Solid arcs represent existing and newly constructed candidate pipes whereas dashed arcs represent candidate pipes that are not built. The figure also provides parts of the physical solution (T in K and p in bar at nodes and q in $\mathrm{kg\,s^{-1}}$ on arcs).

Tab. 5: Relevant parameters of the optimal solution.

Objective (€/day)	P_t **(**kW**)**	P_p **(**kW**)**	P_w **(**kW**)**	P_g **(**kW**)**	P_tl **(**kW**)**
−1380.02	2550.0	2.84	500.0	2149.87	99.87

forward-flow part of the network. The model contains 209 variables, thereof 19 being binary,[1] and 599 constraints. ANTIGONE takes 697 seconds to solve this problem. Note that, if we do not incorporate the additional valid binary inequalities derived in Section 2.7, ANTIGONE needs 5750 seconds to solve the problem. Thus, these inequalities lead to a speed-up factor larger than 8 on the tested instance. Besides Figure 4, Table 5 shows some relevant parameter values as part of the optimal solution, which we will later discuss in detail. Besides the already defined ones, these are the total connected power load

$$P_\mathrm{t} := \sum_{a \in A_\mathrm{c}^\mathrm{e}} P_a + \sum_{a \in A_\mathrm{c}^\mathrm{c}} x_a P_a$$

and the thermal power losses P_tl in the system, which are given by

$$P_\mathrm{tl} := P_\mathrm{w} + P_\mathrm{g} - P_\mathrm{t}.$$

The solution has a rather high pressure at the depot's outlet node of 7.66 bar. This allows to increase the water's velocity in the network and, thus, the mass flow, which in turn allows to reduce temperature differences at the consumers; cf. (12a) or (12b). Thus, the optimal operation in this case is based on significantly increasing the pressure (from the stagnation pressure of 5 bar to 7.66 bar) at the rather high price $C_\mathrm{p} = 0.165\,€/\mathrm{kWh}$ (compared to the lower values for C_w and C_g). This increased outlet pressure at the depot leads to larger mass flows in the system. Thus, the required temperature differences at the consumers can be decreased. This, together with the resulting smaller thermal losses in the pipes, cf. (5), leads to comparably small overall thermal losses in the system, which are coped with by increasing the water temperature at the depot at the rather low prices for C_w and C_g.

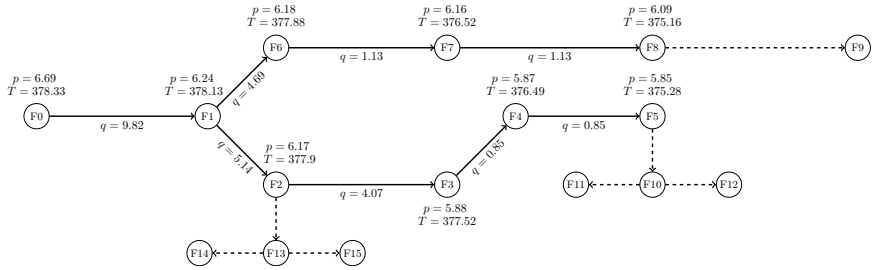

Fig. 5: Solution of the optimization problem when $P_a = 150\,\mathrm{kW}$ for all $a \in A_{\mathrm{c}}^{\mathrm{c}}$.

4.3.1 The Impact of Heat Demand on Expansion Decisions

In Figure 5, we plot the solution for the forward flow network in case that all average consumer demands are reduced to 150 kW. It is clearly visible that this has a strong impact on the investment decision: no new consumer is connected to the network. Although being very important, the effect is rather obvious. Since the network operator mainly earns money by the consumption of connected households, significantly decreased demand leads to less income and thus the potentially new consumers are not worth to be connected.

4.3.2 The Impact of the Distance Between the Existing Network and the New Consumer

We measure the distance of a new consumer to the existing network in terms of the aggregated length of the required new pipes for connecting the new consumer. This distance influences how much the retailer pays to connect the consumer (at least) in two ways. First, the farther away a consumer is from the existing network, the more needs to be paid to install the pipes that connect the new consumer to the network. This immediately influences the objective function; cf. the second term in (19). Second, larger distances lead to larger power and pressure losses in the system: The longer a pipe, the more thermal and pressure losses occur; see the solution (7) of the thermal energy equation and the momentum equation (4).

This explains why consumer (F9,B9) is not connected to the existing network. Indeed, we see that this consumer is located far away from the original network and thus induces high pipe costs and losses. If we, for instance, sufficiently increase

1 Note that we have 7 candidate pipes both in the forward and the backward flow network together with 5 binary variables for the potentially connected new consumers.

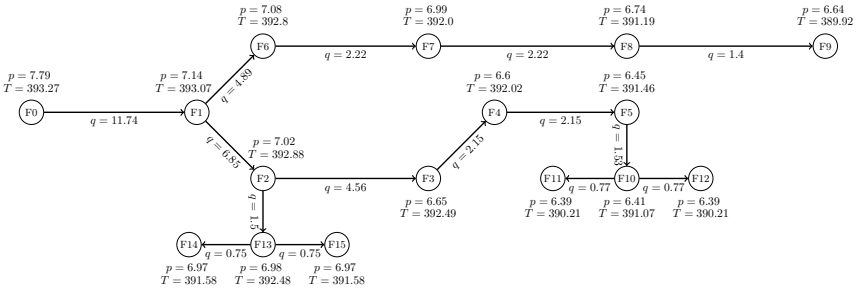

Fig. 6: Solution of the optimization problem when $P_{(\mathsf{F9,B9})} = 350\,\mathrm{kW}$. The arc (F9,B9) is connected since its demand is high enough to overcome the pipe installation costs.

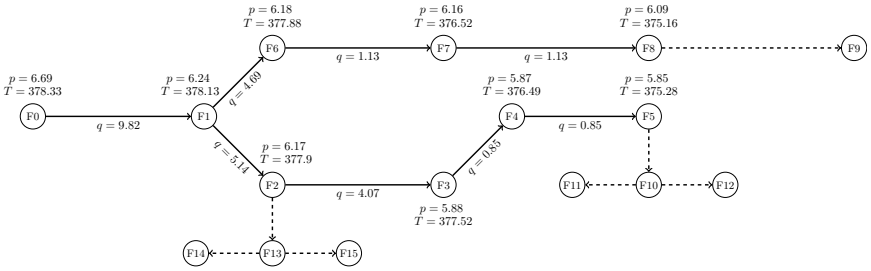

Fig. 7: Solution of the optimization problem when U_a is set to $0.8\,\mathrm{W\,m^{-1}\,K^{-2}}$ for all a in $A_{\mathsf{c}}^{\mathsf{c}}$. No candidate consumers are connected since the additional thermal losses make it financially uninteresting.

the power demand or decrease the distance from this consumer to the existing network, it becomes financially worth to be connect this consumer as shown in Figure 6, which is obtained for $P_{(\mathrm{F9,B9})} = 350\,\mathrm{kW}$.

4.3.3 The Impact of Power Losses

Pressure and thermal losses represent the power loss in the network. Pressure losses (measured in power) correspond to P_{p} since this power is required to propel the water flow in the network. They represent approximately 0.1 % of the total power consumption in the solution (see Table 5) and thus do not have a significant importance for the expansion decisions. Thermal power losses P_{tl} represent 3.76 % of the total power consumption in the solution and, hence, are not negligible. To illustrate the importance of thermal losses, we increase the heat transfer coefficient U_a of all candidate pipes from 0.5 to $0.8\,\mathrm{W\,m^{-1}\,K^{-2}}$. The result is shown in

Figure 7, where no candidate consumer is connected to the existing network at all. This shows that considering thermal power when making expansion decisions is relevant, especially if different insulation techniques for water pipes are available.

5 Conclusion

In this paper, we presented a mixed-integer nonlinear optimization model for the district heating network expansion problem in case of tree-shaped networks. To the best of our knowledge, mixed-integer expansion decisions for district heating networks have not been combined before in the literature with a nonlinear modeling of thermal and hydraulic phenomena as accurate as in this paper. Whereas the accurate incorporation of the hydraulic effects is rather straightforward, the tackling of the energy equation modeling the thermal effects is more complicated. Here, we developed a novel polynomial approximation that is well tailored for optimization. Finally, in our case study we identified three main parameters that mainly govern the expansion decisions:

(i) The estimated average demand of the new consumer. Thus, it is important to have an accurate estimation of the future consumption of households. There are many papers in the literature that estimate the future heat demand of households; see, e.g., [39] for a case study in Sweden or [22, 27] for more general approaches for heat demand estimation. Even more relevant in our context, the authors of [30] try to predict heat demand based on consumer and building characteristics. Based on these predictions, they also estimate the profitability of connecting these new consumers by computing probability distributions to see if these candidate consumers have a high chance of being connected. However, the authors do not consider any network operation or expansion. In the light of the importance of the estimated demand, a highly reasonable topic of future research is to combine these two different branches of literature—namely heat future demand estimation and network expansion.

(ii) The distance of the candidate consumer to the existing network. Thus, one needs to accurately evaluate the pipe building costs and the chosen network layout if multiple consumers shall be connected. This aspect is, in principle, also covered in other papers on district heating networks such as [4] by also considering a price per length of the newly built pipes. However, we are, to the best of our knowledge, the first who measure these effects in the context of nonlinear and non-isothermal physics models.

(iii) Finally, the discussion of thermal power losses highlights the importance of a good pipe insulation. To the best of our knowledge, this aspect was not discussed in the literature before in this context.

To obtain a tractable model, we needed to simplify the problem. Note, however, that we still end up with a nonconvex mixed-integer nonlinear model, which is computationally very challenging. The most important assumption is that we restrict ourselves to the stationary case. Thus, we abstract from time-dependent, i.e. dynamic, effects of physics as well as from certain depot dynamics such as ramping constraints. Second, we only consider a single power-load scenario in the model. Incorporating multiple scenarios, for instance by using stochastic optimization, would allow for a better representation of future demands—and thus, most likely, for a better investment decision. However, this would put a significant additional computational burden. Third, we restricted ourselves to the case of tree-shaped networks to avoid complicating models for temperature mixing at the nodes of the network. Possible future work might also include the further exploitation of this tree-like structure to obtain more effective solution approaches for the problem discussed in this paper. If more general networks are considered, flow directions are not known in advance and one needs mixing models that are nonsmooth and lead to the violation of standard constraint qualifications of nonlinear optimization; see, e.g., [18] for the details. Finally, we abstracted from also choosing the diameters of newly built pipes, which could also be incorporated in the model. All the mentioned aspects are out of the scope of this article but part of our future work.

Acknowledgment: The second author thanks the Deutsche Forschungsgemeinschaft for their support within projects A05 and B08 in the Sonderforschungsbereich/Transregio 154 "Mathematical Modelling, Simulation and Optimization using the Example of Gas Networks". Both authors acknowledge the support by the German Bundesministerium für Bildung und Forschung within the project "EiFer". Moreover, we are very grateful to all the colleagues within the EiFer consortium for many fruitful discussions on the topics of this paper and for providing the data.

References

[1] M. Ameri and Z. Besharati. Optimal design and operation of district heating and cooling networks with cchp systems in a residential complex. *Energy and Buildings*, 110:135–148, 2016.

[2] A. Benonysson, B. Bøhm, and H. F. Ravn. Operational optimization in a

district heating system. *Energy Conversion and Management*, 36(5):297–314, 1995.

[3] M. Blommaert, R. Salenbien, and M. Baelmans. An adjoint approach to thermal network topology optimization, 2018.

[4] C. Bordin, A. Gordini, and D. Vigo. An optimization approach for district heating strategic network design. *European Journal of Operational Research*, 252(1):296–307, 2016.

[5] R. Borsche, M. Eimer, and N. Siedow. A local time stepping method for district heating networks, 2018.

[6] S. Bracco, G. Dentici, and S. Siri. Economic and environmental optimization model for the design and the operation of a combined heat and power distributed generation system in an urban area. *Energy*, 55:1014–1024, 2013.

[7] European Commission. Communication from the cimmission to the european parliament, the european council, the council, the european economic and social committe and the committe of the regions: The european green deal, 2019. Accessed 2020-04-02.

[8] T. Falke, S. Krengel, A.-K. Meinerzhagen, and A. Schnettler. Multi-objective optimization and simulation model for the design of distributed energy systems. *Applied Energy*, 184:1508–1516, 2016.

[9] A. Fügenschuh, B. Geißler, R. Gollmer, A. Morsi, M. E. Pfetsch, J. Rövekamp, M. Schmidt, K. Spreckelsen, and M. C. Steinbach. Physical and technical fundamentals of gas networks. In T. Koch, B. Hiller, M. E. Pfetsch, and L. Schewe, editors, *Evaluating Gas Network Capacities*, SIAM-MOS series on Optimization, chapter 2, pages 17–44. SIAM, 2015.

[10] B. Geißler, A. Morsi, L. Schewe, and M. Schmidt. Solving highly detailed gas transport MINLPs: Block separability and penalty alternating direction methods. *INFORMS Journal on Computing*, 30(2):309–323, 2018.

[11] E. Guelpa, G. Mutani, V. Todeschi, and V. Verda. Reduction of co2 emissions in urban areas through optimal expansion of existing district heating networks. *Journal of Cleaner Production*, 204:117–129, 2018.

[12] C. Haikarainen, F. Pettersson, and H. Saxén. A decomposition procedure for solving two-dimensional distributed energy system design problems. *Applied Thermal Engineering*, 100:30–38, 2016.

[13] E. Hairer, S. P. Nørsett, and G. Wanner. *Solving ordinary differential equations I. Nonstiff problems*. Springer Series in Computational Mathematics, 1993.

[14] F. M. Hante and M. Schmidt. Complementarity-based nonlinear programming techniques for optimal mixing in gas networks. *EURO Journal on Computational Optimization*, 7(3):299–323, 2019.

[15] W. E. Hart, C. D. Laird, J.-P. Watson, D. L. Woodruff, G. A. Hackebeil,

B. L. Nicholson, and J. D. Siirola. *Pyomo-optimization modeling in Python*. Springer, 2017.

[16] W. E. Hart, J.-P. Watson, and D. L. Woodruff. Pyomo: modeling and solving mathematical programs in Python. *Mathematical Programming Computation*, 3(3):219–260, 2011.

[17] S.-A. Hauschild, N. Marheineke, V. Mehrmann, J. Mohring, A. M. Badlyan, M. Rein, and M. Schmidt. Port-hamiltonian modeling of district heating networks. In *Progress in Differential Algebraic Equations II*, Differential-Albergaic Equations Forum. Springer, 2020.

[18] R. Krug, V. Mehrmann, and M. Schmidt. Nonlinear optimization of district heating networks. *Optimization and Engineering*, 2020.

[19] R. Köcher. Beitrag zur berechnung und auslegung von fernwärmenetzen, 2000.

[20] X.-l. Li, L. Duanmu, and H.-w. Shu. Optimal design of district heating and cooling pipe network of seawater-source heat pump. *Energy and Buildings*, 42(1):100–104, 2010. International Conference on Building Energy and Environment (COBEE 2008).

[21] J. E. Marsden and A. J. Chorin. *A mathematical introduction to fluid mechanics*. Springer-Verlag, 1993.

[22] D. Meha, T. Novosel, and N. Duić. Bottom-up and top-down heat demand mapping methods for small municipalities, case gllogoc. *Energy*, 199:117429, 2020.

[23] T. Mertz, S. Serra, A. Henon, and J. Reneaume. A minlp optimization of the configuration and the design of a district heating network: study case on an existing site. *Energy Procedia*, 116:236–248, 2017. 15th International Symposium on District Heating and Cooling, DHC15-2016, 4-7 September 2016, Seoul, South Korea.

[24] T. Mertz, S. Serra, A. Henon, and J.-M. Reneaume. A minlp optimization of the configuration and the design of a district heating network: Academic study cases. *Energy*, 117:450–464, 2016. The 28th International Conference on Efficiency, Cost, Optimization, Simulation and Environmental Impact of Energy Systems - ECOS 2015.

[25] R. Misener and C. A. Floudas. Antigone: Algorithms for continuous / integer global optimization of nonlinear equations. *Journal of Global Optimization*, 59(2):503–526, 2014.

[26] B. Morvaj, R. Evins, and J. Carmeliet. Optimising urban energy systems: Simultaneous system sizing, operation and district heating network layout. *Energy*, 116:619–636, 2016.

[27] T. Novosel, T. Pukšec, N. Duić, and J. Domac. Heat demand mapping and district heating assessment in data-pour areas. *Renewable and Sustainable Energy Reviews*, 131:109987, 2020.

[28] T. Nussbaumer and S. Thalmann. Influence of system design on heat distribution costs in district heating. *Energy*, 101:496–505, 2016.

[29] A. Omu, R. Choudhary, and A. Boies. Distributed energy resource system optimisation using mixed integer linear programming. *Energy Policy*, 61:249–266, 2013.

[30] M. Pagani, P. Maire, W. Korosec, N. Chokani, and R. Abhari. District heat network extension to decarbonise building stock: A bottom-up agent-based approach. *Applied Energy*, 272:115177, 2020.

[31] M. Rein, J. Mohring, T. Damm, and A. Klar. Parametric model order reduction for district heating networks. *PAMM*, 18(1), 2018.

[32] G. Sandou, S. Font, S. Tebbani, A. Hiret, C. Mondon, S. Tebbani, A. Hiret, and C. Mondon. Predictive control of a complex district heating network. In *Proceedings of the 44th IEEE Conference on Decision and Control*, pages 7372–7377, 2005.

[33] M. Schmidt, M. C. Steinbach, and B. M. Willert. High detail stationary optimization models for gas networks. *Optimization and Engineering*, 16(1):131–164, 2015.

[34] M. Schmidt, M. C. Steinbach, and B. M. Willert. The precise NLP model. In T. Koch, B. Hiller, M. E. Pfetsch, and L. Schewe, editors, *Evaluating Gas Network Capacities*, SIAM-MOS series on Optimization, chapter 10, pages 181–210. SIAM, 2015.

[35] M. Schmidt, M. C. Steinbach, and B. M. Willert. High detail stationary optimization models for gas networks: validation and results. *Optimization and Engineering*, 17(2):437–472, 2016.

[36] J. Söderman. Optimisation of structure and operation of district cooling networks in urban regions. *Applied Thermal Engineering*, 27(16):2665–2676, 2007. Selected Papers from the 9th Conference on Process Integration, Modelling and Optimisation for Energy Saving and Pollution Reduction – PRES2006.

[37] TWL. Preise für Fernwärme, 2020. Last accessed 2020-03-25.

[38] F. Verrilli, S. Srinivasan, G. Gambino, M. Canelli, M. Himanka, C. Del Vecchio, M. Sasso, and L. Glielmo. Model predictive control-based optimal operations of district heating system with thermal energy storage and flexible loads. *IEEE Transactions on Automation Science and Engineering*, 14(2):547–557, 2017.

[39] S. Werner. District heating and cooling in sweden. *Energy*, 126:419 – 429, 2017.

A Proof of Lemma 1

Two cases are considered for solving the ODE. First, we consider $v_a = 0$. Then, (5) reduces to

$$\frac{4U_a}{c_\mathrm{p}\rho D_a}(T_a(x) - T_\mathrm{soil}) = 0, \quad x \in [0, L_a].$$

This obviously leads to the first case in (6).

Next, we consider the case $v_a > 0$. In this case, (5) can be rewritten as

$$\frac{\mathrm{d}T_a}{\mathrm{d}x}(x) + \frac{4U_a}{c_\mathrm{p}\rho D_a v_a}T_a(x) = \frac{4U_a}{c_\mathrm{p}\rho D_a v_a}T_\mathrm{soil}, \quad x \in [0, L_a].$$

We know from classical ODE theory, see, e.g., [13], that the first-order ODE of the form

$$\frac{\mathrm{d}y(x)}{\mathrm{d}x} + ay(x) = b,$$

with constants a and b has the solution

$$y(x) = Ce^{-ax} + \frac{b}{a},$$

with C being another constant. This then allows to derive the second case of (6).

To prove continuity and since both cases in (6) are composed of continuous functions it suffices to see that

$$\lim_{v_a \to 0} T_a(x; v_a) = T_\mathrm{soil} = T_a(x; 0)$$

for all $x \in [0, L_a]$. This concludes the proof.

Article 2

Adaptive Nonlinear Optimization of District Heating Networks Based on Model and Discretization Catalogs

Hannes Dänschel, Volker Mehrmann, Marius Roland, Martin Schmidt
Submitted preprint (2022), URL: https://optimization-online.org/2022/01/8779/

Adaptive Nonlinear Optimization of District Heating Networks Based on Model and Discretization Catalogs

Hannes Dänschel, Volker Mehrmann, Marius Roland, and Martin Schmidt

Abstract. We propose an adaptive optimization algorithm for operating district heating networks in a stationary regime. The behavior of hot water flow in the pipe network is modeled using the incompressible Euler equations and a suitably chosen energy equation. By applying different simplifications to these equations, we derive a catalog of models. Our algorithm is based on this catalog and adaptively controls where in the network which model is used. Moreover, the granularity of the applied discretization is controlled in a similar adaptive manner. By doing so, we are able to obtain optimal solutions at low computational costs that satisfy a prescribed tolerance w.r.t. the most accurate modeling level. To adaptively control the switching between different levels and the adaptation of the discretization grids, we derive error formulas and a posteriori error estimators. Under reasonable assumptions we prove that the adaptive algorithm terminates after finitely many iterations. Our numerical results show that the algorithm is able to produce solutions for problem instances that have not been solvable before.

1. Introduction

An efficient and sustainable energy sector is at the core of the fight against the climate crisis. Thus, many countries around the world strive towards an energy turnaround with the overarching goal to replace fossil fuels with energy from renewable resources such as wind and solar power. However, one then faces issues with the high volatility of the fluctuating renewable resources. To overcome this fluctuating nature of wind and solar power, two main approaches are currently seen as the most promising ones: (i) the development and usage of large-scale energy storage systems as well as (ii) sector-coupling.

In this paper, we consider the computation of optimal operation strategies for district heating networks. These networks are used to provide customers with hot water in order to satisfy their heat demand. Thus, a district heating network can be seen both as a large-scale energy storage as well as a key element of successful sector-coupling. The hot water in the pipes of a district heating network is heated in so-called depots in which, usually, waste incineration is used as the primary heat source. If, however, waste incineration is not sufficient for heating the water, gas turbines are used as well. The hot water in the pipeline system can thus be seen as an energy storage that could, for instance, also be filled using power-to-heat technologies in time periods with surplus production of renewables. On the other hand, heat-to-power can be used to smooth the fluctuating nature of renewables in time periods with only small renewable production. Consequently, district heating networks can be seen as sector-coupling entities with inherent storage capabilities.

To make such operational strategies for district heating networks possible, an efficient control of the network is required that does not compromise the heat

Date: August 19, 2022.

2010 *Mathematics Subject Classification.* 90-XX, 90Cxx, 90C11, 90C35, 90C90.

Key words and phrases. District heating networks, Adaptive methods, Nonlinear optimization.

demand of the households that are connected to the network. However, a rigorous physical and technical modeling of hot water flow in pipes leads to hard mathematical optimization problems. At the core of these problems are partial differential equations for modeling both water and heat transport. Additionally, proper models of the depot and the households further increase the level of nonlinearity in the overall model. Finally, the tracking of water temperatures across nodes of the network leads to nonconvex and nonsmooth mixing models that put a significant burden on today's state-of-the-art optimization techniques.

In this paper, we consider the simplified setting of a stationary flow regime. For closed-loop control strategies for instationary variants of the problem we refer to [1, 24, 30] and to [12] for open-loop optimization approaches. Interestingly, the literature on mathematical optimization for district heating networks is rather sparse. An applied case study for a specific district heating network in South Wales is done in [16] and [22] provides more a general discussion of technological aspects and the potentials of district heating networks. In [26], the authors follow a first-discretize-then-optimize approach for the underlying PDE-constrained problem. For the relation between district heating networks and energy storage aspects we refer to [4, 10, 29] and the references therein. Stationary models of hot water flow are also considered in studies on the design and expansion of networks as, e.g., in [2, 5, 23]. Numerical simulation of district heating networks using a local time stepping method is studied in [3] and model order reduction techniques for the hyperbolic equations in district heating networks are discussed in [20] or [19, 21]. Finally, a port-Hamiltonian modeling approach for district heating networks is presented and discussed in [11].

Despite the mentioned simplification of considering stationary flow regimes, the optimization problems at hand are still large-scale and highly nonlinear mathematical programs with complementarity constraints (MPCCs) that are constrained by ordinary differential equations (ODEs). It turns out that these models are extremely hard to solve for realistic or even real-world district heating networks if they are presented to state-of-the-art optimization solvers. Our contribution is the development of an adaptive optimization algorithm that controls the modeling and the discretization of the hot water flow equations in the network. A similar approach has already been developed and tested for natural gas networks in [14]. The main rationale is that simplified (and thus computationally cheaper) models can lead to satisfactory (w.r.t. their physical accuracy) results for some parts of the network whereas other parts require a highly accurate modeling to obtain the required physical accuracy. The problem, however, is that it is not known up-front where which kind of modeling is appropriate. Our adaptive algorithm is based on (i) a catalog of different models of hot water flow and on (ii) different discretization grids for the underlying differential equations. The proposed method then controls the choice of the model and the discretization grid separately for every pipe in the network. The switching between different models and discretization grids is based on rigorous error measures so that we obtain a finite termination proof stating that the method computes a locally optimal point that is feasible w.r.t. the most accurate modeling level and a prescribed tolerance. Besides these theoretical contributions, we also show the effectiveness of our approach in practice and, in particular, illustrate that instances on realistic networks can be solved with the newly proposed method that have been unsolvable before.

The remainder of the paper is structured as follows. In Section 2 we present our modeling of district heating networks and derive the modeling catalog for hot water flow as well as the discretizations of the respective differential equations. After this, we derive exact errors and error estimators in Section 3 both for modeling

as well as discretization errors. These are then used in Section 4 to set up the adaptive optimization algorithm and to prove its finite termination. The algorithm is numerically tested in Section 5 before we close the paper with some concluding remarks and some aspects of potential future work in Section 6.

2. Modeling

We model the district heating network as a directed and connected graph $G = (V, A)$, which has a special structure. First, we have a so-called forward-flow part of the network, which is used to provide the consumers with hot water. Second, the cooled water is transported back to the depot in the so-called backward-flow part. These two parts are connected via the depot in which the cooled water is heated again, and via the consumers who use the temperature difference to satisfy the thermal energy demand in the corresponding household. The set of nodes of the forward-flow part is denoted by V_{ff} and the set of arcs of this part is denoted by A_{ff}, i.e., $a = (u, v) \in A_{\mathrm{ff}}$ implies $u, v \in V_{\mathrm{ff}}$. In analogy, the set of nodes of the backward-flow part is denoted by V_{bf} and the set of arcs of this part is denoted by A_{bf}, i.e., $a = (u, v) \in A_{\mathrm{bf}}$ implies $u, v \in V_{\mathrm{bf}}$. The depot arc is denoted by $a_{\mathrm{d}} = (u, v)$ with $u \in V_{\mathrm{bf}}$ and $v \in V_{\mathrm{ff}}$. The consumers are modeled with arcs $a = (u, v)$ with $u \in V_{\mathrm{ff}}$ and $v \in V_{\mathrm{bf}}$. Finally, all pipes of the forward and the backward flow part are contained in the set of pipes $A_{\mathrm{p}} = A_{\mathrm{ff}} \cup A_{\mathrm{bf}}$.

In the next subsection we present the model for all components of the network, i.e., for pipes, consumers, and the depot.

2.1. Pipes.

We now derive an approximation for the water flow in cylindrical pipes. This derivation is based on the 1-dimensional compressible Euler equations [3, 11, 21]

$$0 = \frac{\partial \rho_a}{\partial t} + v_a \frac{\partial \rho_a}{\partial x} + \rho_a \frac{\partial v_a}{\partial x}, \tag{1a}$$

$$0 = \frac{\partial (\rho_a v_a)}{\partial t} + v_a \frac{\partial (\rho_a v_a)}{\partial x} + \frac{\partial p_a}{\partial x} + \frac{\lambda_a}{2D_a} \rho_a |v_a| v_a + g \rho_a h'_a. \tag{1b}$$

Equation (1a) is the continuity equation and models mass balance, whereas the pressure gradient is described by the momentum equation (1b). Here and in what follows, ρ denotes the density of water, v its velocity, and p its pressure. In (1), the quantities are to be seen as functions in space (x) and time (t), i.e., for instance, $p = p(x, t)$. The diameter of a pipe a is denoted by D_a, λ_a is the pipe's friction coefficient, and h'_a denotes the slope of the pipe. Finally, g is the gravitational acceleration.

The incompressibility of water is modeled as $0 = \rho_a \frac{\partial v_a}{\partial x}$, cf. [11], which implies that

$$0 = \frac{\partial \rho_a}{\partial t} + v_a \frac{\partial \rho_a}{\partial x} \tag{2}$$

holds. Moreover, the further PDEs

$$0 = \frac{\partial e_a}{\partial t} + v_a \frac{\partial e_a}{\partial x} + p_a \frac{\partial v_a}{\partial x} - \frac{\lambda_a}{2D_a} \rho_a |v_a| v_a^2 + \frac{4k_W}{D_a} (T_a - T_{\mathrm{W}}), \tag{3a}$$

$$0 = \frac{\partial s_a}{\partial t} + v_a \frac{\partial s_a}{\partial x} + \frac{\lambda_a \rho_a}{2D_a T_a} |v_a| v_a^2 + \frac{4k_W}{D_a} \frac{(T_a - T_{\mathrm{W}})}{T_a} \tag{3b}$$

model conservation of internal energy density e and entropy density s, respectively; see [11]. The water's temperature is denoted by T_a. The parameters k_W and T_{W} are the heat transfer coefficient and the soil or pipe wall temperature.

The incompressible 1-dimensional Euler equations for the pipe flow arise from a simplification in which the small change (in time) of the pressure energy, and the (small) term of energy and power loss due to dissipation work have been neglected.

If one adds these terms, then it is possible to reformulate these equations in a port-Hamiltonian form [13]. Since the analysis of this energy-based formulation is not complete, we will not consider this extension here. It will be considered in future work.

To use the model in our optimization framework we consider the stationary case. For this, all partial derivatives w.r.t. time are set to zero and System (1)–(3) simplifies to

$$0 = \rho_a \frac{\mathrm{d}v_a}{\mathrm{d}x}, \tag{4a}$$

$$0 = v_a \frac{\mathrm{d}\rho_a}{\mathrm{d}x} + \rho_a \frac{\mathrm{d}v_a}{\mathrm{d}x}, \tag{4b}$$

$$0 = v_a \frac{\mathrm{d}(\rho_a v_a)}{\mathrm{d}x} + \frac{\mathrm{d}p_a}{\mathrm{d}x} + \frac{\lambda_a}{2D_a}\rho_a |v_a| v_a + g\rho_a h_a', \tag{4c}$$

$$0 = v_a \frac{\mathrm{d}e_a}{\mathrm{d}x} + p_a \frac{\mathrm{d}v_a}{\mathrm{d}x} - \frac{\lambda_a}{2D_a}\rho_a |v_a| v_a^2 + \frac{4k_W}{D_a}(T_a - T_\mathrm{W}), \tag{4d}$$

$$0 = v_a \frac{\mathrm{d}s_a}{\mathrm{d}x} + \frac{\lambda_a \rho_a}{2D_a T_a}|v_a| v_a^2 + \frac{4k_W}{D_a}\frac{(T_a - T_\mathrm{W})}{T_a}. \tag{4e}$$

Since $\rho_a > 0$ holds, Equation (4a) implies that $v_a(x) = v_a$ is constant for all pipes. Using this, (4b) leads to that the density $\rho_a(x) = \rho_a$ is constant as well. In addition, we set $\rho_a = \rho$ for all arcs a of the network. With the mass flow

$$q_a = A_a \rho v_a \tag{5}$$

and constant velocities and densities we also have that $q_a(x) = q_a$ is constant for all pipes. In (5), A_a denotes the cross-sectional area of pipe a. By subsuming the discussed simplifications we get the system

$$0 = \frac{\mathrm{d}p_a}{\mathrm{d}x} + \frac{\lambda_a}{2D_a}\rho |v_a| v_a + g\rho h_a', \tag{6a}$$

$$0 = v_a \frac{\mathrm{d}e_a}{\mathrm{d}x} - \frac{\lambda_a}{2D_a}\rho |v_a| v_a^2 + \frac{4k_W}{D_a}(T_a - T_\mathrm{W}), \tag{6b}$$

$$0 = v_a \frac{\mathrm{d}s_a}{\mathrm{d}x} + \frac{\lambda_a \rho}{2D_a T_a}|v_a| v_a^2 + \frac{4k_W}{D_a}\frac{(T_a - T_\mathrm{W})}{T_a}. \tag{6c}$$

In Equation (6a), the pressure gradient term is the only term that depends on the spatial position x. Hence, we obtain the stationary momentum and energy equation

$$0 = \frac{p_a(L_a) - p_a(0)}{L_a} + \frac{\lambda_a}{2D_a}\rho |v_a| v_a + g\rho h_a', \tag{M1a}$$

$$0 = v_a \frac{\mathrm{d}e_a}{\mathrm{d}x} - \frac{\lambda_a}{2D_a}\rho |v_a| v_a^2 + \frac{4k_W}{D_a}(T_a - T_\mathrm{W}). \tag{M1b}$$

In the following, for our optimization framework, we do not consider the entropy equation, which can be solved in a post-processing step once the optimal pressure and internal energy values have been determined.

The system is closed by the state equations

$$\rho = 997\,\mathrm{kg\,m^{-3}}, \tag{7a}$$

$$T_a = \theta_2 (e_a^*)^2 + \theta_1 e_a^* + \theta_0, \tag{7b}$$

in which we set

$$e_a^* := \frac{e_a}{e_0}, \quad e_0 := 10^9\,\mathrm{J\,m^{-3}},$$
$$\theta_2 = 59.2453\,\mathrm{K}, \quad \theta_1 = 220.536\,\mathrm{K}, \quad \theta_0 = 274.93729\,\mathrm{K}.$$

Equation (7b) is known to be a reasonable approximation for $e_a \in [0.2, 0.5]\,\mathrm{GJ\,m^{-3}}$, $T_a \in [323, 403]\,\mathrm{K}$, and $p_a \in [5, 25]\,\mathrm{bar}$; see, e.g., [11].

2.1.1. *Model Catalog.* For the adaptive optimization method developed in this work we employ a catalog of models. In this catalog, System (M1) represents the highest or first modeling level, i.e., the most accurate one.

To derive the second modeling level, we neglect the (small) term $\lambda_a/(2D_a)\rho v_a^2|v_a|$ and get

$$0 = \frac{p_a(L_a) - p_a(0)}{L_a} + \frac{\lambda_a}{2D_a}\rho|v_a|v_a + g\rho h_a', \tag{M2a}$$

$$0 = v_a\frac{\mathrm{d}e_a}{\mathrm{d}x} + \frac{4k_W}{D_a}(T_a - T_\mathrm{W}). \tag{M2b}$$

By further assuming that the first term in (M2b) dominates the second one, we can neglect the term $4k_W/D_a(T_a - T_\mathrm{W})$ and simplify System (M2) to obtain the third level as

$$\begin{aligned} 0 &= \frac{p_a(L_a) - p_a(0)}{L_a} + \frac{\lambda_a}{2D_a}\rho|v_a|v_a + g\rho h_a', \\ 0 &= e_a(L_a) - e_a(0). \end{aligned} \tag{M3}$$

2.1.2. *Exact Solution of the Energy Equation.* The equations (M1b) and (M2b) can be solved analytically. This is done in the following lemma.

Lemma 1. *The differential equation (M1b), i.e.,*

$$0 = v_a\frac{\mathrm{d}e_a}{\mathrm{d}x} - \frac{\lambda_a}{2D_a}\rho|v_a|v_a^2 + \frac{4k_W}{D_a}(T_a - T_W),$$

with initial condition

$$e_a(0) = e_a^0 > 0$$

and state equation (7b) has the exact solution

$$e_a(x) = \frac{\sqrt{\beta^2 - 4\alpha\gamma}}{2\alpha}\frac{1 + \exp\left(\frac{x\sqrt{\beta^2-4\alpha\gamma}}{\zeta}\right)\left(\frac{2\alpha e_a^0 + \beta - \sqrt{\beta^2-4\alpha\gamma}}{2\alpha e_a^0 + \beta + \sqrt{\beta^2-4\alpha\gamma}}\right)}{1 - \exp\left(\frac{x\sqrt{\beta^2-4\alpha\gamma}}{\zeta}\right)\left(\frac{2\alpha e_a^0 + \beta - \sqrt{\beta^2-4\alpha\gamma}}{2\alpha e_a^0 + \beta + \sqrt{\beta^2-4\alpha\gamma}}\right)} - \frac{\beta}{2\alpha}$$

with

$$\begin{aligned} \alpha &:= -\frac{4k_W\theta_2}{D_a(e_0)^2}, \quad \beta := -\frac{4k_W\theta_1}{D_a e_0}, \quad \zeta := v_a, \\ \gamma &:= \frac{\lambda_a}{2D_a}\rho|v_a|v_a^2 - \frac{4k_W}{D_a}(\theta_0 - T_W), \end{aligned} \tag{8}$$

if $4\alpha\gamma - \beta^2 < 0$ is satisfied.

Proof. We combine (M1b) and (7b) to obtain

$$0 = v_a\frac{\mathrm{d}e_a}{\mathrm{d}x} - \frac{\lambda_a}{2D_a}\rho_a|v_a|v_a^2 + \frac{4k_W}{D_a}(\theta_2(e_a^*)^2 + \theta_1 e_a^* + \theta_0 - T_\mathrm{W}).$$

After re-organizing and replacing e_a^* by its definition, the equation reads

$$-\frac{4k_W\theta_2}{D_a(e_0)^2}(e_a)^2 - \frac{4k_W\theta_1}{D_a e_0}e_a - \frac{4k_W}{D_a}(\theta_0 - T_\mathrm{W}) + \frac{\lambda_a}{2D_a}\rho_a|v_a|v_a^2 = v_a\frac{\mathrm{d}e_a}{\mathrm{d}x}. \tag{9}$$

We combine Equation (9) with the definitions in (8) and get

$$\alpha e_a^2 + \beta e_a + \gamma = \zeta\frac{\mathrm{d}e_a}{\mathrm{d}x}. \tag{10}$$

Equation (10) is a Riccati equation with constant coefficients; see, e.g., [18]. Because α, β, γ, and ζ do not depend on x, they can be seen as constants when integrating over x. We re-organize and integrate both sides over x, yielding

$$\int 1 \, \mathrm{d}x = \int \frac{\zeta \frac{\mathrm{d}e_a}{\mathrm{d}x}}{\alpha(e_a)^2 + \beta e_a + \gamma} \, \mathrm{d}x. \tag{11}$$

Applying a variable change in the right-hand side of (11) leads to

$$\frac{x}{\zeta} = \int \frac{1}{\alpha(e_a)^2 + \beta e_a + \gamma} \, \mathrm{d}e_a. \tag{12}$$

We may rewrite

$$\begin{aligned} \alpha(e_a)^2 + \beta e_a + \gamma &= \left((e_a)^2 + \frac{\beta}{\alpha} e_a + \frac{\beta^2}{4\alpha^2} \right) + \frac{4\alpha\gamma - \beta^2}{4\alpha} \\ &= \alpha \left(\left(e_a + \frac{\beta}{2\alpha} \right)^2 + \frac{4\alpha\gamma - \beta^2}{4\alpha^2} \right), \end{aligned}$$

since $4\alpha\gamma - \beta^2 < 0$ holds by assumption. Therefore, we have

$$\alpha \left(\left(e_a + \frac{\beta}{2\alpha} \right)^2 + \frac{4\alpha\gamma - \beta^2}{4\alpha^2} \right) = \alpha \left(\left(e_a + \frac{\beta}{2\alpha} \right)^2 - \left(\frac{\sqrt{\beta^2 - 4\alpha\gamma}}{2\alpha} \right)^2 \right).$$

Going back to (12) we have

$$\begin{aligned} &\int \frac{1}{\alpha(e_a)^2 + \beta e_a + \gamma} \, \mathrm{d}e_a \\ &= \int \frac{1}{\alpha \left(\left(e_a + \frac{\beta}{2\alpha} \right)^2 - \left(\frac{\sqrt{\beta^2 - 4\alpha\gamma}}{2\alpha} \right)^2 \right)} \, \mathrm{d}e_a, \\ &= C_1 \int \frac{\frac{\sqrt{\beta^2 - 4\alpha\gamma}}{\alpha}}{\left(e_a + \frac{\beta}{2\alpha} \right)^2 - \left(\frac{\sqrt{\beta^2 - 4\alpha\gamma}}{2\alpha} \right)^2} \, \mathrm{d}e_a, \\ &= C_1 \int \frac{\frac{\sqrt{\beta^2 - 4\alpha\gamma}}{2\alpha} + \frac{\sqrt{\beta^2 - 4\alpha\gamma}}{2\alpha} + e_a + \frac{\beta}{2\alpha} - e_a - \frac{\beta}{2\alpha}}{\left(e_a + \frac{\beta}{2\alpha} \right)^2 - \left(\frac{\sqrt{\beta^2 - 4\alpha\gamma}}{2\alpha} \right)^2} \, \mathrm{d}e_a, \\ &= C_1 \int \left(\left(e_a + \frac{\beta}{2\alpha} - \frac{\sqrt{\beta^2 - 4\alpha\gamma}}{2\alpha} \right)^{-1} - \left(e_a + \frac{\beta}{2\alpha} + \frac{\sqrt{\beta^2 - 4\alpha\gamma}}{2\alpha} \right)^{-1} \right) \mathrm{d}e_a, \\ &= C_1 \ln \left| \frac{2\alpha e_a + \beta - \sqrt{\beta^2 - 4\alpha\gamma}}{2\alpha e_a + \beta + \sqrt{\beta^2 - 4\alpha\gamma}} \right| + C_2, \end{aligned}$$

where we set

$$C_1 := \frac{1}{\sqrt{\beta^2 - 4\alpha\gamma}}.$$

The internal energy equation thus reduces to

$$\frac{x}{\zeta} = C_1 \ln \left| \frac{2\alpha e_a(x) + \beta - \sqrt{\beta^2 - 4\alpha\gamma}}{2a e_a(x) + \beta + \sqrt{\beta^2 - 4\alpha\gamma}} \right| + C_2.$$

By re-substituting the definition of C_1 we may write

$$\sqrt{\beta^2-4\alpha\gamma}\left(\frac{x}{\zeta}-C_2\right)=\ln\left|\frac{2\alpha e_a(x)+\beta-\sqrt{\beta^2-4\alpha\gamma}}{2ae_a(x)+\beta+\sqrt{\beta^2-4\alpha\gamma}}\right|. \tag{13}$$

We define $C_3 := \exp\left(-C_2\sqrt{\beta^2-4\alpha\gamma}\right)$. Then, (13) leads to

$$C_3\exp\left(\frac{x\sqrt{\beta^2-4\alpha\gamma}}{\zeta}\right)=\left|\frac{2\alpha e_a(x)+\beta-\sqrt{\beta^2-4\alpha\gamma}}{2ae_a(x)+\beta+\sqrt{\beta^2-4\alpha\gamma}}\right|.$$

The constant C_3 then absorbs the $\pm$ sign such that we can write

$$C_3\exp\left(\frac{x\sqrt{\beta^2-4\alpha\gamma}}{\zeta}\right)=\left(\frac{2\alpha e_a(x)+\beta-\sqrt{\beta^2-4\alpha\gamma}}{2ae_a(x)+\beta+\sqrt{\beta^2-4\alpha\gamma}}\right). \tag{14}$$

We compute C_2 using the initial condition at $x=0$ and obtain

$$C_3=\left(\frac{2\alpha e_a^0+\beta-\sqrt{\beta^2-4\alpha\gamma}}{2ae_a^0+\beta+\sqrt{\beta^2-4\alpha\gamma}}\right). \tag{15}$$

Finally, we combine Equation (14) and (15), yielding

$$e_a(x)=\frac{\sqrt{\beta^2-4\alpha\gamma}}{2\alpha}\frac{1+\exp\left(\frac{x\sqrt{\beta^2-4\alpha\gamma}}{\zeta}\right)\left(\frac{2\alpha e_a^0+\beta-\sqrt{\beta^2-4\alpha\gamma}}{2\alpha e_a^0+\beta+\sqrt{\beta^2-4\alpha\gamma}}\right)}{1-\exp\left(\frac{x\sqrt{\beta^2-4\alpha\gamma}}{\zeta}\right)\left(\frac{2\alpha e_a^0+\beta-\sqrt{\beta^2-4\alpha\gamma}}{2\alpha e_a^0+\beta+\sqrt{\beta^2-4\alpha\gamma}}\right)}-\frac{\beta}{2\alpha}. \qquad \square$$

Let us further note that the condition $4\alpha\gamma-\beta^2<0$ of the last lemma is satisfied for usual pipe parameters.

Corollary 1. *The differential equation* (M2b)*, i.e.,*

$$0=v_a\frac{\mathrm{d}e_a}{\mathrm{d}x}+\frac{4k_W}{D_a}(T_a-T_W),$$

with initial condition

$$e_a(0)=e_a^0>0$$

and state equation (7b) *has the solution*

$$e_a(x)=\frac{\sqrt{\beta^2-4\alpha\gamma}}{2\alpha}\frac{1+\exp\left(\frac{x\sqrt{\beta^2-4\alpha\gamma}}{\zeta}\right)\left(\frac{2\alpha e_a^0+\beta-\sqrt{\beta^2-4\alpha\gamma}}{2\alpha e_a^0+\beta+\sqrt{\beta^2-4\alpha\gamma}}\right)}{1-\exp\left(\frac{x\sqrt{\beta^2-4\alpha\gamma}}{\zeta}\right)\left(\frac{2\alpha e_a^0+\beta-\sqrt{\beta^2-4\alpha\gamma}}{2\alpha e_a^0+\beta+\sqrt{\beta^2-4\alpha\gamma}}\right)}-\frac{\beta}{2\alpha}$$

with

$$\alpha:=-\frac{4k_W\theta_2}{D_a(e_0)^2},\quad \beta:=-\frac{4k_W\theta_1}{D_ae_0},\quad \gamma:=-\frac{4k_W}{D_a}(\theta_0-T_W),\quad \zeta:=v_a,$$

if $4\alpha\gamma-\beta^2<0$ *is satisfied.*

The proof is analogous to the one of Lemma 1. Figure 1 shows the exact solution of (M1b) for a specific pipe.

The exact solutions derived in the last lemma and corollary could, in principle, be used as constraints in a nonlinear optimization model. However, the fractions, square roots, and exponential functions would lead to a very badly posed problem resulting in an extreme numerical challenge even for state-of-the-art solvers.

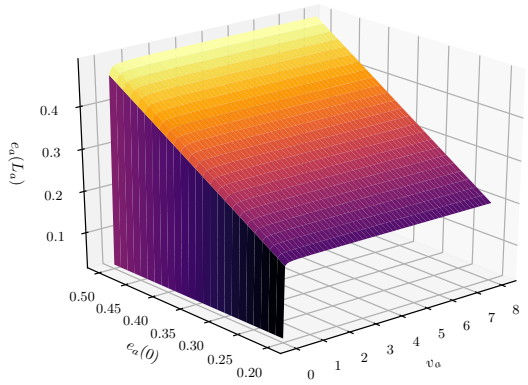

FIGURE 1. Solution of Equation (M1b) for positive velocities and the parameters $k_W = 0.5\,\mathrm{W\,m^{-2}\,K^{-1}}$, $\lambda_a = 0.017$, $D_a = 0.107\,\mathrm{m}$, $L_a = 1000\,\mathrm{m}$, and $T_\mathrm{W} = 278\,\mathrm{K}$. The units of the internal energy density e_a and the velocity v_a are $\mathrm{GJ\,m^{-3}}$ and $\mathrm{m\,s^{-1}}$, respectively.

2.1.3. *Discretization.* In order to solve the optimization problem, we follow the first-discretize-then-optimize approach and introduce an equidistant discretization Γ_a of the spatial domain $[0, L_a]$ using the discretization points $x_k \in \Gamma_a$ such that $0 = x_0 < x_1 < \cdots < x_{n_a} = L_a$ with the step size $\Delta x_a = x_{k+1} - x_k$ for $k = 0, 1, \ldots, n_a - 1$. We use the implicit mid-point rule to discretize the separate levels of the catalog, i.e., Systems (M1)–(M3), as well as the state equation (7b). Using the abbreviation $e_a^k := e_a(x_k)$, we obtain the discretized system

$$\begin{aligned} 0 &= \frac{p_a(L_a) - p_a(0)}{L_a} + \frac{\lambda_a \rho}{2D_a}|v_a|v_a + g\rho h_a', \\ 0 &= v_a \left(\frac{e_a^k - e_a^{k-1}}{\Delta x} \right) - \frac{\lambda_a \rho}{2D_a}|v_a|v_a^2 + \frac{4k_W}{D_a}\left(T_a(e_a^k, e_a^{k-1}) - T_\mathrm{W}\right) \end{aligned} \tag{D1}$$

for all $k = 1, \ldots, n_a$. Discretizing (M2) analogously leads to

$$\begin{aligned} 0 &= \frac{p_a(L_a) - p_a(0)}{L_a} + \frac{\lambda_a \rho}{2D_a}|v_a|v_a + g\rho h_a', \\ 0 &= v_a \left(\frac{e_a^k - e_a^{k-1}}{\Delta x} \right) + \frac{4k_W}{D_a}\left(T_a(e_a^k, e_a^{k-1}) - T_\mathrm{W}\right) \end{aligned} \tag{D2}$$

for all $k = 1, \ldots, n_a$. The discretized systems (D1) and (D2) are closed by the discretized version of the state equation (7b), i.e., by

$$T_a(e_a^k, e_a^{k-1}) := \frac{\theta_2}{4e_0^2}\left(e_a^k + e_a^{k-1}\right)^2 + \frac{\theta_1}{2e_0}\left(e_a^k + e_a^{k-1}\right) + \theta_0 \tag{16}$$

for all $k = 1, \ldots, n_a$. For System (M3), we get

$$\begin{aligned} 0 &= \frac{p_a(L_a) - p_a(0)}{L_a} + \frac{\lambda_a \rho}{2D_a}|v_a|v_a + g\rho h_a', \\ 0 &= e_a(L_a) - e_a(0), \end{aligned} \tag{D3}$$

i.e., a two-point discretization is always exact. The model catalog (both for the original and the discretized version) is depicted in Figure 2.

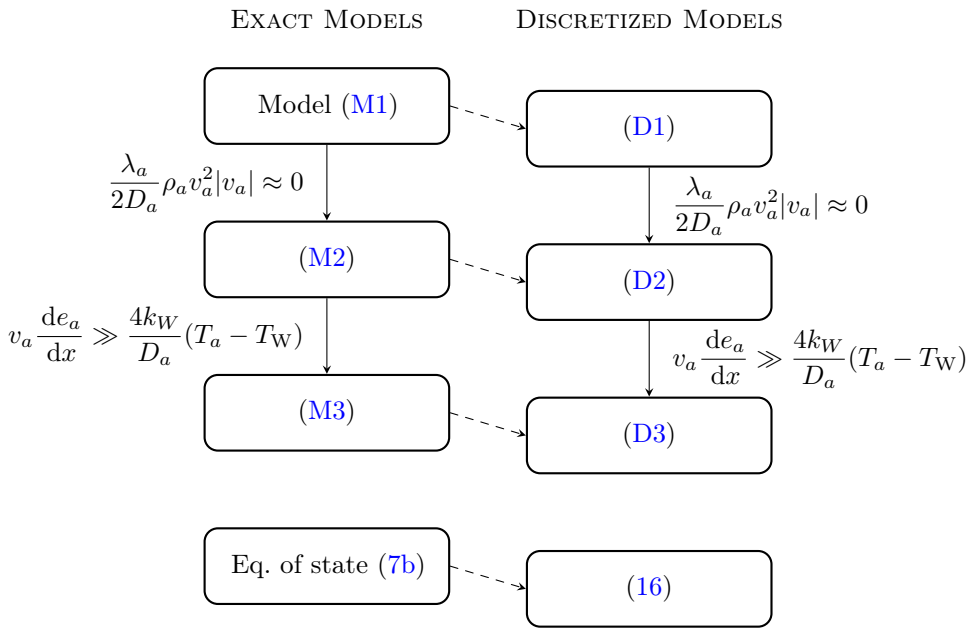

Figure 2. Model catalog for hot water flow in a pipe.

2.2. **Nodes.** In this section, we discuss the modeling of nodes in the district heating network. To this end, we mainly follow the modeling approach presented in [12]. We model mass conservation via

$$\sum_{a\in\delta^{\mathrm{in}}(u)} q_a = \sum_{a\in\delta^{\mathrm{out}}(u)} q_a, \quad u \in V, \tag{17}$$

where $\delta^{\mathrm{in}}(u)$ and $\delta^{\mathrm{out}}(u)$ model the set of in- and outgoing arcs of node u, respectively. We assume continuity of pressure at the nodes and obtain

$$\begin{aligned} p_u &= p_a(0), \quad u \in V,\ a \in \delta^{\mathrm{out}}(u), \\ p_u &= p_a(L_a), \quad u \in V,\ a \in \delta^{\mathrm{in}}(u), \end{aligned} \tag{18}$$

where p_u is the pressure at node u.

Finally, we have to model how the internal energy is mixed at the nodes of the network. To describe this, we use the perfect mixing model

$$\sum_{a\in\delta^{\mathrm{in}}(u)} \frac{e_{a:u}q_a}{\rho_a} = \sum_{a\in\delta^{\mathrm{out}}(u)} \frac{e_{a:u}q_a}{\rho_a}, \tag{19a}$$

$$0 = \beta_a(e_{a:u} - e_u), \quad a \in \delta^{\mathrm{out}}(u), \tag{19b}$$

$$0 = \gamma_a(e_{a:u} - e_u), \quad a \in \delta^{\mathrm{in}}(u), \tag{19c}$$

with

$$q_a = \beta_a - \gamma_a, \quad \beta_a \geq 0, \quad \gamma_a \geq 0, \quad \beta_a\gamma_a = 0 \tag{20}$$

for $a \in \delta(u) = \delta^{\mathrm{in}}(u) \cup \delta^{\mathrm{out}}(u)$. Here and in what follows, we denote with $e_{a:u}$ the internal energy in pipe a at its end node u. For more details and a derivation of this model we refer to [7, 11, 12, 25].

2.3. **Depot and Consumers.** Following [12, 23], for the depot $a_{\mathrm{d}} = (u, v)$ we have the constraints

$$p_u = p_{\mathrm{s}}, \tag{21a}$$

$$P_{\mathrm{p}} = \frac{q_{a_{\mathrm{d}}}}{\rho} \left(p_{a_{\mathrm{d}}:v} - p_{a_{\mathrm{d}}:u} \right), \tag{21b}$$

$$P_{\mathrm{w}} + P_{\mathrm{g}} = \frac{q_{a_{\mathrm{d}}}}{\rho} \left(e_{a_{\mathrm{d}}:v} - e_{a_{\mathrm{d}}:u} \right), \tag{21c}$$

where p_{s} is the so-called stagnation pressure that is used to make the overall pressure profile in the network unique. Moreover, P_{p} is the power required for the pressure increase realized at the depot, P_{w} is the power obtained by waste incineration and P_{g} is the power obtained by burning natural gas. The latter two quantities are used in the depot to increase the internal energy density or, equivalently, the temperature of the water.

In order to model the consumers $a = (u, v) \in A_{\mathrm{c}}$, we use the constraints

$$P_a = \frac{q_a}{\rho} \left(e_{a:v} - e_{a:u} \right), \tag{22a}$$

$$e_{a:u} \geq e_a^{\mathrm{ff}}, \tag{22b}$$

$$e_{a:v} = e^{\mathrm{bf}}, \tag{22c}$$

$$p_v \leq p_u. \tag{22d}$$

The first constraint models how the required thermal energy P_a is obtained in dependence on the mass flow q_a at the consumer and the difference $e_{a:v} - e_{a:u}$ of the internal energy density. The internal energy density at inflow conditions $(e_{a:u})$ needs to be larger than the given threshold e_a^{ff} and, at outflow conditions, it is fixed to the network-wide constant e^{bf}. Finally, the fourth constraint states that the pressure cannot be increased at the household of a consumer.

2.4. **Bounds, Objective Function, and Model Summary.** To complete the model we need to incorporate some technical and physical bounds on the variables of the model and to define a proper objective function. First, we have bounds on the mass flow, i.e.,

$$q_a^- \leq q_a \leq q_a^+, \quad a \in A_{\mathrm{ff}} \cup A_{\mathrm{bf}} \cup A_{\mathrm{c}}, \tag{23}$$

on the nodal pressures,

$$0 \leq p_u \leq p_u^+, \quad u \in V, \tag{24}$$

and on the nodal water temperatures, i.e.,

$$T_u \in [T_u^-, T_u^+], \quad u \in V. \tag{25}$$

Lastly, we incorporate bounds on power consumption, i.e.,

$$P_{\mathrm{p}} \in [0, P_{\mathrm{p}}^+], \quad P_{\mathrm{w}} \in [0, P_{\mathrm{w}}^+], \quad P_{\mathrm{g}} \in [0, P_{\mathrm{g}}^+] \tag{26}$$

for given upper bounds P_{p}^+, P_{w}^+, and P_{g}^+.

Our goal is to minimize the overall costs required to satisfy the heat demand of all the consumers. Thus, the objective function is given by

$$C_{\mathrm{p}} P_{\mathrm{p}} + C_{\mathrm{w}} P_{\mathrm{w}} + C_{\mathrm{g}} P_{\mathrm{g}}, \tag{27}$$

where $C_{\mathrm{p}}, C_{\mathrm{w}}$, and C_{g}, respectively, correspond to the cost of pressure increase, waste incineration, and burning gas.

Taking this all together leads to the discretized and thus finite-dimensional optimization problem

$$\begin{aligned}
\min\quad & \text{objective: (27)},\\
\text{s.t.}\quad & \text{pipe flow and thermal modeling: (16) and (D1), (D2), or (D3)},\\
& \text{mass conservation: (17)},\\
& \text{pressure continuity: (18)},\\
& \text{temperature mixing: (19), (20)},\\
& \text{depot constraints: (21)},\\
& \text{consumer constraints: (22)},\\
& \text{bounds: (23)–(26)}.
\end{aligned} \tag{NLP}$$

This is a highly nonlinear and, depending on the chosen grids, large-scale optimization problem. Moreover, it only possesses very few degrees of freedom since almost all variables are determined by our physical modeling. Both aspects already make the problem very challenging to solve. In addition, however, the model also contains the complementarity constraints (20), which makes it an ODE-constrained mathematical program with complementarity constraints (MPCC). Solving it for real-world networks is very challenging, which is the motivation of the error-based adaptive algorithm that we develop in the two following sections.

3. Error Measures

In this section, we introduce the error measures for the adaptive optimization algorithm that is presented in Section 4. Our approach is based on the work of [14] and adapted for the problem at hand. The algorithm developed here is designed to iteratively solve the nonlinear program (NLP) until its solution y is deemed to be feasible w.r.t. a prescribed tolerance. The algorithm iteratively switches the model level and the step sizes of the discretization grids for each pipe according to a switching strategy presented later on. Both the switching strategy and the feasibility check utilize the error measures in this section.

For the (NLP), four error sources can be identified: errors as introduced by the solver of the optimization problem, round-off errors, errors from switching between Systems (D1)–(D3), and errors due to selecting different step sizes of the discretization of the systems. In this work we will only consider the latter two error sources, which we refer to as model (level) errors and discretization (level) errors, respectively. For a discussion of the neglected solver and round-off errors we refer to Remark 1 below. By investigating the Systems (D1)–(D3) one finds that the only difference between them, and hence the resulting error source, is the energy equation and its discretization. This is why we base the definition of the error in each pipe a on its internal energy density e_a.

In general, utilizing estimates of the error of a system allows for the assessment of the quality of their solution if an exact solution is not available. Hence, this section is used to introduce error estimates for the model and discretization error. However, since we have the analytic solution of the energy equations of Systems (M1)–(M3) at hand, we can compute exact errors for the model and discretization error. Having the exact errors available allows us to compare them to the error estimates presented in this work and, hence, determine their quality.

This section is structured as follows. We start by providing the required notation in Section 3.1. Furthermore, the rules that are used to refine and coarsen the grids in the discretization of Systems (D1)–(D3) are introduced. In Section 3.2, we continue by deriving exact and estimated error measures. We then close this

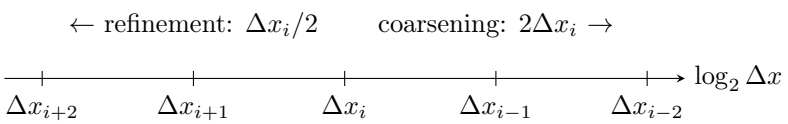

FIGURE 3. Step-size refinement strategy by halving or doubling the current step size Δx_i

section by proving that the error estimates form upper bounds of the exact errors in a first-order approximation.

Remark 1. *Since we want to be able to employ different third-party optimization software packages in our adaptive error control we do not incorporate the errors introduced by the solvers for the optimization problem. However, if error estimates and error control for these errors are available then these can be incorporated as well. It has been observed in the application of adaptive methods for gas networks [14, 28] that round-off errors typically do not contribute much to the global error. For this reason, we also do not consider round-off errors in our adaptive procedure for district heating networks.*

3.1. **Notation.** We start this section by introducing the required quantities and notation. In order to keep the notation lucid, we omit the usage of the subscript a as much as possible in this section. In particular, we drop the subscript a for the model level ($\ell_a \to \ell$), the grid size ($\Delta x_a \to \Delta x$), and for the set of gridpoints ($\Gamma_a \to \Gamma$), if not stated otherwise.

Let y denote the solution of the optimization problem (NLP). For all pipes $a \in A_\mathrm{p}$ it contains the approximate solution $e_a^\ell(x_k; \Delta x)$ for model level ℓ (of pipe model (Dℓ)) and step size Δx (of discretization grid Γ) at every grid point $x_k \in \Gamma$, $k = 1, \dots, n$. In addition, for a given pipe a we denote the exact solution of model (Mℓ), evaluated at $x_k \in \Gamma$ as $e_a^\ell(x_k)$. Furthermore, for the approximate and exact solutions we also utilize the notion of $e_a^\ell(\Gamma; \Delta x) := (e_a^\ell(x_1; \Delta x), \dots, e_a^\ell(x_n; \Delta x))^\top$ and $e_a^\ell(\Gamma) := (e_a^\ell(x_1), \dots, e_a^\ell(x_n))^\top$, respectively.

We continue by defining the grid refinement and coarsening rules. For a given pipe a, consider a sequence of grids $\{\Gamma_i\}$, $i = 0, 1, 2, \dots$, with $\Gamma_i := \{x_{k_i}\}_{k_i=1}^{n_i}$ and $\Delta x_i = x_{k_{i+1}} - x_{k_i}$ for $k_i = 1, \dots, n_i$. Moreover, we refer to Γ_0 as the reference or evaluation grid. It is defined by a given number of grid points n_0 and the corresponding step size $\Delta x_0 := L_a/(n_0 - 1)$. Given an arbitrary grid Γ_i, $i = 0, 1, 2, \dots$, we perform a grid refinement step by halving its step size Δx_i to get $\Delta x_{i+1} = \Delta x_i/2$ of the refined grid Γ_{i+1}. Conversely, we perform a grid coarsening step by doubling Δx_i of grid Γ_i to obtain the coarsened grid Γ_{i-1} with step size $\Delta x_{i-1} = 2\Delta x_i$. Figure 3 depicts a visualization of the grid refinement and coarsening rules. Performing grid refinement and coarsening this way ensures that for every $i = 1, 2, \dots$ it holds that $\Gamma_0 \subset \Gamma_i$. Therefore, providing a fixed number of grid points n_0 enables us to use the reference grid Γ_0 as a common evaluation grid for every refinement and coarsening step.

3.2. **Derivation of Error Measures.** In the following, we introduce two error measures: exact errors and error estimates. To this end, we consider a single pipe $a \in A_\mathrm{p}$. We start by defining the total exact error as

$$\nu_a(y) := \|e_a^1(\Gamma_0) - e_a^\ell(\Gamma_0; \Delta x_i)\|_\infty, \tag{28}$$

where we compare the approximate solution of Model (Dℓ) with grid size Δx_i to the exact solution of Model (M1). Second, we introduce the exact model error via

$$\nu_a^\mathrm{m}(y) := \|e_a^1(\Gamma_0) - e_a^\ell(\Gamma_0)\|_\infty\,, \tag{29}$$

where we compare the solutions of models (Mℓ) and (M1). Next, we define the exact discretization error as

$$\nu_a^{\mathrm{d}}(y) := \|e_a^{\ell}(\Gamma_0) - e_a^{\ell}(\Gamma_0; \Delta x_i)\|_{\infty}, \tag{30}$$

for which we compare the solution of Model (Dℓ) with grid size Δx_i to the exact solution of Model (Mℓ). We continue by introducing error estimates. The (total) error estimate is defined as the sum of a model error estimate and a discretization error estimate. That is,

$$\eta_a(y) := \eta_a^{\mathrm{m}}(y) + \eta_a^{\mathrm{d}}(y) \tag{31}$$

with the model error estimate

$$\eta_a^{\mathrm{m}}(y) := \|e_a^{1}(\Gamma_0; \Delta x_i) - e_a^{\ell}(\Gamma_0; \Delta x_i)\|_{\infty} \tag{32}$$

and the discretization error estimate

$$\eta_a^{\mathrm{d}}(y) := \|e_a^{\ell}(\Gamma_0; \Delta x_i) - e_a^{\ell}(\Gamma_0; \Delta x_{i-1})\|_{\infty}. \tag{33}$$

The model error estimate compares two solutions with the same discretization scheme but different pipe models (D1) and (Dℓ). On the other hand, the discretization error estimate compares two solutions of the same model but with different discretization schemes as given by the step sizes Δx_i and Δx_{i-1}.

By considering the definitions (28)–(33) one finds the relation

$$\begin{aligned}
\nu_a(y) &= \|e_a^{1}(\Gamma_0) - e_a^{\ell}(\Gamma_0; \Delta x_i) + e_a^{\ell}(\Gamma_0) - e_a^{\ell}(\Gamma_0)\|_{\infty} \\
&\leq \|e_a^{1}(\Gamma_0) - e_a^{\ell}(\Gamma_0)\|_{\infty} + \|e_a^{\ell}(\Gamma_0) - e_a^{\ell}(\Gamma_0; \Delta x_i)\|_{\infty} \\
&= \nu_a^{\mathrm{m}}(y) + \nu_a^{\mathrm{d}}(y) \mathrel{\dot{\leq}} \eta_a^{\mathrm{m}}(y) + \eta_a^{\mathrm{d}}(y) = \eta_a(y)
\end{aligned} \tag{34}$$

for $\Delta x_i \to 0$. In the following, we show that the relation (34) holds for $\Delta x_i \to 0$. In particular, we need to show that $\nu_a^{\mathrm{d}}(y) \mathrel{\dot{\leq}} \eta_a^{\mathrm{d}}(y)$ and $\nu_a^{\mathrm{m}}(y) \mathrel{\dot{\leq}} \eta_a^{\mathrm{m}}(y)$ hold, where the relation $f_1(x) \mathrel{\dot{\leq}} f_2(x)$ states that a function f_2 is a first-order upper bound of the function f_1 if and only if $f_1(x) \leq f_2(x) + \phi(x)$ for $x \to 0$ and any function $\phi \in o(\|f_2\|_{\infty})$

We first proceed by showing that $\nu_a^{\mathrm{d}}(y) \mathrel{\dot{\leq}} \eta_a^{\mathrm{d}}(y)$ holds for $\Delta x_i \to 0$. Since we utilize the implicit mid-point rule to get Systems (D1)–(D3) and the fact that its discretization error is of convergence order 2 (see, e.g., [17]) we can write that

$$e_a^{\ell}(x_k) - e_a^{\ell}(x_k; \Delta x_i) = c^{\ell}(x_k)\Delta x_i^2 + \mathcal{O}(\Delta x_i^3)\,, \tag{35}$$

$$e_a^{\ell}(x_k) - e_a^{\ell}(x_k; \Delta x_{i-1}) = 4c^{\ell}(x_k)\Delta x_i^2 + \mathcal{O}(\Delta x_i^3)\,, \tag{36}$$

where we use $\Delta x_{i-1} = 2\Delta x_i$. Here, the function $c^{\ell}(x)$ that arises from the Taylor series expansion of the local discretization error is independet of Δx_i; see, e.g., [27]. Computing the difference between (35) and (36) yields

$$e_a^{\ell}(x_k; \Delta x_i) - e_a^{\ell}(x_k; \Delta x_{i-1}) = 3c^{\ell}(x_k)\Delta x_i^2 + \mathcal{O}(\Delta x_i^3), \tag{37}$$

and, thus,

$$c^{\ell}(x_k)\Delta x_i^2 = \frac{e_a^{\ell}(x_k; \Delta x_i) - e_a^{\ell}(x_k; \Delta x_{i-1})}{3} + \mathcal{O}(\Delta x_i^3). \tag{38}$$

By replacing $c^{\ell}(x_k)\Delta x_i^2$ in (35) with the result of (38), applying the ∞-norm over Γ_0 on both sides, and using the triangle inequality, we find

$$\nu_a^{\mathrm{d}}(y) = \|\frac{e_a^{\ell}(x_k; \Delta x_i) - e_a^{\ell}(x_k; \Delta x_{i-1})}{3} + \mathcal{O}(\Delta x_i^3)\|_{\infty} \leq \frac{1}{3}\eta_a^{\mathrm{d}}(y) + \|\mathcal{O}(\Delta x_i^3)\|_{\infty}.$$

Since $\eta_a^{\mathrm{d}}(y) \in \mathcal{O}(\Delta x_i^2)$ holds as shown in (37), we get that $\nu_a^{\mathrm{d}}(y) \mathrel{\dot{\leq}} \eta_a^{\mathrm{d}}(y)$ holds for $\Delta x_i \to 0$.

Finally, we show that $\nu_a^{\mathrm{m}}(y) \dot{\leq} \eta_a^{\mathrm{m}}(y)$. The ideas are rather similar. By applying the ∞-norm over Γ_0 and the triangle inequality to the difference between (35) with (M1) and current model level $\ell \in \{(\mathrm{M1}), (\mathrm{M2}), (\mathrm{M3})\}$ we get

$$\begin{aligned}\nu_a^{\mathrm{m}}(y) &= \|e_a^{\ell}(x_k;\Delta x_i) - e_a^1(x_k;\Delta x_i) + (c^{\ell}(x_k) - c^1(x_k))\Delta x_i^2 + \mathcal{O}(\Delta x_i^3)\|_\infty \\ &\leq \eta_a^{\mathrm{m}}(y) + \|\mathcal{O}(\Delta x_i^2)\|_\infty.\end{aligned}$$

Since $\eta_a^{\mathrm{m}}(y) \in \mathcal{O}(1)$, we get that $\nu_a^{\mathrm{m}}(y) \dot{\leq} \eta_a^{\mathrm{m}}(y)$ holds for $\Delta x_i \to 0$.

Remark 2 (Computing error estimates)**.** *Observing the definitions of the error estimates* (31)–(33) *yields that not only the energy* $e_a^{\ell}(\Gamma_0;\Delta x_i)$*, as a part of the solution* y*, is required to compute the estimates but also the values* $e_a^1(\Gamma_0;\Delta x_i)$ *and* $e_a^{\ell}(\Gamma_0;\Delta x_{i-1})$*, which are not given in terms of the solution* y*. One could compute these values by recomputing the* (NLP) *with appropriately modified pipe levels and step sizes. However, this is computationally very costly. An alternative approach is to explicitly solve the modified (w.r.t. appropriately modified model levels and step sizes) energy equations of the Systems* (D1)–(D3) *by means of implicit numerical integration. Fortunately, this is not required in this work since the energy equations of the Systems* (D1)–(D3) *together with Equation* (16) *allow for solving them algebraically for the energies* e_a^k*,* $k = 0, 1, \ldots, n$ *in linear time.*

In the following section we present the algorithm that adaptively switches the previously introduced models and their discretizations by means of a switching strategy.

4. Adaptive algorithm

In this section, we present and analyze the adaptive optimization algorithm. This algorithm is based on the work in [14] and adapted for the district heating network problem studied in this paper. The algorithm iteratively solves the (NLP) while adaptively switching the pipe model levels and discretization step sizes to achieve a locally optimal solution that is feasible w.r.t. to some prescribed tolerance. The adaptive switching is implemented via marking and switching strategies, which are based on the error measures presented in the previous section.

Given an a-priori error tolerance $\varepsilon > 0$, our method aims at computing a finite sequence of solutions of the nonlinear problem (NLP) in order to achieve a solution y with an estimated average error less or equal to ε. This motivates the following definition.

Definition 1. *Let* $\varepsilon > 0$ *be a given tolerance. The solution* y *of the* (NLP) *is called* ε*-feasible if*

$$\bar{\eta}(y) := \frac{1}{|A_p|} \sum_{a \in A_p} \eta_a(y) \leq \varepsilon,$$

where $\bar{\eta}(y)$ *is called the* total average error estimate.

The remainder of this section is structured as follows. We first provide the switching and marking strategies used by our algorithm in Section 4.1. Then, we present the adaptive algorithm and prove its convergence in Section 4.2.

4.1. Switching and Marking Strategies.

We now define switching strategies to compute new pipe levels ℓ_a^{new} and new step sizes $\Delta x_a^{\mathrm{new}}$. Let $\varepsilon > 0$ be a tolerance and $\tau \geq 1$ be a tuning parameter. First, we introduce the model level switching rules. Consider the pipe sets

$$A_{\mathrm{p}}^{>\varepsilon} := \{a \in A_{\mathrm{p}} \colon \eta_a^{\mathrm{m}}(y;\ell_a) - \eta_a^{\mathrm{m}}(y;\ell_a^{\mathrm{new}}) > \varepsilon\} \tag{39}$$

and

$$A_{\mathrm{p}}^{<\tau\varepsilon} := \{a \in A_{\mathrm{p}} \colon \eta_a^{\mathrm{m}}(y;\ell_a^{\mathrm{new}}) - \eta_a^{\mathrm{m}}(y;\ell_a) < \tau\varepsilon\}. \tag{40}$$

The set $A_{\mathrm{p}}^{>\varepsilon}$ ($A_{\mathrm{p}}^{<\tau\varepsilon}$) contains all the pipes for which the new model level ℓ_a^{new} decreases (increases) the model error estimate compared to the current model level ℓ_a w.r.t. the error tolerance ε. In order to switch-up the model level ($\ell_a^{\mathrm{new}} < \ell_a$), we apply the rule

$$\ell_a^{\mathrm{new}} = \begin{cases} \ell_a - 1, & \ell_a > 1 \ \wedge \ \eta_a^{\mathrm{m}}(y;\ell_a) - \eta_a^{\mathrm{m}}(y;\ell_a - 1) > \varepsilon, \\ 1, & \text{otherwise.} \end{cases} \tag{41}$$

Similarly, for down-switching of the model level ($\ell_a^{\mathrm{new}} > \ell_a$), we apply the rule

$$\ell_a^{\mathrm{new}} = \min\{\ell_a + 1, \ell_{\max}\} \tag{42}$$

with $\ell_{\max} = 3$ in our setting. According to the rules defined in Section 3.1, we apply the following grid refinement and coarsening rule:

$$\Delta x_a^{\mathrm{new}} = \begin{cases} 1/2\,\Delta x_a, & \text{for a grid refinement,} \\ 2\,\Delta x_a, & \text{for a grid coarsening.} \end{cases} \tag{43}$$

Based on the switching strategies defined in (39)–(43) we can now present our marking strategies that decide for which pipes we switch up or down the model level and for which pipes we refine or coarsen the step size. Let the sets $\mathcal{R}, \mathcal{U} \subseteq A_{\mathrm{p}}$ represent all pipes marked for grid refinement and model level up-switching, respectively. Furthermore, let the sets $\mathcal{C}, \mathcal{D} \subseteq A_{\mathrm{p}}$ represent all pipes marked for grid coarsening and model level down-switching, respectively. To avoid unnecessary switching we use threshold parameters $\Theta_{\mathcal{R}}$, $\Theta_{\mathcal{U}}$, $\Theta_{\mathcal{C}}$, $\Theta_{\mathcal{D}} \in (0,1)$. We determine $\mathcal{R}$ and $\mathcal{U}$ by finding the minimum subset of pipes $a \in A_{\mathrm{p}}$ such that

$$\Theta_{\mathcal{R}} \sum_{a \in A_{\mathrm{p}}} \eta_a^{\mathrm{d}}(y) \leq \sum_{a \in \mathcal{R}} \eta_a^{\mathrm{d}}(y) \tag{44}$$

and

$$\Theta_{\mathcal{U}} \sum_{a \in A_{\mathrm{p}}^{>\varepsilon}} \left(\eta_a^{\mathrm{m}}(y;\ell_a) - \eta_a^{\mathrm{m}}(y;\ell_a^{\mathrm{new}})\right) \leq \sum_{a \in \mathcal{U}} \left(\eta_a^{\mathrm{m}}(y;\ell_a) - \eta_a^{\mathrm{m}}(y;\ell_a^{\mathrm{new}})\right) \tag{45}$$

are satisfied, where in (45), the rule in (41) is applied. Similarly, in order to determine $\mathcal{C}$ and $\mathcal{D}$, we have to find the maximum subset of all pipes $a \in A_{\mathrm{p}}$ such that

$$\Theta_{\mathcal{C}} \sum_{a \in A_{\mathrm{p}}} \eta_a^{\mathrm{d}}(y) \geq \sum_{a \in \mathcal{C}} \eta_a^{\mathrm{d}}(y) \tag{46}$$

and

$$\Theta_{\mathcal{D}} \sum_{a \in A_{\mathrm{p}}^{<\tau\varepsilon}} \left(\eta_a^{\mathrm{m}}(y;\ell_a^{\mathrm{new}}) - \eta_a^{\mathrm{m}}(y;\ell_a)\right) \geq \sum_{a \in \mathcal{D}} \left(\eta_a^{\mathrm{m}}(y;\ell_a^{\mathrm{new}}) - \eta_a^{\mathrm{m}}(y;\ell_a)\right) \tag{47}$$

hold, where in (47), the rule in (42) is applied.

Remark 3. *Note that Definition 1 is based on the total error estimate as introduced in the previous section. Since the total exact error is upper bounded by the total error estimate via (34) one also has that the solution y of the (NLP) is ε-feasible w.r.t. the total average exact error $\bar{\nu}(y)$, i.e., $\bar{\nu}(y) \leq \varepsilon$ holds with where*

$$\bar{\nu}(y) := \frac{1}{|A_p|} \sum_{a \in A_p} \nu_a(y).$$

Thus, whenever error estimates are used for the switching and marking strategies, the exact errors can be used as well.

As used before in Section 3.2, the first-order approximation of the discretization error estimator in $x \in [0, L_a]$ of a discretization scheme of order β reads $\eta_a^{\mathrm{d}}(x) \doteq c(x)\Delta x_a^{\beta}$, where $c(x)$ is independent of Δx_a. This allows us to write

$$\eta_a^{\mathrm{d,new}}(x) = \left(\frac{\Delta x_a^{\mathrm{new}}}{\Delta x_a}\right)^{\beta} \eta_a^{\mathrm{d}}(x)$$

for the new discretization error estimator after a grid refinement or coarsening. Since the implicit mid-point rule is used in our case, $\beta = 2$ holds, leading to

$$\eta_a^{\mathrm{d,new}}(x) = \begin{cases} \eta_a^{\mathrm{d}}(x)/4, & \text{for a grid refinement,} \\ 4\,\eta_a^{\mathrm{d}}(x), & \text{for a grid coarsening.} \end{cases} \tag{48}$$

This also naturally holds for the exact discretization error estimator $\nu_a^{\mathrm{d}}(x)$.

4.2. **Adaptive Algorithm.** In this section we present the adaptive optimization algorithm. The algorithm is formally given in Algorithm 1 and described in the following.

The input of the algorithm comprise of a complete description of the network, including initial and boundary conditions, the error tolerance $\varepsilon > 0$ as well as initial values for the parameters $\Theta_{\mathcal{R}}^0, \Theta_{\mathcal{U}}^0, \Theta_{\mathcal{C}}^0, \Theta_{\mathcal{D}}^0 \in (0,1)$, $\tau^0 \leq 1$, $\mu^0 \in \mathbb{N}_+$. The output of the algorithm is an ε-feasible solution y of the nonlinear problem (NLP) according to Definition 1.

The algorithm starts by initializing model levels and grid sizes for each pipe. It then solves the (NLP) for the first time and checks for ε-feasibility. Since it is likely that after the first iteration the feasibility check fails, the algorithm enters two nested loops: the outer loop for down-switching and coarsening and the inner loop for up-switching and refinement. In this description we will also refer to the outer loop as the k-loop and to the inner loop as the j-loop.

Next, the inner loop is entered and the up-switching and refinement sets $\mathcal{U}$ and $\mathcal{R}$ are determined. This step is followed by up-switching and refining of each pipe accordingly. Each j-loop finishes by re-solving the (NLP) with the new configuration w.r.t. pipe model levels and grid sizes and it checks for feasibility. The inner loop continues until either a feasible solution y is found or a maximum number of inner loop iterations μ^k is reached.

What follows in the outer loop is the computation of the coarsening and down-switching sets $\mathcal{C}$ and $\mathcal{D}$, respectively. This step is succeeded by updating the pipe model levels and step sizes. Similar to the inner loop, the outer loop finishes by re-solving the (NLP) and checking for feasibility.

We first show that the algorithm is finite if we only apply changes to the discretization step sizes while fixing the model levels for all pipes.

Lemma 2. *Suppose that the model level $\ell_a \in \{1,2,3\}$ is fixed for every pipe $a \in A_p$. Let the resulting set of model levels be denoted by $\mathcal{M}$. Suppose further that $\eta_a(y) = \eta_a^d(y)$ holds in (31) and that every (NLP) is solved to local optimality. Consider Algorithm 1 without applying the model switching steps in Lines 11 and 19. Then, the algorithm terminates after a finite number of refinements in Line 13 and coarsenings in Line 21 with an ε-feasible solution w.r.t. model level set $\mathcal{M}$ if there exists a constant $C > 0$ such that*

$$\frac{1}{4}\Theta_{\mathcal{R}}^k \mu^k \geq \Theta_{\mathcal{C}}^k + C \tag{49}$$

holds and if the step sizes of the initial discretizations are chosen sufficiently small.

Proof. We focus on the total discretization error defined as

$$\eta^{\mathrm{d}}(y^j) := \sum_{a \in A_{\mathrm{p}}} \eta_a^{\mathrm{d}}(y^j)$$

Algorithm 1: Adaptive Model and Discretization Level Control

Input: Network (V, A), initial and boundary conditions, error tolerance $\varepsilon > 0$, initial parameters $\Theta^0_{\mathcal{R}}, \Theta^0_{\mathcal{U}}, \Theta^0_{\mathcal{C}}, \Theta^0_{\mathcal{D}} \in (0,1)$, $\tau^0 \leq 1$, $\mu^0 \in \mathbb{N}_+$
Output: ε-feasible solution y of (NLP)

foreach $a \in A_p$ **do**
  Initialize model level ℓ_a^0 and step size Δx_a^0
$y^0 \leftarrow$ Solve (NLP)
if y^0 *is* ε*-feasible* **then**
  return $y \leftarrow y^0$
for $k = 1, 2, \ldots$ **do**
  Update parameters $\Theta^k_{\mathcal{R}}, \Theta^k_{\mathcal{U}}, \Theta^k_{\mathcal{C}}, \Theta^k_{\mathcal{D}}, \mu^k, \tau^k$
  for $j = 1, \ldots, \mu^k$ **do**
    Compute sets $\mathcal{U}^{k,j}, \mathcal{R}^{k,j} \subseteq A_{\mathrm{p}}$ according to (44), (45)
    foreach $a \in \mathcal{U}^{k,j}$ **do**
      Switch-up the model level $\ell_a^{k,j}$ according to (41)
    foreach $a \in \mathcal{R}^{k,j}$ **do**
      Refine step size $\Delta x_a^{k,j}$ according to (43)
    $y^{k,j} \leftarrow$ Solve (NLP)
    if $y^{k,j}$ *is* ε*-feasible* **then**
      return $y \leftarrow y^{k,j}$
  Compute sets $\mathcal{D}^k, \mathcal{C}^k \subseteq A_{\mathrm{p}}$ according to (46), (47)
  foreach $a \in \mathcal{D}^k$ **do**
    Switch-down the model level ℓ_a^k according to (42)
  foreach $a \in \mathcal{C}^k$ **do**
    Coarsen step size Δx_a^k according to (43)
  $y^k \leftarrow$ Solve (NLP)
  if y^k *is* ε*-feasible* **then**
    return $y \leftarrow y^k$

(up-switching & refinement; down-switching & coarsening)

and show that this quantity is positively bounded away from zero for one outer-loop iteration k containing μ inner refinement steps and one coarsening step. For the sake of simplicity we drop the k index.

Hence, we first look at the influence of one inner refinement for-loop iteration $j \in \{1, \ldots, \mu\}$ on $\eta^{\mathrm{d}}(y^j)$. Thus,

$$\begin{aligned}
&\sum_{a \in A_{\mathrm{p}}} \eta_a^{\mathrm{d}}(y^{j-1}) - \sum_{a \in A_{\mathrm{p}}} \eta_a^{\mathrm{d}}(y^j) \\
&= \sum_{a \in A_{\mathrm{p}} \setminus \mathcal{R}^j} \eta_a^{\mathrm{d}}(y^{j-1}) + \sum_{a \in \mathcal{R}^j} \eta_a^{\mathrm{d}}(y^{j-1}) - \sum_{a \in A_{\mathrm{p}} \setminus \mathcal{R}^j} \eta_a^{\mathrm{d}}(y^j) - \sum_{a \in \mathcal{R}^j} \eta_a^{\mathrm{d}}(y^j) \\
&= \sum_{a \in \mathcal{R}^j} \eta_a^{\mathrm{d}}(y^{j-1}) - \sum_{a \in \mathcal{R}^j} \frac{1}{4} \eta_a^{\mathrm{d}}(y^{j-1}) \\
&= \frac{3}{4} \sum_{a \in \mathcal{R}^j} \eta_a^{\mathrm{d}}(y^{j-1}),
\end{aligned} \tag{50}$$

where we use that $\eta_a^{\mathrm{d}}(y^j)$ equals $1/4$ of $\eta_a^{\mathrm{d}}(y^{j-1})$ if Δx_a is chosen small enough.

Summing up Equation (50) over all $j \in \{1, \dots, \mu\}$ gives the total error decrease in the inner for-loop:

$$\begin{aligned}
&\sum_{j=1}^{\mu} \left(\sum_{a \in A_\mathrm{p}} \eta_a^\mathrm{d}(y^{j-1}) - \sum_{a \in A_\mathrm{p}} \eta_a^\mathrm{d}(y^j) \right) \\
&= \sum_{a \in A_\mathrm{p}} \eta_a^\mathrm{d}(y^0) - \sum_{a \in A_\mathrm{p}} \eta_a^\mathrm{d}(y^\mu) \\
&= \frac{3}{4} \sum_{j=1}^{\mu} \sum_{a \in \mathcal{R}^j} \eta_a^\mathrm{d}(y^{j-1}).
\end{aligned}$$

We now focus on the final coarsening step of the outer for-loop. For the sake of simplicity we say that $y^{\mu+1}$ corresponds to the solution of the (NLP) after the coarsening step. Thus,

$$\begin{aligned}
&\sum_{a \in A_\mathrm{p}} \eta_a^\mathrm{d}(y^{\mu+1}) - \sum_{a \in A_\mathrm{p}} \eta_a^\mathrm{d}(y^\mu) \\
&= \sum_{a \in A_\mathrm{p} \setminus \mathcal{C}} \eta_a^\mathrm{d}(y^{\mu+1}) + \sum_{a \in \mathcal{C}} \eta_a^\mathrm{d}(y^{\mu+1}) - \sum_{a \in A_\mathrm{p} \setminus \mathcal{C}} \eta_a^\mathrm{d}(y^\mu) - \sum_{a \in \mathcal{C}} \eta_a^\mathrm{d}(y^\mu) \\
&= 4 \sum_{a \in \mathcal{C}} \eta_a^\mathrm{d}(y^\mu) - \sum_{a \in \mathcal{C}} \eta_a^\mathrm{d}(y^\mu) \\
&= 3 \sum_{a \in \mathcal{C}} \eta_a^\mathrm{d}(y^\mu)
\end{aligned}$$

holds, where we again use that $\eta_a^\mathrm{d}(y^{\mu+1})$ equals $4\eta_a^\mathrm{d}(y^\mu)$ if Δx_a is chosen small enough.

We now prove that the total error decrease in each iteration of the outer for loop of Algorithm 1 is positive and uniformly bounded away from zero. Hence, we consider

$$\sum_{a \in A_\mathrm{p}} \eta_a^\mathrm{d}(y^0) - \sum_{a \in A_\mathrm{p}} \eta_a^\mathrm{d}(y^{\mu+1}) = \frac{3}{4} \sum_{j=1}^{\mu} \sum_{a \in \mathcal{R}^j} \eta_a^\mathrm{d}(y^{j-1}) - 3 \sum_{a \in \mathcal{C}} \eta_a^\mathrm{d}(y^\mu).$$

Then, using

$$\eta_a^\mathrm{d}(y^j) \geq \eta_a^\mathrm{d}(y^\mu) \quad \text{for all} \quad j = 1, \dots, \mu,$$

(44), (49), and (46), we obtain

$$\begin{aligned}
&\frac{3}{4} \sum_{j=1}^{\mu} \sum_{a \in \mathcal{R}^j} \eta_a^\mathrm{d}(y^{j-1}) \geq \frac{3}{4} \Theta_\mathcal{R} \sum_{j=1}^{\mu} \sum_{a \in A_\mathrm{p}} \eta_a^\mathrm{d}(y^{j-1}) \geq \frac{3}{4} \Theta_\mathcal{R} \sum_{j=1}^{\mu} \sum_{a \in A_\mathrm{p}} \eta_a^\mathrm{d}(y^\mu) \\
&= \frac{3}{4} \Theta_\mathcal{R} \mu \sum_{a \in A_\mathrm{p}} \eta_a^\mathrm{d}(y^\mu) \geq 3(\Theta_\mathcal{C} + C) \sum_{a \in A_\mathrm{p}} \eta_a^\mathrm{d}(y^\mu) \geq 3\Theta_\mathcal{C} \sum_{a \in A_\mathrm{p}} \eta_a^\mathrm{d}(y^\mu) + C|A_\mathrm{p}|\varepsilon \\
&\geq 3 \sum_{a \in \mathcal{C}} \eta_a^\mathrm{d}(y^\mu) + C|A_\mathrm{p}|\varepsilon,
\end{aligned}$$

which completes the proof. □

Next, we show that the algorithm is finite if we only apply model level changes while the discretization step sizes are kept fixed.

Lemma 3. *Suppose that the discretization stepsize Δx_a is fixed for every pipe $a \in A_p$. Suppose further that $\eta_a(y) = \eta_a^m(y)$ holds in (31) and that every (NLP) is solved to local optimality. Consider Algorithm 1 without applying the discretization refinements in Line 13 and the coarsening step in Line 21. Then, the algorithm*

terminates after a finite number of model switches in Lines 11 and 19 with an ε-feasible solution with respect to the step sizes Δx_a, $a \in A_p$, if there exists a constant $C > 0$ such that

$$\Theta_{\mathcal{U}}^k \mu^k \geq \tau^k \Theta_{\mathcal{D}}^k |A_p| + C. \tag{51}$$

The proof of this lemma is the same as in [14], which is why we omit it here.

Lemma 4. *Let y^μ and $y^{\mu+1}$ be the solution of the optimization problem before and after a refinement or coarsening step, respectively. Let $\eta_a^d(y)$ and $\eta_a^m(y)$ be the discretization and model error estimator for a given solution y of (NLP) as defined in (33) and (32). Then, if*

$$\eta_a^d(y^\mu) \ll \eta_a^m(y^\mu)$$

is satisfied, it holds that

$$\eta_a^m(y^{\mu+1}) = \eta_a^m(y^\mu). \tag{52}$$

Proof. For $x \in \Gamma_0$ we introduce $\eta_a^{\mathrm{d}}(x; \ell_a, \Delta x_i)$ and $\eta_a^{\mathrm{m}}(x; \ell_a, \Delta x_i)$ as the local discretization error estimator and the local model error estimator evaluated at x using the model level ℓ_a and the step size Δx_i such that

$$\begin{aligned}
\eta_a^{\mathrm{d}}(x; \ell_a, \Delta x_i) &:= e_a^{\ell_a}(x; \Delta x_i) - e_a^{\ell_a}(x; \Delta x_{i-1}), \\
\eta_a^{\mathrm{m}}(x; \ell_a, \Delta x_i) &:= e_a^{1}(x; \Delta x_i) - e_a^{\ell_a}(x; \Delta x_i)
\end{aligned}$$

holds. Since $\eta_a^{\mathrm{d}}(x; \ell_a, \Delta x_i)$ uses the same step sizes Δx_i and Δx_{i-1} for all ℓ_a, we have

$$|\eta_a^{\mathrm{d}}(x; \ell_a, \Delta x_i)| \ll |\eta_a^{\mathrm{m}}(x; \ell_a, \Delta x_i)| \iff |\eta_a^{\mathrm{d}}(x; 1, \Delta x_i)| \ll |\eta_a^{\mathrm{m}}(x; \ell_a, \Delta x_i)|. \tag{53}$$

We now focus on the coarsening step and prove Equation (52). The proof for the refinement step is analogous to the coarsening step and is therefore not presented. By definition and due to the coarsening step, we have

$$\begin{aligned}
\eta_a^{\mathrm{m}}(y^{\mu+1}) &= \max_{x \in \Gamma_0} |e_a^1(x; \Delta x_{i-1}) - e_a^{\ell_a}(x; \Delta x_{i-1})| \\
&= \max_{x \in \Gamma_0} |e_a^1(x; \Delta x_{i-1}) - e_a^{\ell_a}(x; \Delta x_{i-1}) + e_a^1(x; \Delta x_i) \\
&\qquad\qquad - e_a^1(x; \Delta x_i) + e_a^{\ell_a}(x; \Delta x_i) - e_a^{\ell_a}(x; \Delta x_i)| \\
&= \max_{x \in \Gamma_0} |\eta_a^{\mathrm{m}}(x; \ell_a, \Delta x_i) - \eta_a^{\mathrm{d}}(x; 1, \Delta x_i) + \eta_a^{\mathrm{d}}(x; \ell_a, \Delta x_i)|.
\end{aligned}$$

Using (53), we finally obtain

$$\eta_a^{\mathrm{m}}(y^{\mu+1}) = \max_{x \in \Gamma_0} |\eta_a^{\mathrm{m}}(x; \ell_a, \Delta x_i)| =: \eta_a^{\mathrm{m}}(y^\mu). \qquad \square$$

We also have a corresponding result for the estimators of the discretization error. For this result, we make the following assumption.

Assumption 1. *Let y^μ and $y^{\mu+1}$ be the solution of the optimization problem before and after a model up- or down-switching step, respectively. Moreover, let us denote with λ^μ and $\lambda^{\mu+1}$ the corresponding sensitivities. Then, there exists a constant $C > 0$ with $\|\lambda^\mu - \lambda^{\mu+1}\| \leq C$.*

Before we now state the next lemma, we briefly discuss this assumption. Informally speaking, it states that the difference of the sensitivities (i.e., of the dual variables) of the optimization problems before and after a model up- or down-switching step is bounded by a constant. We are convinced that this assumption holds for the different models in our catalog.

Lemma 5. *Let y^μ and $y^{\mu+1}$ respectively be the solution of the optimization problem before and after a model up or down switching step. Let $\eta_a^d(y)$ and $\eta_a^m(y)$ be the discretization and model error estimator for a given solution y of (NLP) as defined in (33) and (32). Finally, suppose that Assumption 1 holds. Then,*

$$\eta_a^d(y^{\mu+1}) = \eta_a^d(y^\mu) \tag{54}$$

holds.

Proof. As long as Assumption 1 holds, the error estimate for the discretization error is independent of the used model and we immediately get the desired result. □

We are now ready to prove our main theorem on the finiteness of the proposed algorithm.

Theorem 1 (Finite termination)**.** *Suppose that $\eta_a^d \ll \eta_a^m$ for every $a \in A_p$ and that every (NLP) is solved to local optimality. Moreover, suppose that Assumption 1 holds. Then, Algorithm 1 terminates after a finite number of refinements, coarsenings, and model switches in Lines 11, 13, 19, and 21 with an ε-feasible solution w.r.t. the reference problem if there exist constants $C_1, C_2 > 0$ such that*

$$\frac{1}{4}\Theta_{\mathcal{R}}^k \mu^k \geq \Theta_{\mathcal{C}}^k + C_1 \quad \text{and} \quad \Theta_{\mathcal{U}}^k \mu^k \geq \tau^k \Theta_{\mathcal{D}}^k |A_p| + C_2$$

hold for all k.

Proof. We first focus on the average total error estimator decrease between two subsequent inner loop iterations of Algorithm 1. Hence,

$$\begin{aligned}
\bar{\eta}(y^{j-1}) - \bar{\eta}(y^j) &= \sum_{a\in A_\mathrm{p}} \eta_a(y^{j-1}) - \sum_{a\in A_\mathrm{p}} \eta_a(y^j) \\
&= \sum_{a\in A_\mathrm{p}} \eta_a^\mathrm{m}(y^{j-1}) + \sum_{a\in A_\mathrm{p}} \eta_a^\mathrm{d}(y^{j-1}) - \sum_{a\in A_\mathrm{p}} \eta_a^\mathrm{m}(y^j) - \sum_{a\in A_\mathrm{p}} \eta_a^\mathrm{d}(y^j) \\
&= \sum_{a\in A_\mathrm{p}\setminus(\mathcal{R}_j\cup\mathcal{U}_j)} \eta_a^\mathrm{m}(y^{j-1}) + \sum_{a\in\mathcal{U}_j} \eta_a^\mathrm{m}(y^{j-1}) + \sum_{a\in\mathcal{R}_j\setminus\mathcal{U}_j} \eta_a^\mathrm{m}(y^{j-1}) \\
&\quad - \sum_{a\in A_\mathrm{p}\setminus(\mathcal{R}_j\cup\mathcal{U}_j)} \eta_a^\mathrm{m}(y^j) - \sum_{a\in\mathcal{U}_j} \eta_a^\mathrm{m}(y^j) - \sum_{a\in\mathcal{R}_j\setminus\mathcal{U}_j} \eta_a^\mathrm{m}(y^j) \\
&\quad + \sum_{a\in A_\mathrm{p}\setminus(\mathcal{R}_j\cup\mathcal{U}_j)} \eta_a^\mathrm{d}(y^{j-1}) + \sum_{a\in\mathcal{R}_j} \eta_a^\mathrm{d}(y^{j-1}) + \sum_{a\in\mathcal{U}_j\setminus\mathcal{R}_j} \eta_a^\mathrm{d}(y^{j-1}) \\
&\quad - \sum_{a\in A_\mathrm{p}\setminus(\mathcal{R}_j\cup\mathcal{U}_j)} \eta_a^\mathrm{d}(y^j) - \sum_{a\in\mathcal{R}_j} \eta_a^\mathrm{d}(y^j) - \sum_{a\in\mathcal{U}_j\setminus\mathcal{R}_j} \eta_a^\mathrm{d}(y^j) \\
&= \sum_{a\in\mathcal{U}_j} \eta_a^\mathrm{m}(y^{j-1}) - \sum_{a\in\mathcal{U}_j} \eta_a^\mathrm{m}(y^j) + \sum_{a\in\mathcal{R}_j} \eta_a^\mathrm{d}(y^{j-1}) - \sum_{a\in\mathcal{R}_j} \eta_a^\mathrm{d}(y^j) \\
&= \sum_{a\in\mathcal{U}_j} \eta_a^\mathrm{m}(y^{j-1}) - \sum_{a\in\mathcal{U}_j} \eta_a^\mathrm{m}(y^j) + \sum_{a\in\mathcal{R}_j} \frac{3}{4}\eta_a^\mathrm{d}(y^{j-1})
\end{aligned}$$

holds, where we use Lemma 4, Lemma 5, and Equation (48). Taking the sum over all $j = 1, \dots, \mu$ inner loop iterations gives

$$\begin{aligned}
&\sum_{j=1}^{\mu} \bar{\eta}(y^{j-1}) - \bar{\eta}(y^j) \\
&= \bar{\eta}(y^0) - \bar{\eta}(y^\mu) \\
&= \sum_{j=1}^{\mu} \left(\sum_{a\in\mathcal{U}_j} \eta_a^\mathrm{m}(y^{j-1}) - \sum_{a\in\mathcal{U}_j} \eta_a^\mathrm{m}(y^j) + \sum_{a\in\mathcal{R}_j} \frac{3}{4}\eta_a^\mathrm{d}(y^{j-1}) \right).
\end{aligned}$$

Next, we focus on the outer loop iterations of Algorithm 1. We evaluate the average total error increase due to the coarsening and down-switching. Hence,

$$\begin{aligned}
\bar{\eta}(y^{\mu+1}) - \bar{\eta}(y^{\mu}) &= \sum_{a\in A_\mathrm{p}} \eta_a^\mathrm{m}(y^{\mu+1}) + \sum_{a\in A_\mathrm{p}} \eta_a^\mathrm{d}(y^{\mu+1}) - \sum_{a\in A_\mathrm{p}} \eta_a^\mathrm{m}(y^{\mu}) - \sum_{a\in A_\mathrm{p}} \eta_a^\mathrm{d}(y^{\mu}) \\
&= \sum_{a\in A_\mathrm{p}\setminus(\mathcal{C}\cup\mathcal{D})} \eta_a^\mathrm{m}(y^{\mu+1}) + \sum_{a\in\mathcal{D}} \eta_a^\mathrm{m}(y^{\mu+1}) + \sum_{a\in\mathcal{C}\setminus\mathcal{D}} \eta_a^\mathrm{m}(y^{\mu+1}) \\
&\quad - \sum_{a\in A_\mathrm{p}\setminus(\mathcal{C}\cup\mathcal{D})} \eta_a^\mathrm{m}(y^{\mu}) - \sum_{a\in\mathcal{D}} \eta_a^\mathrm{m}(y^{\mu}) - \sum_{a\in\mathcal{C}\setminus\mathcal{D}} \eta_a^\mathrm{m}(y^{\mu}) \\
&\quad + \sum_{a\in A_\mathrm{p}\setminus(\mathcal{C}\cup\mathcal{D})} \eta_a^\mathrm{d}(y^{\mu+1}) + \sum_{a\in\mathcal{C}} \eta_a^\mathrm{d}(y^{\mu+1}) + \sum_{a\in\mathcal{D}\setminus\mathcal{C}} \eta_a^\mathrm{d}(y^{\mu+1}) \\
&\quad - \sum_{a\in A_\mathrm{p}\setminus(\mathcal{C}\cup\mathcal{D})} \eta_a^\mathrm{d}(y^{\mu}) - \sum_{a\in\mathcal{C}} \eta_a^\mathrm{d}(y^{\mu}) - \sum_{a\in\mathcal{D}\setminus\mathcal{C}} \eta_a^\mathrm{d}(y^{\mu}) \\
&= \sum_{a\in\mathcal{D}} \eta_a^\mathrm{m}(y^{\mu+1}) - \sum_{a\in\mathcal{D}} \eta_a^\mathrm{m}(y^{\mu}) + \sum_{a\in\mathcal{C}} \eta_a^\mathrm{d}(y^{\mu+1}) - \sum_{a\in\mathcal{C}} \eta_a^\mathrm{d}(y^{\mu}) \\
&= \sum_{a\in\mathcal{D}} \eta_a^\mathrm{m}(y^{\mu+1}) - \sum_{a\in\mathcal{D}} \eta_a^\mathrm{m}(y^{\mu}) + 3\sum_{a\in\mathcal{C}} \eta_a^\mathrm{d}(y^{\mu}),
\end{aligned}$$

where we use Lemma 4, Lemma 5, and Equation (48).

It suffices to prove that the inner loop average total error decrease is always greater than the outer loop average total error increase, i.e.,

$$\begin{aligned}
&\sum_{j=1}^{\mu} \left(\sum_{a\in\mathcal{U}_j} \eta_a^\mathrm{m}(y^{j-1}) - \sum_{a\in\mathcal{U}_j} \eta_a^\mathrm{m}(y^{j}) + \sum_{a\in\mathcal{R}_j} \frac{3}{4} \eta_a^\mathrm{d}(y^{j-1}) \right) \\
&> \sum_{a\in\mathcal{D}} \eta_a^\mathrm{m}(y^{\mu+1}) - \sum_{a\in\mathcal{D}} \eta_a^\mathrm{m}(y^{\mu}) + 3\sum_{a\in\mathcal{C}} \eta_a^\mathrm{d}(y^{\mu}).
\end{aligned}$$

Using the proofs of Lemma 2 and 3, we obtain

$$\begin{aligned}
&\sum_{j=1}^{\mu} \left(\sum_{a\in\mathcal{U}_j} \eta_a^\mathrm{m}(y^{j-1}) - \sum_{a\in\mathcal{U}_j} \eta_a^\mathrm{m}(y^{j}) + \sum_{a\in\mathcal{R}_j} \frac{3}{4} \eta_a^\mathrm{d}(y^{j-1}) \right) \\
&\geq \Theta_\mathcal{U}\mu\varepsilon + \frac{3}{4}\Theta_\mathcal{R}\mu \sum_{a\in A_\mathrm{p}} \eta_a^\mathrm{d}(y^{\mu}) \\
&\geq (\tau\Theta_\mathcal{D}|A_\mathrm{p}| + C_2)\varepsilon + 3(\Theta_\mathcal{C} + C_1) \sum_{a\in A_\mathrm{p}} \eta_a^\mathrm{d}(y^{\mu}) \\
&\geq \sum_{a\in\mathcal{D}} (\eta_a^\mathrm{m}(y^{\mu+1}) - \eta_a^\mathrm{m}(y^{\mu})) + C_2\varepsilon + 3\sum_{a\in\mathcal{C}} \eta_a^\mathrm{d}(y^{\mu}) + C_1|A_\mathrm{p}|\varepsilon.
\end{aligned}$$

This concludes the proof. □

5. Numerical Results

In this section we present numerical results and for this we first discuss the software and hardware setup. Then, the considered instances are presented and, afterward, the parameterization of the adaptive algorithm is explained.

5.1. **Software and Hardware Setup.** We implemented the models in Python 3.7.4 using the Pyomo 6.2 package [8, 9] and solve the resulting NLPs using the NLP solver CONOPT4 4.24 [6], which is interfaced via the Pyomo-GAMS interface. We also tested other solvers and concluded that CONOPT4 is the most reliable solver that performs best for our application. We used the default GAMS settings. The

TABLE 1. Characteristics of the test networks.

Network	# pipes	# depots	# consumers	total pipe length (m)
AROMA	18	1	5	7262.4
STREET	162	1	32	7627.1

TABLE 2. Parameters used for the numerical results.

Parameter	Value
ε	$10^{-6}\,\mathrm{GJ\,m^{-3}}$
$\Theta_{\mathcal{R}}$	0.9
$\Theta_{\mathcal{U}}$	0.4
$\Theta_{\mathcal{C}}$	0.45
$\Theta_{\mathcal{D}}$	0.2
τ	5
μ	4

computations were executed on a computer with an Intel(R) Core(TM) i7-8550U processor with eight threads at 1.90 GHz and 16 GB RAM.

5.2. **Test Instances.** The two networks considered in this section are the so-called AROMA and STREET networks; see also [12] where they have been used as well. AROMA is an academic test network, whereas STREET is a part of an existing real-world district heating network. Both networks contain cycles but the much larger STREET network only contains a single cycle so that the overall network is almost tree-shaped. Table 1 shows the main characteristics of these networks.

The cost of waste incineration, of natural gas, and of increasing the pressure of the water in the depot are taken from [15] and are set to $C_{\mathrm{w}} = 0\,€/\mathrm{kWh}$, $C_{\mathrm{g}} = 0.0415\,€/\mathrm{kWh}$, and $C_{\mathrm{p}} = 0.165\,€/\mathrm{kWh}$. Additionally, the gas and pressure power variables P_{g} and P_{p} are left unbounded above, whereas the waste power variable P_{w} is bounded above by 10 kW. Scarce waste incineration power P_{w} implies an increased consumption of costly power (P_{p} and P_{g}) to satisfy the total customer demand and thus yields a non-trivial optimization problem.

5.3. **Parameterization of the Algorithm.** Table 2 shows the parameters used for obtaining the numerical results. These parameters are kept constant over the course of the iterations of the algorithm to simplify the interpretation of the results. It should be noted that the parameters do not satisfy the second inequality in Theorem 1. We choose this parameterization despite this fact because the algorithm still converges using these settings and allows for switching down the model level of more pipes and, hence, keeps the optimization model more tractable over the course of the iterations. One could, e.g., by increasing μ, easily satisfy both inequalities of Theorem 1. For the first iteration of the adaptive algorithm we use $\Delta x_a = L_a/2$ and $\ell_a = 3$ for all $a \in A_{\mathrm{p}}$. This forces us to take the reference grid $\Gamma_0 = \{0, L_a\}$ for all $a \in A_{\mathrm{p}}$. The assumption that the initial granularity of the discretization is sufficiently fine is not satisfied here but does (in practice) not harm the overall convergence of the algorithm and is therefore kept large.

5.4. **Discussion of the Results Obtained by Using Error Estimators.** Let us first note that none of the tested optimization solvers converges to a feasible point for both the AROMA and the STREET network when using (M1) and $\Delta x_a = L_a/10$

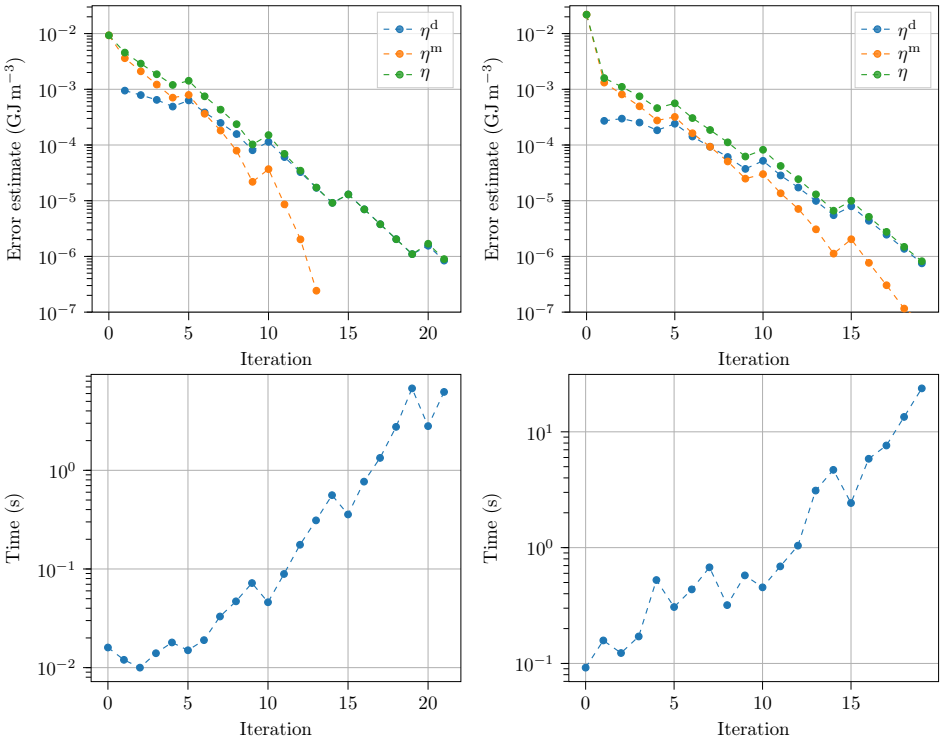

FIGURE 4. Error estimator values (top) and computation times (bottom) over the course of the iterations of the adaptive algorithm using error estimators; AROMA network (left) and STREET network (right).

for all $a \in A_{\mathrm{p}}$ since this spatial discretization already leads to a highly nonlinear problem of a size that is very hard to be tackled by state-of-the-art NLP solvers.

The two upper plots in Figure 4 show a steady decrease of the values of the error estimators over the course of the iterations of the adaptive algorithm. Small increases in the error can be observed every five iterations of the algorithm. These arise from the increase of the model level and the coarsening of the discretizations (outer loop) that is carried out after four refinement steps in which we increase the model's accuracy (inner loop). The error plots thus confirm that the algorithm steadily decreases the total error over the course of one outer loop iteration.

The results show that the algorithm works as expected and that it terminates after a finite number of iterations with a locally optimal solution of a model that has a physical accuracy for which state-of-the-art solvers are not able to compute a solution from scratch. This is one of the most important contributions of this paper: We can solve realistic instances that have not been solvable before. Additionally, the two lower plots in Figure 4 show the computation times for the separate models of Type (NLP) that we solve in every iteration. Although we warmstart every new problem with the solution of the previous one, we observe an increase of solution times due to the higher complexity of the successive models that we solve.

Next, Figure 5 shows the proportion of pipes inside the sets $\mathcal{U}$, $\mathcal{R}$, $\mathcal{D}$, and $\mathcal{C}$ before solving (NLP) for every iteration of the algorithm. The discretization sets represent a larger proportion of pipes when compared to the sets for switching between the model levels. This originates from the parameter selection that favors changes of the discretization and is explained by the fact that the model level of a specific pipe

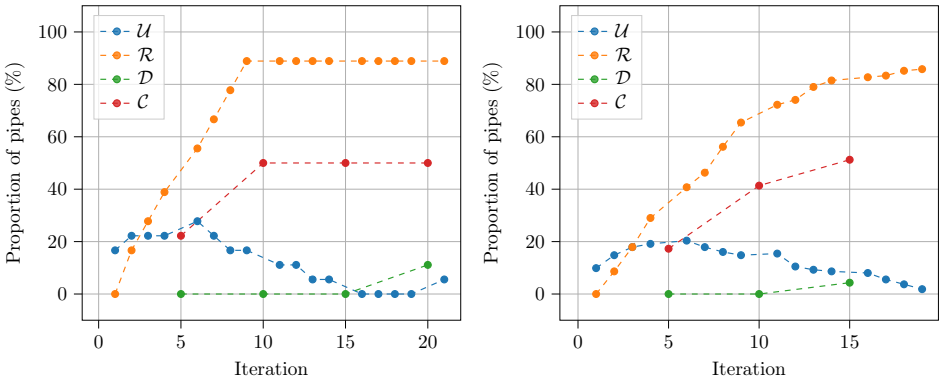

FIGURE 5. Proportion of pipes inside sets $\mathcal{U}, \mathcal{R}, \mathcal{D}$, and $\mathcal{C}$ over the course of iterations of the adaptive algorithm using the error estimators; AROMA (left) and STREET (right).

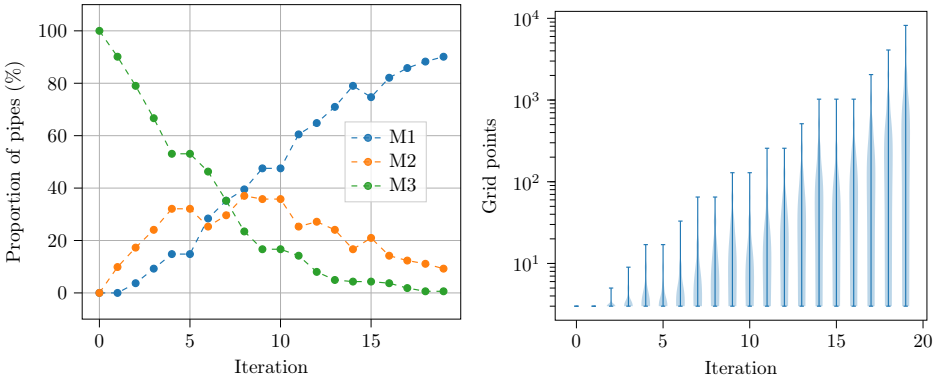

FIGURE 6. Proportion of pipes inside each model level set (left) and violin plots of the quantity of grid points (right) over the iterations of our adaptive algorithm using the error estimators applied on the STREET network.

can only be increased twice—unlike the discretization step size that may need to be halved more often. The right plot of Figure 6 shows violin plots for the amount of grid points in the pipes over the iterations of the algorithm applied to the STREET network. The plot confirms the idea behind the parameter selection. Besides this, Figure 5 illustrates that the down-switching set $\mathcal{D}$ stays empty until the last outer loop iteration for both networks. This is a result of the set $A_{\mathrm{p}}^{<\tau\varepsilon}$ being empty for the first outer-loop iterations of the algorithm, which forces $\mathcal{D}$ to be empty. The amount of pipes in each model level is shown in the left plot of Figure 6. Roughly 90 % of all pipes end up in the most accurate model level whereas the remaining stay in the intermediate level.

Overall, we see that the behavior of the algorithm is comparable when applied to the two different networks, which indicates that the algorithm is robust.

5.5. **Discussion of the Results Obtained by Using Exact Errors.** We now compare the impact of using the error estimators defined in (31)–(33) when employing the exact errors as defined in (28)–(30). To this end, we only consider the larger STREET network. Figure 7 shows the previously discussed plots using exact errors. Both approaches need 19 iterations to reach the desired tolerance. However, when

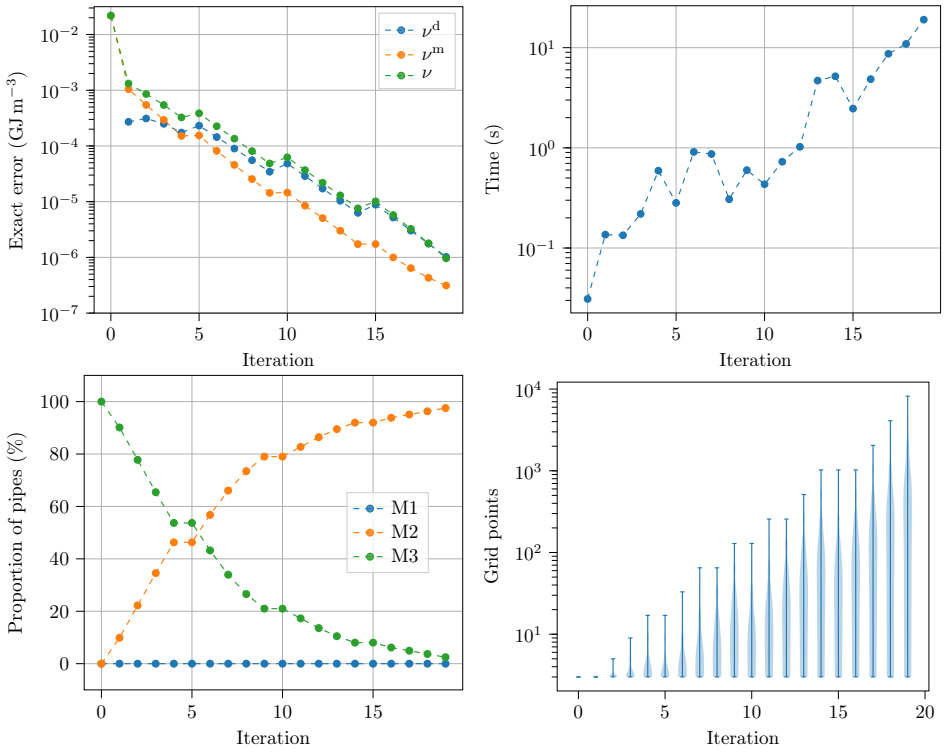

FIGURE 7. Exact error values (top-left), computation time (top-right), proportion of pipes inside each model level set (bottom-left), and violin plots of the quantity of grid points (bottom-right) over the course of the iterations of the adaptive algorithm using the exact errors applied on the STREET network.

looking at the distribution of model levels, we see that in the case of using error estimators, a much higher proportion of pipes are modeled using the most accurate model (M1), which is not the case for any pipe in the exact error case; see the bottom-left plot in Figure 7. Thus, it seems that the error estimators overestimate the importance of switching to the most accurate model level. Consequently, using the error estimators instead of the exact errors introduces a larger amount of nonlinearities to the models that are solved in each iteration. This is an interesting aspect and shows that it might be beneficial to use exact errors if they are available like for the ODEs that we consider in this paper. Nevertheless, the computation times show very similar behavior for both approaches, which makes clear that using error estimators (especially in cases in which exact error formulas are not available) also leads to an effective method.

5.6. **Is Physical Accuracy Worth the Effort?** Let us close this section with a brief analysis of whether the physical accuracy guaranteed by our adaptive method is worth the computational effort. The answer is a clear "Yes". To illustrate this, Figure 8 shows the values of some forward flow variables (pressures, temperatures, and mass flows) that are part of the (NLP) of the AROMA network solved in the first iteration as well as in the last iteration of the adaptive algorithm. The parameter setup used in this test case is the same as presented in Section 5.2. Note that the solution of the first iteration (top figure) corresponds to a rather coarse physical

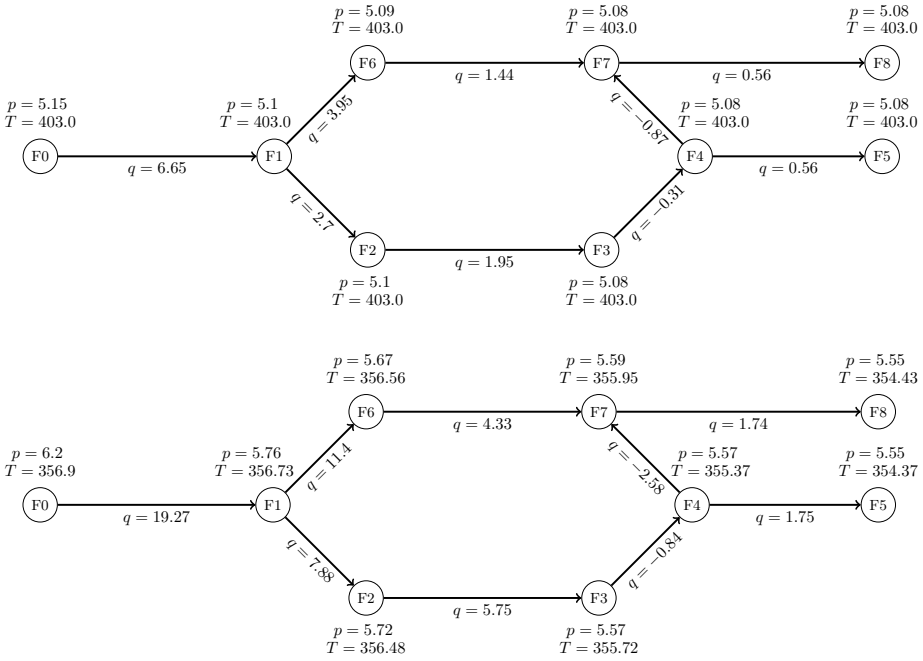

FIGURE 8. Forward flow solution of the AROMA network using the error estimators after the first (top figure) and last (bottom figure) iteration of the adaptive algorithm. Temperatures in K, pressures in bar, and mass flows in $\mathrm{kg\,s^{-1}}$.

modeling whereas the solution of the last iteration (bottom figure) satisfies the prescribed tolerance and is very accurate.

The difference of the solution values are obvious. The first solution has no temperature losses at all (see (M3)) and all temperature values are at the upper bound. Moreover, the mass flow values are comparably small. This changes completely in the final solution. The temperatures have decreased around 50 K and mass flows have increased by up to a factor of 3. The pressures have also changed by around 10 %. It is clearly visible that the physical solution and the control of the network changes significantly if the physical accuracy is increased. Thus, there is a strong need for computing highly accurate solutions if the resulting controls shall be practically useful.

6. CONCLUSION

In this paper, we set up a catalog of models for the hot water flow in pipes of district heating networks. For all entries of this catalog, we also derived suitable discretizations to obtain finite-dimensional optimization problems for the energy-efficient control of these networks that still ensures that the demand of all customers are satisfied. Based on these different models, we designed an iterative and adaptive optimization method that automatically adapts the model level in the catalog as well as the granularity of the discretization to finally obtain a local optimal control that is feasible w.r.t. a user-specified tolerance. We show finite termination of this algorithm and present very convincing numerical results that particularly show that we can now solve realistic instances that are not solvable with state-of-the-art commercial NLP solvers.

For our future work, we plan to extend our modeling and solution approach to the case of instationary hot water flow modeling. While we are confident that the overall ideas can be carried over to this PDE-setting, this will most likely require some more technical derivations compared to the ODE-case considered in this paper.

Acknowledgments

We acknowledge the support by the German Bundesministerium für Bildung und Forschung within the project "EiFer". Moreover, we are very grateful to all the colleagues within the EiFer consortium for many fruitful discussions on the topics of this paper and for providing the data. We also thank the Deutsche Forschungsgemeinschaft for their support within projects A05, B03, B08, and Z01 in the Sonderforschungsbereich/Transregio 154 "Mathematical Modelling, Simulation and Optimization using the Example of Gas Networks".

References

[1] A. Benonysson, B. Bøhm, and H. F. Ravn. "Operational optimization in a district heating system." In: *Energy Conversion and Management* 36.5 (1995), pp. 297–314. DOI: 10.1016/0196-8904(95)98895-T.

[2] C. Bordin, A. Gordini, and D. Vigo. "An optimization approach for district heating strategic network design." In: *European Journal of Operational Research* 252.1 (2016), pp. 296–307. DOI: 10.1016/j.ejor.2015.12.049.

[3] R. Borsche, M. Eimer, and N. Siedow. *A local time stepping method for district heating networks*. 2018. URL: https://kluedo.ub.uni-kl.de/frontdoor/deliver/index/docId/5140/file/district_heating.pdf.

[4] F. Colella, A. Sciacovelli, and V. Verda. "Numerical analysis of a medium scale latent energy storage unit for district heating systems." In: *Energy* 45.1 (2012). The 24th International Conference on Efficiency, Cost, Optimization, Simulation and Environmental Impact of Energy, ECOS 2011, pp. 397–406. DOI: 10.1016/j.energy.2012.03.043.

[5] J. Dorfner and T. Hamacher. "Large-Scale District Heating Network Optimization." In: *IEEE Transactions on Smart Grid* 5.4 (2014), pp. 1884–1891. DOI: 10.1109/TSG.2013.2295856.

[6] A. S. Drud. "CONOPT—a large-scale GRG code." In: *ORSA Journal on computing* 6.2 (1994), pp. 207–216.

[7] F. M. Hante and M. Schmidt. "Complementarity-based nonlinear programming techniques for optimal mixing in gas networks." In: *EURO Journal on Computational Optimization* 7.3 (2019), pp. 299–323. DOI: 10.1007/s13675-019-00112-w.

[8] W. E. Hart, J.-P. Watson, and D. L. Woodruff. "Pyomo: modeling and solving mathematical programs in Python." In: *Mathematical Programming Computation* 3.3 (2011), pp. 219–260. DOI: 10.1007/s12532-011-0026-8.

[9] W. E. Hart, C. D. Laird, J.-P. Watson, D. L. Woodruff, G. A. Hackebeil, B. L. Nicholson, and J. D. Siirola. *Pyomo-optimization modeling in Python*. Springer, 2017. DOI: 10.1007/978-1-4614-3226-5.

[10] I. B. Hassine and U. Eicker. "Impact of load structure variation and solar thermal energy integration on an existing district heating network." In: *Applied Thermal Engineering* 50.2 (2013). Combined Special Issues: ECP 2011 and IMPRES 2010, pp. 1437–1446. DOI: 10.1016/j.applthermaleng.2011.12.037.

[11] S.-A. Hauschild, N. Marheineke, V. Mehrmann, J. Mohring, A. M. Badlyan, M. Rein, and M. Schmidt. "Port-Hamiltonian modeling of district heating networks." In: *Progress in Differential Algebraic Equations II*. Ed. by T. Reis, S. Grundel, and S. Schöps. Differential-Albergaic Equations Forum. Springer, 2020. DOI: 10.1007/978-3-030-53905-4_11.

[12] R. Krug, V. Mehrmann, and M. Schmidt. "Nonlinear Optimization of District Heating Networks." In: *Optimization and Engineering* 22.2 (2021), pp. 783–819. DOI: 10.1007/s11081-020-09549-0.

[13] V. Mehrmann and R. Morandin. "Structure-preserving discretization for port-Hamiltonian descriptor systems." In: *58th IEEE Conference on Decision and Control (CDC), 9.-12.12.19, Nice*. IEEE, 2019, pp. 6863–6868.

[14] V. Mehrmann, M. Schmidt, and J. J. Stolwijk. "Model and Discretization Error Adaptivity Within Stationary Gas Transport Optimization." In: *Vietnam Journal of Mathematics* 46.4 (2018), pp. 779–801. DOI: 10.1007/s10013-018-0303-1.

[15] T. Nussbaumer and S. Thalmann. "Influence of system design on heat distribution costs in district heating." In: *Energy* 101 (2016), pp. 496–505. DOI: 10.1016/j.energy.2016.02.062.

[16] M. Pirouti, A. Bagdanavicius, J. Ekanayake, J. Wu, and N. Jenkins. "Energy consumption and economic analyses of a district heating network." In: *Energy* 57 (2013), pp. 149–159. DOI: 10.1016/j.energy.2013.01.065.

[17] A. Quarteroni, R. Sacco, and F. Saleri. *Numerical mathematics*. Vol. 37. Springer Science & Business Media, 2010.

[18] W. T. Reid. *Riccati Differential Equations*. Vol. 86. Mathematics in Science and Engineering. Elsevier, 1972. DOI: 10.1016/S0076-5392(08)61166-2.

[19] M. Rein, J. Mohring, T. Damm, and A. Klar. *Model order reduction of hyperbolic systems at the example of district heating networks*. Tech. rep. 2019. URL: https://arxiv.org/abs/1903.03342.

[20] M. Rein, J. Mohring, T. Damm, and A. Klar. *Optimal control of district heating networks using a reduced order model*. Tech. rep. 2019. URL: http://publica.fraunhofer.de/documents/N-596673.html.

[21] M. Rein, J. Mohring, T. Damm, and A. Klar. "Parametric model order reduction for district heating networks." In: *PAMM* 18.1 (2018). DOI: 10.1002/pamm.201800192.

[22] B. Rezaie and M. A. Rosen. "District heating and cooling: Review of technology and potential enhancements." In: *Applied Energy* 93 (2012), pp. 2–10. DOI: 10.1016/j.apenergy.2011.04.020.

[23] M. Roland and M. Schmidt. "Mixed-Integer Nonlinear Optimization for District Heating Network Expansion." In: *at - Automatisierungstechnik* (2020). Special Issue "Mathematical Innovations fostering the Energy Transition – Control, Optimization and Uncertainty Quantification". DOI: 10.1515/auto-2020-0063. Forthcoming.

[24] G. Sandou, S. Font, S. Tebbani, A. Hiret, C. Mondon, S. Tebbani, A. Hiret, and C. Mondon. "Predictive Control of a Complex District Heating Network." In: *Proceedings of the 44th IEEE Conference on Decision and Control*. 2005, pp. 7372–7377. DOI: 10.1109/CDC.2005.1583351.

[25] M. Schmidt, M. C. Steinbach, and B. M. Willert. "High detail stationary optimization models for gas networks: validation and results." In: *Optimization and Engineering* 17.2 (2016), pp. 437–472. DOI: 10.1007/s11081-015-9300-3.

[26] G. Schweiger, P.-O. Larsson, F. Magnusson, P. Lauenburg, and S. Velut. "District heating and cooling systems – Framework for Modelica-based simulation and dynamic optimization." In: *Energy* 137 (2017), pp. 566–578. DOI: 10.1016/j.energy.2017.05.115.

[27] J. Stoer and R. Bulirsch. *Introduction to Numerical Analysis*. 3rd ed. Springer, New York, NY, 2002. DOI: 10.1007/978-0-387-21738-3.

[28] J. Stolwijk and V. Mehrmann. "Error Analysis and Model Adaptivity for Flows in Gas Networks." In: *Analele Stiintifice ale Universitatii Ovidius Constanta, Seria Matematica* 26 (July 2018), pp. 231–266. DOI: 10.2478/auom-2018-0027.

[29] V. Verda and F. Colella. "Primary energy savings through thermal storage in district heating networks." In: *Energy* 36.7 (2011), pp. 4278–4286. DOI: 10.1016/j.energy.2011.04.015.

[30] F. Verrilli, S. Srinivasan, G. Gambino, M. Canelli, M. Himanka, C. Del Vecchio, M. Sasso, and L. Glielmo. "Model Predictive Control-Based Optimal Operations of District Heating System With Thermal Energy Storage and Flexible Loads." In: *IEEE Transactions on Automation Science and Engineering* 14.2 (2017), pp. 547–557. DOI: 10.1109/TASE.2016.2618948.

(H. Dänschel, V. Mehrmann) TU Berlin, Inst. f. Mathematik, MA 4-5, Str. des 17. Juni 135, 10623 Berlin, Germany
Email address: daenschel@math.tu-berlin.de
Email address: mehrmann@math.tu-berlin.de

(M. Roland, M. Schmidt) Trier University, Department of Mathematics, Universitätsring 15, 54296 Trier, Germany
Email address: roland@uni-trier.de
Email address: martin.schmidt@uni-trier.de

Article 3

Exact and Heuristic Solution Techniques for Mixed-Integer Quantile Minimization Problems

Diego Cattaruzza, Martine Labbé, Matteo Petris, Marius Roland, Martin Schmidt

Submitted preprint (2022), URL: https://optimization-online.org/2021/11/8673/

Exact and Heuristic Solution Techniques for Mixed-Integer Quantile Minimization Problems

Diego Cattaruzza, Martine Labbé, Matteo Petris, Marius Roland, Martin Schmidt

Abstract. We consider mixed-integer linear quantile minimization problems that yield large-scale problems that are very hard to solve for real-world instances. We motivate the study of this problem class by two important real-world problems: a maintenance planning problem for electricity networks and a quantile-based variant of the classic portfolio optimization problem. For these problems, we develop valid inequalities and present an overlapping alternating direction method. Moreover, we discuss an adaptive scenario clustering method for which we prove that it terminates after a finite number of iterations with a global optimal solution. We study the computational impact of all presented techniques and finally show that their combination leads to an overall method that can solve the maintenance planning problem on large-scale real-world instances provided by the EURO/ROADEF challenge 2020[1] and that they also lead to significant improvements when solving a quantile-version of the classic portfolio optimization problem.

1. Introduction

Many real-world planning and investment problems face a significant amount of uncertainty since they inevitably need to incorporate aspects that lie in the future and are thus unknown at the time of decision making. Consequently, usual objective functions in this context combine the minimization of expected costs (or the maximization of expected profits) with some kind of risk minimization. In this paper, we consider general planning and investment problems in which we minimize a convex combination of expected costs and the risk's quantile. In other words, the objective function is a combination of the expected value and the Value at Risk (VaR) of some function that is linear in the problem's variables. It is well known that VaR is nothing but the τ-quantile. It is a measure of risk used in various domains. In portfolio optimization, [8, 9] consider the problem of maximizing the VaR subject to a lower bound on the expected return while [1, 2, 4, 16] maximize the expected return given a lower bound on the VaR.

Limiting the VaR of a random variable is a particular type of chance constraint since it is equivalent to setting up a lower bound on the probability that the random variable takes a value larger than the said limit. Chance-constrained formulations have been proposed for various applications such as the design of reliable networks [25], the packing of objects with random weights [26], or the allocation of scarce vaccines to prevent the occurrence of disease epidemics [27]. Moreover, the VaR is also used in real-world regulatory frameworks such as Basel or Solvency.

Date: August 19, 2022.

2020 *Mathematics Subject Classification.* 90B25, 90C11, 90C90, 90C15.

Key words and phrases. Quantile Minimization, Value-at-Risk (VaR), Mixed-Integer Optimization, Valid Inequalities, Adaptive Clustering.

[1] See https://www.roadef.org/challenge/2020/en/index.php.

Besides considering the quantile minimization, which already poses a computational challenge on its own, we study both continuous and mixed-integer linear settings, which are required by many real-world problems to properly model planning or investment decisions. Thus, in total, we consider the challenging class of mixed-integer linear quantile minimization problems. To this end, stochasticity is modeled via finite scenario sets, which leads to large-scale mixed-integer linear problems that can hardly be solved with state-of-the-art solvers.

Throughout the paper we use two examples for the general class of problems under consideration: A maintenance planning problem in electricity networks as it was posed in the EURO/ROADEF challenge 2020 and a variant of the classic portfolio optimization problem. The grid operation based outage maintenance planning problem (MPP) consists in determining the start time of maintenance interventions in a high-voltage transmission network over a given time horizon. Each of the interventions lasts a certain number of time units that depends on the start time of the intervention. All interventions must be planned and finished before the end of the time horizon. Further, some interventions cannot take place at the same time. Finally, each intervention consumes resources and the total amount of resources used at each time step is bounded from below and above. The objective is to minimize the risk of the maintenance plan. More precisely, a set of scenarios is given and for each such scenario, we know, at each time period, the risk value of each intervention. The goal is to minimize a combination of the expectation and the quantile of the risk.

The second problem is a variant of the well-known portfolio optimization problem. The goal in portfolio optimization is twofold: maximize the return and minimize the risk for which different measures have been proposed; see, e.g., [4, 9, 16, 18]. Among them, the VaR or τ-quantile has attracted particular attention, namely because it is used to measure market risk by regulators; see, e.g., [3] and the references therein.

As we already mentioned above, the studied models lead to large-scale mixed-integer linear problems (MILPs). For these problems, we develop tailored solution techniques. In Section 2, we introduce the general problem class and the two specific examples. In Section 3, we propose problem-tailored valid inequalities. They are derived from duality theory applied to a properly chosen linear optimization problem that models the quantile. In Section 4, we present an overlapping alternating direction method that serves as a primal heuristic for quickly computing feasible points of good quality. In Section 5, we then present an adaptive scenario clustering method for which we prove that it computes an approximate global optimal solution after finitely many iterations. We illustrate the computational impact of all presented techniques in our numerical study in Section 6 before we close this paper with some concluding remarks and a brief discussion of potential future research in Section 7.

2. Problem Statement

In this section, we first state the general problem class that we consider in the following. Afterward, we present two specific examples for the general modeling framework to underline the importance of the studied class of problems.

We consider a discrete set of indices $t \in \mathcal{T} = \{1, \dots, T\}$. With this at hand, the general problem is given by

$$\min_{x} \quad \alpha \sum_{t \in \mathcal{T}} \mathbb{E}[c_t^\top x] + (1-\alpha) \sum_{t \in \mathcal{T}} f\left(\mathbb{Q}[c_t^\top x]\right) \tag{1a}$$

$$\text{s.t.} \quad x \in X \subseteq \mathbb{R}^N. \tag{1b}$$

The feasible set X is a non-empty and closed set that may also include integrality restrictions for all or some of the variables. For each index t, we are given a finite

set $\mathcal{S}_t$ of scenarios and for each scenario $s \in \mathcal{S}_t$, c_t^s is the respective cost vector and $p_t^s \in [0,1]$ is the associated probability with $\sum_{s\in\mathcal{S}_t} p_t^s = 1$. The expected value is then defined as

$$\mathbb{E}[c_t^\top x] = \sum_{s\in\mathcal{S}_t} p_t^s (c_t^s)^\top x$$

and the τ-quantile is given by

$$\mathbb{Q}[c_t^\top x] = \min\left\{ q \in \mathbb{R} \colon \sum_{s\in\mathcal{N}(q)} p_t^s \geq \tau \right\}, \quad \mathcal{N}(q) = \left\{ s \in \mathcal{S}_t \colon (c_t^s)^\top x \leq q \right\}.$$

Further, $\alpha \in [0,1]$ is a scaling factor that either puts more emphasis on the expected value terms $\mathbb{E}[c_t^\top x]$ or on the τ-quantile terms $f(\mathbb{Q}[c_t^\top x])$, where f is an arbitrary function depending on the τ-quantile $\mathbb{Q}[\cdot]$.

Usually, the τ-quantile $\mathbb{Q}[\cdot]$ cannot be stated in closed form. However, it can be expressed by the solution of the following quantile optimization problem in an extended variable space:

$$\begin{aligned}
\mathbb{Q}[c_t^\top x] = \underset{q_t, y_t^s}{\arg\min} \quad & q_t && \text{(2a)}\\
\text{s.t.} \quad & q_t \geq (c_t^s)^\top x + M_t^s (y_t^s - 1), \quad s \in \mathcal{S}_t, && \text{(2b)}\\
& \sum_{s\in\mathcal{S}_t} y_t^s p_t \geq \tau, && \text{(2c)}\\
& y_t^s \in \{0,1\}, \quad s \in \mathcal{S}_t, && \text{(2d)}
\end{aligned}$$

where M_t^s are sufficiently large numbers. We will discuss specific choices of these parameters later when we consider concrete examples. Using such a technique leads to the reformulation

$$\begin{aligned}
\min_{x,z} \quad & \alpha \sum_{t\in\mathcal{T}} \mathbb{E}[c_t^\top x] + (1-\alpha) \sum_{t\in\mathcal{T}} g(z_t) && \text{(3a)}\\
\text{s.t.} \quad & x \in X, \quad z_t \in Z_t(x),\ t \in \mathcal{T}, && \text{(3b)}
\end{aligned}$$

where the (possibly mixed-integer) constraint sets $Z_t(x)$, which are required to model the quantile, depend on the original variables x. Moreover, we have $z = (z_t)_{t\in\mathcal{T}}$ and g is an arbitrary function depending on the newly introduced variable vector z.

To highlight the generality of this class of optimization models, we now consider two examples in the following subsections.

2.1. **The Maintenance Planning Problem.** Let $\mathcal{I}$ denote the set of interventions to be scheduled, let $\mathcal{T} = \{1, \dots, T\}$ be the set of time indices representing the time horizon, i.e., the set of time steps at which interventions can take place, and let $\mathcal{R}$ be the set of resources used for the interventions. Further, for each time $t \in \mathcal{T}$, $\mathcal{S}_t$ represents the set of scenarios at this time, which all have the same probability, i.e., $p_t^s = p_t = 1/|\mathcal{S}_t|$ holds for all $t \in \mathcal{T}$. The duration of intervention $i \in \mathcal{I}$, if it starts at time $t \in \mathcal{T}$, is given by Δ_t^i. The amount of resource r used at time t by intervention i starting at time t' is given by $r_{t',t}^i$. The total amount of resource r used by all interventions in process at time t must be at least l_t^r and cannot be larger than u_t^r. Moreover, $\sigma_{t',t}^{i,s}$ denotes the risk in scenario s at time t of intervention i if it starts at time t'. We are also given a set $\mathcal{D}$ of triplets (i,j,t) such that intervention i and j cannot be both in process at time t.

Intervention preemption is not allowed and each intervention must be terminated at time T. We thus denote by $\mathcal{T}(i) = \{t \in \mathcal{T} \colon t + \Delta_t^i \leq T\}$ the set of feasible starting times of intervention i. Further, we denote by $\mathcal{T}(i,t) = \{t' \in \mathcal{T} \colon t' \leq t,\ t' + \Delta_{t'}^i \geq t\}$ the set of starting times of intervention i for which the intervention is in process at time t.

To model the maintenance planning problem (MPP), we use a set of binary variables x: for $i \in \mathcal{I}$ and $t \in \mathcal{T}(i)$, we have $x_t^i = 1$ if intervention i starts at time t. Further, for $t \in \mathcal{T}$, q_t and ε_t are continuous variables representing the τ-quantile as well as the maximum of zero and the difference between the τ-quantile and the average of the risk at time t for the different scenarios in $\mathcal{S}_t$, respectively. We now present the MILP:

$$\min_{x,\varepsilon,q} \quad \alpha \frac{1}{T} \sum_{t\in\mathcal{T}} \frac{1}{|\mathcal{S}_t|} \sum_{s\in\mathcal{S}_t} \sum_{i\in\mathcal{I}} \sum_{t'\in\mathcal{T}(i,t)} \sigma_{t',t}^{i,s} x_{t'}^i + (1-\alpha)\frac{1}{T}\sum_{t\in\mathcal{T}} \varepsilon_t \tag{4a}$$

$$\text{s.t.} \quad \sum_{t\in\mathcal{T}(i)} x_t^i = 1, \quad i \in \mathcal{I}, \tag{4b}$$

$$l_t^r \le \sum_{i\in\mathcal{I}} \sum_{t'\in\mathcal{T}(i,t)} r_{t',t}^i x_{t'}^i \le u_t^r, \quad r \in \mathcal{R},\, t \in \mathcal{T}, \tag{4c}$$

$$\sum_{t'\in\mathcal{T}(i,t)} x_{t'}^i + \sum_{t'\in\mathcal{T}(j,t)} x_{t'}^j \le 1, \quad (i,j,t) \in \mathcal{D}, \tag{4d}$$

$$\varepsilon_t \ge q_t - \frac{1}{|\mathcal{S}_t|} \sum_{s\in\mathcal{S}_t} \sum_{i\in\mathcal{I}} \sum_{t'\in\mathcal{T}(i,t)} \sigma_{t',t}^{i,s} x_{t'}^i, \quad t \in \mathcal{T}, \tag{4e}$$

$$\varepsilon_t \ge 0, \quad t \in \mathcal{T}, \tag{4f}$$

$$x_t^i \in \{0,1\}, \quad i \in \mathcal{I},\, t \in \mathcal{T}, \tag{4g}$$

$$q_t \in Z_t(x), \quad t \in \mathcal{T}, \tag{4h}$$

with $x = (x_t)_{t\in\mathcal{T}}$ and $x_t = (x_t^i)_{i\in\mathcal{I}}$. Analogous vector notation is used to define ε and q.

This problem is the one of the EURO/ROADEF challenge 2020. The first term of the objective function represents the average risk and the second term represents the average excess, i.e., the average of the maximum of zero and the difference between the risk's τ-quantile and the risk's average. They are weighted with coefficients α and $(1-\alpha)$, $\alpha \in [0,1]$, respectively. Constraints (4b) specify that each intervention must start in exactly one time period. Constraints (4c) indicate that the amount of each resource must be within its lower and upper bounds at each time period. Constraints (4d) forbid pairs of interventions to be in process at the same time when they are in conflict. Constraints (4e) together with the objective function define the excess, at each time t, as the difference between the τ-quantile and the average of the risks. Note that we used that all scenarios have the same probability in this setting while defining the quantile. Finally, (4f)–(4g) specify the type of the different variables.

The set $Z_t(x)$ appearing in Constraints (4h) is the set of optimal solutions of the following problem that states that the quantile denoted by q_t must be the smallest value larger than or equal to at least $p_t = \lceil \tau|\mathcal{S}_t| \rceil$ risk values $\sum_{i\in\mathcal{I}} \sum_{t'\in\mathcal{T}(i,t)} \sigma_{t',t}^{i,s} x_{t'}^i$. To this end, it uses the variables y_t^s that take binary values. Thus, we have

$$Z_t(x) = \arg\min_{q_t, y_t^s} \quad q_t \tag{5a}$$

$$\text{s.t.} \quad q_t \ge \sum_{i\in\mathcal{I}} \sum_{t'\in\mathcal{T}(i,t)} \sigma_{t',t}^{i,s} x_{t'}^i + M_t^s (y_t^s - 1), \quad s \in \mathcal{S}_t, \tag{5b}$$

$$\sum_{s\in\mathcal{S}_t} y_t^s p_t \ge \tau, \tag{5c}$$

$$y_t^s \in \{0,1\}, \quad s \in \mathcal{S}_t. \tag{5d}$$

Given that the objective function (4a) to be minimized is non-decreasing in the quantiles q_t, we can replace Constraints (4h) by Constraints (5b)–(5d). Note further

that Problem (5) also ensures that every quantile is non-negative if all risks are non-negative.

Constraints (5b) involve the big-M constants M_t^s that must be an upper bound on $\sum_{i\in\mathcal{I}}\sum_{t'\in\mathcal{T}(i,t)}\sigma_{t',t}^{i,s}x_{t'}^i$. Given that variables x_t^i satisfy (4b), we can choose

$$M_t^s = \sum_{i\in\mathcal{I}} \max_{t'\in\mathcal{T}(i,t)} \sigma_{t',t}^{i,s}.$$

A stronger big-M can be computed via

$$M_t^s = \max \quad \sum_{i\in\mathcal{I}}\sum_{t'\in\mathcal{T}(i,t)} \sigma_{t',t}^{i,s}x_{t'}^i \tag{6a}$$

$$\text{s.t.} \quad (4b), (4c), (4d) \quad \text{and} \quad x_t^i \in \{0,1\},\ i\in\mathcal{I},\ t'\in\mathcal{T}(i,t). \tag{6b}$$

A compromise consists in solving the LP relaxation of (6).

Finally, to show that Problem (4) is a special instance of the general problem (1), we first note that for every scenario $s\in\mathcal{S}_t$, the random variable in the maintenance planning problem is given by

$$(c_t^s)^\top x = \sum_{i\in\mathcal{I}}\sum_{t'\in\mathcal{T}(i,t)} \sigma_{t',t}^{i,s}x_{t'}^i, \quad s\in\mathcal{S}_t,$$

with associated probability $p_t^s = 1/|\mathcal{S}_t|$. Then, we replace the excess ε_t in the second term of the objective function with

$$f(\mathbb{Q}[c_t^\top x]) = \max\left\{0,\ \mathbb{Q}[c_t^\top x] - \frac{1}{|\mathcal{S}_t|}\sum_{s\in\mathcal{S}_t}\sum_{i\in\mathcal{I}}\sum_{t'\in\mathcal{T}(i,t)} \sigma_{t',t}^{i,s}x_{t'}^i\right\}.$$

Thus, the variables ε_t, $t\in\mathcal{T}$, and Constraints (4e), (4f) and (4h) are not required anymore.

By putting this all together and by re-scaling the objective function with T, for X defined by (4b)–(4d) and (4g), we obtain

$$\min \quad \alpha\sum_{t\in\mathcal{T}}\mathbb{E}[c_t^\top x] + (1-\alpha)\sum_{t\in\mathcal{T}} f(\mathbb{Q}[c_t^\top x]) \quad \text{s.t.} \quad x = (x_t)_{t\in\mathcal{T}} \in X,$$

which is exactly of the general form (1).

2.2. **Portfolio Optimization.** In the classic portfolio optimization problem [19] we are given a budget B that we need to invest in a set of n equities so that the expected return is maximized while the corresponding risk, calculated by the standard deviation, is limited to be at most of a given value.

In recent years the risk measure that has mostly been used in the financial community is the Value-at-risk (VaR) [4]: to minimize the portfolio's risk, one wishes that, for a given value of the parameter τ, that the corresponding quantile (or VaR) is large.

According to [2], the VaR at the $100\tau\,\%$ confidence level of a risky portfolio is the rate of return v^q such that $F(-v^q) = 1-\tau$ and $F(\cdot)$ is the cumulative distribution function of the portfolio's rate of return at the end of the period.

Let r_i be the return of equity i after, e.g., one year, which is a random variable. Moreover, let $x\in\mathbb{R}^n$ be the vector describing the investment. This means that we invest x_iB in equity i and it holds

$$\sum_{i=1}^n x_i = 1, \quad x\geq 0.$$

The return of the entire portfolio is then given by $r^\top x$.

The resulting general model for portfolio optimization reads

$$\max_{x} \quad \alpha\mathbb{E}[r^\top x] + (1-\alpha)\mathbb{Q}[r^\top x] \tag{7a}$$

$$\text{s.t.} \quad x \in X = \left\{ x \in \mathbb{R}^n \colon \sum_{i=1}^{n} x_i = 1,\ \mathbb{E}[r^\top x] \geq \rho,\ x \geq 0 \right\} \tag{7b}$$

with $\alpha \in [0,1]$ and ρ is the minimum expected return of the portfolio.

This model is a particular case of Model (1) with $\mathcal{T}$ being a singleton and f being the identity. Furthermore, to fit into our general framework it remains to change the sign of all observed returns and minimize the objective function.

For $\alpha = 0$ this problem amounts to minimize the VaR with a minimum expected return. This is the model proposed in [9] and we can deduct from [4] that it is strongly NP-hard. However, (7) also encompasses the possibility of a linear combination of both objectives or to relax the constraint of a minimal expected return by choosing a value for ρ that is sufficiently small.

A common approach to determine an optimal portfolio consists in using historical or simulated data. In this context, return vectors r^s with their associated probability p^s are given for a set $\mathcal{S}$ of scenarios so that

$$\mathbb{E}[r^\top x] = \sum_{s \in \mathcal{S}} p^s (r^s)^\top x$$

and

$$\mathbb{Q}[r^\top x] = \max \left\{ q \colon \sum_{s \in \mathcal{N}(q)} p^s \geq 1 - \tau \right\}, \quad \mathcal{N}(q) = \left\{ s \in \mathcal{S} \colon (r^s)^\top x \geq q \right\}$$

holds. Finally, the portfolio optimization problem (POP) can then be formulated as the MILP

$$\max_{x,q,y} \quad \alpha \sum_{s \in \mathcal{S}} p^s (r^s)^\top x + (1-\alpha) q \tag{8a}$$

$$\text{s.t.} \quad x \in X, \tag{8b}$$

$$q \leq (r^s)^\top x + M^s y^s, \quad s \in \mathcal{S}, \tag{8c}$$

$$\sum_{s \in \mathcal{S}} p^s y^s \leq \tau, \tag{8d}$$

$$y^s \in \{0,1\}, \quad s \in \mathcal{S}, \tag{8e}$$

where M^s is a sufficiently large constant that can be set equal to

$$\min \left\{ q \colon \sum_{s' \in \mathcal{M}(q)} p^{s'} \geq \tau \right\} - \min_i r_i^s \quad \text{with} \quad \mathcal{M}(q) = \left\{ s' \in \mathcal{S} \colon \max_i r_i^{s'} \leq q \right\}.$$

Again, this is a special case of Model (3) in which $z = (q, y)$ as well as $g(z) = q$ holds and $Z(x)$ is defined by Constraints (8c)–(8e).

3. Valid Inequalities

For the ease of notation, we omit the index t in this section when there is no possible ambiguity. Lower bounds on the variable q representing the τ-quantile can be obtained in two different ways. The first one uses the strong-duality property of linear optimization while the second one is based on a combinatorial argument.

In what follows, we set $p(\bar{\mathcal{S}}) = \sum_{s \in \bar{\mathcal{S}}} p^s$ and $c_i(\bar{\mathcal{S}}) = \sum_{s \in \bar{\mathcal{S}}} c_i^s$ for $\bar{\mathcal{S}} \subseteq \mathcal{S}$.

Proposition 1. *The following inequality is valid for the quantile problem (2) for all subsets $\bar{\mathcal{S}} \subseteq \mathcal{S}$ with $p(\bar{\mathcal{S}}) < \tau$:*

$$\big(\tau - p(\bar{\mathcal{S}})\big)\, q \geq \sum_{i=1}^{n} \big(b_i - c_i(\bar{\mathcal{S}})\big)\, x_i \tag{9}$$

with

$$b_i = \min_{w} \left\{ \sum_{s\in\mathcal{S}} c_i^s w^s \colon \sum_{s\in\mathcal{S}} w^s = \tau,\ 0 \leq w^s \leq p^s,\ s \in \mathcal{S} \right\}.$$

Furthermore, it can be separated in polynomial time.

Proof. Let us consider $d^s := (c^s)^\top x$ and p^s, $s \in \mathcal{S}$, as the realizations of a discrete random variable and its corresponding probability. It is well known, see, e.g., [18], that the τ-quantile q is the optimal solution of the linear optimization problem

$$\max_{u,q} \quad \tau q - \sum_{s\in\mathcal{S}} p^s u^s \tag{10a}$$

$$\text{s.t.} \quad q - u^s \leq d^s, \quad u^s \geq 0, \quad s \in \mathcal{S}, \tag{10b}$$

$$q \in \mathbb{R}. \tag{10c}$$

The dual of this problem reads

$$\min_{w} \quad \sum_{s\in\mathcal{S}} d^s w^s \tag{11a}$$

$$\text{s.t.} \quad \sum_{s\in\mathcal{S}} w^s = \tau, \tag{11b}$$

$$0 \leq w^s \leq p^s, \quad s \in \mathcal{S}. \tag{11c}$$

Using strong duality of linear optimization, the quantile q must satisfy

$$\tau q \geq \sum_{s\in\mathcal{S}} d^s w^s + \sum_{s\in\mathcal{S}} p^s u^s.$$

Since $u^s \geq \max\{q - d^s, 0\}$, the following inequality is valid for all $\bar{\mathcal{S}} \subseteq \mathcal{S}$:

$$\tau q \geq \sum_{s\in\mathcal{S}} d^s w^s + \sum_{s\in\bar{\mathcal{S}}} p^s (q - d^s). \tag{12}$$

In our general framework, the realization d^s is a linear function $\sum_{i=1}^n c_i^s x_i$ so that the resulting inequality (12) is nonlinear. However, the linear inequality (9) can be obtained by noticing that

$$\sum_{s\in\mathcal{S}} d^s w^s = \sum_{s\in\mathcal{S}} \sum_{i=1}^{n} c_i^s x_i w^s \geq \sum_{i=1}^{n} b_i x_i, \quad b_i = \min_{w} \left\{ \sum_{s\in\mathcal{S}} c_i^s w^s \colon (11b), (11c) \right\} \tag{13}$$

and by rearranging terms.

The separation problem for Inequality (9) is easy. Given a solution $\bar{x}, \bar{q}$, it suffices to choose $\bar{\mathcal{S}} = \{s \in \mathcal{S} \colon \bar{q} > \sum_{i=1}^n c_i^s \bar{x}_i\}$ and check whether the resulting inequality (9) is violated. □

Note that these inequalities can be seen as a special case of the valid inequalities discussed in [15] for bilevel optimization.

The second approach to derive a lower bound on the τ-quantile uses a covering argument and can be seen as a generalization of the idea proposed by [21] for the case where at most k linear inequalities among n given ones are allowed to be violated. In our context, if for a subset $\bar{\mathcal{S}}$ of scenarios the probability satisfies $p(\bar{\mathcal{S}}) < \tau$, then $q \geq (c^s)^\top x$ holds for some scenarios $s \in \mathcal{S} \setminus \bar{\mathcal{S}}$.

Proposition 2. *The following inequality is valid for the quantile problem (2) for all subsets $\bar{\mathcal{S}} \subseteq \mathcal{S}$ with $p(\bar{\mathcal{S}}) < \tau$:*

$$\big(\tau - p(\bar{\mathcal{S}})\big)\, q \geq \sum_{i=1}^{n} b_i(\bar{\mathcal{S}}) x_i \tag{14}$$

where

$$b_i(\bar{\mathcal{S}}) = \min_{w} \left\{ \sum_{s \in \mathcal{S} \setminus \bar{\mathcal{S}}} c_i^s w^s : \sum_{s \in \mathcal{S} \setminus \bar{\mathcal{S}}} w^s = \tau - p(\bar{\mathcal{S}}), 0 \leq w^s \leq p^s, s \in \mathcal{S} \setminus \bar{\mathcal{S}} \right\}.$$

Proof. Since $p(\bar{\mathcal{S}}) < \tau$ holds, there exists a subset $\mathcal{S}^c \subset \mathcal{S} \setminus \bar{\mathcal{S}}$ such that $p(\mathcal{S}^c) > \tau - p(\bar{\mathcal{S}})$ and $q \geq (c^s)^\top x$ holds for all $s \in \mathcal{S}^c$. Taking a weighted sum of these inequalities with coefficients v^s for $s \in \mathcal{S}^c$ with $\sum_{s \in \mathcal{S}^c} v^s = \tau - p(\bar{\mathcal{S}})$ and $0 \leq v^s \leq p^s$ yields

$$\big(\tau - p(\bar{\mathcal{S}})\big)\, q \geq \sum_{i=1}^{n} \sum_{s \in \mathcal{S}^c} v^s c_i^s x_i. \tag{15}$$

Inequality (14) is obtained by additionally using that $\sum_{s \in \mathcal{S}^c} v^s c_i^s \geq b_i(\bar{\mathcal{S}})$ holds. □

Let us remark that the definitions of b_i and $b_i(\bar{\mathcal{S}})$ imply that $b_i = b_i(\emptyset)$. To avoid any ambiguities in the sequel we will rather use the notation $b_i(\emptyset)$.

The following example shows that a priori there is no dominance relation between the inequalities in (14).

Example 1. *Consider four scenarios $s \in \{1,2,3,4\}$ with equal probability $1/4$ and four variables x_i with $i \in \{1,2,3,4\}$ and let $c_i^s = 0$, if $i = s$ and $c_i^s = 1$ otherwise. If $\tau = 3/4$, then the inequalities in (14) are the following (after rescaling):*

- $q \geq 2/3 \sum_{i=1}^{4} x_i$, *for* $\bar{\mathcal{S}} = \emptyset$
- $q \geq \sum_{i \in \bar{\mathcal{S}}} x_i + 1/2 \sum_{i \notin \bar{\mathcal{S}}} x_i$, *if* $|\bar{\mathcal{S}}| = 1$
- $q \geq \sum_{i \in \bar{\mathcal{S}}} x_i$, *if* $|\bar{\mathcal{S}}| = 2$.

None of them is dominated by a nonegative linear combination of the others.

As shown in the following proposition, the separation of the inequalities in (14) is difficult at least for a fixed value of $p(\bar{\mathcal{S}})$.

Proposition 3. *For a fixed value of $p(\bar{\mathcal{S}})$, the separation problem for the inequalities in (14) is NP-hard even in the special case where $p^s = 1/|\mathcal{S}|$ for all $s \in \mathcal{S}$, $\tau = k/|\mathcal{S}|$, and $c_i^s \in \{0,1\}$.*

Proof. Under the above conditions, the decision version (D-SEP) of the separation problem of (14) for a point (x^*, q^*) consists in determining whether there exists a subset $\bar{\mathcal{S}}$ such that $|\bar{\mathcal{S}}| = B$ and

$$|\mathcal{S}| \sum_{i=1}^{n} b_i(\bar{\mathcal{S}}) x_i^* > q^*(k - B) \tag{16}$$

holds.

This problem clearly belongs to NP. Further, we show that CLIQUE reduces to it; see, e.g., Problem GT19 in [10]. To this end, for an instance of CLIQUE given by a graph $G = (V, E)$ and an integer B, we define an instance of (D-SEP) as follows. We set $\mathcal{S} = V$, $I = E$, $k = B + 1$, $x_i^* = x^*$ for all i, $q^* = x^*(B(B-1)/2 - 1)$, and $c_i^s = 0$ if edge i is incident to vertex s and $c_i^s = 1$ otherwise. Then, $|\mathcal{S}| b_i(\bar{\mathcal{S}}) =$

$\min\left\{c_i^s : s \in \mathcal{S} \setminus \bar{\mathcal{S}}\right\} = 1$ if both end vertices of i belong to $\bar{\mathcal{S}}$ and 0 otherwise. Hence, (16) reads

$$x^*|\mathcal{S}| \sum_{i=1}^{n} b_i(\bar{\mathcal{S}}) = x^*|E(\bar{\mathcal{S}})| > q^*(k-B) = x^*(B(B-1)/2 - 1)$$

and is satisfied if and only if $\bar{\mathcal{S}}$ is a clique of size B. □

The following proposition shows that the inequalities in (14) are stronger than the inequalities in (9).

Proposition 4. *For $\bar{\mathcal{S}} \in \mathcal{S}$, Inequality (14) dominates Inequality (9).*

Proof. The left-hand sides of both inequalities are equal. Further, we have

$$b_i(\emptyset) = \min_w \left\{ \sum_{s\in\mathcal{S}} c_i^s w^s : \sum_{s\in S} w^s = \tau, 0 \le w^s \le p^s, s \in S \right\} \le c_i(\bar{\mathcal{S}}) + b_i(\bar{\mathcal{S}})$$

Hence, the ith coefficient of (14) is larger than or equal to the corresponding one of (9). □

The above results suggest to use the separation procedure for Inequality (9) but to add the corresponding stronger inequality (14).

3.1. **Application to the Maintenance Planning Problem.** First recall that, in the MPP, we have a set of scenarios $\mathcal{S}_t$ for each time step t and $p^s = 1/|\mathcal{S}_t|$ holds for all $s \in \mathcal{S}_t$.

The following proposition shows how to adapt the valid inequalities (9) and (14) to MPP.

Proposition 5. *The following two inequalities are valid for the MPP (4) for all subsets $\bar{\mathcal{S}} \subseteq \mathcal{S}_t$ with $|\bar{\mathcal{S}}| < \lceil \tau|\mathcal{S}_t| \rceil$:*

$$\left(\lceil \tau|\mathcal{S}_t| \rceil - |\bar{\mathcal{S}}|\right) q_t \ge \sum_{i\in I} \sum_{t'\in\mathcal{T}(i,t)} \left(b^i_{t,t'}(\emptyset) - \sum_{s\in\bar{\mathcal{S}}} \sigma^{i,s}_{t',t} x^i_{t'} \right) \tag{17}$$

and

$$\left(\lceil \tau|\mathcal{S}_t| \rceil - |\bar{\mathcal{S}}|\right) q_t \ge \sum_{i\in I} \sum_{t'\in\mathcal{T}(i,t)} b^i_{t,t'}(\bar{\mathcal{S}}) x^i_{t'}, \tag{18}$$

where

$$b^i_{t,t'}(\bar{\mathcal{S}}) = \min_w \left\{ \sum_{s\in\mathcal{S}\setminus\bar{\mathcal{S}}} \sigma^{i,s}_{t',t} w^s : \sum_{s\in\mathcal{S}\setminus\bar{\mathcal{S}}} w^s = \lceil \tau|\mathcal{S}|\rceil - |\bar{\mathcal{S}}|, 0 \le w^s \le 1, s \in \mathcal{S}\setminus\bar{\mathcal{S}} \right\}$$

holds. In addition, Inequality (17) can be separated in polynomial time but is dominated by Inequality (18), whose separation is NP-hard.

Proof. The objective function of Problem (10) can be rewritten as

$$\max_{u,q} \quad \lceil \tau|\mathcal{S}|\rceil q - \sum_{s\in\mathcal{S}} u^s, \tag{19}$$

which leads to the dual formulation

$$\min_w \quad \sum_{s\in\mathcal{S}} d^s w^s \tag{20a}$$

$$\text{s.t.} \quad \sum_{s\in\mathcal{S}} w^s = \lceil \tau|\mathcal{S}|\rceil, \tag{20b}$$

$$0 \le w^s \le 1, \quad s \in \mathcal{S}. \tag{20c}$$

Note that in the MPP, we need to select $\lceil \tau|\mathcal{S}| \rceil$ scenarios with a risk lower than or equal to the quantile, which allows us to use the constant in the right-hand side of (20b) and in the objective function (19). Next, by strong duality, the quantile must then satisfy

$$\lceil \tau|\mathcal{S}| \rceil q \geq \sum_{s \in \bar{\mathcal{S}}} d^s w^s + \sum_{s \in \bar{\mathcal{S}}} (q - d^s). \tag{21}$$

After re-introducing the t-index and bounding the nonlinear terms as in (13), Inequality (21) applied to the MPP reads

$$\lceil \tau|\mathcal{S}_t| \rceil q_t \geq \sum_{i \in I} \sum_{t' \in \mathcal{T}(i,t)} b^i_{t,t'}(\emptyset) x^i_{t'} + \sum_{s \in \bar{\mathcal{S}}} \left(q_t - \sum_{i \in \mathcal{I}} \sum_{t' \in \mathcal{T}(i,t)} \sigma^{i,s}_{t',t} x^i_{t'} \right), \quad t \in \mathcal{T}, \tag{22}$$

with

$$b^i_{t,t'}(\emptyset) = \min_w \left\{ \sum_{s \in \mathcal{S}} \sigma^{i,s}_{t',t} w^s : (20b), (20c) \right\}.$$

The coefficient $b^i_{t,t'}(\emptyset)$ is the sum of the $\lceil \tau|\mathcal{S}| \rceil$ smallest risk values $\sigma^{i,s}_{t',t}$ of intervention $i \in \mathcal{I}$ at time $t \in \mathcal{T}$ that has started at $t' \in \mathcal{T}(i,t)$.

By grouping the terms in q in the left-hand side, Inequality (22) becomes (17) and its separation can be done in polynomial time since it suffices to include in $\bar{\mathcal{S}}$ each scenario $s \in \mathcal{S}_t$ if the value of the second term of the right-hand side of (22) is positive for the current solution.

The proofs of the validity of Inequality (17), of the NP-hardness of its separation, and the fact that it dominates Inequality (17) are similar to those of Propositions 2–4 while taking again into account that the scenarios of a set $\mathcal{S}_t$ have equal probability. □

3.2. **Application to the Portfolio Optimization Problem.** In the case of the portfolio optimization problem, given that $-q$ is the $(1-\tau)$-quantile of the linear functions $-(r^s)^\top x$, we can directly apply Propositions 2–4 with the modified data $\tilde{c}^s = -r^s$, $\tilde{\tau} = 1 - \tau$, and variables $\tilde{q} = -q$. The following proposition summarizes these results.

Proposition 6. *The following two inequalities are valid for the portfolio optimization problem (8) for all subsets $\bar{\mathcal{S}} \subseteq \mathcal{S}$ with $p(\bar{\mathcal{S}}) < 1 - \tau$:*

$$(1 - \tau - p(\bar{\mathcal{S}}))q \leq \sum_{i \in I} (b_i(\emptyset) - \sum_{s \in \bar{\mathcal{S}}} p^s r^s_i) x_i, \tag{23}$$

and

$$(1 - \tau - p(\bar{\mathcal{S}}))q \leq \sum_{i \in I} b_i(\bar{\mathcal{S}}) x_i, \tag{24}$$

where

$$b_i(\bar{\mathcal{S}}) = \max_w \left\{ \sum_{s \in \mathcal{S} \setminus \bar{\mathcal{S}}} r^s_i w^s : \sum_{s \in \mathcal{S} \setminus \bar{\mathcal{S}}} w^s = 1 - \tau - p(\bar{\mathcal{S}}), 0 \leq w^s \leq p^s, s \in \mathcal{S} \setminus \bar{\mathcal{S}} \right\}$$

holds. In addition, Inequality (23) can be separated in polynomial time but is dominated by Inequality (24), whose separation is NP-hard.

4. An Overlapping Alternating Direction Method

In this section, we describe an overlapping alternating direction method to solve Problem (3). Alternating Direction Methods (ADMs) have been initially proposed in [7, 13] as extensions of Lagrangian methods. They are iterative procedures typically used to tackle problems defined by means of two vectors of decision variables, which are subject to some coupling constraints. Instead of solving the monolithic original problem, at each iteration of an ADM, one sequentially solves two smaller subproblems each of which determines a new value for one of the variable vectors, having fixed the value of the other one. In recent years, ADMs have been exploited to solve large-scale optimization problems in the field of gas transport [11, 12], machine learning [5, 17], bilevel problems [14], or supply chain problems [22]. In our work, we devise an overlapping ADM (OADM), which can be seen as a variant of an ADM to solve problems for which the vector of variables is partitioned into three subvectors. As in usual ADMs, two subproblems related to two variable subvectors are identified and solved sequentially. However, the remaining variable subvector is to be determined in both subproblems, since it is part of both. The idea behind OADMs can be traced back to overlapping Schwarz methods (see, e.g., [6, 20]) used in the field of partial differential equations to solve boundary value problems defined on a domain that is a union of some intersecting subdomains. Recently, it also has been applied very successfully to graph-structured problems; see, e.g., [23].

In the following, we present an OADM for Problem (3), which is motivated by the special structure of the problem itself and by our formulation for the quantile. We observe that Problem (3) makes use of the pair (x, z) of variable vectors, where z is introduced only to reformulate the term of the objective function (3a) that is related to the quantile. Specifically, $z \in Z_t(x)$, $t \in \mathcal{T}$, encodes the formulation of the quantile. In both of our applications, sets of constraints $Z_t(x)$, $t \in \mathcal{T}$, are defined over two vectors of variables; see Problem (5) and (8). Hence, in this section, we generalize the setting of Problem (3) by considering it defined over the 3-tuple (x, z_1, z_2) of variable vectors, where z_1 and z_2 are two subvectors of z, i.e., $z = (z_1, z_2)$. In what follows, we may still write z in lieu of (z_1, z_2) if the explicit decomposition is not required. In our OADM, we identify a subproblem related to x and one related to z_1. The variable vector z_2 is overlapping, i.e., it is part of the optimization for both subproblems. Finally, we highlight that our OADM enjoys two special features. The value of z depends only on the one of x (see, e.g., Constraints (3b)) and z has no influence on the feasible set of the problem, i.e., at each iteration, solving the two subproblems provides feasible points for Problem (3).

We apply the OADM outlined in Algorithm 1 to determine a feasible point of Problem (3), which improves on an initial one (x^0, z_1^0, z_2^0) in terms of the objective function value. The initial point (x^0, z_1^0, z_2^0) is defined by

$$x^0 \in \arg\min_x \left\{ \alpha \sum_{t \in \mathcal{T}} \mathbb{E}[c_t^\top x] \colon x \in X \right\},$$
$$z^0 = (z_1^0, z_2^0) \in \left\{ z = (z_t)_{t \in \mathcal{T}} \colon z_t = (z_{1,t}, z_{2,t}) \in Z_t(x^0) \right\}.$$

Specifically, x^0 is chosen among the solutions of the problem obtained by Problem (3) after removing the constraints and the objective function term involving the variable vector z. Clearly, (x^0, z^0) is a feasible point of Problem (3).

Now, we describe the iterative procedure outlined in Algorithm 1. In what follows, we write

$$v(x, z) := \alpha \sum_{t \in \mathcal{T}} \mathbb{E}[c_t^\top x] + (1 - \alpha) \sum_{t \in \mathcal{T}} g(z_t)$$

to lighten the notation. In Line 1, we set the iteration counter j to zero. In iteration $j+1$, the algorithm first solves Problem (3) in the direction of (x, z_2) while having fixed the value of z_1 to z_1^j to determine a new value (x^{j+1}, z_2^{j+1}) for (x, z_2); see Line 3. Then, Problem (3) is solved in the direction of (z_1, z_2) while having fixed the value of x to x^{j+1} to determine a new value (z_1^{j+1}, z_2^{j+1}) for (z_1, z_2). Finally, the algorithm stops (Line 7) once a given stopping criterion is met such as that a time limit is reached or that the improvement of the value of the feasible points is less than a given threshold.

Algorithm 1: An Overlapping Alternating Direction Method

Input : An initial feasible point $(x^0, z^0 = (z_1^0, z_2^0))$ of Problem (3).
Output : A feasible point $(x^j, z^j = (z_1^j, z_2^j))$ of Problem (3).

1 Set $j \leftarrow 0$.
2 **while** *stopping criterion is not satisfied* **do**
3 Compute $(x^{j+1}, z_2^{j+1}) \in \arg\min_{x, z_2} \{v(x, z_1^j, z_{2,t}) \colon x \in X, (z_{1,t}^j, z_2) \in Z_t(x), t \in \mathcal{T}\}$.
4 Compute $z^{j+1} = (z_1^{j+1}, z_2^{j+1}) \in \arg\min_{z=(z_1,z_2)} \{v(x^{j+1}, z) \colon z_t \in Z_t(x^{j+1}), t \in \mathcal{T}\}$.
5 Increment $j \leftarrow j + 1$.
6 **end**
7 **return** (x^j, z^j)

4.1. **Application to the Maintenance Planning Problem.** In this section, we discuss how Algorithm 1 is applied to the MPP. Specifically, we apply our OADM to the variant of Problem (4) that makes use of Constraints (5). This problem is defined on four vectors of variables: $x = (x_t)_{t\in\mathcal{T}}$ with $x_t = (x_t^i)_{i\in\mathcal{I}}$, $y = (y_t)_{t\in\mathcal{T}}$ with $y_t = (y_t^s)_{s\in\mathcal{S}_t}$, $q = (q_t)_{t\in\mathcal{T}}$, and $\varepsilon = (\varepsilon_t)_{t\in\mathcal{T}}$. In the OADM for the MPP, variable vectors x and y play the role of x and z_1 and variable vectors q and ε play the role of the overlapping variables z_2 in Algorithm 1. Hence, Problem (4) is solved in the direction of x and y and, in both directions, q and ε are also part of the optimization. Here, we consider the variable vector ε as part of z. This leads to a re-definition of the sets $Z_t(x)$, $t \in \mathcal{T}$, where Constraints (4e) and (4f) are included.

An initial point $(x^0, y^0, q^0, \varepsilon^0)$ of Problem (4) is retrieved as for the general case. First, we select a planning x^0 for the interventions among the feasible solutions of the problem obtained by Problem (4) without taking into account the quantile related variables, constraints, and the objective function term, i.e.,

$$x^0 \in \arg\min_x \left\{ \alpha \frac{1}{T} \sum_{t\in\mathcal{T}} \frac{1}{|\mathcal{S}_t|} \sum_{s\in\mathcal{S}_t} \sum_{i\in\mathcal{I}} \sum_{t'\in\mathcal{T}(i,t)} \sigma_{t',t}^{i,s} x_{t'}^i \colon (4b), (4c), (4d), (4g) \right\}.$$

Then, we determine values y^0, q^0, and ε^0 for variable vectors y, q, and ε as when solving the problem in the direction of y. We do so as follows.

In iteration $j+1$, the subproblem in the x-direction corresponds to finding a maintenance planning for the interventions of $\mathcal{I}$ in the time horizon $\mathcal{T}$ while having fixed the scenarios used to calculate the quantile at each time instant. Hence, the values x^{j+1} for x are selected among the feasible points of Problem (4) with the values of variables in vector y fixed to y^j. We observe that this subproblem is NP-hard. Indeed, it can be reduced to the resource constrained scheduling problem; see, e.g., [10]. Differently, solving the subproblem in the direction of y corresponds to computing the value of the objective function (4a) having fixed a planning for

the interventions x^{j+1}. This can be done in a polynomial time. Specifically, given a time instant $t \in \mathcal{T}$, we first need to compute risk values σ_t^s related to each scenario $s \in \mathcal{S}_t$ as

$$\sigma_t^s = \sum_{i \in \mathcal{I}} \sum_{t' \in \mathcal{T}(i,t)} \sigma_{t',t}^{i,s} (x^{j+1})_{t'}^i.$$

Then, we sort the scenarios in $\mathcal{S}_t$ by non-decreasing values of σ_t^s. The first p_t scenarios appearing in this order are those for which we set $(y^{j+1})_t^s = 1$. For the others, we set $(y^{j+1})_t^s = 0$. This procedure is repeated for each time period $t \in \mathcal{T}$.

4.2. **Application to the Portfolio Optimization Problem.** The OADM for the portfolio optimization problem is applied to the MILP (8), which makes use of variable vectors $x \in X$, $y = (y^s)_{s \in \mathcal{S}}$, and a variable q. It sequentially solves a subproblem in the x-direction and one in the y-direction. The variable q is part of both optimization tasks. Solving the subproblem in the x-directions corresponds to maximizing the portfolio revenue, having fixed the scenario selection. This problem is modeled as a linear program (see the MILP (8)) and can thus be efficiently solved. Solving the subproblem in the y-direction corresponds to computing the value of the objective function (8a) knowing the portfolio composition. This can be done in polynomial time.

The initial point computation and the iterative procedure are analogous to the one discussed for the MPP. Hence, we do not report the details here.

5. An Adaptive Scenario Clustering Approach

This section presents an adaptive scenario clustering algorithm (ASCA) for solving Problem (1) in the case function f is nondecreasing. Given $t \in \mathcal{T}$, let us first denote with $\bar{c}_t$ the average cost at t, i.e.,

$$\bar{c}_t = \frac{1}{|\mathcal{S}_t|} \sum_{s \in \mathcal{S}_t} c_t^s,$$

which allows to rewrite the objective function (1a) as

$$\min \quad \alpha \sum_{t \in \mathcal{T}} \bar{c}_t x + (1-\alpha) \sum_{t \in \mathcal{T}} f\left(\mathbb{Q}[c_t^\top x]\right). \tag{25}$$

Observe that the scenarios only have an impact on the quantile computations, i.e., on the second term in (25). Thus, a large number of scenarios can make the resolution of the problem computationally hard. Therefore, a way to approximate the general problem is to reduce the size of each $\mathcal{S}_t$ by clustering its scenarios. This allows to heuristically find feasible solutions of good quality quickly.

More precisely, let $\mathcal{C}_t$ be a partition of $\mathcal{S}_t$ into $K_t \leq |\mathcal{S}_t|$ nonempty clusters. Each cluster $\gamma \in \mathcal{C}_t$ has a cost vector c_t^γ and a probability p_t^γ. The ASCA consists in solving a sequence of instances of Problem (1)—each defined over a clustered scenario set $\mathcal{C}_t$ instead of the original set $\mathcal{S}_t$. The probability p_t^γ of cluster $\gamma \in \mathcal{C}_t$ is given by

$$p_t^\gamma = \sum_{s \in \gamma} p_t^s,$$

which satisfies

$$\sum_{\gamma \in \mathcal{C}_t} p_t^\gamma = 1. \tag{26}$$

We now present two strategies to associate a cost vector to each cluster of scenarios. First, the average scenario clustering (ASC) associates with each cluster

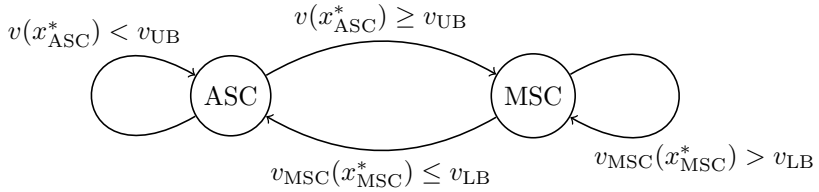

FIGURE 1. State diagram of the adaptive scenario clustering algorithm.

$\gamma \in \mathcal{C}_t$ a cost vector c_t^γ defined as follows:

$$(c_t^\gamma)_i = \frac{1}{|\gamma|} \sum_{s \in \gamma} (c_t^s)_i, \quad i \in N.$$

Let us indicate with $\mathcal{C}_t^{\text{ASC}}$ the corresponding clustering of scenarios.

Further, the minimum scenario clustering (MSC) associates with each cluster $\gamma \in \mathcal{C}_t$ a cost vector c_t^γ defined as

$$(c_t^\gamma)_i = \min \left\{ (c_t^s)_i \colon s \in \gamma \right\}, \quad i \in N.$$

Let us indicate with $\mathcal{C}_t^{\text{MSC}}$ the corresponding clustering of scenarios.

Proposition 7. *Let x^* be an optimal solution of Problem (1) and let x^*_{ASC} as well as x^*_{MSC} denote optimal solutions of Problem (1) solved on the scenarios set $\mathcal{C}_t^{ASC}$ and $\mathcal{C}_t^{MSC}$, respectively. For a vector $x \in X$, let $v(x)$ and $v_{MSC}(x)$ denote the objective value w.r.t. x and (1a) defined over $\mathcal{S}_t$ and $\mathcal{C}_t^{MSC}$, respectively. Then,*

$$v_{MSC}(x^*_{MSC}) \leq v(x^*) \leq \min\{v(x^*_{ASC}), v(x^*_{MSC})\}$$

holds.

Proof. We get the first inequality by construction of the MSC, hence $v_{\text{MSC}}(x^*_{\text{MSC}}) \leq v_{\text{MSC}}(x^*) \leq v(x^*)$. The second inequality is due to x^* being optimal for Problem (1). □

Thus, both ASC and MSC allow to compute a bound on $v(x^*)$ while solving Problem (1) over clustered scenario sets.

Corollary 1. *Let x^* be an optimal solution of Problem (1) and let x^*_{ASC} as well as x^*_{MSC} denote optimal solutions of Problem (1) solved for the scenarios set $\mathcal{C}_t^{ASC}$ and $\mathcal{C}_t^{MSC}$, respectively. For a vector $x \in X$, let $v(x)$ and $v_{MSC}(x)$ denote the objective value w.r.t. x and (1a) defined over $\mathcal{S}_t$ and $\mathcal{C}_t^{MSC}$, respectively. Then, if*

$$v_{MSC}(x^*_{MSC}) = \min\{v(x^*_{ASC}), v(x^*_{MSC})\}$$

holds, x^*_{ASC} or x^*_{MSC} is an optimal solution of Problem (1).

Additionally, solving Problem (1) with the MSC can be improved using the valid inequality (14).

Proposition 8. *Given $\mathcal{C}_t^{MSC}$ for a specific $t \in \mathcal{T}$. Let γ be a cluster in $\mathcal{C}_t^{MSC}$ such that $p_t^\gamma > 1 - \tau$ holds. Then, in Problem (2) defining the quantile of t, it holds that*

$$y_t^\gamma = 1,$$

and the resulting inequality (2b) is dominated by the valid inequality (14) for $\bar{\mathcal{S}} = \mathcal{S}_t \setminus \gamma$.

Algorithm 2: Adaptive Scenario Clustering Algorithm.

Input : Threshold parameter $\varepsilon \in (0,1)$.

Set $\mathcal{C}_t^0 \leftarrow \{\mathcal{S}_t\}$ for all $t \in \mathcal{T}$, i.e., we start with a single cluster per index t.
Set $j \leftarrow 0$, $v_{\text{UB}} \leftarrow +\infty$, $v_{\text{LB}} \leftarrow -\infty$, and $\kappa \leftarrow$ true.
while $(v_{UB} - v_{LB})/v_{UB} \geq \varepsilon$ **do**
  if κ **then**
    Solve Problem (1) on $\mathcal{C}_t^{\text{ASC},j}$, let x^*_{ASC} denote the optimal solution.
    if $v(x^*_{ASC}) < v_{UB}$ **then**
      set $x_{\text{UB}} \leftarrow x^*_{\text{ASC}}$ and $v_{\text{UB}} \leftarrow v(x^*_{\text{ASC}})$
    else
      set $\kappa \leftarrow$ false.
    end
  else
    Solve Problem (1) on $\mathcal{C}_t^{\text{MSC}^+,j}$, let $x^*_{\text{MSC}^+}$ denote the optimal solution.
    if $v_{MSC^+}(x^*_{MSC^+}) > v_{LB}$ **then**
      set $x_{\text{LB}} \leftarrow x^*_{\text{MSC}^+}$ and $v_{\text{LB}} \leftarrow v_{\text{MSC}^+}(x^*_{\text{MSC}^+})$
    else
      set $\kappa \leftarrow$ true.
    end
    if $v(x^*_{MSC^+}) < v_{UB}$ **then**
      set $x_{\text{UB}} \leftarrow x^*_{\text{MSC}^+}$ and $v_{\text{UB}} \leftarrow v(x^*_{\text{MSC}^+})$.
    end
  end
  Update $j \leftarrow j+1$ and refine $\mathcal{C}_t^{j-1}$, yielding $\mathcal{C}_t^j$.
end
return x_{UB}

Proof. Since $p_t^\gamma > 1-\tau$, (2c) and (2d) imply $y_t^\gamma = 1$. Furthermore, the definition of $b_i(\bar{\mathcal{S}}_t)$ with $\bar{\mathcal{S}} = \mathcal{S}_t \setminus \gamma$ implies

$$\frac{b_i(\mathcal{S}_t \setminus \gamma)}{\tau - p(\mathcal{S}_t \setminus \gamma)} \geq (c_t^\gamma)_i, \quad i \in N, \tag{27}$$

so that (14) dominates (2b). □

Proposition 8 hence tells us that given the set

$$\mathcal{B} := \{\gamma \in \mathcal{C}_t^{\text{MSC}} : p_t^\gamma > 1-\tau\},$$

we can replace the quantile constraint (2b) associated to $\gamma \in \mathcal{B}$ by the valid inequality (14) applied on the set $\mathcal{S}_t \setminus \gamma$ in the MSC. Furthermore, Constraint (2c) reduces to

$$\sum_{\gamma \in \mathcal{C}_t^{\text{MSC}}} y_t^\gamma p_t^\gamma \geq \tau - \sum_{\gamma \in \mathcal{B}} p_t^\gamma.$$

We denote by MSC^+ the resulting optimization problem. By construction, we thus have that

$$v_{\text{MSC}}(x^*_{\text{MSC}}) \leq v_{\text{MSC}^+}(x^*_{\text{MSC}^+}) \leq v(x^*)$$

holds.

For what follows, we define v_{UB} and v_{LB} as the current best upper and lower bounds on $v(x^*)$. Additionally, $\mathcal{C}_t^j$ stands for the clustering of $\mathcal{S}_t$ for $t \in \mathcal{T}$ in iteration j of the algorithm. We indicate with $\mathcal{C}_t^{\text{ASC},j}$ and $\mathcal{C}_t^{\text{MSC}^+,j}$ the instance of $\mathcal{C}_t^j$ where the cost vectors are calculated using ASC and MSC^+, respectively.

Algorithm 2 states the pseudo-code of our adaptive algorithm and Figure 1 shows a state diagram of the inner while loop of the algorithm. The algorithm solves a sequence of problems of Type (1) defined over $\mathcal{C}_t^{\text{ASC}}$ and $\mathcal{C}_t^{\text{MSC}^+}$ to improve the lower or upper bound on $v(x^*)$ as shown in Proposition 7. After each resolution, the algorithm refines the previous clustering $\mathcal{C}_t^{j-1}$, yielding $\mathcal{C}_t^j$ for all $t \in \mathcal{T}$. The resulting clustering $\mathcal{C}_t^j$ allows to have a better representation of the scenario set $\mathcal{S}_t$. This makes the next resolution of Problem (1) defined over $\mathcal{C}_t^{\text{ASC}}$ or $\mathcal{C}_t^{\text{MSC}^+}$ harder to solve. However, the new clustering of scenarios will likely allow to compute a better lower or upper bound on $v(x^*)$. The sequence of resolutions over $\mathcal{C}_t^{\text{ASC}}$ is then interrupted and switched to the resolution over $\mathcal{C}_t^{\text{MSC}^+}$ when $v(x^*_{\text{ASC}}) \geq v_{\text{UB}}$. Similarly, the sequence of resolution of Problem (1) over $\mathcal{C}_t^{\text{MSC}^+}$ is interrupted and switched to $\mathcal{C}_t^{\text{ASC}}$ when $v_{\text{MSC}^+}(x^*_{\text{MSC}^+}) \leq v_{\text{LB}}$. Finally, the algorithm terminates once we achieve a relative gap smaller than a prescribed tolerance ε, i.e.,

$$\frac{v_{\text{UB}} - v_{\text{LB}}}{v_{\text{UB}}} \leq \varepsilon.$$

Theorem 1. *Let x^* be an optimal solution of Problem (1) and let $v(x^*)$ be its value. Moreover, let $\mathcal{C}_t^j$ be the clustering of $\mathcal{S}_t$ for index $t \in \mathcal{T}$ in iteration j. Suppose further that there exists an index $t \in \mathcal{T}$ such that*

$$|\mathcal{C}_t^j| > |\mathcal{C}_t^{j-1}|, \tag{28}$$

for all iterations j. Then, Algorithm 2 terminates after a finite number of cluster refinements with a point $x \in X$ such that

$$\frac{v(x) - v(x^*)}{v(x)} \leq \varepsilon. \tag{29}$$

Proof. Due to Inequality (28), each iteration of Algorithm 2 increases the size of $\mathcal{C}_t^j$ for at least one $t \in \mathcal{T}$. Therefore, if the termination criterion $(v_{\text{UB}} - v_{\text{LB}})/v_{\text{UB}} \leq \varepsilon$ is never satisfied, $\mathcal{C}_t^j$ will increase in size over the iterations until being equal to $\mathcal{S}_t$. If $\mathcal{C}_t^j$ equals $\mathcal{S}_t$ for all $t \in \mathcal{T}$, then $|\gamma| = 1$ for all $\gamma \in \mathcal{C}_t^j$.

The cost vectors c_t^γ for each $\gamma \in \mathcal{C}_t^j$ correspond to the cost vector associated with the single scenario in γ for both ASC and MSC clustering strategies. Otherwise, if $(v_{\text{UB}} - v_{\text{LB}})/v_{\text{UB}} \leq \varepsilon$ is satisfied, we know that x_{ASC} also satisfies Inequality (29) by Proposition 7. □

Remark 1. *We close this section with the discussion of two features of the ASCA.*

- *The cluster refinement step in Line 21 of Algorithm 2 is done using kernel density estimation (KDE). KDE allows to estimate the probability density function of a random variable by using a set of samples of this random variable [24]. The local minima of the estimated probability density function then yield a splitting of the random variable samples. In our case, for a given $t \in \mathcal{T}$ and $\gamma \in \mathcal{C}_t$ as well as a point $x \in X$, we compute the KDE of $(c_t^s)^\top x$ using all $s \in \gamma$, which results in a splitting of γ. We use x^*_{ASC} or x^*_{MSC} depending on whether the previous iteration $j-1$ of the ASCA used $\mathcal{C}_t^{ASC,j-1}$ or $\mathcal{C}_t^{MSC,j-1}$. Additionally, only a subset of time steps $\overline{\mathcal{T}} \subseteq \mathcal{T}$ is selected for re-clustering after each iteration of the ASCA. Given a parameter $\Theta \in (0,1)$, we compute this refinement set $\overline{\mathcal{T}}$ to be the minimal subset of $\mathcal{T}$ satisfying*

$$\sum_{t \in \overline{\mathcal{T}}} \left| \mathbb{Q}[c_t^\top x; \mathcal{C}_t^{j-1}] - \mathbb{Q}[c_t^\top x] \right| > \Theta \sum_{t \in \mathcal{T}} \left| \mathbb{Q}[c_t^\top x; \mathcal{C}_t^{j-1}] - \mathbb{Q}[c_t^\top x] \right|.$$

Here, $\mathbb{Q}[\cdot]$ is the original quantile, whereas $\mathbb{Q}[\cdot; \mathcal{C}_t^{j-1}]$ denotes the quantile's approximation based on the clustering $\mathcal{C}_t^{j-1}$. Hence, we select the subset of

indices $t \in \mathcal{T}$ that have the biggest difference between their clustered and their real quantile value for a chosen x.

- *The solution processes in Lines 5 and 12 of Algorithm 2 can benefit from a series of improvements. First, every valid inequality from MSC$^+$ obtained through Proposition 8 is kept in the subsequent MSC$^+$ and ASC problems even if the associated cluster is split in the refinement step. Second, the OADM discussed in Section 4 is applied first, as a heuristic, for every MILP. Here, we use x_{LB} and x_{UB} (see Algorithm 2) as initial iterates for the OADM provided that we are in the corresponding clustered problem. Third, we use the valid inequalities in (14) to speed up the MILP solution process.*

6. Numerical Results

In this section, we present and discuss the results obtained by testing our methods on the maintenance planning and on the portfolio optimization problem.

In what follows, we make use of the following notation. When assessing the performance of our MILP models, we consider the following three configurations. We write MILP meaning that we solve Model (4) when considering the MPP and Model (8) when considering the POP, both without valid inequalities. We write MILP_{VI} and $\text{MILP}_{\text{VI}^*}$ meaning that we solve Model (4) enriched with Inequalities (17) and Inequalities (18), when considering the MPP. In the case of the POP, MILP_{VI} and $\text{MILP}_{\text{VI}^*}$ stand for Model (8) enriched with Inequalities (23) and (24), respectively. Furthermore, we add the superscript OADM to the notation yet introduced, when the corresponding configuration is warm-started with an initial solution found by OADM as described in Section 4. For example, in the case of the MPP, $\text{MILP}_{\text{VI}^*}^{\text{OADM}}$ means that Model (4) enriched with Inequalities (18) is warm-started with an initial solution found by the OADM. Let $\mathcal{M}$ denote the set of considered methods. For $m \in \mathcal{M}$ we denote by v_{LB}^m and v_{UB}^m the best lower and upper bound values found by method m on a given problem instance. For the sake of simplicity, we will additionaly use v_{LB} and v_{UB} when discussing the upper or lower bound without referring to a specific method.

In the following, we make some further comments regarding the tests we will discuss in Sections 6.1 and 6.2. In configurations MILP_{VI} and $\text{MILP}_{\text{VI}^*}$, we separate valid inequalities only at the root node of the branch-and-bound tree, as preliminary results showed that this is the best strategy. Indeed, separating them at each node of the tree significantly reduces the time left to explore the tree itself, leading to poor primal bounds—in particular in the case of the MPP. Moreover, the valid inequalities considered in $\text{MILP}_{\text{VI}^*}$ dominate the ones considered in MILP_{VI}; see Proposition 4. In the case of the MPP, this is reflected in the results obtained by performing some preliminary tests. Hence, in Section 6.1 we only discuss the results obtained by $\text{MILP}_{\text{VI}^*}$. This behavior does not occur when considering the POP. Thus, in Section 6.2, we discuss the results of both configurations. Finally, we remark that the solver does not struggle to provide feasible solutions of good quality on the POP instances when solving MILP, MILP_{VI} or $\text{MILP}_{\text{VI}^*}$; see Section 6.2. Consequently, we do not consider the inclusion of OADM and ASCA in the solution procedure for this problem.

All computations have been executed on a remote server with 64 GB RAM and an AMD Opteron 6176 SE processor with 12 cores and 2.30 GHz. The techniques presented in this paper have been coded in C++14 and are compiled using g++ version 9.3.0. All MILP models are solved using Gurobi 9.1.0. The time limit is set to 90 min for which the time for reading the instance is ignored.

6.1. Numerical Results for the Maintenance Planning Problem.

We first present the numerical results of the proposed methods when applied to the

EURO/ROADEF 2020 challenge instances. Table 1 shows the main characteristics of the these instances. Their names start with a capital letter that, based on their alphabetical order, correspond to a different phases of the EURO/ROADEF 2020 challenge. Hence, instances with a name starting with a letter appearing later in the alphabet are more likely to be computationally challenging. Note that we omit to list those instances that are trivial due to a very small number of scenarios.

The size of some instances makes the time to complete multiple OADM iterations too large w.r.t. the total computational time allowed. Thus, we set the stopping criterion of the OADM so that only the first iteration is applied. Finally, the ASCA computational parameters are given in Table 2 and have been chosen based on our preliminary numerical tests.

Because of the large amount of EURO/ROADEF instances we use the bar plots in Figures 2–5 to visually compare the different methods. Let $\mathcal{M}'$ be the subset of methods of $\mathcal{M}$ considered in the bar plot. Then, for all $m \in \mathcal{M}'$ the bar plots show the re-scaled value of v^m_{LB} (left side) and v^m_{UB} (right side) on all instances. The bars' lengths are determined as follows. The left side of the bar plots is equal to $\min_{m' \in \mathcal{M}'}\{v^{m'}_{\mathrm{LB}} \colon v^{m'}_{\mathrm{LB}} > 0\}/v^m_{\mathrm{LB}}$. The numerator $\min_{m' \in \mathcal{M}'}\{v^{m'}_{\mathrm{LB}} \colon v^{m'}_{\mathrm{LB}} > 0\}$ takes the value of the smallest lower bound obtained by the methods in $\mathcal{M}'$ while ignoring a lower bound if the method m' does not improve on $v^{m'}_{\mathrm{LB}} = 0$. We apply a similar rule for the right side of the bar plots using $v^m_{\mathrm{UB}} / \max_{m' \in \mathcal{M}'}\{v^{m'}_{\mathrm{UB}} \colon v^{m'}_{\mathrm{UB}} < \infty\}$. Here, $\max_{m' \in \mathcal{M}'}\{v^m_{\mathrm{UB}} \colon v^{m'}_{\mathrm{UB}} < \infty\}$ takes the value of the largest upper bound obtained by the two compared methods without considering $v^{m'}_{\mathrm{UB}}$ if no incumbent is found during the solution process of m'. The rescaling of v_{LB} or v_{UB} is constant for a specific instance and therefore allows to easily visualize how they compare for two different methods.

Hence, bars close to zero mean that the corresponding method performs better compared to the other method on the respective bound. However, we would like to draw attention to the fact that the spacing between the sides of the bars is not representative of the relative gap given by $(v_{\mathrm{UB}} - v_{\mathrm{LB}})/v_{\mathrm{LB}}$.

Figure 2 shows a comparison between the results obtained by MILP with those obtained by $\mathrm{MILP}_{\mathrm{VI}^*}$. We observe that $\mathrm{MILP}_{\mathrm{VI}^*}$ systematically outperforms MILP, yielding a great improvement on both v_{LB} and v_{UB}, where the lower bound improves more significantly than the upper bound. However, we remark that $\mathrm{MILP}_{\mathrm{VI}^*}$ fails to provide an incumbent solution for some instances within the time limit for which MILP succeeds in doing so; see, e.g., B03. Most likely, this has two reasons. First, additional time is needed to separate violated inequalities in the first node of the branch and bound tree. Second, the model's relaxations are a bit harder to solve after adding valid inequalities due their increased size.

To counteract this effect, we also tested to apply the OADM described in Section 4 to the MILP model with valid inequalities for the MPP as a primal root node heuristic. Figure 3 shows the comparison of $\mathrm{MILP}_{\mathrm{VI}^*}$ and $\mathrm{MILP}^{\mathrm{OADM}}_{\mathrm{VI}^*}$. In the latter configuration, the point to warm-start is the result of a single iteration of the OADM. The resulting bar plot only displays the instances with a significant difference in v_{LB} or v_{UB}. Note that the one iteration of the OADM allows to obtain an incumbent solutions for all the instances where the resolution of $\mathrm{MILP}_{\mathrm{VI}^*}$ fails to do so. For the remaining instances, we see that activating a single OADM step mostly performs worse in terms of v_{UB}. Also, for instance X05 and C13, the time spent in one OADM iteration is rather long—hence harming the impact of the valid inequalities on v_{LB}.

Figure 4 shows the results obtained by the ASCA presented in Section 5 when compared to the results obtained by MILP. One can observe that ASCA provides better results in terms of both v_{LB} and v_{UB}. However, it fails to get a strictly positive

TABLE 1. Characteristics of all the EURO/ROADEF 2020 challenge instances.

ID	$\lvert\mathcal{I}\rvert$	$\lvert\mathcal{R}\rvert$	$\lvert\mathcal{T}\rvert$	$\sum_{t\in\mathcal{T}} \frac{\lvert\mathcal{S}_t\rvert}{\lvert\mathcal{T}\rvert}$	$\lvert\mathcal{D}\rvert$
A02	89	9	90	120.0	1869
A05	180	9	182	120.0	6791
A08	18	9	17	645.59	29
A11	54	9	53	639.53	96
A14	108	10	53	160.3	438
A15	108	10	53	320.06	438
B01	100	9	53	191.45	553
B02	100	9	53	191.45	404
B03	706	9	53	63.49	23674
B04	706	9	53	63.49	23674
B05	706	9	53	63.49	27276
B06	100	9	53	255.42	404
B07	250	9	53	191.45	3787
B08	119	9	42	254.07	550
B09	120	9	42	127.4	730
B10	398	9	25	192.4	3231
B11	100	9	53	191.45	679
B12	495	9	102	63.91	20205
B13	99	9	102	159.51	148
B14	297	9	191	95.5	14448
B15	495	9	250	63.38	61786
C01	120	9	53	191.45	1080
C02	120	9	53	191.45	828
C03	706	9	53	63.49	24260
C04	706	9	53	63.49	23638
C05	706	9	53	63.49	27276
C06	280	9	53	191.45	3404
C07	120	9	42	126.76	578
C08	426	9	25	192.88	3405
C09	110	9	53	191.45	718
C10	522	9	102	63.24	26250
C11	89	9	102	191.05	1474
C12	298	9	191	95.21	13996
C13	505	9	230	63.4	44384
C14	465	9	220	95.34	53628
C15	528	9	300	50.69	69715
X01	120	9	53	191.45	917
X02	706	9	53	63.49	24464
X03	280	9	53	191.45	3299
X04	426	9	25	188.84	4509
X05	467	9	220	95.3	48595
X06	528	9	300	50.64	79180
X07	209	9	300	63.52	8873
X08	209	9	300	63.6	6032
X09	548	9	30	156.97	8942
X10	460	9	35	159.54	7083
X11	521	9	131	63.35	35112
X12	522	9	131	63.92	35241
X13	336	9	212	95.27	19978
X14	613	9	180	63.73	57762
X15	613	9	180	63.32	64400

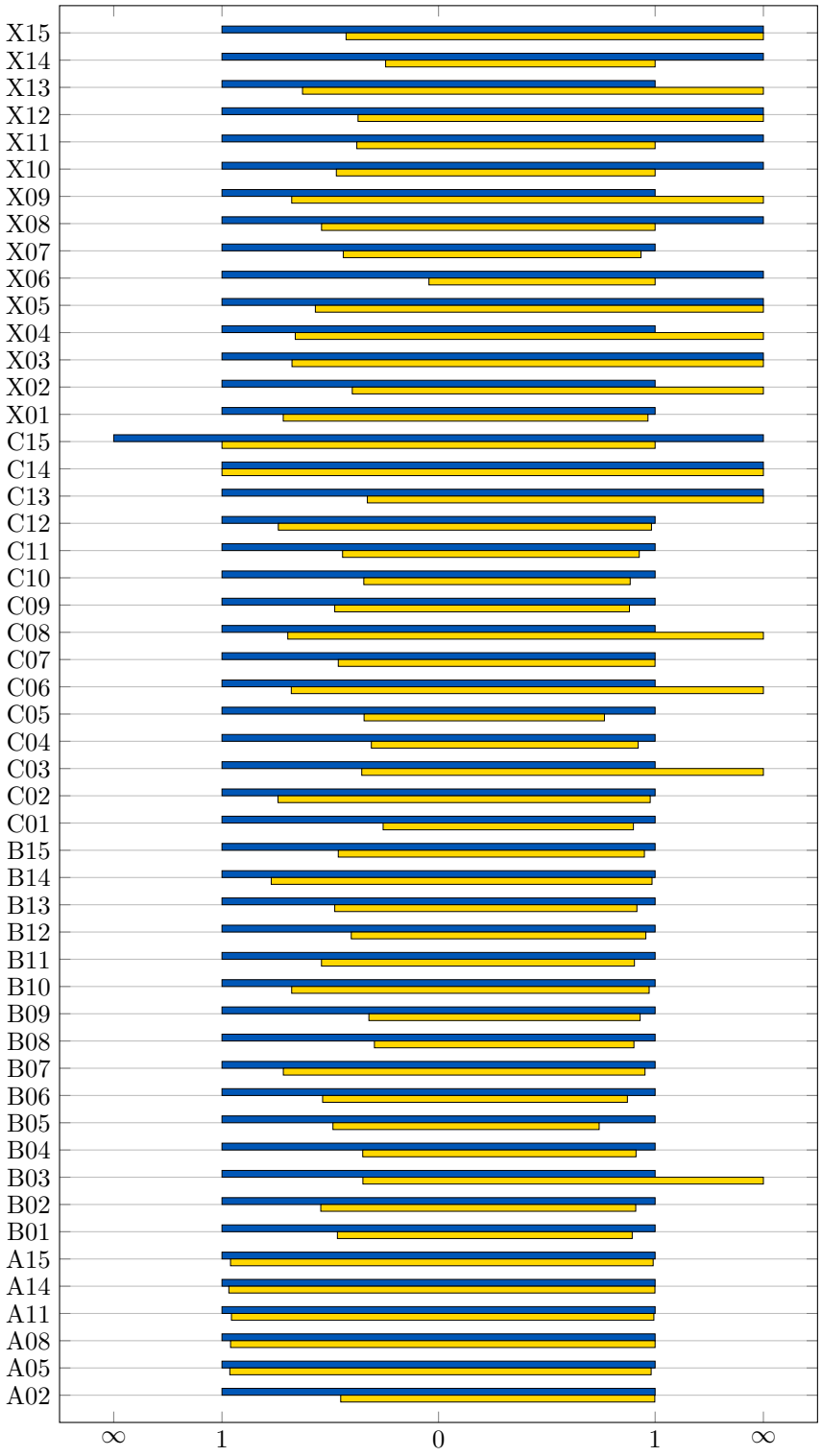

FIGURE 2. Bar plot for $\min_{m' \in \mathcal{M}'}\{v_{\mathrm{LB}}^{m'} \colon v_{\mathrm{LB}}^{m'} > 0\}/v_{\mathrm{LB}}^{m}$ (left side) and $v_{\mathrm{UB}}^{m}/\max_{m' \in \mathcal{M}'}\{v_{\mathrm{UB}}^{m'} \colon v_{\mathrm{UB}}^{m'} < \infty\}$ (right side), where $\mathcal{M}'$ is composed of MILP (blue) and $\mathrm{MILP}_{\mathrm{VI}^*}$ (yellow).

TABLE 2. OADM parameters.

Θ	OADM gap (Line 3)	OADM gap (Line 4)	Solver gap (Lines 5,12)
0.25	0.0025	0	0.025

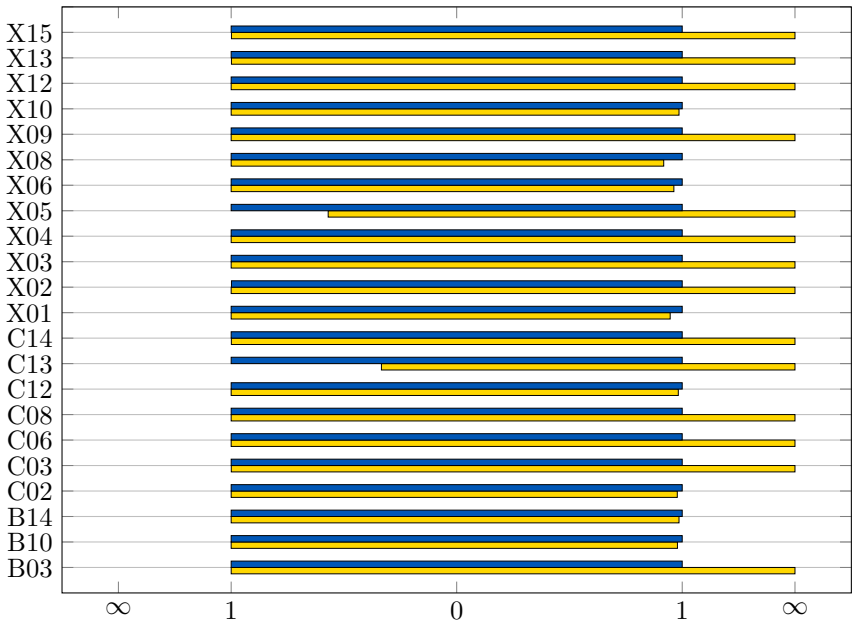

FIGURE 3. Bar plot for $\min_{m' \in \mathcal{M}'}\{v_{\mathrm{LB}}^{m'} \colon v_{\mathrm{LB}}^{m'} > 0\}/v_{\mathrm{LB}}^{m}$ (left side) and $v_{\mathrm{UB}}^{m}/\max_{m' \in \mathcal{M}'}\{v_{\mathrm{UB}}^{m'} \colon v_{\mathrm{UB}}^{m'} < \infty\}$ (right side), where $\mathcal{M}'$ is composed of $\mathrm{MILP}_{\mathrm{VI}^*}^{\mathrm{OADM}}$ (blue) and $\mathrm{MILP}_{\mathrm{VI}^*}$ (yellow). Only the instances with a significant difference in the results for v_{LB} and v_{UB} are displayed.

value for v_{LB} for some of the more computationally challenging instances. As it is is the case for $\mathrm{MILP}_{\mathrm{VI}^*}$, both for v_{LB} and v_{UB} we see that ASCA outperforms MILP. For those instances for which ASCA fails to obtain a strictly positive value for v_{LB}, ASCA keeps improving v_{UB} using the ASC problem during the initial iterations of the algorithm. Since v_{UB} keeps decreasing in every iteration, ASCA never enters the MSC^+ problem before reaching the given time limit. Thus, it never improves on the $v_{\mathrm{LB}} = 0$ lower bound. Similarly, MILP fails to compute incumbent solutions for some of the more computationally challenging instances and, hence, does not decrease the $v_{\mathrm{UB}} = \infty$ bound. On the contrary, ASCA always finds an improved incumbent solution since it is designed to start solving the ASC problem in order to decrease the value of v_{UB}.

We close the comparison of the methods with Figure 5, which compares ASCA and $\mathrm{MILP}_{\mathrm{VI}^*}^{\mathrm{OADM}}$, i.e., it compares the methods that perform best in terms of v_{UB} and v_{LB}. Considering the values of v_{LB}, we see that $\mathrm{MILP}_{\mathrm{VI}^*}^{\mathrm{OADM}}$ always outperforms ASCA except for the instances C14 and X05. The opposite situation occurs when the two configurations are compared w.r.t. the values of v_{UB}. The detailed results obtained on the EURO/ROADEF instances with our methods are reported in Tables 5 and 6.

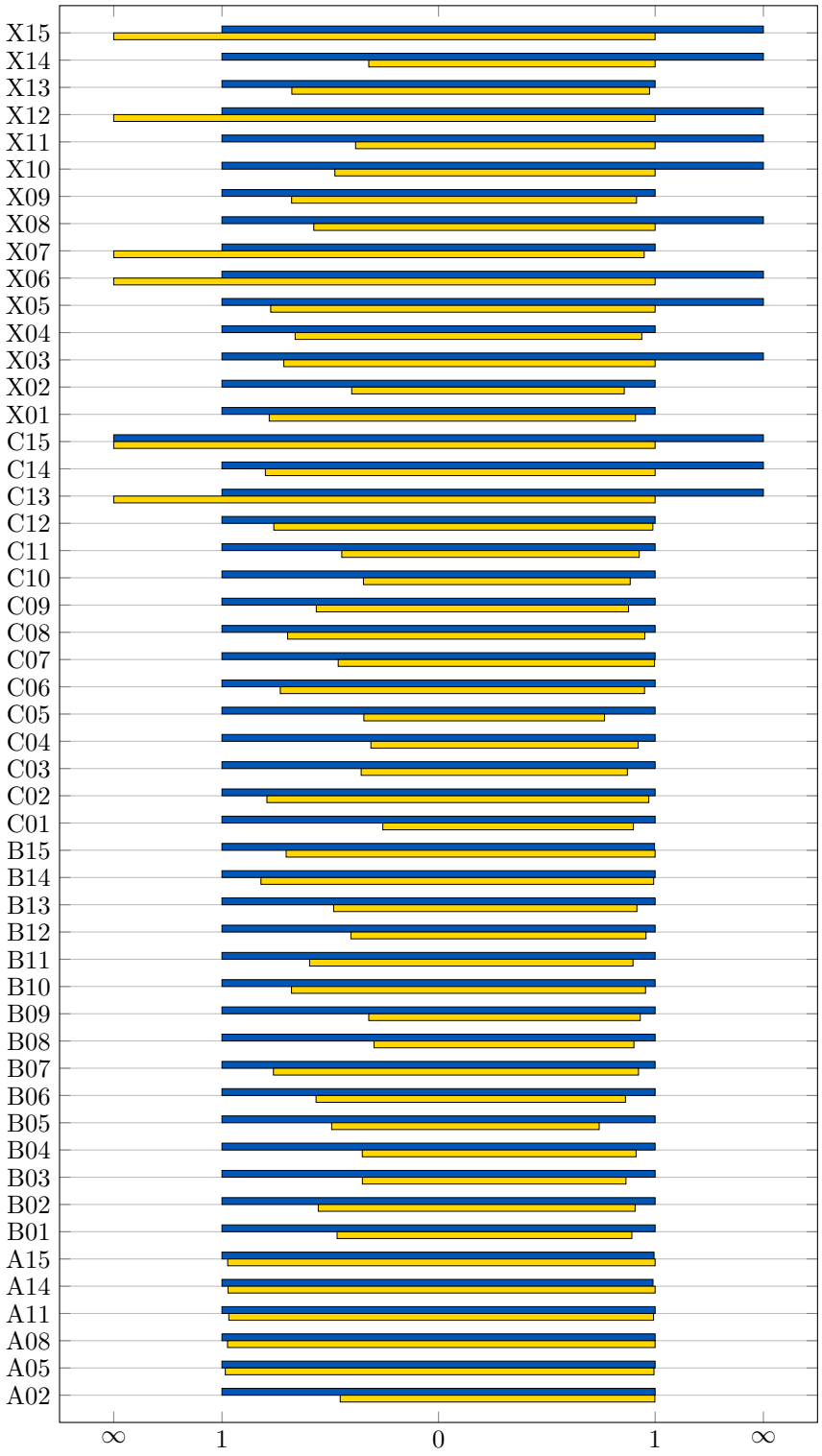

FIGURE 4. Bar plot for $\min_{m' \in \mathcal{M}'}\{v_{\mathrm{LB}}^{m'} \colon v_{\mathrm{LB}}^{m'} > 0\}/v_{\mathrm{LB}}^{m}$ (left side) and $v_{\mathrm{UB}}^{m}/\max_{m' \in \mathcal{M}'}\{v_{\mathrm{UB}}^{m'} \colon v_{\mathrm{UB}}^{m'} < \infty\}$ (right side), where $\mathcal{M}'$ is composed of MILP (blue) and ASCA (yellow).

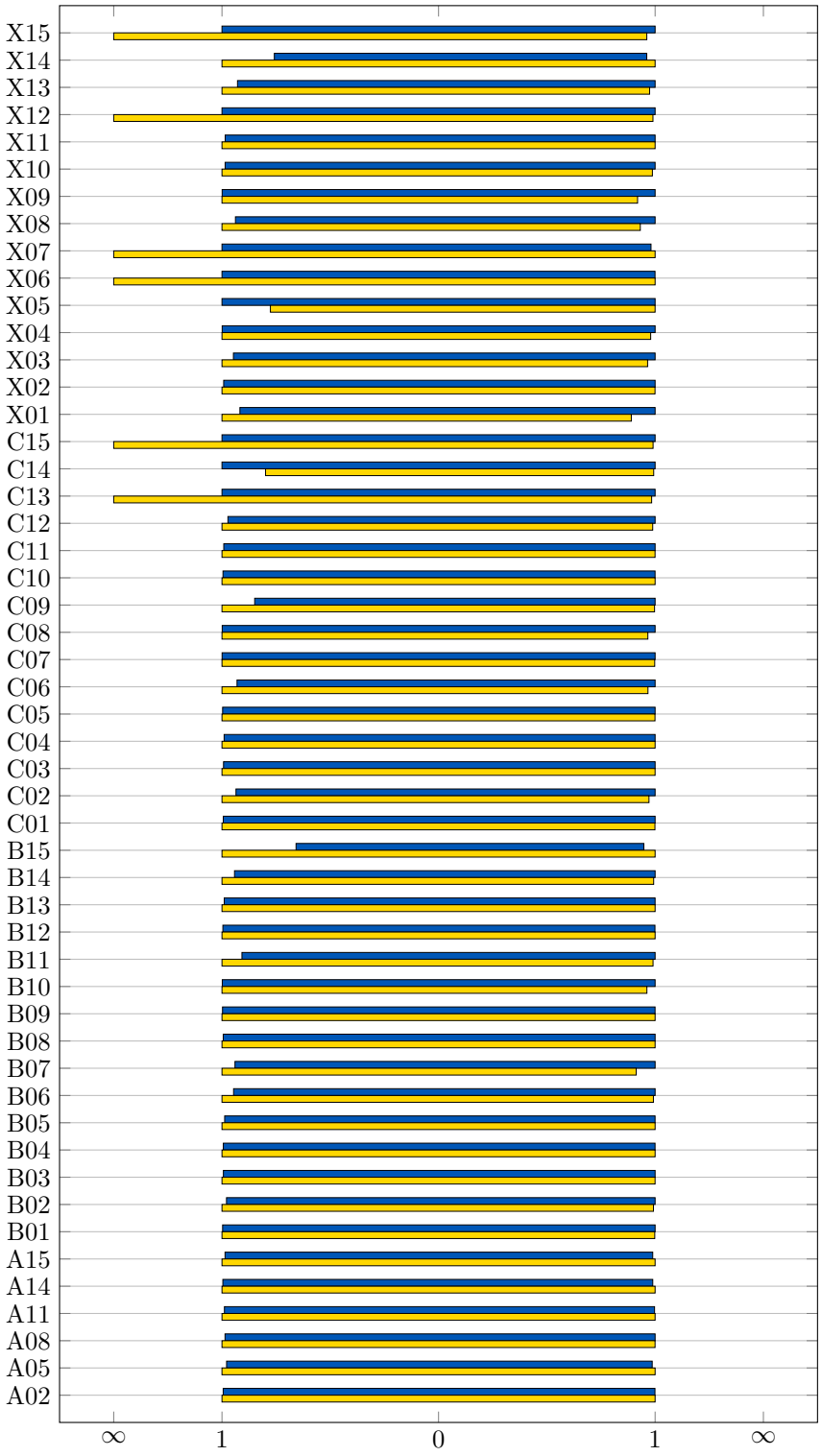

FIGURE 5. Bar plot for $\min_{m' \in \mathcal{M}'}\{v_{\mathrm{LB}}^{m'} \colon v_{\mathrm{LB}}^{m'} > 0\}/v_{\mathrm{LB}}^{m}$ (left side) and $v_{\mathrm{UB}}^{m}/\max_{m' \in \mathcal{M}'}\{v_{\mathrm{UB}}^{m'} \colon v_{\mathrm{UB}}^{m'} < \infty\}$ (right side), where $\mathcal{M}'$ is composed of $\mathrm{MILP}_{\mathrm{VI}^*}^{\mathrm{OADM}}$ (blue) and ASCA (yellow).

6.2. **Numerical Results for the Portfolio Optimization Problem.** We build a test set of 24 instances for the portfolio optimization problem following the procedure used in [21] to generate instances for the probabilistically chance-constrained portfolio optimization model. Our instances are characterized by $n \in \{20, 200\}$ equities and $|\mathcal{S}| = 200$ equiprobable scenarios with $p^s = 1/|\mathcal{S}|$, $s \in \mathcal{S}$. We draw the components of return vectors r^s, $s \in \mathcal{S}$, using an independent uniform distribution law on the interval $[80, 150]$. This means, we generate equities whose returns range between a 20 % loss and a 50 % profit on the investment. The minimum expected return ρ is set to 110, forcing an average portfolio return of 10 % w.r.t. the invested budget. We consider the VaR confidence level of 7.5 %, 15 %, and 22.5 %, i.e., $\tau \in \{0.075, 0.15, 0.225\}$ holds. Finally, the objective function weight α takes values in set $\{0, 0.25, 0.5, 0.75\}$: Smaller values of α favor risk minimization over return maximization—larger values of α favor the opposite behavior.

First, we discuss the results obtained by solving MILP, MILP_{VI}, and $\text{MILP}_{\text{VI}^*}$ on the entire set of 24 instances. For $\text{MILP}_{\text{VI}^*}$, where the separation of the inequalities in (24) is NP-hard (see Proposition 6), we separate them by means of the same procedure employed for the inequalities in (23). By doing so, the time spent to separate and build the two families of valid inequalities differs of a factor of ten. However, in both cases, this time remains negligible w.r.t. the computational time limit since it is always less than 4 s.

Table 3 reports the results obtained by solving the instances with the three configurations. Each row of the table corresponds to an instance for which its parameterization is summarized in columns two to six of the table. Then, for each approach, we include three columns. The first and second columns contain the lower and upper bounds (v_{LB} and v_{UB}), respectively. The third is a mixed time/gap (t_{solve}/gap) column reporting either the computational time if the model is solved to global optimality within the time limit or the relative optimality gap in percentage ($100\,(v_{\text{UB}} - v_{\text{LB}})/v_{\text{LB}}$) otherwise.

In general, all three configurations yield comparable results. The solver provides feasible points of comparable value (v_{LB}) on all the instances and it manages to prove the optimality of the same four instances (W1, W4, W7, W10) on average in 436, 438, and 604 seconds, respectively. The average optimality gap returned by the solver on the instances for which optimality is not proven within the time limit is 3.4 % for the plain MILP and 2.6 % for both configurations involving valid inequalities.

To assess the impact of the two families of valid inequalities, we focus on those instances that are not solved to optimality. In what follows, the upper bound improvement of a configuration against another one, e.g., MILP against MILP_{VI}, is computed as $(v_{\text{UB}}^{\text{MILP}} - v_{\text{UB}}^{\text{MILP}_{\text{VI}}})/v_{\text{UB}}^{\text{MILP}}$, where $v_{\text{UB}}^{\text{MILP}}$ and $v_{\text{UB}}^{\text{MILP}_{\text{VI}}}$ are the upper bounds returned by the solver for the configurations MILP and MILP_{VI}, respectively. The improvements regarding the optimality gap are computed analogously.

First, we observe that the introduction of either inequalities (23) or (24) yields benefits in terms of both decreasing the upper bound and reducing the optimality gap. Indeed, the upper bound and integrality gap improvements on average are equal to 0.8 % and 18 % when comparing MILP to MILP_{VI} and they are equal to 0.7 % and 16 % when comparing MILP to $\text{MILP}_{\text{VI}^*}$. The same trend emerges when analyzing the values of the upper bound and the optimality gap after the solution of the root node of the branch-and-bound tree; see Table 4.

As mentioned in the introduction of this section, although inequalities (23) are dominated by inequalities (24) (see Proposition 6), this relation is not reflected in the computational results. Indeed, when comparing MILP_{VI} to $\text{MILP}_{\text{VI}^*}$, the upper bound improvement in percent becomes negligible and the optimality gap tends

to be smaller for MILP_{VI}—on average of 3 %. Conversely, a slight dominance of configuration $\text{MILP}_{\text{VI}^*}$ over configuration MILP_{VI} arises from the results obtained after the solution of the root node; see Table 4. To explain this behavior, we note that the separation procedure for inequalities (24) is heuristic.

TABLE 3. Results obtained by solving the instances of the portfolio optimization problem with configurations MILP, MILP_{VI} and $\text{MILP}_{\text{VI}^*}$ within a time limit of 90 minutes.

	Parameters					MILP			MILP_{VI}			$\text{MILP}_{\text{VI}^*}$		
ID	Assets	$\lvert\mathcal{S}\rvert$	α	ρ	τ	v_{LB}	v_{UB}	t_{solve}(s)/gap(%)	v_{LB}	v_{UB}	t_{solve}(s)/gap(%)	v_{LB}	v_{UB}	t_{solve}(s)/gap(%)
W1	20	200	0	110	0.075	111.05	111.05	934.522s	111.05	111.05	1058.42s	111.05	111.05	885.981s
W2	20	200	0	110	0.15	112.629	114.825	1.95%	112.629	114.772	1.90%	112.629	114.837	1.96%
W3	20	200	0	110	0.225	113.844	119.218	4.72%	113.719	118.829	4.49%	113.82	120.508	5.88%
W4	20	200	0.25	110	0.075	112.558	112.558	370.782s	112.558	112.558	380.56s	112.558	112.558	1226.77s
W5	20	200	0.25	110	0.15	113.33	115.169	1.62%	113.258	115.409	1.90%	113.33	115.39	1.82%
W6	20	200	0.25	110	0.225	115.051	119.067	3.49%	115.054	119.716	4.05%	115.007	119.544	3.95%
W7	20	200	0.5	110	0.075	113.778	113.778	325.911s	113.778	113.778	113.778s	113.778	113.778	206.893s
W8	20	200	0.5	110	0.15	114.345	115.705	1.19%	114.385	115.734	1.18%	114.375	116.205	1.60%
W9	20	200	0.5	110	0.225	114.959	117.764	2.44%	114.907	118.117	2.79%	114.876	118.1	2.81%
W10	20	200	0.75	110	0.075	114.31	114.31	113.189s	114.31	114.31	92.8553s	114.31	114.31	126.28s
W11	20	200	0.75	110	0.15	114.642	115.362	0.63%	114.678	115.271	0.52%	114.678	115.33	0.57%
W12	20	200	0.75	110	0.225	115.126	115.813	0.60%	115.126	115.96	0.72%	115.126	115.874	0.65%
W13	400	200	0	110	0.075	116.551	120.701	3.56%	116.545	119.155	2.24%	116.612	119.165	2.19%
W14	400	200	0	110	0.15	117.094	125.632	7.29%	117.219	122.351	4.38%	117.226	122.363	4.38%
W15	400	200	0	110	0.225	117.595	130.208	10.73%	117.811	125.778	6.76%	117.812	125.736	6.73%
W16	400	200	0.25	110	0.075	116.738	119.85	2.67%	116.762	118.696	1.66%	116.745	118.705	1.68%
W17	400	200	0.25	110	0.15	117.203	123.38	5.27%	117.233	121.102	3.30%	117.229	121.131	3.33%
W18	400	200	0.25	110	0.225	117.775	126.679	7.56%	117.829	123.704	4.99%	117.715	123.727	5.11%
W19	400	200	0.5	110	0.075	116.909	118.83	1.64%	116.9	118.112	1.04%	116.907	118.122	1.04%
W20	400	200	0.5	110	0.15	117.378	121.241	3.29%	117.332	120.073	2.34%	117.33	120.087	2.35%
W21	400	200	0.5	110	0.225	117.583	123.293	4.86%	117.684	121.521	3.26%	117.654	121.509	3.28%
W22	400	200	0.75	110	0.075	117.25	118.136	0.76%	117.24	117.78	0.46%	117.25	117.785	0.46%
W23	400	200	0.75	110	0.15	117.199	119.012	1.55%	117.209	118.547	1.14%	117.222	118.517	1.10%
W24	400	200	0.75	110	0.225	117.659	120.392	2.32%	117.677	119.695	1.71%	117.715	119.752	1.73%

TABLE 4. Average upper bound and integrality gap percentage improvements after the resolution of the root node of the branch-and-bound tree

Comparison	avg. v_{UB} impr.(%)	avg. gap impr.(%)
MILP vs. $\mathrm{MILP}_{\mathrm{VI}}$	1.73	34.50
MILP vs. $\mathrm{MILP}_{\mathrm{VI}^*}$	1.77	39.15
$\mathrm{MILP}_{\mathrm{VI}}$ vs. $\mathrm{MILP}_{\mathrm{VI}^*}$	0.05	4.85

Finally, as opposed to the MPP, the solver does not fail to provide feasible points of good quality on the instances of the portfolio optimization problem. Indeed, the average optimality gap already after the resolution of root node is rather small. It is equal to 11.5 %, 6.1 %, and 5.6 % for configurations MILP, $\mathrm{MILP}_{\mathrm{VI}}$ and $\mathrm{MILP}_{\mathrm{VI}^*}$, respectively.

7. Conclusion

In this paper we considered several solution techniques for mixed-integer quantile minimization problems. We stated the problem in a very general form and developed techniques to strengthen the dual bound (via tailored valid inequalities), to find good primal solutions quickly (via the overlapping ADM), and to derive provably optimal solutions using a problem-specific approach (via the adaptive clustering method). Our numerical results on the maintenance planning problem of the EURO/ROADEF challenge 2020 and on the quantile-based version of the portfolio optimization problem show that the combination of these techniques significantly outperforms the application of general-purpose MILP solvers.

We briefly touched the field of chance constraints that is highly related to the quantile minimization problems discussed in this paper. Thus, a natural topic of future research will be to investigate on how to transfer our novel techniques to improve solution methods for chance-constrained problems.

Acknowledgments

Martine Labbé has been partially supported by the Fonds de la Recherche Scientifique - FNRS under Grant(s) no PDR T0098.18. Marius Roland and Martin Schmidt acknowledge the support by the German Bundesministerium für Bildung und Forschung within the project "EiFer". Martin Schmidt thanks the DFG for their support within the projects A05 and B08 in CRC TRR 154.

References

[1] G. J. Alexander and A. M. Baptista. "A comparison of VaR and CVaR constraints on portfolio selection with the mean-variance model." In: *Management science* 50.9 (2004), pp. 1261–1273.

[2] G. J. Alexander and A. M. Baptista. "Economic implications of using a mean-VaR model for portfolio selection: A comparison with mean-variance analysis." In: *Journal of Economic Dynamics and Control* 26.7-8 (2002), pp. 1159–1193.

[3] P. Artzner, F. Delbaen, J.-M. Eber, and D. Heath. "Coherent measures of risk." In: *Mathematical Finance* 9.3 (1999), pp. 203–228.

[4] S. Benati and R. Rizzi. "A mixed integer linear programming formulation of the optimal mean/Value-at-Risk portfolio problem." In: *European Journal of Operational Research* 176 (2007), pp. 423–434.

[5] S. Boyd, N. Parikh, and E. Chu. *Distributed optimization and statistical learning via the alternating direction method of multipliers*. Now Publishers Inc., 2011.

[6] P. F. Fischer. "An Overlapping Schwarz Method for Spectral Element Solution of the Incompressible Navier–Stokes Equations." In: *Journal of Computational Physics* 133.1 (1997), pp. 84–101. DOI: 10.1006/jcph.1997.5651.

[7] D. Gabay and B. Mercier. "A dual algorithm for the solution of nonlinear variational problems via finite element approximation." In: *Computers & Mathematics with Applications* 2.1 (1976), pp. 17–40.

[8] A. A. Gaivoronski and G. Pflug. "Finding optimal portfolios with constraints on value at risk." In: *Proceedings III Stockholm seminar on risk behavior and risk management*. 1999.

[9] A. A. Gaivoronski and G. Pflug. "Value-at-Risk in Portfolio Optimization: Properties and Computational Approach." In: *Journal of Risk* 7.2 (2005), pp. 1–31.

[10] M. R. Garey and D. S. Johnson. *Computers and intractability*. Vol. 174. San Francisco: freeman, 1979.

[11] B. Geißler, A. Morsi, L. Schewe, and M. Schmidt. "Solving power-constrained gas transportation problems using an MIP-based alternating direction method." In: *Computers & Chemical Engineering* 82 (2015), pp. 303–317.

[12] B. Geißler, A. Morsi, L. Schewe, and M. Schmidt. "Solving Highly Detailed Gas Transport MINLPs: Block Separability and Penalty Alternating Direction Methods." In: *INFORMS Journal on Computing* 30.2 (2018), pp. 309–323. DOI: 10.1287/ijoc.2017.0780.

[13] R. Glowinski and A. Marroco. "Sur l'approximation, par éléments finis d'ordre un, et la résolution, par pénalisation-dualité d'une classe de problèmes de Dirichlet non linéaires." In: *ESAIM: Mathematical Modelling and Numerical Analysis-Modélisation Mathématique et Analyse Numérique* 9.R2 (1975), pp. 41–76.

[14] T. Kleinert and M. Schmidt. "Computing Feasible Points of Bilevel Problems with a Penalty Alternating Direction Method." In: *INFORMS Journal on Computing* (2019). DOI: 10.1287/ijoc.2019.0945. Forthcoming.

[15] T. Kleinert, M. Labbé, F. Plein, and M. Schmidt. "Closing the Gap in Linear Bilevel Optimization: A New Valid Primal-Dual Inequality." In: *Optimization Letters* 15 (2021), pp. 1027–1040. DOI: 10.1007/s11590-020-01660-6.

[16] C.-C. Lin. "Comments on "A mixed integer linear programming formulation of the optimal mean/Value-at-Risk portfolio problem"." In: *European Journal of Operational Research* 194 (2009), pp. 339–341.

[17] R. Liu, Z. Lin, and Z. Su. "Linearized alternating direction method with parallel splitting and adaptive penalty for separable convex programs in machine learning." In: *Asian Conference on Machine Learning*. PMLR. 2013, pp. 116–132.

[18] R. Mansini, W. Ogryczak, and M. G. Speranza. "LP solvable models for portfolio optimization: A classification and computational comparison." In: *IMA Journal of Management Mathematics* 14.3 (2003), pp. 187–220.

[19] H. Markowitz. "Portfolio Selection." In: *The Journal of Finance* 7.1 (1952), pp. 77–91. DOI: 10.1111/j.1540-6261.1952.tb01525.x.

[20] S. Na, S. Shin, M. Anitescu, and V. M. Zavala. *On the Convergence of Overlapping Schwarz Decomposition for Nonlinear Optimal Control*. 2021.

[21] F. Qiu, S. Ahmed, S. S. Dey, and L. A. Wolsey. "Covering linear programming with violations." In: *INFORMS Journal on Computing* 26.3 (2014), pp. 531–546.

[22] L. Schewe, M. Schmidt, and D. Weninger. "A decomposition heuristic for mixed-integer supply chain problem." In: *Operations Research Letters* 48.3 (2020), pp. 225–232. DOI: 10.1016/j.orl.2020.02.006.

[23] S. Shin, V. M. Zavala, and M. Anitescu. "Decentralized Schemes With Overlap for Solving Graph-Structured Optimization Problems." In: *IEEE Transactions on Control of Network Systems* 7.3 (2020), pp. 1225–1236. DOI: 10.1109/TCNS.2020.2967805.

[24] B. W. Silverman. *Density estimation for statistics and data analysis*. Routledge, 2018. DOI: 10.1201/9781315140919.

[25] Y. Song and J. R. Luedtke. "Branch-and-cut approaches for chance-constrained formulations of reliable network design problems." In: *Mathematical Programming Computation* 5.4 (2013), pp. 397–432.

[26] Y. Song, J. R. Luedtke, and S. Kücükyavuz. "Chance-constrained binary packing problems." In: *INFORMS Journal on Computing* 26.4 (2014), pp. 735–747.

[27] M. W. Tanner and L. Ntaimo. "IIS branch-and-cut for joint chance-constrained stochastic programs and application to optimal vaccine allocation." In: *European Journal of Operational Research* 207.1 (2010), pp. 290–296.

Appendix A. Detailed Results for the Instances of the EURO/ROADEF Challenge 2020

Table 5. Results for all methods applied to the A and B instances of the EURO/ROADEF challenge 2020.

	MILP			$\text{MILP}_{\text{VI}^*}$			$\text{MILP}_{\text{VI}^*}^{\text{OADM}}$			ASCA		
ID	v_{UB}	v_{LB}	gap (%)	v_{UB}	v_{LB}	gap (%)	v_{UB}	v_{LB}	gap (%)	v_{UB}	v_{LB}	gap (%)
A02	4682.57	2075.8	55.67	4676.16	4594.49	1.75	4673.88	4596.33	1.66	4676.99	4570.84	2.27
A05	649.25	593.35	8.61	637.36	615.61	3.41	637.087	615.65	3.36	645.767	602.549	6.69
A08	744.35	710.52	4.54	744.29	739.85	0.6	744.469	739.58	0.66	744.293	729.207	2.03
A11	500.37	456.27	8.81	497.47	477.1	4.09	495.499	476.5	3.83	496.744	471.108	5.16
A14	2275.96	2093.47	8.02	2274.39	2161.94	4.94	2273.4	2161.6	4.92	2298.28	2153.18	6.31
A15	2297.72	2078.2	9.55	2277.11	2163.3	5	2283.86	2164.64	5.22	2309.31	2134.33	7.58
B01	4466.12	1793.44	59.84	3994.03	3839.8	3.86	3992.4	3838.76	3.85	3986.2	3827.57	3.98
B02	4757.6	2000.87	57.94	4332.3	3679.17	15.08	4351.97	3679.01	15.46	4318.82	3602.24	16.59
B03	40780.7	11894.1	70.83	-	34043.6	-	35300.4	34038.7	3.57	35294.3	33815.8	4.19
B04	38202.7	11782.5	69.16	34837.5	33653.8	3.4	34836.2	33660.7	3.37	34845.6	33452.3	4
B05	3234.52	1133.02	64.97	2399.01	2323.41	3.15	2398.92	2324.26	3.11	2399.45	2295.4	4.34
B06	4982.95	1972.34	60.42	4345.36	3684.41	15.21	4335.23	3683.91	15.02	4301.25	3486.57	18.94
B07	8200.08	4396.8	46.38	7817.26	6134.58	21.53	8295.25	6134.69	26.05	7570.9	5766.54	23.83
B08	8242.35	2144.27	73.98	7436.35	7240.81	2.63	7436.3	7239.54	2.65	7436.08	7197.57	3.21
B09	8050.04	2336.22	70.98	7493.25	7262.21	3.08	7495.97	7264.14	3.09	7497.76	7246.02	3.36
B10	11112.6	5745.84	48.29	10806.9	8472.26	21.6	11040.6	8472.3	23.26	10621.9	8461.01	20.34
B11	4061.66	1723.11	57.58	3673.93	3187.98	13.23	3682.11	3187.97	13.42	3646.96	2894.26	20.64
B12	39281.9	14788.8	62.35	37602.8	36690.9	2.42	37606	36690.6	2.43	37632.1	36540.5	2.9
B13	5486.03	2321.9	57.68	5025.11	4843.72	3.61	5025.11	4842.8	3.63	5025.45	4792.55	4.63
B14	12212.5	7428.6	39.17	12039.4	9615.35	20.13	12212.5	9615.35	21.27	12131.2	9059.02	25.32
B15	23749	9867.61	58.45	22574.4	21309.8	5.6	22573.8	21309.8	5.6	23812	14022.6	41.11

TABLE 6. Results for all methods applied to the C and X instances of the EURO/ROADEF challenge 2020.

	MILP			$\text{MILP}_{\text{VI}^*}$			$\text{MILP}_{\text{VI}^*}^{\text{OADM}}$			ASCA		
ID	v_{UB}	v_{LB}	gap (%)	v_{UB}	v_{LB}	gap (%)	v_{UB}	v_{LB}	gap (%)	v_{UB}	v_{LB}	gap (%)
C01	9467.7	2107.45	77.74	8518.94	8233.48	3.35	8524.85	8236.19	3.39	8518.43	8187.43	3.89
C02	3662.99	2201.19	39.91	3580.33	2969.05	17.07	3660.18	2968.88	18.89	3556.65	2777.08	21.92
C03	38448.1	11297.3	70.62	-	31856.5	-	33529.6	31840.7	5.04	33525.9	31611.4	5.71
C04	40790.2	11304.7	72.29	37602.3	36430.4	3.12	37603	36542.9	2.82	37603.5	36183	3.78
C05	4134.92	1061.68	74.32	3167.83	3086.67	2.56	3170.99	3086.54	2.66	3169.41	3077.42	2.9
C06	8910.6	4582.13	48.58	-	6738.91	-	8764.45	6738.76	23.11	8475.4	6270.43	26.02
C07	6101.87	2730.57	55.25	6099.53	5897.3	3.32	6096.17	5895.13	3.3	6085.14	5892.19	3.17
C08	11771.2	6391.58	45.7	-	9180.71	-	11600.4	9180.72	20.86	11212	9171.45	18.2
C09	6421.51	2099.57	67.3	5660.99	4379.42	22.64	5648.66	4380.04	22.46	5634.22	3718.77	34
C10	48983	14502	70.39	43348.8	42013	3.08	43345.1	42013.7	3.07	43353.6	41817.9	3.54
C11	6205.78	2437.72	60.72	5751.26	5499.78	4.37	5751.26	5500.1	4.37	5749.96	5454.68	5.14
C12	13171.7	6946.82	47.26	12951.5	9389.39	27.5	13179.9	9389.62	28.76	13034.2	9132.07	29.94
C13	-	13602	-	-	41378.6	-	45607.4	13809.1	69.72	44878.5	-	-
C14	-	10695.8	-	-	10695.2	-	28329.9	10686.2	62.28	28145.9	13376.2	52.48
C15	-	-	-	43437.7	14076.3	67.59	43554.5	14076.3	67.68	43147.5	-	-
X01	4435.85	2058.52	53.59	4289.81	2870.42	33.09	4531.54	2870.43	36.66	4033.74	2632.89	34.73
X02	37594.5	12194.5	67.56	-	30607.4	-	32254.8	30649	4.98	32242.2	30407.8	5.69
X03	-	4390.86	-	-	6487.7	-	8427.73	6487.59	23.02	8136.08	6145.04	24.47
X04	12120.1	5962.21	50.81	-	9011.92	-	11612.5	9011.77	22.4	11375.2	9003.65	20.85
X05	-	10068.4	-	-	17700.1	-	23650.5	10086.6	57.35	23649.5	12989.2	45.08
X06	-	718.87	-	47607.6	16203.8	65.96	49435.5	16203.8	67.22	49454.9	-	-
X07	14203.8	5594.45	60.61	13278.1	12713	4.26	13233.1	12712.9	3.93	13488.2	-	-
X08	-	5351.69	-	13944.4	9904.99	28.97	15190	9904.84	34.79	14151.4	9289.43	34.36
X09	22170.2	8743.09	60.56	-	12894.9	-	22053.1	12894.9	41.53	20266.9	12885.2	36.42
X10	-	7445.86	-	17380.9	15778.7	9.22	17630.9	15777.9	10.51	17410.8	15549	10.69
X11	-	14384	-	39132.3	38112.8	2.61	39133.9	38113.4	2.61	39133.7	37551.6	4.04
X12	-	13952.3	-	-	37534.1	-	48594.8	37534.3	22.76	48113	-	-
X13	16409.2	8819.77	46.25	-	14040.4	-	16403.5	14022.8	14.51	15987.2	13018	18.57
X14	-	18718.5	-	79583.7	76588.3	3.76	79589.1	76587.7	3.77	82782	58069.3	29.85
X15	-	16558.7	-	-	38778.4	-	49584.7	38729.5	21.89	47679.5	-	-

(D. Cattaruzza, M. Petris) Univ. Lille, CNRS, Centrale Lille, Inria, UMR 9189 - CRIStAL Lille, France

(M. Labbé) (A) Université Libre de Bruxelles, Department of Computer Science, Boulevard du Triomphe, CP212, 1050 Brussels, Belgium; (B) Inria Lille - Nord Europe, Parc scientifique de la Haute Borne, 40, av. Halley - Bât A - Park Plaza, 59650 Villeneuve d'Ascq, France

Email address: martine.labbe@ulb.be

(M. Roland, M. Schmidt) Trier University, Department of Mathematics, Universitätsring 15, 54296 Trier, Germany

Email address: roland@uni-trier.de, martin.schmidt@uni-trier.de